# UTILITY APPLICATION FOR UNITED STATES PATENT

# GENE SEGREGATION AND BIOLOGICAL SAMPLE CLASSIFICATION METHODS

Inventor:

Guennadi V. Glinskii, a citizen of United States of America,

residing at

939 Coast Boulevard, #4M, La Jolla, CA 92037

Assignee:

Sidney Kimmel Cancer Center

10835 Altman Row San Diego, CA 92121

a CALIFORNIA NON-PROFIT CORPORATION

Entity:

Small

Correspondence Address:

Fenwick & West LLP
Silicon Valley Center
801 California Street

Mountain View, CA 94041

(650) 988-8500

Filing Date:

September 10, 2003

Express Mail No: EV342133757US

## TITLE OF INVENTION

[0001] Gene segregation and biological sample classification methods.

# CROSS-REFERENCE TO RELATED APPLICATIONS

[0002] This application claims the benefit of U.S. Provisional Application 60/410,018 filed September 10, 2002, U.S. Provisional Application 60/411,155 filed September 16, 2002, U.S. Provisional Application 60/429,168 filed November 25, 2002, U.S. Provisional Application 60/444,348 filed January 31, 2003, and U.S. Provisional Application 60/460,826 filed April 3, 2003, each of which is incorporated by reference in its entirety.

#### FIELD OF THE INVENTION

[0003] The present invention relates to methods for gene segregation to identify clusters of genes associated with biological sample phenotypes and for classifying biological samples on the basis of gene expression patterns derived from those samples.

# STATEMENT REGARDING FEDERALLY SPONSORED RESEARCH

[0004] This invention was made using federal funds awarded by the National Institutes of Health, National Cancer Institute under contract number 1RO1CA89827-01. The government has certain rights to this invention.

# **BACKGROUND OF THE INVENTION**

[0005] For many years established human cancer cell lines have been used as models to study human cancers because, to a large degree, they faithfully recapitulate many biological features of human tumors. Established human cancer cell lines maintained *in vitro* are not expected to fully recapitulate the gene expression patterns of human clinical cancers. This essentially precludes their use as model systems for global gene expression analysis of human tumors. It is likely that the longer that cancer cell lines are maintained

in vitro, the more they degrade as models for transcription changes in human clinical cancers.

[0006] Recent experiments using established human prostate and breast cancer cell line models indicate that this degradation may be at least partly reversed by using established cancer cell lines to generate experimental tumors in mice and to develop xenograft-derived cell lines from these experimental tumors (Glinsky, G.V., Glinskii, A.B., McClelland, M., Krones-Herzig, A., Mercola, D., Welsh, J. 2002. Microarray gene expression analysis of tumor progression in the nude mouse model of human prostate cancer. In Proceedings of the 93<sup>rd</sup> Annual Meeting of the American Association for Cancer Research, April 6-10, San Francisco, CA, 43: 462 (Abstract#4480), incorporated herein by reference). Furthermore, the study of differential gene expression observed using cell lines maintained in vitro and in cell line-induced experimental tumors in mice avoids many of the problems associated with cellular heterogeneity and experimental manipulation of clinical samples. It appears that the in vitro and in vivo human prostate cancer progression models partially recapitulate gene expression behavior of clinical prostate tumor samples, at least with respect to the consensus differentially regulated gene class that has been recently defined for multiple xenograft-derived human prostate cancer cell lines (Glinsky, G.V., Glinskii, A.B., McClelland, M., Krones-Herzig, A., Mercola, D., Welsh, J. 2002. Microarray gene expression analysis of tumor progression in the nude mouse model of human prostate cancer. In Proceedings of the 93<sup>rd</sup> Annual Meeting of the American Association for Cancer Research, April 6-10, San Francisco, CA, 43: 462 (Abstract#4480), incorporated herein by reference).

While several useful methods of classification of human and other tumors are [0007] known, these methods tend to be a highly subjective in nature and at best semiquantitative. Recent advances in global gene expression analysis of human tumors using cDNA or oligonucleotide microarray technologies set the stage for the development of improved quantitative methods for human tumor classification (see, e.g., Magee, J.A., Araki, T., Patil, S., Ehrig, T., True, L., Humphrey, P.A., Catalona, W.J., Watson, M.A., Milbrandt, J. Expression profiling reveals hepsin overexpression in prostate cancer. Cancer Res., 61: 5692-5696, 2001; Dhanasekaran, S.M., Barrette, T.R., Ghosh, D., Shah, R., Varambally, S., Kurachi, K., Pienta, K.J., Rubin, M.A., Chinnalyan, A.M. Delineation of prognostic biomarkers in prostate cancer. Nature, 412:822-826, 2001; Welsh, J.B., Sapinoso, L.M., Su, A.I., Kern, S.G., Wang-Rodriguez, J., Moskaluk, C.A., Frierson, H.F., Jr., Hampton, G.M. Analysis of gene expression identifies candidate markers and pharmacological targets in prostate cancer. Cancer Res., 61: 5974-5978, 2001; Luo, J., Duggan, D.J., Chen, Y., Sauvageot, J., Ewing, C.M., Bittner, M.L., Trent, J.M., Isaacs, W.B. Human prostate cancer and benign prostatic hyperplasia: molecular dissection by gene expression profiling. Cancer Res., 61: 4683-4688, 2001; Stamey, TA, Warrington, JA, Caldwell, MC, Chen, Z, Fan, Z, Mahadevappa, M, McNeal, JE, Nolley, R, Zhang, Z. Molecular genetic profiling of Gleason grade 4/5 prostate cancers compared to benign prostatic hyperplasia. J. Urol., 166: 2171-2177, 2001; Luo, J., Dunn, T, Ewing, C, Sauvageot, J., Chen, Y., Trent, J., Isaacs, W. Gene expression signature of benign prostatic hyperplasia revealed by cDNA microarray analysis. Prostate, 51: 189-200, 2002; Singh, D., Febbo, P.G., Ross, K., Jackson, D.G., Manola, C.L., Tamayo, P., Renshaw, A.A., D'Amico, A.V., Richie, J.P., Lander, E.S., Loda, M., Kantoff, P.W., Golub, T.R., Sellers,

W.R. Gene expression correlates of clinical prostate cancer behavior. Cancer Cell, 1: 203-209, 2002; Rhodes, D.R., Barrette, T.R., Rubin, M.A., Ghosh, D., Chinnaiyan, A.M. Meta-analysis of microarrays: interstudy validation of gene expression profiles reveals pathways dysregulation in prostate cancer. Cancer Res., 62: 4427-4433, 2002; Pollack, J.R., Perou, C.M., Alizadeh, A.A., Eisen, M.B., Pergamenschikov, A., Williams, C.F., Jeffrey, S.S., Botstein, D., Brown, P.O. Genome-wide analysis of DNA-copy number changes using cDNA microarrays. Nature Genetics. 1999. 23: 41-46; Forozan, F., Mahlamaki, E.H., Monni, O., Chen, Y., Veldman, R., Jiang, Y., Gooden, G.C., Ethier, S.P., Kallioniemi, A., Kallioniemi, O-P. Comparative genomic hybridization analysis of 38 breast cancer cell lines: a basis for interpreting complementary DNA microarray data. Cancer Res. 2000. 60: 4519-4525; Perou CM, Jeffrey SS, van de Rijn M, et al. Distinctive gene expression patterns in human mammary epithelial cells and breast cancers. Proc Natl Acad Sci USA. 1999. 96:9212-9217; Perou CM, Sorlie T, Eisen MB, et al. Molecular portrait of human breast tumors. Nature. 2000. 406:747-752; Clark, EA, Golub TR, Lander ES, Hynes RO. Genomic analysis of metastasis reveals an essential role for RhoC. Nature 2000. 406:532-535; Welsh, J.B., Zarrinkar, P.P., Sapinoso, L.M., Kern, S.G., Behling, C.A., Monk, B.J., Lockhart, D.J., Burger, R.A., Hampton, G.M. Analysis of gene expression profiles in normal and neoplastic ovarian tissue samples identifies candidate molecular markers of epithelial ovarian cancer. Proc Natl Acad Sci USA. 2001. 98:1176-1181, incorporated herein by reference). However, direct attempts to identify genes differentially regulated in tumors that are useful for tumor classification, clinical management and prognosis have produced limited success, in part, because of intrinsic cellular heterogeneity and variability in cellular composition of clinical samples,

the statistically underdetermined nature of the problem in which the number of variables (e.g., expression data points) exceeds the number of observations (i.e., independent samples from which the data are gathered), and the absence of a uniform, readily accessible and reproducible reference standard against which differential expression can be evaluated.

[0008] In the context of clinical tumor samples, an acceptable reference standard against which differential gene expression can be evaluated should meet the following requirements:

[0009] Individual clinical tumors should display different degrees of resemblance between their gene expression patterns as compared to the gene expression pattern exhibited by the reference standard samples;

[0010] The degree of resemblance between the gene expression patterns in individual clinical samples and that of the reference standard samples should be susceptible to quantitative measurement; and

[0011] Quantitative measurements of the degree of resemblance between clinical samples and the reference standard samples should correlate with biological, clinical, and pathohistological features of individual human tumors enabling their use as a basis for classification of clinical tumor samples.

[0012] In a more general sense, gene expression drives the acquisition of cellular phenotypes during differentiation of precursor or stem cells. Identification of genes that are differentially expressed between precursor cells and differentiated cells, or between different types of differentiated cells is an important step for understanding the molecular processes underlying differentiation. The ability to control differentiation of precursor or

stem cells so as to direct the cells down a desired differentiation pathway is an important goal, as it represents a tissue engineering solution to the problem of alleviating the shortage of tissue and organs useful for grafting and transplantation. Furthermore, normal and transformed cell-type specific markers, useful for, e.g., molecular-recognition-based targeting of therapeutics such as e.g., rituximab and other recognition based therapeutics, can be identified from sets of genes concordantly regulated in particular normal and transformed cell types.

Attempts to identify directly genes that are differentially regulated in various [0013]cell lines suffer from some of the same difficulties referenced above for tumor samples. One of the most common problems for the array-based study is that they usually generate vast data sets. For example, gene expression analysis of a single tumor cell line and a single normal epithelial counterpart typically identifies many thousands of transcripts as differentially expressed at a statistically significant level. Up to 40-50% of the surveyed genes will be identified as differentially expressed when one compares gene expression profiles of normal epithelial and stromal cells. Obviously, any meaningful design of follow-up clinical and/or experimental validation experiments would require an application of further data reduction steps. Our work makes contribution to the solution of this problem by providing a convenient and simple data reduction technique. Two possible approaches seem to be appropriate: one can narrow a set of candidate genes identified in cell lines to those that maintain similar transcript abundance (or other type of gene expression) behavior in a relevant set of clinical tumor samples and design a hypothesis-driven study aimed at identifying potential biologically important genes and/or pathways using cell lines as a model system. Alternatively, one can identify or

design cell lines that recapitulate gene expression behavior identified in clinical samples and again use the model system for the assessment of the biological relevance of the gene expression changes. During the last two years or so a third approach is rapidly emerging. It is based on simultaneous analysis of gene expression and DNA copy number changes with an aim to identify the genes that acquired mRNA abundance changes due to the amplification or deletion of the corresponding genes. The cancer cell lines are certainly attractive model systems to undertake such validation study. Suitable reference standards also are needed against which gene expression patterns can be evaluated in normal (*i.e.*, not tumor) cells and/or tissues. Here again, acceptable reference standards would be expected to have the following properties:

- [0014] Different types of normal cells and/or tissues should display different degrees of resemblance between their gene expression patterns as compared to the gene expression pattern exhibited by the reference standard samples;
- [0015] The degree of resemblance between the gene expression patterns in individual normal cells and that of the reference standard samples should be susceptible to quantitative measurement; and
- [0016] Quantitative measurements of the degree of resemblance between normal cells and the reference standard samples should correlate with biological features of different normal cell types so as to provide a basis for the classification of differentiation state and cell type.
- [0017] There thus exist in the art a need for improved methods of biological sample classification, for improved methods of identifying genes that are differentially expressed or regulated in biological samples such as tumors and normal cells, for reference

standards that can be used in accordance with these methods, and for identified sets of coordinately regulated genes, the expression patterns of which can be used for classifying samples and for developing cell- or tissue-specific markers. The present invention addresses these and other shortcomings of the art.

## **BRIEF SUMMARY OF THE INVENTION**

[0018] Broadly, it is an object of the invention to provide improved quantitative methods for classifying tumor and normal samples.

[0019] It is a further object of the invention to provide useful reference standards for classifying tumors and normal samples.

[0020] It is a still further object of the invention to provide methods for classifying tumor and normal samples on the basis of gene expression data.

[0021] Thus, in one aspect, the invention provides a method for classifying a sample in which a first reference set of expressed genes is identified, the first reference set consisting of genes that are differentially expressed between a first set of tumor cell lines and a set of control cell lines, a second reference set of expressed genes is identified, the second reference set consisting of genes that are differentially expressed between a first set of samples and a second set of samples, wherein the first and second samples differ with respect to a sample classification, a concordance set of expressed genes is identified, the concordance set consisting of genes that are common to the first and second reference sets and wherein, preferably, the direction of the differential expression is the same in the first and second reference sets, identifying a minimum segregation set of expressed genes within the concordance set, the minimum segregation set consisting of a subset of expressed genes within the concordance set selected so that a first correlation coefficient between an average fold-change or difference of the gene expression data from the lines

and an average fold-change or difference of the gene expression data from the samples exceeds a pre-determined value, calculating for the expressed genes within the minimum segregation set a second correlation coefficient between the average fold-change or difference of the gene expression data from the cell lines and a fold-change or difference of the gene expression data from an unclassified sample, and classifying the unclassified sample as belonging to the first set of samples or the second set of samples according to the sign of the second correlation coefficient.

[0022] In a preferred embodiment, the first set of samples and the second set of samples comprise tumor cells and/or tissues containing tumor cells, that differ with respect to a tumor classification such as, e.g., benign versus malignant growth, local and/or systemic recurrence, invasiveness, metastatic propensity, metastatic tumors versus localized primary tumors, degree of dedifferentiation (poor, moderate, or well differentiated tumors), tumor grade, Gleason score, survival prognosis, disease free survival, lymph node status, patient age, hormone receptor status, PSA level, and histologic type.

[0023] In another embodiment, reference sets are obtained without the use of cell lines, but instead rely solely on the use of clinical samples. In this embodiment, a first reference set is obtained by looking at differential expression among two or more sets of clinical samples, preferably using average expression values, wherein the two or more sets differ with respect to a known phenotype. A concordance set is then obtained by determining concordance between the differentially expressed genes established using the two or more clinical sample groups and one or more individual samples within the group

that demonstrate the best fit (highest correlation coefficient) between the individual sample(s) and the average group measurements.

[0024] In other preferred embodiments, the gene expression data is selected from the group consisting of mRNA quantification data, cDNA quantification data, cRNA quantification data, and protein quantification data.

In another aspect, the invention provides for a method for identifying a set of [0025]genes in which a first reference set of expressed genes is identified, the first reference set consisting of genes that are differentially expressed between a first set of tumor cell lines and a set of control cell lines, a second reference set of expressed genes is identified, the second reference set consisting of genes that are differentially expressed between a first set of samples and a second set of samples, wherein the first and second samples differ with respect to a sample classification, a concordance set of expressed genes is identified, the concordance set consisting of genes that are common to the first and second reference sets and wherein, preferably, the direction of the differential expression is the same in the first and second reference sets, and identifying a minimum segregation set of expressed genes within the concordance set, the minimum segregation set consisting of a subset of expressed genes within the concordance set selected so that a first correlation coefficient between an average fold-change or difference of the gene expression data from the lines and an average fold-change or difference of the gene expression data from the samples exceeds a pre-determined value.

[0026] In another embodiment, the minimum segregation set is determined without use of cell line data. This embodiment is preferred when no appropriate cell lines are available. In this embodiment, two or more groups of clinical samples, differing with

respect to a known phenotype are used to generate a first reference set. Preferably, this is accomplished by determining average fold expression changes (optionally log transformed), and identifying a set of differentially expressed genes that are consistently (i.e., up- or down-regulated) in one group as compared to another group. The second reference set is obtained by determining for individual sample(s) within a group, fold-expression changes for genes within the first reference set, and finding those genes concordantly over- or under-expressed, in the individual sample(s) *cf.* the first reference set, and identifying those individual samples for which the individual gene expression values are most highly correlated with the expression of the genes in the first reference set. This essentially consists of calculating phenotype association indices for the individual gene expression measurements within the sample, and selecting as the second reference those genes identified as being concordantly expressed in the most highly correlated individual sample(s).

[0027] In yet another preferred embodiment, the invention provides minimum segregation sets of expressed genes. Such sets have utility as tools for, e.g., sample classification or prognostication, and as sources of cell- or tissue-specific markers. The markers can be used as, e.g., targets for delivery of cell- or tissue-specific reagents or drugs, or to monitor drug effects on a molecular scale.

[0028] In yet another preferred embodiment, the invention provides a kit comprising a set of reagents useful for determining the expression of a subset of genes identified using the methods of the invention, along with instructions for their use. The reagents can be affixed to a solid support and used in a hybridization reaction, or alternatively can be primers for use in nucleic acid amplification reactions.

[0029] Additional advantages and aspects of the present invention are now described with reference to the detailed description and drawings, below.

## BRIEF DESCRIPTION OF THE DRAWINGS

[0030] Fig. 1 is a scatter plot showing correlation of the expression profiles in 5 xenograft-derived human prostate carcinoma cell lines and 8 recurrent versus 13 non-recurrent human prostate tumors for 19 genes of the concordance set.

[0031] Fig. 2 is a scatter plot showing correlation of the expression profiles in 5 xenograft-derived human prostate carcinoma cell lines and 8 recurrent versus 13 non-recurrent human prostate tumors for 9 genes of the PC3/LNCap recurrence minimum segregation set (recurrence cluster).

[0032] Fig. 3 is a graph showing phenotype association indices for 9 genes of the recurrence cluster in individual human prostate tumors exhibiting recurrent (samples 1-8) or non-recurrent (samples 12-24) clinical behavior.

[0033] Fig. 4 is a graph showing phenotype association indices for 54 genes of the prostate cancer/normal tissue discrimination minimum segregation set (i.e., cluster) in 24 individual prostate tumors (samples 1-25 [one tumor sample run in duplicate]), 2 normal prostate stroma (NPS) samples (samples 28 and 29), and 9 adjacent normal tissue samples (samples 32-40).

[0034] Fig. 5 is a scatter plot showing correlation of the expression profiles in 5 xenograft-derived human prostate carcinoma cell lines and 24 prostate cancer tissue samples versus 9 adjacent normal prostate samples for 54 genes of the concordance set.

[0035] Fig. 6 is a graph showing phenotype association indices for 10 genes of the prostate cancer/normal tissue minimum segregation set (i.e. cluster) in 24 prostate tumors

(samples 1-25 [one tumor sample run in duplicate]), and 9 adjacent normal tissue samples (samples 29-37).

[0036] Fig. 7 is a graph showing phenotype association indices for 5 genes of the prostate cancer/normal tissue minimum segregation set (i.e., cluster) in 24 prostate tumors (samples 1-25 [one tumor sample run in duplicate]), and 9 adjacent normal tissue samples (samples 29-37).

[0037] Fig. 8 is a graph showing phenotype association indices for 10 genes of the prostate cancer/normal tissue minimum segregation set (i.e., cluster) in 47 prostate tumors (samples 1-47), and 47 adjacent normal tissue samples (samples 51-97).

[0038] Fig. 9 is a graph showing phenotype association indices for 5 genes of the prostate cancer/normal tissue minimum segregation set (i.e., cluster) in 47 prostate tumors (samples 1-47), and 47 adjacent normal tissue samples (samples 51-97).

[0039] Fig. 10 is a scatter plot showing correlation of the expression profiles in 5 xenograft-derived human prostate carcinoma cell lines and 14 invasive versus 38 non-invasive human prostate cancer tissue samples for 104 genes of the concordance set.

[0040] Fig. 11 is a scatter plot showing correlation of the expression profiles in 5 xenograft-derived human prostate carcinoma cell lines and 14 invasive versus 38 non-invasive human prostate cancer tissue samples for 20 genes of the invasion minimum segregation set 1 (i.e., invasion cluster 1).

[0041] Fig. 12 is a graph showing phenotype association indices for 20 genes of invasion cluster 1 in 14 invasive (samples 1-14) and 38 non-invasive (samples 20-57) human prostate tumor samples.

- [0042] Fig. 13 is a scatter plot showing correlation of the expression profiles in 5 xenograft-derived human prostate carcinoma cell lines and 12 invasive versus 17 non-invasive (surgical margins 1+) human prostate cancer tissue samples for 12 genes of the invasion minimum segregation set 2 (i.e., invasion cluster 2).
- [0043] Fig. 14 is a graph showing phenotype association indices for 12 genes of invasion cluster 2 in 12 invasive (samples 1-12) and 17 non-invasive (samples 17-33) human prostate tumor samples.
- [0044] Fig. 15 is a scatter plot showing correlation of the expression profiles in 5 xenograft-derived human prostate carcinoma cell lines and 11 invasive versus 7 non-invasive (invasion clusters 1&2 +) human prostate cancer tissue samples for 10 genes of the invasion minimum segregation class 3 (i.e., invasion cluster 3).
- [0045] Fig. 16 is a graph showing phenotype association indices for 10 genes of invasion cluster 3 in 11 invasive (samples 1-11) and 7 non-invasive (samples 16-22) human prostate tumor samples.
- [0046] Fig. 17 is a scatter plot showing correlation of the expression profiles in 5 xenograft-derived human prostate carcinoma cell lines and 3 invasive versus 21 non-invasive human prostate cancer tissue samples for 13 genes of the invasion minimum segregation class 4 (i.e., invasion cluster 4).
- [0047] Fig. 18 is a graph showing phenotype association indices for 13 genes of invasion cluster 4 in 3 invasive (samples 1-3) and 21 non-invasive (samples 8-28) human prostate tumor samples.
- [0048] Fig. 19 is a scatter plot showing correlation of the expression profiles in 5 xenograft-derived human prostate carcinoma cell lines and 6 high Gleason grade versus

46 low Gleason grade human prostate cancer tissue samples for 58 genes of the concordance set.

[0049] Fig. 20 is a scatter plot showing correlation of the expression profiles in 5 xenograft-derived human prostate carcinoma cell lines and 6 high Gleason grade versus 46 low Gleason grade human prostate cancer tissue samples for 17 genes of the high grade minimum segregation set 1 (high grade cluster 1).

[0050] Fig. 21 is a scatter plot showing correlation of the expression profiles in 5 xenograft-derived human prostate carcinoma cell lines and 6 high Gleason grade versus 20 low Gleason grade human prostate cancer tissue samples for 12 genes of the high grade minimum segregation set 2 (high grade cluster 2).

[0051] Fig. 22 is a scatter plot showing correlation of the expression profiles in 5 xenograft-derived human prostate carcinoma cell lines and 6 high Gleason grade versus 16 low Gleason grade human prostate cancer tissue samples for 7 genes of the high grade minimum segregation set 3 (high grade cluster 3).

[0052] Fig. 23 is a scatter plot showing correlation of the expression profiles in 5 xenograft-derived human prostate carcinoma cell lines and 6 high Gleason grade versus 46 low Gleason grade human prostate cancer tissue samples for 38 genes of the ALT high grade minimum segregation set (ALT high grade cluster).

[0053] Fig. 24 is a scatter plot showing correlation of the expression profiles in 5 xenograft-derived human prostate carcinoma cell lines and 6 high Gleason grade versus 17 low Gleason grade human prostate cancer tissue samples for 5 genes of the high grade minimum segregation set 4 (high grade cluster 4).

[0054] Fig. 25 is a scatter plot showing correlation of the expression profiles in 5 xenograft-derived human prostate carcinoma cell lines and 6 high Gleason grade versus 17 low Gleason grade human prostate cancer tissue samples for 4 genes of the high grade minimum segregation set 5 (high grade cluster 5).

[0055] Fig. 26 is a scatter plot showing correlation of the expression profiles in 5 xenograft-derived human prostate carcinoma cell lines and 6 high Gleason grade versus 17 low Gleason grade human prostate cancer tissue samples for 7 genes of the high grade minimum segregation set 6 (high grade cluster 6).

[0056] Fig. 27 is a scatter plot showing correlation of the expression profiles in 5 xenograft-derived human prostate carcinoma cell lines and 6 high Gleason grade versus 17 low Gleason grade human prostate cancer tissue samples for 13 genes of the high grade minimum segregation set 7 (high grade cluster 7).

[0057] Fig. 28 is a graph showing phenotype association indices for 54 genes of the BPH minimum segregation class (i.e. cluster) in 8 patients with benign prostatic hypertrophy (BPH) (samples 1-8) and 9 patients with prostate cancer (samples 13-21).

[0058] Fig. 29 is a graph showing phenotype association indices for 14 genes of the BPH minimum segregation class (i.e. cluster) MAGEA1 in 8 patients with benign prostatic hypertrophy (BPH) (samples 1-8) and 9 patients with prostate cancer (samples 12-20).

[0059] Fig. 30 is a graph showing phenotype association indices for 17 genes of the metastasis minimum segregation class 1 (i.e. metastasis cluster 1) in 5 patients with benign prostatic hypertrophy (BPH) (samples 7-11), 3 adjacent normal prostate (ANP) samples (samples 1-3), 1 patient with prostatitis (sample 5), 10 patients with localized

prostate cancer (samples 13-22), and 7 patients with metastatic prostate cancer (MPC)(samples 24-30).

[0060] Fig. 31 is a graph showing phenotype association indices for 19 genes of the metastasis minimum segregation class 2 (i.e. metastasis cluster 2) in 5 patients with benign prostatic hypertrophy (BPH) (samples 7-11), 3 adjacent normal prostate (ANP) samples (samples 1-3), 1 patient with prostatitis (sample 5), 10 patients with localized prostate cancer (samples 13-22), and 7 patients with metastatic prostate cancer (MPC)(samples 24-30).

[0061] Fig. 32 is a graph showing phenotype association indices for 17 genes of the metastasis minimum segregation class 1 (i.e. metastasis cluster 1) in 14 patients with benign prostatic hypertrophy (BPH) (samples 1-14), 4 adjacent normal prostate (ANP) samples (samples 17-20), 1 patient with prostatitis (sample 23), 10 patients with localized prostate cancer (LPC) (samples 26-39), and 20 patients with metastatic prostate cancer (MPC)(samples 42-61).

[0062] Fig. 33 is a graph showing phenotype association indices for 19 genes of the metastasis minimum segregation class 2 (i.e. metastasis cluster 2) in 14 patients with benign prostatic hypertrophy (BPH) (samples 1-14), 4 adjacent normal prostate (ANP) samples (samples 17-20), 1 patient with prostatitis (sample 23), 14 patients with localized prostate cancer (LPC) (samples 26-39), and 20 patients with metastatic prostate cancer (MPC)(samples 42-61).

[0063] Fig. 34 is a graph showing phenotype association indices for 6 genes of the Q-PCR-based poor prognosis predictor minimum segregation set (i.e. cluster) in 34 patients with breast cancer who developed distant metastases within 5 years of diagnosis (samples

1-34) and in 44 patients who continued to be disease-free for at least five years (samples 37-80).

[0064] Fig. 35 is a graph showing phenotype association indices for 14 genes of the Q-PCR-based good prognosis predictor minimum segregation set (i.e. cluster) in 34 patients with breast cancer who developed distant metastases within 5 years of diagnosis (samples 1-34) and in 44 patients who continued to be disease-free for at least five years (samples 37-80).

[0065] Fig. 36 is a graph showing phenotype association indices for 13 genes of the Q-PCR-based good prognosis predictor minimum segregation set (i.e. cluster) in 34 patients with breast cancer who developed distant metastases within 5 years of diagnosis (samples 1-34) and in 44 patients who continued to be disease-free for at least five years (samples 37-80).

[0066] Fig. 37 is a graph showing phenotype association indices for 13 genes of the Q-PCR-based good prognosis predictor minimum segregation set (i.e. cluster) in 11 patients with breast cancer who developed distant metastases within 5 years of diagnosis (samples 1-11) and in 8 patients who continued to be disease-free for at least five years (samples 14-21).

[0067] Fig. 38 is a graph showing phenotype association indices for 11 genes of the ovarian cancer poor prognosis predictor minimum segregation set (i.e. cluster) in 3 poorly differentiated tumors (samples 1-3) and in 11 tumors of well and moderate differentiation (samples 6-16).

[0068] Fig. 39 is a graph showing phenotype association indices for 10 genes of the ovarian cancer good prognosis predictor minimum segregation set (i.e. cluster) in 3

poorly differentiated tumors (samples 1-3) and in 11 tumors of well and moderate differentiation (samples 6-16).

[0069] Fig. 40 is a scatter plot showing correlation of the expression profiles in non small cell lung carcinoma ("NSCLC") cell lines and normal bronchial epithelial cells versus 139 human adenocarcinoma tissue samples versus 17 normal human lung samples for 13 genes of the human lung adenocarcinoma minimum segregation set 1 (lung adenocarcinoma cluster 1).

[0070] Fig. 41 is a scatter plot showing correlation of the expression profiles in non small cell lung carcinoma ("NSCLC") cell lines and normal bronchial epithelial cells and 139 human adenocarcinoma tissue samples versus 17 normal human lung samples for 26 genes of the human lung adenocarcinoma minimum segregation set 2 (lung adenocarcinoma cluster 2).

[0071] Fig. 42 is a graph showing phenotype association indices for 13 genes of the lung adenocarcinoma minimum segregation set 1 (lung adenocarcinoma cluster 1) in 17 normal lung specimens (samples 1-17) and 139 patients with lung adenocarcinoma (samples 20-158).

[0072] Fig. 43 is a graph showing phenotype association indices for 26 genes of the lung adenocarcinoma minimum segregation set 2 (lung adenocarcinoma cluster 2) in 17 normal lung specimens (samples 1-17) and 139 patients with lung adenocarcinoma (samples 20-158).

[0073] Fig. 44 is a scatter plot showing correlation of the expression profiles in non small cell lung carcinoma ("NSCLC") cell lines and normal bronchial epithelial cells and 34 human NSCLC patients with poor prognosis tissue samples versus 16 human NSCLC

patients with good prognosis tissue samples for 38 genes of the lung adenocarcinoma poor prognosis minimum segregation set 1 (poor prognosis cluster 1).

[0074] Fig. 45 is a graph showing phenotype association indices for 38 genes of the lung adenocarcinoma poor prognosis minimum segregation set 1 (poor prognosis cluster 1) in 34 human NSCLC patients with poor prognosis (samples 1-34) 16 human NSCLC patients with good prognosis (samples 37-52).

[0075] Fig. 46. Xenografts of human prostate cancer derived from the PC-3M-LN4 highly metastatic cell variant and growing in a metastasis promoting orthotopic setting exhibit pro-invasive and pro-angiogenic gene expression profiles. Expression profiling of the 12,625 transcripts in the orthotopic ("OR") and subcutaneous ("s.c." or "SC") xenografts derived from the cell variants of the PC-3 lineage was carried out. (A1 – A4) Expression pattern of the matrix metalloproteinases (MMPs). (B1 – B4) Expression pattern of the components of plasminogen / plasminogen activator system. (C1 – C4) Proangiogenic switch in PC-3M-LN4 orthotopic xenografts: increased levels of expression of interleukin 8, angiopoietin-2, and osteopontin and decreased level of expression of a protease and angiogenesis inhibitor maspin. (D1 – D4) Cadherin switch in PC-3M-LN4 orthotopic xenografts: increased level of expression of non-epithelial cadherins (OB-cadherin-2 and VE-cadherin) and decreased level of expression of epithelial E-cadherin.

[0076] Fig. 47. Correlation of gene expression profiles 8-gene prostate cancer recurrence signature cluster (A) in highly metastatic orthotopic xenografts and the recurrent versus non-recurrent prostate tumors or 5-gene prostate cancer invasion signature in invasive versus non-invasive human prostate tumors (B).

[0077] Fig. 48. Correlation of expression profiles in orthotopic xenografts and clinical samples for 131-gene prostate cancer metastasis signature cluster (A), 37-gene prostate cancer metastasis signature (B), 12-gene prostate cancer metastasis signature (C), 9-gene prostate cancer metastasis signature (D).

[0078] Fig. 49. Gene expression patterns of selected gene clusters in highly metastatic orthotopic xenografts are discriminators of the metastatic and primary human prostate carcinomas. The classification accuracy of the clinical samples is shown for clusters of 131 genes (A), 37 genes (B), 9 genes (C), and a family of 6 metastasis segregation clusters (D).

[0079] Fig. 50 Gene expression patterns of the selected gene clusters in highly metastatic orthotopic xenografts are discriminators of invasive (Fig. 50A) and recurrent (Fig. 50B) phenotypes of human prostate tumors. Fig. 50A, phenotype association indices for 5 gene prostate cancer invasion predictor. Bars 1-8 tumors with positive surgical margins and prostate capsule penetration ("PSM & PCP"); bars 11-16 tumors with positive surgical margins ("PSM"); bars 19-30 tumors with prostate capsule penetration ("PCP"); bars 33-58 non-invasive tumors. Fig. 50B, phenotype association indices for 8 gene prostate cancer recurrence predictor. Bars 1-8 recurrent tumors; bars 11-23 non-recurrent tumors.

[0080] Fig. 51. Gene expression profiles of selected gene clusters in highly metastatic PC3MLN4 orthotopic xenografts are concordant with the expression patterns of these genes in the recurrent (A), invasive (B), and metastatic (C) human prostate tumors. For each figure, bars show average fold change in gene expression compared to respective control for individual genes within clusters.

[0081] Fig. 52. Gene expression profiles of the 25-gene recurrence predictor signature in highly metastatic PC3MLN4 orthotopic xenografts are concordant with the expression patterns of these genes in the recurrent human prostate tumors. Figure 52A – correlation of expression profiles in orthotopic xenografts and clinical samples for 25-gene prostate cancer recurrence predictor cluster. Fig 52B – Change in expression for each transcript are plotted as Log10Fold Change Average expression level in PC-3MLN4OR versus Average expression level in PC-3MLN4SC and Log10Fold Change Average expression level in recurrent prostate tumors versus Average expression level in non-recurrent prostate tumors.

[0082] Fig. 53 is a bar graph illustrating phenotypic association indices for transcripts of the 25 genes prostate cancer recurrence predictor cluster in 8 recurrent and 13 non-recurrent human prostate tumors.

[0083] Fig. 54 is a bar graph illustrating expression profile of the 12 gene recurrence predictor signature in PC-3MLN4 orthotopic xenografts and recurrent human prostate tumors.

[0084] Fig. 55 is a scatter plot illustrating correlation of the expression profiles of the 12 genes recurrence predictor cluster in PC-3MLN4 orthotopic xenografts and recurrent human prostate tumors.

[0085] Fig. 56 is a bar graph illustrating phenotypic association indices for transcripts of the 12 genes prostate cancer recurrence predictor cluster in 8 recurrent and 13 non-recurrent human prostate tumors.

[0086] Fig. 57. Phenotype association indices (PAIs) defined by the expression profile of the prostate cancer recurrence predictor signature 1 for 21 prostate carcinoma samples comprising a signature discovery (training) data set.

[0087] Fig. 58. Kaplan-Meier analysis of the probability that patients would remain disease-free among 21 prostate cancer patients comprising a signature discovery group according to whether they had a good-prognosis or poor-prognosis signatures defined by the recurrence predictor signature 1 (Fig. 58A), recurrence predictor signature 2 (Fig. 58B), recurrence predictor signature 3 (Fig. 58C), and the recurrence predictor algorithm that takes into account calls from all three signatures (Fig. 58D).

[0088] Fig. 59. Kaplan-Meier analysis of the probability that patients would remain disease-free among 79 prostate cancer patients comprising a signature validation group for all patients (Fig. 59A), patients with high (Fig. 59B) or low (Fig. 59C) preoperative PSA level in blood according to whether they had a good-prognosis or poor-prognosis signatures defined by the recurrence predictor algorithm or whether they had high or low preoperative PSA level in the blood (Fig. 59D).

[0089] Fig. 60. Kaplan-Meier analysis of the probability that patients would remain disease-free among prostate cancer patients with Gleason sum 6 & 7 tumors (Fig. 60A) and patients with Gleason sum 8 & 9 tumors (Fig. 60B) according to whether they had a good-prognosis or poor-prognosis signatures defined by the recurrence predictor algorithm or whether they had Gleason sum 8 & 9 or Gleason sum 6 & 7 prostate tumors (Fig. 60C).

[0090] Fig. 61. Kaplan-Meier analysis of the probability that patients would remain disease-free among 79 prostate cancer patients comprising a signature validation group

for all patients (Fig. 61A), patients with poor prognosis (Fig. 61B) or good prognosis (Fig. 60C) defined by the Kattan nomogram according to whether they had a good-prognosis or poor-prognosis signatures defined by the recurrence predictor algorithm (Figs. 61B and 61C) or whether they had poor or good prognosis defined by the Kattan nomogram (Fig. 61A).

[0091] Fig. 62. Kaplan-Meier analysis of the probability that patients would remain disease-free among prostate cancer patients with stage 1C tumors (Fig. 62A) and patients with stage 2A tumors (Fig. 62B) according to whether they had a good-prognosis or poor-prognosis signatures defined by the recurrence predictor algorithm.

[0092] Fig. 63. Kaplan Meier survival curves. Fig. 63A Survival of 151 breast cancer patients with lymph node negative disease (stratified by 14 gene signature). Fig. 63B Survival of 109 breast cancer patients with estrogen receptor positive tumors and lymph node negative disease (stratified by 14 gene signature); Fig. 63C Survival of 42 breast cancer patients with estrogen receptor negative tumors and lymph node negative disease (stratified by 4 and/or 3 gene signatures).

[0093] Fig. 64. Kaplan Meier survival curves. Fig. 64A Survival of breast cancer patients with estrogen receptor positive and estrogen receptor negative tumors; Fig. 64B Survival or 69 breast cancer patients with estrogen receptor negative tumors (stratified by 5 and/or three gene signatures).

[0094] Fig. 65. Metastasis-free survival of 78 breast cancer patients. Fig. 65A survival stratified by 4 gene signature; Fig. 65B survival stratified by 6 gene signature; Fig. 65C, survival stratified by 13 gene signature; Fig. 65D survival stratified by 14 gene signature.

[0095] Fig. 66. Survival of breast cancer patients classified into subgroups using gene signatures. Fig. 66A Survival of 144 breast cancer patients with lymph node positive disease stratified according to 14 gene survival predictor cluster; Fig. 66B Survival of 117 breast cancer patients with estrogen receptor positive tumors and lymph node positive disease stratified according to 14 gene survival predictor cluster; Fig. 66C Survival of 27 breast cancer patients with estrogen receptor negative tumors and lymph node positive disease stratified according to 4 and 3 gene signatures.

[0096] Fig. 67. Survival of estrogen receptor positive breast cancer patients. Fig. 67A stratified according to positive and negative 14 gene signature; Fig. 67B stratified according to relative values of 14 gene signature.

[0097] Fig. 68. Survival of breast cancer patients. Fig. 68A Survival of 295 breast cancer patients with positive and negative 14 gene signature (0.00 cut off); Fig. 68B Survival of 295 breast cancer patients with positive and negative 14 gene signature (-0.55 cut off); Fig. 68C Survival of breast cancer patients with positive and negative 14-gene signature; Fig. 68D Survival of breast cancer patients with positive and negative 14 gene signature; Fig. 68E Survival of breast cancer patients classified based on relative values of the 14 gene signature.

# DETAILED DESCRIPTION OF THE PREFERRED EMBODIMENTS Definitions

[0098] All terms, unless specifically defined below, are intended to have their ordinary meanings as understood by those of skill in the art. Claimed masses and volumes are intended to encompass variations in the sated quantities compatible with the practice of the invention. Such variations are contemplated to be within, e.g. about + 10 – 20 percent of the stated quantities. In case of conflict between the specific definitions

contained in this section and the ordinary meanings as understood by those of skill in the art, the definitions supplied below are to control.

[0099] "Identifying a set of expressed genes" refers to any method now known or later developed to assess gene expression, including but not limited to measurements relating to the biological processes of nucleic acid amplification, transcription, RNA splicing, and translation. Thus, direct and indirect measures of gene copy number (e.g., as by fluorescence in situ hybridization or other type of quantitative hybridization measurement, or by quantitative PCR), transcript concentration (e.g., as by Northern blotting, expression array measurements or quantitative RT-PCR), and protein concentration (e.g., by quantitative 2-D gel electrophoresis, mass spectrometry, Western blotting, ELISA, or other method for determining protein concentration) are intended to be encompassed within the scope of the definition.

[00100] "Differentially expressed" refers to the existence of a difference in the expression level of a gene as compared between two sample classes. Differences in the expression levels of "differentially expressed" genes preferably are statistically significant.

[00101] "Tumor" is to be construed broadly to refer to any and all types of solid and diffuse malignant neoplasias including but not limited to sarcomas, carcinomas, leukaemias, lymphomas, etc., and includes by way of example, but not limitation, tumors found within prostate, breast, colon, lung, and ovarian tissues.

[00102] A "tumor cell line" refers to a transformed cell line derived from a tumor sample. Usually, a "tumor cell line" is capable of generating a tumor upon explant into an appropriate host. A "tumor cell line" line usually retains, in vitro, properties in

loss of contact inhibition, and will undergo essentially unlimited cell divisions in vitro.

[00103] A "control cell line" refers to a non-transformed, usually primary culture of a

normally differentiated cell type. In the practice of the invention, it is preferable to use a

common with the tumor from which it is derived, including, e.g., loss of differentiation,

"control cell line" and a "tumor cell line" that are related with respect to the tissue of

origin, to improve the likelihood that observed gene expression differences are related to

gene expression changes underlying the transformation from control cell to tumor.

[00104] An "unclassified sample" refers to a sample for which classification is obtained by applying the methods of the present invention. An "unclassified sample" may be one that has been classified previously using the methods of the present invention, or through the use of other molecular biological or pathohistological analyses. Alternatively, an "unclassified sample" may be one on which no classification has been carried out prior to the use of the sample for classification by the methods of the present invention.

[00105] "According to the sign of" a correlation coefficient refers to a determination based on the sign, i.e., positive or negative, of the referenced correlation coefficient. For example, a sample may be classified as belonging to a first set of samples if the sign of the correlation coefficient is positive, or as belonging to a second set of samples if the correlation coefficient is negative.

[00106] "Orthotopic" refers to the placement of cells in an organ or tissue of origin, and is intended to encompass placement within the same species or in a different species from which the cells are originally derived.

[00107] "Ectopic" refers to the placement of cells in an organ or tissue other than the organ or tissue of origin, and is intended to encompass placement within the same species or in a different species from which the cells are originally derived.

## <u>Introduction</u>

unprecedented opportunity to study the genetic basis of human cancer progression.

During malignant progression, genomic instability leads to continuously emerging phenotypic diversity, clonal evolution, and clonal selection resulting in the remarkable cellular heterogeneity of tumors. The phenotypic diversity of cancer cells is associated with significant mutation-driven changes in gene expression, although not all mutations and differences in gene expression are crucial or even relevant to the malignant phenotype. It therefore is important to identify expression changes that are highly relevant and characteristic of malignant phenotypes and progression pathways, more than one of which may exist (Hanahan, D., Weinberg, R.A. The hallmarks of cancer. Cell. 2000. 100: 57-70, incorporated herein by reference.). The methods of the present invention address this goal by providing analytical techniques to identify those expression changes highly correlated with and indeed predictive of certain clinically relevant features of malignant phenotypes and progression pathways.

[00109] In a broad and general sense, as applied to the analysis of tumor samples, the methods of the invention use gene expression data from a set of tumor cell lines and compare those data with gene expression data from a set of control cell lines to identify those genes that are differentially expressed in the tumor cell lines as compared to the control cell lines. In preferred embodiments, each of these sets includes more than a

single member, although it is contemplated to be within the scope of the present invention to practice embodiments in which either or both of the set of tumor cell lines and the set of control cell lines includes only one member. The identified genes are referred to as a first reference set of expressed genes. Preferably, the control cell line and the tumor cell lines are related insofar as the control cell lines represent physiologically normal cells from the tissue or organ from which the tumor represented by the tumor cell lines arose. For example, if the tumor cell lines are derived from a prostate tumor, the control cell lines preferably are primary cultures of normal prostate epithelial cells. In the preferred embodiments, more than one tumor cell line and more than one control cell line is used to generate the reference set so as to reduce the number of genes in the first reference set by eliminating those genes that are not consistently differentially expressed between the tumor and control cell lines.

[00110] In other embodiments, the method may be practiced using only one tumor cell line and one control cell line, and identifying the set of genes differentially expressed between the tumor cell line and the control cell line. However, by carrying out a series of comparison between multiple control cell lines and multiple tumor cell lines the first reference set is more likely to contain only those genes that are consistently differentially expressed between the normal and tumor classes of cell lines (*i.e.*, a gene is included within the first reference set if its expression level is always higher in each of the tumor cell lines examined as compared to each of the control cell lines examined, or if its expression level is always lower in each of the tumor cell lines examined as compared to each of the control cell lines examined as compared to each of the control cell lines examined as compared to

[00111] In yet another embodiment, exemplified below as Example 6, the methods of the invention may be practiced without the use of cell lines, using instead data derived only from clinical samples. In a similar manner, the methods of the invention may be practiced using only data derived from cell lines.

For example, consider an embodiment in which the first reference set is [00112] derived using data obtained from three separate control cell lines and six separate tumor cell lines. For each gene considered for inclusion within the first reference set, pairwise comparisons are carried out for each of the 3 x 6 or 18 pairwise combinations between control cell lines and tumor cell lines. A candidate gene will be included in the first reference set if each of the 18 pairwise comparisons reveals the gene to be consistently differentially expressed (i.e., gene expression always is higher in the control cell line or always higher in the tumor cell line for each of the 18 pairwise comparisons). As one of ordinary skill readily will appreciate, it may sometimes be necessary to scale the datasets prior to carrying out the pairwise comparisons. Such scaling may be routinely implemented in the analysis software provided by commercial suppliers of expression arrays or array readers (such as, e.g., Affymetrix, Santa Clara, CA). For a general discussion of data scaling for and differential gene expression analysis, see, e.g., Affymetrix Microarray Suite 4.0 User Guide, Affymetrix, Santa Clara, CA, incorporated herein by reference.

[00113] The first reference set therefore is a set of genes that have met a screening criterion requiring that the genes be differentially expressed between tumor and control cell lines. This criterion reflects the hypothesis that differences in the tumor and control cell phenotypes are driven, at least in part, by differences in gene expression patterns in

the tumor and control cells. In the practice of the invention, generating a first reference set typically results in an order of magnitude or greater reduction in the number of genes that remain under consideration for inclusion in a cluster or for use in the sample classification methods.

[00114] Because the tumor and control cell lines have at some point been cultured in vitro, their gene expression patterns likely will not exactly correspond with the expression patterns of their counterparts grown in vivo. Consequently, the methods of the invention use additional steps to establish a second reference set of expressed genes that are differentially expressed in cells of biological samples that differ with respect to a classification. The classification may be an outcome predictor or cellular phenotype or any type of classification that may be used for classifying biological samples. The classification may be binary (i.e., for two mutually exclusive classes such as, e.g., invasive/non-invasive, metastatic/non-metastatic, etc.), or may be continuously or discretely variable (i.e., a classification that can assume more than two values such as, e.g., Gleason scores, survival odds, etc.) The only requirement is that the classified trait must be something that can be observed and characterized by the assignment of a variable or other type of identifier so that samples belonging to the same class may be grouped together during the analysis.

[00115] The second reference set of expressed genes may be obtained following essentially the same techniques described above for the first reference set, except sets of samples obtained from *in vivo* sources are used instead of sets of cell lines. In embodiments of the invention directed toward tumor analysis, classification or prognostication, the sample sets preferably consist of tumor samples obtained from

patients that are analyzed without any intervening tissue culturing steps so that the gene expression patterns reflect as closely as possible the pattern within cells growing in their undisturbed, *in vivo* environment. Here again, the goal is to obtain a reference set that includes genes differentially expressed between samples belonging to different classifications. As is the case with the first reference set, it is preferable to include several independent samples within a classified set and to carry out a plurality of pairwise comparisons to identify differentially expressed genes for inclusion into the second reference set.

[00116] For example, assume the classification of interest is invasiveness (e.g., turning on whether tumor-free surgical margins are observed). It is preferable to use as the sample sets a number of invasive samples and a number of non-invasive samples. The number of pairwise comparisons that can be carried out is of course equal to the product of the numbers of independent samples in each category. Ideally, each of these pairwise comparisons is carried out and the same consistently differentially expressed criterion described above is used to select genes for inclusion into the second reference set.

[00117] It is contemplated, that in certain instances, especially, e.g., when the variance within a sample set is low, it will not be necessary to carry out all pairwise comparisons to select genes for inclusion into the first or second reference set. In practice, one of ordinary skill can readily determine whether it is advantageous to carry out all pairwise comparisons, or fewer than all pairwise comparisons by examining the convergence behavior of the reference sets as additional comparisons are carried out. If the sets

apparently converge prior to completion of all possible pairwise comparisons, then the

added benefit of exhaustive comparison may be small and so can be avoided.

[00118]Similar principles drive the selection of the numbers of cell lines and cell samples used to derive the first and second reference sets as apply to the study of other cell and molecular biological phenomena. One of ordinary skill readily will appreciate that the accuracy of the reference sets can increase as more cell lines and samples are used so that statistical noise is minimized. It currently is contemplated that preferred numbers of different cell lines and samples per set used for calculating reference sets be in the range of 2 to 50 per set, or in the range of 2 to 25, or in the range of 2 to 10, or in the range of 3 to 5 per set. While not preferred, it also is contemplated to be within the scope of the present invention to use sets consisting of a single type of cell in one or more of the four sets of input cells used to calculate the first and second reference sets (i.e., tumor cell lines, control cell lines, first sample, and second sample). Direct statistical analysis using T-test and/or Mann-Whitney test for identification of genes differentially expressed in sets of biological samples that differ with respect to a classification is also applicable to the methods of the present invention. The average expression values for genes across the first and second sets of biological samples that differ with respect to a classification are used for calculation of fold expression changes (see below). [00119] After the first and second reference sets of differentially expressed genes are identified, a concordance set of expressed genes is identified. The concordance set is obtained by comparing the first and second reference sets. Two criteria preferably are used to identify genes for inclusion into the concordance set: 1) the candidate gene is present in first and second reference sets; 2) the direction of the candidate gene's differential is the same in the first and second reference sets. Again, as one of ordinary skill readily will recognize, there is a certain degree of arbitrariness to the sign of the

differential, as it is determined by, e.g., the direction of the comparison between samples [sample 1/sample 2, cf. sample 2/sample 1, or alternatively, sample 1 – sample 2, cf. sample 2 – sample 1]. In any event, the arbitrariness does not affect the results because the direction of the comparison is the same across the entire set of expressed genes. The first criterion is, in general, required for inclusion of a gene within the concordance set, while the second criterion is preferred, but optional. In practical terms, identification of a single reference set of differentially expressed genes could serve as a starting point for identification of a concordant set of transcripts. For example, one can identify a reference set of differentially regulated genes in a panel of biological samples subject to a classification and proceed directly to identification of a concordant set of differentially regulated genes in cell lines.

[00120] Once the concordance set has been established, information about the rank order of expression differences is used to establish another subset of genes. This subset is referred to as the minimum segregation set. The minimum segregation set may conveniently be selected by generating a scatter plot from which may be determined correlations between the –fold expression change or difference in the cell lines and the samples. In preferred embodiments, the –fold expression change is used, and is calculated by obtaining for gene x the ratio of the average expression value obtained across all tumor cell lines and across all control cell lines, and across the first and in the second sample sets, *i.e.*,

-fold change =  $\langle expression \rangle_1 / \langle expression \rangle_2$ 

[00121] where  $\langle \text{expression} \rangle_1$  is the average expression for gene x across all observations in set 1, and likewise,  $\langle \text{expression} \rangle_2$  is the average expression for gene x

across all observations in set 2. Explicitly,  $\langle \text{expression} \rangle = \frac{1}{N} \sum_{n=1}^{N} E_n$ , where N equals the number of observations of expression value E for gene x in the set. In the case of the cell line data, set 1 preferably correspond to the tumor cell line set, and set 2 preferably corresponds to the control cell line set. Similarly, for the sample data, set 1 preferably corresponds to the first set of samples and set 2 preferably corresponds to the second set of samples.

[00122] In another preferred embodiment, differences in expression values are used and are calculated as:

difference =  $\langle expression \rangle_1$  -  $\langle expression \rangle_2$ ,

[00123] where <expression><sub>1</sub> and <expression><sub>2</sub> have the same meanings as in the – fold change expression.

[00124] In other embodiments, preferred if the number of observations of gene x expression in each set is small, (i.e., on the order of one or two), a modified average fold change across all observations, <expression><sub>m</sub>, can be used in lieu of <expression><sub>1</sub>/<expression><sub>2</sub> to improve the performance of the method. The modified average fold change <expression><sub>m</sub> explicitly is defined as:

 $\langle expression \rangle_m = \langle expression \rangle_1 / \langle expression_1 + expression_2 \rangle$ [00125] which is equal to:

$$\langle \text{expression} \rangle_{\text{m}} = \frac{\frac{1}{N} \sum_{n=1}^{N} E_n}{\frac{1}{N+M} \sum_{n=1}^{N+M} E_n},$$

[00126] where there are N observations of expression value E for gene x from set 1 and M observations of expression value E for gene x from set 2. Improvement in the

method performance can be determined using samples of known classification, and assessing the overall accuracy of the method in classifying known samples using  $\langle \exp ression \rangle_m$  in lieu of  $\langle \exp ression \rangle_1 / \langle \exp ression \rangle_2$ .

[00127] Consider the following observations of expression values E for gene x in which N = M = 5:

Expression Values, E, for gene x				
Set 1 Data	Set 2 Data			
5	1			
4	2			
8	1			
7	4			
3	2			
sum = 27	sum = 10			
<expression $>$ 1 = 27/5 = 5.4	$\langle \text{expression} \rangle_2 = 10/5 = 2$			
<expression>1/<expression></expression></expression>	$ssion>_2 = 5.4/2 = 2.7$			
<expression $>$ <sub>m</sub> = $<$ expression $>$ <sub>1</sub> $/<$ expression $>$	ession <sub>1</sub> +expression <sub>2</sub> > = $5.4/3.7 = 1.3$			

[00128] A scatter plot can be generated for genes within the concordance set in which each gene is assigned a point in the scatter plot. The (x,y) location of that point will be, or will be proportional to, the –fold expression change or difference in the cell line data (e.g., x), and the –fold expression change or difference in the sample data (e.g., y). Of course, the selection of the data assigned to be plotted on the abscissa and that to be plotted on the ordinate is arbitrary, so that one could have the x value correspond to the sample data and the y value correspond to the cell line data. In preferred embodiments, the –fold expression change or difference data is logarithmically transformed prior to plotting said data on the scatter plot.

[00129] The scatter plot potentially will be populated by data points that fall within any of the four quadrants of a graph in which the axes intersect at (0,0). Define quadrant I as negative x, positive y, quadrant III as positive x, negative y, and quadrant IV as negative x, negative y. The minimum segregation class is selected so as to include genes that fall within quadrants II and IV, and preferably to include only those genes within quadrants II and IV whose –fold expression changes or differences are highly positively correlated between the cell line and sample data.

Alternatively, the minimum segregation class may be selected so as to include genes that fall within quadrants I and III, and preferably to include only those genes within quadrants I and III whose –fold expression changes or differences are highly negatively correlated between the cell line and sample data.

[00130] The scatter plots described above provide a convenient graphical representation of the data used in the clustering and classification methods of the present invention, although it is not necessary to generate such plots in the practice of the invention. Correlation coefficients can be generated for arrays of data without first plotting the data as described above. The expression data can be sorted by the values of the fold expression changes or differences and subsets of highly correlated data can be selected visually or with the aid of, e.g., regression analysis. Correlation coefficients may then be calculated on the subset of data.

[00131] Genes whose expression changes are highly correlated (positively or negatively) between the cell line and sample data may be identified by calculating a correlation coefficient for one or more subsets of genes that fall within quadrants II and IV (or alternatively for those that fall within quadrants I and III) of a scatter plot, and

selecting as the minimum segregation set, those genes for which the correlation coefficient exceeds a predetermined value. Any one of a number of commonly used correlation coefficients may be used, including correlation coefficients generated for linear and non-linear regression lines through the data. Representative correlation coefficients include the correlation coefficient,  $\rho_{x,y}$ , that ranges between -1 and +1, such as is generated by Microsoft Excel's CORREL function, the Pearson product moment correlation coefficient, r, that also ranges between -1 and +1, that that reflects the extent of a linear relationship between two data sets, such as is generated by Microsoft Excel's PEARSON function, or the square of the Pearson product moment correlation coefficient,  $r^2$ , through data points in known y's and known x's, such as is generated by Microsoft Excel's RSQ function. The  $r^2$  value can be interpreted as the proportion of the variance in y attributable to the variance in x.

[00132] In a preferred embodiment, the –fold expression change or difference data are logarithmically transformed (e.g.,  $\log_{10}$  transformed), and the minimum segregation set is selected so that the correlation coefficient,  $\rho_{x,y}$ , is greater than or equal to 0.8, or is greater than or equal to 0.9, or is greater than or equal to 0.95, or is greater than or equal to 0.995. One of ordinary skill can readily work out equivalent values for other types of transformations (e.g. natural log transformations) and other types of correlation coefficients either mathematically, or empirically using samples of known classification.

[00133] The method can be terminated at the step of selecting the minimum segregation set. This set will consist of a collection or cluster of genes that is coordinately regulated during processes that result in phenotypic changes between the types of samples that comprise the sample sets.

[00134] The method may be continued, as described immediately below, to classify a sample as belonging to the first sample set or to the second sample set. The classification method uses a minimum segregation set of expressed genes to calculate a second correlation coefficient referred to as a "phenotype association index." The method contemplates several different embodiments for calculating the second correlation coefficient. In a preferred embodiment, the second correlation coefficient is calculated by determining for an individual sample for which classification is sought, the -fold expression change for each gene x within the minimum segregation set. Preferably, the – fold expression change is determined with respect to the average value of expression for gene x across all samples used to identify the minimum segregation set. In the table above, assume set 1 data correspond to a first set of samples and that set 2 data correspond to a second set of samples. The average expression value for gene x across these samples is equal to 3.7. In this preferred embodiment, the -fold expression change is determined by computing the ratio of the expression value for gene x in the individual sample to the 3.7 average value across all the samples used to identify the minimum segregation set. For example, if the observed gene x expression value in the sample is 7, then the –fold expression change calculated according to this embodiment is 7/3.7 = 1.9. If the data were logarithmically transformed prior to identifying the minimum segregation set, then the same logarithmic transformation is carried out on the individual sample data prior to calculating the correlation coefficient.

[00135] In this preferred embodiment the classification is made according to the sign of this second correlation coefficient (phenotype association index). Given the setup outlined above, using -fold expression changes <expression><sub>1</sub>/<expression<sub>1</sub> +

expression<sub>2</sub>> for the sample sets to calculate the minimum segregation set, a positive correlation coefficient obtained for the classified sample indicates that the sample is a member of sample set 1, while a negative correlation coefficient indicates the sample belongs to sample set 2.

[00136] In a refinement of this preferred embodiment, the magnitude of the correlation coefficient can be used as a threshold for classification. The larger the magnitude of the correlation coefficient, the greater the confidence that the classification is accurate. As one of ordinary skill readily will appreciate, the appropriate threshold can be determined through the use of test data that seek to classify samples of known classification using the methods of the present invention. The threshold is adjusted so that a desired level of accuracy (e.g., greater than about 70% or greater than about 80%, or greater than about 90% or greater than about 95% or greater than about 99% accuracy is obtained). This accuracy refers to the likelihood that an assigned classification is correct. Of course, the tradeoff for the higher confidence is an increase in the fraction of samples that are unable to be classified according to the method. That is, the increase in confidence comes at the cost of a loss in sensitivity.

[00137] In another preferred embodiment, multiple minimum segregation sets can be identified and used to increase the sensitivity of the method. Here again, test data from samples of known classification are used to identify the minimum segregation sets and classify the individual samples. In a preferred embodiment, successive minimum segregation classes are identified using expression data from true positive and false positive samples. The expression data from these samples is again broken down into two sample sets, with the true positives assigned to, e.g., sample set 1, and the false positives

assigned to sample set 2. The re-apportioned expression data are used to identify another concordance set and another minimum segregation set. This additional minimum segregation set is used to re-score the samples with particular attention paid to the ability of the set to properly classify the false positives.

[00138] Several such iterations can be done, and criteria developed to improve the accuracy of the method by evaluating the behavior of known samples against a number of minimum segregation sets. Such analysis can be used to show, *e.g.*, that true positives score with the correct phenotype association index in, *e.g.*, 3 of 3 minimum segregation sets.

[00139] As one of ordinary skill will recognize, a similar approach can be used with false negatives, wherein the true negatives and the false negatives are used in an iterative embodiment of the invention, with the false negatives re-assigned to sample set 1 and the true negatives assigned to sample set 2. Blended methods also may be used in which, e.g., the true positives and false negatives are assigned to sample set 1 and the true negatives and false positives assigned to sample set 2, or any other logical combination that uses mis-classified samples to iteratively obtain minimum segregation sets that are used either alone or in conjunction with other sets to improve the accuracy of the classification methods of the present invention.

[00140] While the clustering and classification methods have been described primarily with reference to tumor samples, they are readily applicable to any biological analysis for which appropriate cell lines and samples can be obtained. These include by way of example, but not limitation, omnipotent stem cells, pluripotent precursor cells, various terminally differentiated cells, *etc.* The clustering methods applied to cell differentiation

analyses will identify gene clusters that are coordinately regulated in differentiation programs. These genes are useful not only from a basic research point of view (e.g., to identify novel transcription factors or response elements), but also to identify gene products specifically expressed in one but not another cell type. Such gene products are useful for, e.g., targeting of therapeutic molecules using reagents that have affinity for the specifically expressed gene products.

[00141] Application of the methods of the present invention to the study and classification of cancers represents an important advance made possible in large part by the ready availability of gene expression data. Recent gene expression analysis data revealed that direct comparison of expression profiles for individual tumors to identify the transcriptome of human cancer progression is extremely challenging. Continuous phenotypic changes in cancer cells during tumor progression, individual phenotypic variations, intrinsic cellular heterogeneity, and variability in cellular composition of the primary and metastatic tumors render extremely problematic the selection of the gene expression changes relevant to tumor progression and metastasis. Furthermore, the use of human tumors and metastatic material, itself, limits the direct manipulation of variables that might otherwise reveal regulatory defects that are not apparent in the ground state expression patterns of *in vivo* tumors.

[00142] A complementary experimental approach to the extensive clinical sampling was developed employing gene expression analysis of selected cancer cell lines representing divergent clinically relevant variants of cancer progression (Table 1). These cell lines were surveyed under various *in vitro* and *in vivo* conditions that model microenvironments favorable to the malignant phenotype, including differential serum

withdrawal responsiveness in vitro and induction of experimental tumors in nude mice, ultimately to identify expression changes characteristic of human cancer progression. These cell lines provide a representative group of tumor cell lines that can be used in the practice of the methods of the invention (although other transformed cell lines, such as are readily available from depositories such as ATCC or commercial suppliers also can be used). The methods of the invention also may be practiced using, e.g., one or more of the 38 human breast cancer cell lines described in Forozan, F., Mahlamaki, E.H., Monni, O., Chen, Y., Veldman, R., Jiang, Y., Gooden, G.C., Ethier, S.P., Kallioniemi, A., Kallioniemi, O-P. Comparative genomic hybridization analysis of 38 breast cancer cell lines: a basis for interpreting complementary DNA microarray data. Cancer Res. 2000. 60: 4519-4525, incorporated herein by reference. The methods of the invention also may be practiced using one or more of the 60 human cancer cell lines representing multiple forms of human cancer and utilized in the National Cancer Institute's screen for anticancer drug was described in Ross, TD, Scherf, U, Eisen, MB, Perou, CM, Rees, C, Spellman, P, Iyer, V, Jeffrey, SS, Van de Rijn, M, Waltham, M, Pergamenschikov, A, Lee, JCF, Lashkari, D, Shalon, D, Myers, TG, Weinstein, JN, Botstein, D, Brown, PO. Systematic variation in gene expression patterns in human cancer cell lines. Nature Genetics, 24: 227-235, 2000, incorporated herein by reference. Classification of the human cancer cell lines based on the observed gene expression profiles revealed a correspondence to the tissue of origins of the corresponding tumors from which the cell lines were derived (Ross, DT, et al, 2000).

[00143] Each cell line and experimental condition provided a criterion that a gene met in order to be retained in the next step of analysis. Thus, the cancer cell lines represented

in Table 1 are especially useful for the practice of the clustering and classification methods of the invention. Each step in the gene selection process (i.e., identification of a first and a second reference set, identification of a concordance set and finally, identification of a minimum segregation set) can be thought of as a cut-off criterion that allows genes to pass to the next stage in the analysis. The identified set of candidate genes that satisfies these criteria comprises genes, the differential expression of which is associated with certain features of the malignant phenotype and that is relatively insensitive to significant alterations in cell type and environmental context. Consequently, these genes represent reliable starting points for identifying genes that are commonly altered in human cancer and represent a consensus transcriptome of cancer progression. Other cell line combinations suitable for practicing the methods of the present invention are set forth in Tables 2 – 4. Table 2 lists representative cell line combinations for normal cells and certain cancers (e.g., breast, prostate, lung). These combinations are especially useful for identifying genetic markers that serve as diagnostics for a malignant phenotype. Such markers, in addition to providing diagnostic information, can also provide drug discovery targets. Table 2 also lists representative cell line combinations for precursor and differentiated cells, useful for identifying differentiation markers. Such markers can be used to screen for agents that activate differentiation programs to further basic research, as well as tissue engineering work. Table 3 lists additional tumor cell/control cell line combinations useful for practicing the methods of the invention to identify markers of malignant phenotype for diagnostic as well as drug discovery purposes. Table 4 provides additional primary tumor/ metastatic

tumor cell line combinations useful for practicing the methods of the invention to identify markers of metastatic potential for diagnostic, prognostic and therapeutic applications.

Table 1	Table 1: Model Human Cancer Cell Systems Exhibiting Graded Metastatic					
Potential						
CELLS	DEFINITION	METASTATIC	REMARKS			
		POTENTIAL				
Breast	A panel of human	Metastatic potential	This series of cells			
Cancer	breast carcinoma cell	varies from 0 (MDA-	exhibits differential			
(metastatic	lines of graded	MB-361) to 10-90%	metastatic potential in			
potential)	metastatic potential.	(MDA-MB-435 and	nude mice, differential			
MDAMB-	High met variant	variants) incidence of	homotypic aggregation			
361 (0)	(lung2), low met	lung metastasis in	and clonogenic growth			
MDAMB-	revertant (Br), and	nude mice following	properties, differential			
468 (5%)	blood-survival variant	orthotopic	sensitivity toward			
MDAMB-	(Bl3) were derived	implantation.	apoptosis, in vivo and			
231 (30%)	from parental MB-435		vitro sensitivity to			
MDA-MB-	cells.	,	glycoamines, galectin-			
435 (60%)		·	dependent adhesion.			
MB-						
435lung2						
(90%)						
MB-435Br						
(10%)						
MB-						
435Bl3 (?)						
	Į.	1	1			

PC3			High metastatic
System			potential is associated
(Prostate-1)	Parental, 1 in vivo	Poorly metastatic	with high resistance
PC-3M	passage	Small prostate tumors	toward apoptosis.
PC-3M-	4 in vivo serial	Metastatic	Glycoamine-sensitive
Pro4	passages in prostate		cell lines. From liver
	4 in vivo serial	Highly metastatic	met. of splenic PC3
PC-3M-	passage; LN4 > Pro4		implant.
LN4	-		Exhibit rapid large
			prostate tumor growth.
			Exhibit small prostate
			tumors, large LN
			metastatic tumors.
LNCap			Only androgen-sensitive
System			system. This panel
(Prostate-2)	parental		exhibits differential
LNCaP	5 in vivo serial	Poorly metastatic	metastatic potential,
LNCaP-	passages in prostate	1	differential sensitivity
Pro5	3 in vivo serial	Highly metastatic	toward apoptosis, and in
	passages; LN3 > Pro5	1	vitro glycoamine
LNCaP-			sensitivity. LN3 exhibit
LN3			decreased androgen
		1	dependency, increased
			PSA level, high
			frequency and load of
			regional LN metastasis.

BPE	SV40 large T antigen	Approximately 11%	
System	immortalized benign	tumorigenicity with 6	Cell line system suitable
(Prostate-3)	prostate epithelial	mo. latency.	for determination of the
P69	cells (BPE).		gene expression changes
2182		Lung and diaphragm	associated with
M12	3 serial passages in	metastases.	alterations within major
	vivo as xenograft		tumor suppressor
			pathways.
Colon	Colon carcinoma cell	Differential capability	High metastatic
cancer	lines selected from a	to generate liver	potential within this cell
KM12-C	single parental cell	metastasis following	line system is associated
KM12-SP	line for differential	intrasplenic	with increased
KM12-SM	metastatic potential	implantation in nude	expression of a sialyl
KM12-L4	through in vivo	mice.	Lewis family of
	passages in nude mice.		glycoantigens and
			higher selectin-mediated
			adhesion.

References: Pettaway, C. et al. Clin. Cancer Res., 2: 1627, 1996; Bae, V. et al. Int. J. Cancer, 58:721, 1994; Plymate, et al. J. Clin. Endocrinol., Met. 81: 3709, 1996; Morikawa et al. Cancer Res., 48: 1943, 1988; Morikawa et al. Cancer Res., 48: 6863, 1988; Schackert et al. Am. J. Pathol., 136: 95, 1990; Zhang et al. Cancer Res., 51: 2029, 1991; Zhang et al. Invasion Metastasis, 11: 204, 1991; Price et al. Cancer Res., 50: 717, 1990; Mukhopadhyay et al. Clin Exp Met., 17: 325, 1999; Glinsky et al. Clin. Exper. Metastasis, 14: 253, 1996; Glinsky et al. Cancer Res., 56: 5319, 1996; Glinsky et al. Cancer Lett., 115: 185, 1997; McConkey et al. Cancer Res., 56: 5594, 1996; Glinsky et al. Transf Med Rev 14: 326, 2000 (incorporated herein by reference).

Table 2 – Representative Cell Line Combinations				
Breast Cancer				
Tumor Cell Line	Control Cell Line	Reference/comments		

See Table 1	Clonetics <sup>TM</sup> human mammary epithelial cells (Cat. # CC2551 from Cambrex, Inc., East Rutherford, NJ)	ATCC collection, incorporated herein by reference; Cambrex, Inc. 2002 Biotech Catalog, incorporated herein by reference
Tumor Cell Line	Control Cell Line	Reference/comments
See Table 1	Clonetics <sup>TM</sup> prostate epithelial cells (Cat. # CC2555 from Cambrex, Inc., East Rutherford, NJ)	ATCC collection, incorporated herein by reference; Cambrex, Inc. 2002 Biotech Catalog, incorporated herein by reference
	Lung Cancer	
Tumor Cell Line	Control Cell Line	Reference/comments
See Table 3	ATCC# CCL-256.1; NCI-BL2126; peripheral blood; Clonetics the bronchial epithelial cells (Cat. # CC2540 from Cambrex, Inc., East Rutherford, NJ); Clonetics the small airway epithelial cells (Cat. # CC2547 from Cambrex, Inc., East Rutherford, NJ); See Table 3	ATCC collection, incorporated herein by reference; Cambrex, Inc. 2002 Biotech Catalog, incorporated herein by reference
	Other types of cancers	
Tumor Cell Line	Control Cell Line	Reference/comments
See Table 3	See Table 3	
	Differentiation Pathway	
Precursor/Stem Cell Line	Differentiated Cell Line	Reference/comments

CD133+ cells Cat. # 2M-	mononuclear cells Cat	ATCC collection,
102A – bone marrow	#2M-125C; CD4+ T-cells	incorporated herein by
derived; Cat # 2G102 – G-	Cat. # 1C-200; human	reference; Cambrex, Inc.
CSF derived; Cat. # 2L-	astrocytes Cat. # CC2565;	2002 Biotech Catalog,
102A – fetal liver derived;	human hepatocytes Cat. #	incorporated herein by
CD36+ erythroid	CC2591; NHEM neonatal	reference
progenitors Cat # 2C-250;	melanocytes Cat. #	
cord blood CD19+ B cells	CC2513; SkMC - Skeletal	
Cat # 1C-300; dendritic	Muscle Cells Cat. #	
cell precursors Cat # 2P-	CC2561 (all from	
105; NHNP neural	Cambrex, Inc., East	•
progenitor cells Cat. #	Rutherford, NJ)	
CC2599; hMSC -		
mesenchymal stem cells,		
human bone marrow Cat. #		
PT-2501 (all from		
Cambrex, Inc., East		
Rutherford, NJ)		

	Table 3 – Representative Tumor/Control Cell Line							
Con	Combinations Available from American Type Culture Collection (ATCC)							
	Tumo	r Cell Line		C	ontrol Cell Lin	e		
ATCC		Cancer	Tissue	ATCC		Tissue		
No.	Name	Туре	Source	No.	Name	Source		
CCL-256	NCI-H2126	carcinoma; non- small cell lung cancer	lung	CCL-256.1	NCI-BL2126	peripheral blood		
CRL-5868	NCI-H1395	adenocarcinoma	lung	CRL-5957	NCI-BL1395	peripheral blood		
CRL-5882	NCI-H1648	adenocarcinoma	lung	CRL-5954	NCI-BL1648	peripheral blood		
CRL-5911	NCI-H2009	adenocarcinoma	lung	CRL-5961	NCI-BL2009	peripheral blood		

CRL-5985	NCI-H2122	adenocarcinoma	pleural effusion	CRL-5967	NCI-BL2122	peripheral blood
CRL-5922	NCI-H2087	adenocarcinoma	lymph node (metastasis)		NCI-BL2087	peripheral blood
CRL-5886	NCI-H1672	carcinoma; classic small cell lung cancer	lung	CRL-5959	NCI-BL1672	peripheral blood
CRL-5929	NCI-H2171	carcinoma; small cell lung cancer	lung	CRL-5969	NCI-BL2171	peripheral blood
CRL-5931	NCI-H2195	carcinoma; small cell lung cancer	lung	CRL-5956	NCI-BL2195	peripheral blood
CRL-5858	NCI-H1184	carcinoma; small cell lung cancer	lymph node (metastasis)	}	NCI-BL1184	peripheral blood
HTB-172	NCI-H209	carcinoma; small cell lung cancer	bone marrow (metastasis)	CRL-5948	NCI-BL209	peripheral blood
CRL-5983	NCI-H2107	carcinoma; small cell lung cancer	bone marrow (metastasis)		NCI-BL2107	peripheral blood
HTB-120	NCI-H128	carcinoma; small cell lung cancer	pleural effusion	CRL-5947	NCI-BL128	peripheral blood
CRL-5915	NCI-H2052	mesothelioma	pleural effusion	CRL-5963	NCI-BL2052	peripheral blood
CRL-5893	NCI-H1770	neuroendocrine carcinoma	lymph node (metastasis)	ļ	NCI-BL1770	peripheral blood

HTB-126	Hs 578T	ductal	mammary	HTB-125	Hs 578Bst	mammary
		carcinoma	gland;			gland;
			breast			breast
CRL-2320	HCC1008	ductal	mammary	CRL-2319	HCC1007 BL	peripheral
		carcinoma	gland;			blood
			breast			
CRL-2338	HCC1954	ductal	mammary	CRL-2339	HCC1954 BL	peripheral
		carcinoma	gland;			blood
			breast			
CRL-2314	НСС38	primary ductal	mammary	CRL-2346	HCC38 BL	peripheral
		carcinoma	gland;			blood
			breast			
CRL-2321	HCC1143	primary ductal	mammary	CRL-2362	HCC1143 BL	peripheral
		carcinoma	gland;			blood
			breast		·	
CRL-2322	HCC1187	primary ductal	mammary	CRL-2323	HCC1187 BL	peripheral
		carcinoma	gland;			blood
	·		breast			
CRL-2324	HCC1395	primary ductal	mammary	CRL-2325	HCC1395 BL	peripheral
		carcinoma	gland;			blood
			breast			
CRL-2331	HCC1599	primary ductal	mammary	CRL-2332	HCC1599 BL	peripheral
		carcinoma	gland;			blood
			breast			
CRL-2336	HCC1937	primary ductal	mammary	CRL-2337	HCC1937 BL	peripheral
		carcinoma	gland;			blood
			breast			

CIGE-23-10].	HCC2157	primary ductal	mammary	CRL-2341	HCC2157 BL	peripheral
1		carcinoma	gland;			blood
			breast			
CRL-2343	HCC2218	primary ductal	mammary	CRL-2363	HCC2218 BL	peripheral
	;	carcinoma	gland;			blood
			breast			
CRL-7345	Hs 574.T	ductal	mammary	CRL-7346	Hs 574.Sk	skin
		carcinoma	gland;			
			breast			
CRL-7482	Hs 742.T	scirrhous	mammary	CRL-7481	Hs 742.Sk	skin
		adenocarcinoma	gland;			
			breast			
CRL-7365	Hs 605.T	carcinoma	mammary	CRL-7364	Hs 605.Sk	skin
		\$	gland;			
	i		breast			
CRL-7368	Hs 606	carcinoma	mammary	CRL-7367	Hs 606.Sk	skin
			gland;			
			breast			_
CRL-1974	COLO 829	malignant	skin	CRL-1980	COLO 829BL	peripheral
		melanoma	:			blood
CRL-7762	TE 354.T	basal cell	skin	CRL-7761	TE 353.Sk	skin
		carcinoma				
CRL-7677	Hs 925.T	pagetoid	skin	CRL-7676	Hs 925.Sk	skin
		sarcoma				
CRL-7672	Hs 919.T	benign osteoid	bone	CRL-7671	Hs 919.Sk	skin
		osteoma				
CRL-7554	Hs 821.T	giant cell	bone	CRL-7553	Hs 821.Sk	skin
		sarcoma				

CRL-7552	Hs 820.T	heterophilic osteofication	bone	CRL-7551	Hs 820.Sk	skin
CRL-7444	Hs 704.T	osteosarcoma	bone	CRL-7443	Hs 704.Sk	skin
CRL-7448	Hs 707(A).T	osteosarcoma	bone	CRL-7449	Hs 707(B).Ep	skin
CRL-7471	Hs 735.T	osteosarcoma	bone	CRL-7865	Hs 735.Sk	skin
CRL-7595	Hs 860.T	osteosarcoma	bone	CRL-7519	Hs 791.Sk	skin
CRL-7622	Hs 888.T	osteosarcoma	bone	CCL-211	Hs888Lu	lung
CRL-7626	Hs 889.T	osteosarcoma	bone	CRL-7625	Hs 889.Sk	skin
CRL-7628	Hs 890.T	osteosarcoma	bone	CRL-7627	Hs 890.Sk	skin
CRL-7453	Hs 709.T	periostitis; granuloma	bone	CRL-7452	Hs 709.Sk	skin
CRL-7886	Hs 789.T	transitional cell carcinoma	ureter	CRL-7518	Hs 789.Sk	skin
CRL-7547	Hs 814.T	giant cell sarcoma	vertebral column	CRL-7546	Hs 814.Sk	skin

Table 4 – Representative Primary Tumor/Metastatic Tumor Cell Line Combinations Available from American Type Culture Collection (ATCC)											
	Primar	y Cell Line	Metastatic Cell Line								
ATCC No.	Name	Disease	Tissue	ATCC No.	Name	Tissue					
CCL-228	SW480	colorectal adenocarcinoma	colon	CCL-227	SW620	lymph node					
CRL-1864	RF-1	gastric adenocarcinoma	stomach	CRL-1863	RF-48	ascites					
CRL-1675	WM-115	melanoma	skin	CRL-1676	WM-266-4	n/a					

CRL-7425	Hs	melanoma	skin	CRL-7426	Hs 688(B).T	lymph
	688(A).T					node

[00144] Application of the methods of the invention to the study of particular cancers is described generally below, and is followed by specific working examples demonstrating aspects of the invention.

### Prostate Cancer

[00145] As many as 50% of men, aged 70 years and over have microscopic foci of prostate cancer without clinical evidence of disease (Trump, D. L., Robertson, C. N., Holland, J. F., Frei, E., Bast, R. C., Kufe, D. W., Morton, D. L., and Weishselbaum, R. R. Neoplasms of the prostate. In: D. L. Trump, C. N. Robertson, J. F. Holland, E. Frei, R. C. Bast, D. W. Kufe, D. L. Morton, and R. R. Weishselbaum (eds.), Cancer Med, Vol. 3, pp. 1562-86. Philadelphia: Lea & Febiger, 1993.). Although some prostate cancers remain indolent and confined to the gland, other prostate cancers behave more aggressively and metastasize if not adequately treated. Prostate cancer is the second most lethal neoplasia in males after lung cancer. Because of widespread screening programs utilizing serum PSA values, many more cases of early stage disease are being diagnosed. In 1988 approximately 50% of patients were diagnosed with early stage disease (stage I and II). Today, about 75% of patients have early stage disease that is potentially curable. [00146] Unfortunately, the only potentially curative therapy for prostate cancer consists of radical prostatectomy or other local therapies such as external irradiation, implanted irradiation seeds, or cryotherapy. The use of prostatectomy has increased in step with the amount of diagnosed early stage prostate cancer. SEER data indicates an increase in prostatectomies from 17.4 per 100,000 in 1988 to 54.6 per 100,000 in 1992.

Insufficient treatment leads to local disease extension and metastasis. Current methods, such as Gleason scores are not perfectly reliably correlated with whether a tumor is aggressive or indolent. Thus, developing a treatment strategy appropriate for any individual is difficult. The recognition of those genetic changes that portend metastatic prostate cancer would, therefore, be a breakthrough. The methods of the present invention readily identify such genetic changes.

#### **Breast Cancer**

Breast cancer is the most common cancer among women in North America [00147] and Western Europe and is the second leading cause of female cancer death in the United States. In the United States, age-adjusted breast cancer incidence rates have considerably increased during last century. Approximately 40% of patients diagnosed with breast cancer have disease that has regional or distant metastases and, at present, there is no efficient curative therapy for breast cancer patients with advanced metastatic disease. Thus, developing a treatment strategy appropriate for any individual with early stage disease is difficult and insufficient treatment leads to local disease extension and metastasis. Therefore, there is an urgent clinical need for novel diagnostic methods that would allow early identification of those breast cancer patients who are likely to develop metastatic disease and would require the most aggressive and advanced forms of therapy for increased chance of survival. The identification of those genetic changes that distinguish aggressive metastatic disease and predict metastatic behavior would, therefore, be a breakthrough. The methods of the present invention provide information that allows prognostication of aggressive metastatic disease.

[00148] Recent gene expression analysis of human tumor samples employing cDNA microarray technology underscores the difficulties in identification of the cellular origin of differentially expressed transcripts in clinical samples due to the remarkable cellular heterogeneity and variability in cellular compositions of human tumors (Golub, T.R., Slonim, D.K., Tamayo, P., Huard, C., Gaasenbeek, M., Mesirov, J.P., Coller, H., Loh, M.L., Downing, J.R., Caliguri, M.A., Bloomfield, C.D., Lander, E.S. 1999. Molecular classification of cancer: class discovery and class prediction by gene expression monitoring. Science, 286: 531-537; Perou CM, Jeffrey SS, van de Rijn M, et al. Distinctive gene expression patterns in human mammary epithelial cells and breast cancers. Proc Natl Acad Sci USA. 1999. 96:9212-9217; Perou CM, Sorlie T, Eisen MB, et al. Molecular portrait of human breast tumors. Nature. 2000. 406:747-752, incorporated herein by reference). However, a cDNA microarray analysis of gene expression in melanoma cell lines of distinct metastatic potential, was successfully employed for identification of RhoC as an essential gene for the acquisition of metastatic phenotype by melanoma cells (Clark, EA, Golub TR, Lander ES, Hynes RO. Genomic analysis of metastasis reveals an essential role for RhoC. Nature 2000. 406:532-535, incorporated herein by reference). Established human cancer cell lines were utilized for parallel comparisons of the alterations in DNA copy number and gene expression associated with human breast cancer (Pollack, J.R., Perou, C.M., Alizadeh, A.A., Eisen, M.B., Pergamenschikov, A., Williams, C.F., Jeffrey, S.S., Botstein, D., Brown, P.O. Genome-wide analysis of DNA-copy number changes using cDNA microarrays. Nature Genetics. 1999. 23: 41-46; Forozan, F., Mahlamaki, E.H., Monni, O., Chen, Y., Veldman, R., Jiang, Y., Gooden, G.C., Ethier, S.P., Kallioniemi, A., Kallioniemi, O-P. Comparative genomic hybridization analysis of 38 breast cancer cell lines: a basis for interpreting complementary DNA microarray data. Cancer Res. 2000. 60: 4519-4525, incorporated herein by reference). Thus, model systems are a reasonable source of gene candidates to be studied in the much more heterogeneous environment of real human tumors.

[00149] Analysis of gene expression in normal and neoplastic ovarian human tissues using methods of the present invention revealed that high malignant potential ovarian cancers exhibited gene expression profile somewhat similar to the ovarian cancer cell lines (Welsh, J.B., Zarrinkar, P.P., Sapinoso, L.M., Kern, S.G., Behling, C.A., Monk, B.J., Lockhart, D.J., Burger, R.A., Hampton, G.M. Analysis of gene expression profiles in normal and neoplastic ovarian tissue samples identifies candidate molecular markers of epithelial ovarian cancer. Proc Natl Acad Sci USA. 2001. 98:1176-1181, incorporated herein by reference), further validating the complementary gene expression analysis

### Metastasis

[00150] Cancer cells have exceedingly low survival rates in the circulation (reviewed in [Glinsky, G.V. 1993. Cell adhesion and metastasis: is the site specificity of cancer metastasis determined by leukocyte-endothelial cell recognition and adhesion? Crit. Rev. Onc./Hemat., 14: 229-278, incorporated herein by reference). Even if the bloodstream contains many cancer cells, there may be no clinical or pathohistological evidence of metastatic dissemination into the target organs (Williams, W.R. The theory of Metastasis. In The Natural History of Cancer. 1908; 442-448; Goldmann, E. 1907. The growth of malignant disease in man and the lower animals, with special reference to the vascular system. Proc. R. Soc. Med., 1: 1-13; Schmidt, M.B. In Die Verbreitungswege der

approach utilizing selected established cancer cell lines and clinical samples.

Karzinome und die bezienhung generalisiertes sarkome su den leukamischen neubildungen. Fischer, Jena, 1903, incorporated herein by reference). The levels of metastatic efficiency at the intramicrovascular (postintravasation) phase of metastatic dissemination were shown to be only 0.2% and 0.003% in high and low metastatic variants of B16 melanoma cells, respectively, injected at a concentration of 105 cells into the tail veins of laboratory mice (Weiss, L. 1990. Metastatic inefficiency. Adv. Cancer Res., 54: 159-211; Weiss, L., Mayhew, E., Glaves-Rapp, D., Holmes, J.C. 1982. Metastatic inefficiency in mice bearing B16 melanomas. Br. J. Cancer, 45: 44-53, incorporated herein by reference). The fate of cancer cells in the circulation is a rapid phase of intramicrovascular cancer cell death, which is completed in <5 minutes and accounts for 85% of arrested cancer cells. This is followed by a slow phase of cell death, which accounts for the vast majority of the remainder (Weiss, L. 1988. Biomechanical destruction of cancer cells in the hart: a rate regulator of hematogenous metastasis. Invas. Metastasis, 8: 228-237; Weiss, L., Orr, F.W., Honn, K.V. 1988. Interactions of cancer cells with the microvasculature during metastasis. FSEB J., 2: 12-21; Weiss, L., Harlos, J.P., Elkin, G. 1989. Mechanism of mechanical trauma to Ehrlich ascites tumor cells in vitro and its relationship to rapid intravascular death during metastasis. Int. J. Cancer, 44: 143-148, incorporated herein by reference).

[00151] For example, the number of tumor cells in the lungs declined very rapidly after intravenous injection *i.e.*, 90-99% had disappeared after 24 hours (Hewitt, H.B., Blake, A. 1975. Quantitative studies of translymphonodal passage of tumor cells naturally disseminating from a nonimmunogenic murine squamous carcinoma. Br. J. Cancer, 31: 25-35; Fidler, I.J. 1970. Metastasis: quantitative analysis of distribution and

fate of tumor emboli labeled with 125I-5 iodo-2'-deoxyuridine. J. Natl. Cancer Inst., 45: 773-782; Proctor, J.W. 1976. Rat sarcoma model supports both soil seed and mechanical theories of metastatic spread. Br. J. Cancer, 34: 651-654; Proctor, J.W., Auclair, B.G., Rudenstam, C.M. 1976. The distribution and fate of blood-born 125IudR-labeled tumor cells in immune syngeneic rats. Int. J. Cancer, 18: 255-262; Weston, B.J., Carter, R.L., Eastry, G.C., Connell, D.I., Davies, A.J.C. 1974. The growth and metastasis of an allografted lymphoma in normal, deprived and reconstituted mice. Int. J. Cancer, 14: 176-185; Kodama, M., Kodama, T. 1975. Enhancing effect of hydrocortisone on hematogenous metastasis of Ehrlich ascites tumor in mice. Cancer Res., 35: 1015-1021, incorporated herein by reference) and after 3 days generally less than 1% remained (Fidler, I.J. 1970. Metastasis: quantitative analysis of distribution and fate of tumor emboli labeled with 125I-5 iodo-2'-deoxyuridine. J. Natl. Cancer Inst., 45: 773-782; Weston, B.J., Carter, R.L., Eastry, G.C., Connell, D.I., Davies, A.J.C. 1974. The growth and metastasis of an allografted lymphoma in normal, deprived and reconstituted mice. Int. J. Cancer, 14: 176-185; Kodama, M., Kodama, T. 1975. Enhancing effect of hydrocortisone on hematogenous metastasis of Ehrlich ascites tumor in mice. Cancer Res., 35: 1015-1021, incorporated herein by reference). This decline is due to a rapid degeneration of cancer cells (Fidler, I.J. 1970. Metastasis: quantitative analysis of distribution and fate of tumor emboli labeled with 125I-5 iodo-2'-deoxyuridine. J. Natl. Cancer Inst., 45: 773-782; Roos, E., Dingemans, K.P. 1979. Mechanisms of metastasis. Biochim. Biophys. Acta, 560: 135-166, incorporated herein by reference). Therefore, the individual 'average' cancer cell survives only a short time in the circulation. The successful metastatic cancer cells are able to find a largely unknown survival and escape

route. Patients at high risk for metastatic disease could be better managed if gene expression patterns correlated with a clinical metastatic phenotype are identified. The methods of the present invention identify such gene expression patterns. Patients' tumor samples can be tested to see whether the gene expression pattern is associated with an increased risk of metastasis, and if so, the patients can be treated with more aggressive therapies to lower the risk of metastasis. As explained in greater detail below, the present invention provides for methods that allow identification of such gene expression patterns, and sample classification based on those patterns.

## Models of human cancer metastasis of graded metastatic potential

[00152] We have acquired several well-established and characterized model human cancer cell systems of graded metastatic potential (Table 1). The collection of these human cancer cell line panels provides different backgrounds upon which increased metastatic potential is superimposed. We have studied these cell line systems extensively for many years both *in vitro* and *in vivo* (Glinsky, G.V. 1998. Failure of Apoptosis and Cancer Metastasis. Berlin/Heidelberg: Springer-Verlag, pp. 178 *et seq.*; Glinsky, G.V., Mossine, V.V., Price, J.E., Bielenberg, D., Glinsky, V.V., Ananthaswamy, H.N., Feather, M.S. 1996. Inhibition of colony formation in agarose of metastatic human breast carcinoma and melanoma cells by synthetic glycoamines. Clin. Exp. Metastasis, 14: 253-267; Glinsky, G.V., Price, J.E., Glinsky, V.V., Mossine, V.V., Kiriakova, G., Metcalf, J.B. 1996. Inhibition of human breast cancer metastasis in nude mice by synthetic glycoamines. Cancer Res., 56: 5319-5324; Glinsky, G.V., Glinsky, V.V. 1996. Apoptosis and metastasis: a superior resistance of metastatic cancer cells to the programmed cell death. Cancer Lett., 101: 43-51; Glinsky, G.V., Glinsky, V.V., Ivanova, A.B., Hueser,

C.N. 1997. Apoptosis and metastasis: increased apoptosis resistance of metastatic cancer cells is associated with the profound deficiency of apoptosis execution mechanisms.

Cancer Lett., 115: 185-193, incorporated herein by reference) and, therefore, have considerable experience in the maintenance of cell lines preserving graded metastatic potentials. These models provide an excellent opportunity to test whether concordant changes in gene expression underlie the metastasis process and to test the efficacy of drugs designed to block one or more crucial targets.

[00153] Four important features of the selected models have been documented (Glinsky, G.V. 1997. Apoptosis in metastatic cancer cells. Crit. Rev. Onc/Hemat., 25:175-186; Glinsky, G.V. 1998. Anti-adhesion cancer therapy. Cancer and Metastasis Reviews, 17: 171-185. Glinsky, G.V. 1998. Failure of Apoptosis and Cancer Metastasis. Berlin/Heidelberg: Springer-Verlag, pp 178 et seq.; Glinsky, G.V., Mossine, V.V., Price, J.E., Bielenberg, D., Glinsky, V.V., Ananthaswamy, H.N., Feather, M.S. 1996. Inhibition of colony formation in agarose of metastatic human breast carcinoma and melanoma cells by synthetic glycoamines. Clin. Exp. Metastasis, 14: 253-267; Glinsky, G.V., Price, J.E., Glinsky, V.V., Mossine, V.V., Kiriakova, G., Metcalf, J.B. 1996. Inhibition of human breast cancer metastasis in nude mice by synthetic glycoamines. Cancer Res., 56: 5319-5324; Glinsky, G.V., Glinsky, V.V. 1996. Apoptosis and metastasis: a superior resistance of metastatic cancer cells to the programmed cell death. Cancer Lett., 101: 43-51; Glinsky, G.V., Glinsky, V.V., Ivanova, A.B., Hueser, C.N. 1997. Apoptosis and metastasis: increased apoptosis resistance of metastatic cancer cells is associated with the profound deficiency of apoptosis execution mechanisms. Cancer Lett., 115: 185-193, incorporated herein by reference): a) highly metastatic cell variants possess an increased

survival ability, high clonogenic growth potential, and enhanced resistance to apoptosis compared to parental or poorly metastatic counterparts; b) treatment of highly metastatic cell variants with certain synthetic glycoamine analogues caused inhibition of clonogenic growth and survival and reversal of apoptosis resistance in vitro, as well as significant reduction of metastatic potential in vivo; c) these cell lines maintain their distinct in vivo metastatic potentials during in vitro passage for at least several months, indicating that metastatic ability is preserved in vitro; d) differential transcription profiles of four metastasis-associated genes between high and low metastatic cell variants was shown to be similar in vitro and in vivo (Greene, G.F., Kitadai, Y., Pettaway, C.A., von Eschenbach, A.C., Bucana, C.D., Fidler, I.J. 1997. Correlation of metastasis-related gene expression with metastatic potential in human prostate carcinoma cells implanted in nude mice using an in situ messenger RNA hybridization technique. American J. Pathology, 150: 1571-1582, incorporated herein by reference) indicating the potential relevance of in vitro gene expression patterns to the metastatic phenotype. Thus, in accordance with the methods of the present invention, these cellular systems can be used to identify relevant gene expression patterns associated with phenotypes of interest (such as, e.g., metastasis, invasiveness, etc.) by comparing patterns of differential gene expression in one or more independently selected cell line variants with those in different types of clinical human cancer samples.

### Orthotopic Model of Human Cancer Metastasis in Nude Mice

[00154] When human tumor cells are injected into ectopic sites in nude mice most do not metastasize (Fidler, I.J. The nude mouse model for studies of human cancer · metastasis. In: V. Schirrmacher and R. Schwartz-Abliez (eds.). pp. 11-17. Berlin:

Springer-Verlag, 1989; Fidler, I.J. Critical factors in the biology of human cancer metastasis. 1990. Cancer Res., 50, 6130-6138, incorporated herein by reference). The normal host tissue environment influences metastatic ability of cancer cells in such a way that many human and animal tumors transplanted into nude mice metastasize only if placed in the orthotopic organ (Fidler, I.J. The nude mouse model for studies of human cancer metastasis. In: V. Schirrmacher and R. Schwartz-Abliez (eds.). pp. 11-17. Berlin: Springer-Verlag, 1989; Fidler, I.J. Critical factors in the biology of human cancer metastasis. 1990. Cancer Res., 50, 6130-6138; Fidler, I.J., Naito, S., Pathak, S. 1990. Orthotopic implantation is essential for the selection, growth and metastasis of human renal cell cancer in nude mice. Cancer Metastasis Rev., 9, 149-165; Giavazzi, R., Campbell, D.E., Jessup, J.M., Cleary, K., and Fidler, I.J. 1986. Metastatic behavior of tumor cells isolated from primary and metastatic human colorectal carcinomas implanted into different sites in nude mice. Cancer Res., 46: 1928-1948; Naito, S., von Eschenbach, A.C., Giavazzi, R., and Fidler, I.J. 1986. Growth and metastasis of tumor cells isolated from a renal cell carcinoma implanted into different organs of nude mice. Cancer Res., 46: 4109-4115; McLemore, T.L., et al. 1987. Novel intrapulmonary model for orthotopic propagation of human lung cancer in athymic nude mice. Cancer Res., 47: 5132-5140, incorporated herein by reference). These observations pointed out the unique opportunity to study gene expression changes associated with aggressive metastatic phenotype. A comparison of gene expression patterns using the same high metastatic variant implanted at orthotopic (metastasis promoting model) and ectopic (metastasis suppressing model) sites should provide unique information regarding differential gene expression profiles associated with metastatic behavior in vivo.

Several orthotopic models of human cancer metastasis have been developed [00155](Fu, X., Herrera, H., and Hoffman, R.M. 1992. Orthotopic growth and metastasis of human prostate carcinoma in nude mice after transplantation of histologically intact tissue. Int. J.Cancer, 52: 987-990; Stephenson, R.A., Dinney, C.P.N., Gohji, K., Ordonez, N.G., Killion, J.J., and Fidler, I.J. 1992. Metastatic model for human prostate cancer using orthotopic implantation in nude mice. J. Natl. Cancer Inst., 84: 951-957; Pettaway, C.A., Stephenson, R.A., and Fidler, I.J. 1993. Development of orthotopic models of metastatic human prostate cancer. Cancer Bull. (Houst.), 45: 424-429; An, Z., Wang, X., Geller, J., Moossa, A.R., and Hoffman, R.M. 1998. Surgical orthotopic implantation allows high lung and lymph node metastasis expression of human prostate carcinoma cell line PC-3 in nude mice. The Prostate, 34: 169-174; Wang, X., An, Z., Geller, J., and Hoffman, R.M. 1999. High-malignancy orthotopic mouse model of human prostate cancer LNCaP. The Prostate, 39: 182-186; Yang, M., Jiang, P., Sun, F.-X., Hasegawa, S., Baranov, E., Chishima, T., Shimada, H., Moosa, A.R., and Hofman, R.M. 1999. A fluorescent orthotopic bone metastasis model of human prostate cancer. Cancer Res., 59: 781-786, incorporated herein by reference). The orthotopic model of human cancer metastasis in nude mice was used for in vivo selection of highly and poorly metastatic cell variants, employing either established panels of human cancer cell lines or cell variants derived from the same parental cell lines (Giavazzi, R., Campbell, D.E., Jessup, J.M., Cleary, K., and Fidler, I.J. 1986. Metastatic behavior of tumor cells isolated from primary and metastatic human colorectal carcinomas implanted into different sites in nude mice. Cancer Res., 46: 1928-1948; Morikawa, K., Walker, S.M., Jessup, J.M., Cleary, K., and Fidler, I.J. 1988. In vivo selection of highly metastatic cells from surgical

specimens of different primary human colon carcinoma implanted in nude mice. Cancer Res., 48: 1943-1948; Dinney, C.P.N. *et al.* 1995. Isolation and characterization of metastatic variants from human transitional cell carcinoma passaged by orthotopic implantation in athymic nude mice. J. Urol., 154: 1532-1538, incorporated herein by reference).

This approach was successfully applied to develop a human breast cancer [00156] model of graded metastatic potential (see Glinsky, G.V., Mossine, V.V., Price, J.E., Bielenberg, D., Glinsky, V.V., Ananthaswamy, H.N., Feather, M.S. 1996. Inhibition of colony formation in agarose of metastatic human breast carcinoma and melanoma cells by synthetic glycoamines. Clin. Exp. Metastasis, 14: 253-267; Glinsky, G.V., Price, J.E., Glinsky, V.V., Mossine, V.V., Kiriakova, G., Metcalf, J.B. 1996. Inhibition of human breast cancer metastasis in nude mice by synthetic glycoamines. Cancer Res., 56: 5319-5324, incorporated herein by reference) as well as three independent panels of human prostate cancer cell lines with distinct metastatic potential (Pettaway, C.A., Pathak, S., Greene, G., Ramirez, E., Wilson, M.R., Killion, J.J., and Fidler, I.J. 1996. Selection of highly metastatic variants of different human prostatic carcinomas using orthotopic implantation in nude mice. Clinical Cancer Res., 2: 1627-1636; Bae, V.L., Jackson-Cook, C.K., Brothman, A.R., Maygarden, S.J., and Ware, J. Tumorugenicity of SV40 T antigen immortalized human prostate epithelial cells: association with decreased epidermal growth factor receptor (EGFR) expression. Int. J. Cancer 1994;58:721-29; Plymate, et al., The effect of the IGF system in human prostate epithelial cells of immortalization and transformation by SV-40 T antigen. J. Clin. Endocrinol. Met. 1996:81;3709-16; Jackson-Cook, C., Bae, V., Edelman W., Brothman, A., and Ware, J. Cytogenetic characterization

of the human prostate cancer cell line P69SV40T and its novel tumorigenic sublines M2182 and M15. Cancer Genet. & Cytogenet 1996;87:14-23; Bae, V.L., Jackson-Cook, C.K., Maygarden, S.J., Plymate, S.R., Chen, J., and Ware, J.L. Metastatic subline of an SV40 large T antigen immortalized human prostate epithelial cell line. Prostate 1998;34:275-82, incorporated herein by reference). Recent experimental evidence indicates that enhancement of metastatic capability of human cancer cells transplanted orthotopically is associated with differential expression of several metastasis-associated genes that have been implicated earlier in certain key features of the metastatic phenotype (Greene, G.F., Kitadai, Y., Pettaway, C.A., von Eschenbach, A.C., Bucana, C.D., Fidler, I.J. 1997. Correlation of metastasis-related gene expression with metastatic potential in human prostate carcinoma cells implanted in nude mice using an in situ messenger RNA hybridization technique. American J. Pathology, 150: 1571-1582, incorporated herein by reference). These data support the rationale for the methods of the present invention to identify gene expression profiles associated with the phenotypes of clinical tumor samples based on a combination of *in vitro* gene expression analysis in one or more cell lines having a phenotype of interest (e.g., metastatic potential, invasiveness, etc.) and gene expression analysis of clinical samples.

[00157] A similar rationale supports the use of the methods of the present invention to identify gene expression patterns correlated with specific differentiation pathways associated with defined cell types (e.g., liver, skin, bone, muscle, blood, etc.), although in this instance, the preferred relevant comparisons are the gene expression profiles of one or more stem cell lines with that of the terminally differentiated cell type. (See, e.g., Table 2, supra.) In a related method of the present invention, expression analysis may be

carried out on one or more different cell types using sets of genes (i.e., gene clusters) previously identified in, e.g., a biological sample analysis experiment such as the described tumor classification methods, to identify concordantly regulated genes that can be used as tissue-specific markers, or to screen for agents that may affect cellular differentiation or other aspects of cellular phenotype. Phenotype association indices can be calculated for normally differentiated tissue samples by calculating a correlation coefficient for a particular normally differentiated tissue sample against, e.g., -fold expression changes or expression differences for a minimum segregation set identified in a cancer analysis, as described above. The -fold expression changes or expression differences for the normally differentiated tissue sample can be calculated with reference to average values of gene x expression across a collection of different normal tissue samples. Expression data derived from the large collections of normal human and mouse tissue samples are available as supplemental data reported by Su, A.I. et al. Large-scale analysis of the human and mouse transcriptomes. PNAS 99: 4465-4470, 2002, incorporated herein by reference, and are available from the publicly accessible website http://expression.gnf.org, incorporated herein by reference.

[00158] Three possible outcomes are observed. In the first, no correlation is observed between the minimum segregation set and the normal tissue sample expression data implying that the regulatory pathway represented by the transcript abundance rank order within the minimum segregation set is not active. In the second, a positive correlation is seen between the –fold expression changes or differences in the minimum segregation set and the normal tissue sample implying that the regulatory pathway represented by the transcript abundance rank order within the minimum segregation set is active. In this

outcome, the minimum segregation set represents a cluster of genes involved in a differentiation program and/or regulatory pathway that operates in the normal tissue sample and in the tumor cell lines. In the third outcome, a negative correlation is seen between the –fold expression changes or differences in the minimum segregation set and the normal tissue sample implying that the alternative regulatory pathway to one represented by the transcript abundance rank order within the minimum segregation set is active. In this outcome, the minimum segregation set represents a cluster of genes coregulated in a differentiation program and/or regulatory pathway that operates in the normal tissue samples but that has failed in the tumor cell lines. Because the expression rank order of the genes within the minimum segregation class was derived from a comparison of the fold expression changes in tumor cell lines versus normal epithelial cells of the organ of cancer origin, this scenario may serve as an indicator of an active tumor suppression pathway.

Gene expression profiles of human normal prostate epithelial cells and prostate cancer cell lines in culture

[00159] To identify genes expression of which is consistently altered in human prostate cancer cell lines, we searched for genes whose differential expression is retained as cells diverge through mutation, genomic instability, and possibly epigenetic mechanisms during repeated cycles of *in vivo* prostate cancer growth and progression in nude mice. To model this behavior, cell lines established from LNCap- and PC3-derived human prostate carcinoma xenografts were studied. Parental LNCap and PC3 cell lines represent divergent clinically relevant prostate cancer progression variants. LNCap is a relatively less aggressive, androgen-dependent cell line with wild-type p53, and PC3 is an aggressive, p53 mutated (21), and androgen independent cell line. The five cell lines,

LNCapLN3, LNCapPro5, PC3M, PC3MLN4, PC3MPro4 (Pettaway, C. A., Pathak, S., Greene, G., Ramirez, E., Wilson, M. R., Killion, J. J. and Fidler, I. J. Selection of highly metastatic variants of different human prostatic carcinomas using orthotopic implantation in nude mice. Clin Cancer Res. 1996;2:1627-36, incorporated herein by reference) represent lineages that have been derived from xenografts passaged repeatedly in the mouse to model prostate cancer growth and metastatic progression (*see* Table 1 and accompanying legend). The number of successive *in vivo* progression and in vitro expansion cycles varied from 1 to 5 in different lineages (Table 1).

[00160] The model design was based on the following considerations. Genes regulated similarly in five lineages would be expected to biased towards those genes that are relatively insensitive to the individual genetic differences in the cell's *in vitro* regulatory program. Furthermore, genes that are sensitive to environmental perturbations may be a source of changes that are stress-induced or are handling artifacts. This consideration also is relevant for changes associated with surgically-derived samples isolated from patients. We chose the early response to serum starvation (two hours) as a convenient method to identify and remove genes that are sensitive to environmental perturbations. Following these criteria, we identified 214 transcripts that are differentially expressed in the same direction in all five prostate cancer cell lines, relative to normal prostate epithelium (NPE), regardless of the presence or absence of serum (vs. 292 observed using data from high serum alone). 43 of these genes were consistently upregulated and 171 were consistently down-regulated at least two-fold in all five cancer cell lines relative to NPE.

[00161] Of the 78 genes excluded by this experimental condition, only the Id3 protein and two alternatively spliced transcripts from the Id1 gene showed a common differential response to serum withdrawal within all five PC3- and LNCap-derived cell lines. Id1 and Id3 gene products are dominant negative regulators of the HLH transcription factors (Lyden, D., Young, A.Z., Zagzag, D., Yan, W., Gerald, W., O'Reilly, R., Bader, B.L., Hynes, R.O., Zhuang, Y., Manova, K., Benezra, R. Id1 and Id3 are required for neurogenesis, angiogenesis and vascularization of tumor xenografts. Nature 1999;401:670-77, incorporated herein by reference). The remaining 75 genes were differentially regulated with respect to serum withdrawal in ways that depended on the cell type. This is consistent with the view that the serum withdrawal criterion removes genes that are sensitive to both external environmental variables and internal cell line-specific context.

# Gene expression profiles of PC3-derived orthotopic tumors

[00162] To test whether the altered gene expression pattern of 214 genes identified in vitro is maintained in vivo, the common set of differentially expressed genes identified in the five cell lines relative to NPE were compared with genes that were differentially expressed in orthotopic tumors induced in nude mice using donor tumors for the PC3 lineage.

[00163] We identified a concordant gene expression profile for two tumors each independently derived from the three cell lines PC3 parental, PC3M, and PC3MLN4. 79 % (170 of 214 genes) of the transcripts differentially expressed in five prostate cancer cell lines in vitro were also differentially regulated in the same direction in vivo in all six orthotopic tumors. This gene set is exhaustively authenticated in thirty separate

comparisons, which should, theoretically, put their regulation in these systems beyond doubt. Nevertheless, a sample of twelve up- and two down-regulated genes was tested using Q-PCR on an ABI7900 using the vendor's recommended protocols available at <a href="http://www.appliedbiosystems.com/support/tutorials/">http://www.appliedbiosystems.com/support/tutorials/</a> (incorporated herein by reference). This PCR experiment used a further new batch of RNA from normal human prostate epithelial cell line and PC3M cells and human transcript-specific pairs of PCR primers. For several genes two separate sets of primers were designed and tested. Regulation was confirmed in the correct direction for these 14 genes, although the arrays tended to underestimate the magnitude of the change.

[00164] Therefore, the differential expression pattern of many of the prostate cancer-associated transcripts of PC3/LNCap consensus class identified *in vitro* using cell line concordance and media shift refractivity is retained in vivo in orthotopic human prostate tumors in mice. In the context of present invention, these data suggest that human prostate carcinoma xenografts may serve as a useful source of samples for identification of the reference standard data sets.

In vivo versus in vitro selection of human prostate cancer-associated genes

[00165] To determine whether the consensus set of 214 differentially expressed genes

identified here is retained in the parental cell lines, the PC3 and LNCaP cell lines that

have not been serially passaged through mice were examined by microarray analysis,

both in high and low serum. When concordance analysis was performed comparing the

consensus list of 214 genes and genes that were differentially regulated relative to NPE in

parental PC3 and LNCap cell lines, the majority of the down-regulated transcripts (133

genes; 78%) were similarly down-regulated in all 7 cell lines. However, only a small

fraction (10 genes; 23%) of up-regulated transcripts was similarly differentially regulated in both parental cell lines. Thus, when compared with the five tumor-derived cell lines, PC3 and LNCaP parental cell lines have substantially smaller similarity with respect to the up-regulated transcripts, indicating that the transcripts with increased mRNA abundance levels in a set of 214 genes do not reflect *in vitro* selection. The significant degree of conservation of the consensus set of 214 genes in both xenograft-derived and plastic-maintained series of cancer cell lines supports the notion that plastic maintained cancer cell lines may serve as a useful source of samples for identification of the reference standard data sets.

## Comparison with clinical human prostate tumors

[00166] While the genes described here are of undoubted interest as their expression is consistently altered in the multiple mouse model systems of human prostate cancer, it is not possible to say, as yet, whether they are of relevance to human disease. However, the expression levels of the genes in our stable set were analyzed published data from a group of clinical samples (Welsh, J.B., Sapinoso, L.M., Su, A.I., Kern, S.G., Wang-Rodriguez, J., Moskaluk, C.A., Frierson, H.F., Jr., Hampton, G.M. Analysis of gene expression identifies candidate markers and pharmacological targets in prostate cancer. Cancer Res., 61: 5974-5978, 2001, (supplemental data obtained from <a href="http://www.gnf.org/cancer/prostate">http://www.gnf.org/cancer/prostate</a>), incorporated herein by reference).

[00167] These data must be treated with caution because the human clinical samples are highly heterogeneous, consisting of different amounts of cells of epithelial, stromal, and other origins. Nevertheless, of the genes that could be cross-referenced, 31 out of 41 up-regulated genes (76%) were more highly expressed in the majority of 24 human

tumors than in a normal epithelial cell line. 32 of these genes were more highly expressed in the majority of tumors than the average expression found in nine adjacent normal prostate tissue samples. Similarly, 141 of 166 down-regulated genes (88%) were down regulated in tumors relative to normal epithelial cells, and 122 were down-regulated in tumors relative to adjacent normal prostate tissue. The similarity in the altered regulation of many of these genes in clinical tumors is an indication that these genes are relevant to the human disease.

## Materials and Methods

Cell culture. Cell lines used in this study are described in Table 1. The PC3-[00168] and LNCap-derived cell lines were developed by consecutive serial orthotopic implantation, either from metastases to the lymph node (for the LN series), or reimplanted from the prostate (Pro series). This procedure generated cell variants with differing tumorigenicity, frequency and latency of regional lymph node metastasis (Pettaway, C. A., Pathak, S., Greene, G., Ramirez, E., Wilson, M. R., Killion, J. J. and Fidler, I. J. Selection of highly metastatic variants of different human prostatic carcinomas using orthotopic implantation in nude mice. Clin Cancer Res. 1996;2:1627-36, incorporated herein by reference). The LNCaP and PC-3 panels of human prostate carcinoma cell lines of graded metastatic potential were provided by Dr. C. Pettaway (M.D. Anderson Cancer Center, Houston, TX) and described earlier (Pettaway, C. A., Pathak, S., Greene, G., Ramirez, E., Wilson, M. R., Killion, J. J. and Fidler, I. J. Selection of highly metastatic variants of different human prostatic carcinomas using orthotopic implantation in nude mice. Clin Cancer Res. 1996;2:1627-36, incorporated herein by reference). A third progression model is represented by the P69 cell line, an SV40 large

T-antigen-immortalized prostate epithelial line, and M12, a metastatic derivative of P69 (Bae, V.L., Jackson-Cook, C.K., Brothman, A.R., Maygarden, S.J., and Ware, J. Tumorugenicity of SV40 T antigen immortalized human prostate epithelial cells: association with decreased epidermal growth factor receptor (EGFR) expression. Int. J. Cancer 1994;58:721-29; Jackson-Cook, C., Bae, V., Edelman W., Brothman, A., and Ware, J. Cytogenetic characterization of the human prostate cancer cell line P69SV40T and its novel tumorigenic sublines M2182 and M15. Cancer Genet. & Cytogenet 1996;87:14-23; Bae, V.L., Jackson-Cook, C.K., Maygarden, S.J., Plymate, S.R., Chen, J., and Ware, J.L. Metastatic subline of an SV40 large T antigen immortalized human prostate epithelial cell line. Prostate 1998;34:275-82, incorporated herein by reference). The P69 cell line and M12 cell line were obtained from Dr. S. Plymate and Dr. J. Ware. Two primary human prostate epithelial and one primary human prostate stromal cell line were obtained from Clonetics/BioWhittaker (San Diego, CA) and grown in complete prostate epithelial and stromal growth medium provided by the supplier. Except where noted, other cell lines were grown in RPMI1640 supplemented with 10% fetal bovine serum and gentamycin (Gibco BRL) to 70-80% confluence and subjected to serum starvation as described (14-16), or maintained in fresh complete media, supplemented with 10% FBS.

[00169] RNA extraction. For gene expression analysis, cells were harvested in lysis buffer 2 hrs after the last media change at 70-80% confluence and total RNA or mRNA was extracted using the RNeasy (Qiagen, Chatsworth, CA) or FastTract kits (Invitrogen, Carlsbad, CA). Cell lines were not split more than 5 times, except where noted.

and sublines (Table 1) were developed by surgical orthotopic implantation as previously described (An, Z., Wang, X., Geller, J., Moossa, A.R., Hoffman, R.M. Surgical orthotopic implantation allows high lung and lymph node metastatic expression of human prostate carcinoma cell line PC-3 in nude mice. Prostate 1998;34:169-74, incorporated herein by reference). Briefly, 2 x 10<sup>6</sup> cultured PC3 cells, PC3M cells, or PC3M sublines were injected subcutaneously into male athymic mice, and allowed to develop into firm palpable and visible tumors over the course of 2 - 4 weeks. Intact tissue was harvested from a single subcutaneous tumor and surgically implanted in the ventral lateral lobes of the prostate gland in a series of six athymic mice per cell line subtype. The mice were examined periodically for suprapubic masses, which appeared for all subline cell types, in the order PC3MLN4 >PC3M>>PC3. Tumor-bearing mice were sacrificed by CO<sub>2</sub> inhalation over dry ice and necropsy was carried out in a  $2-4^{\circ}$ C cold room. Typically, bilaterally symmetric prostate gland tumors in the shape of greatly distended prostate glands were apparent. Prostate tumor tissue was excised and snap frozen in liquid nitrogen. The elapsed time from sacrifice to snap freezing was < 20 min. A systematic gross and microscopic post mortem examination was carried out. [00171] Tissue processing for mRNA isolation. Fresh frozen orthotopic tumor was

Orthotopic xenografts. Orthotopic xenografts of human prostate PC3 cells

[00170]

[00171] Tissue processing for mRNA isolation. Fresh frozen orthotopic tumor was examined by use of hematoxylin and eosin stained frozen sections. Orthotopic tumors of all sublines exhibited similar morphology consisting of sheets of monotonous closely packed tumor cells with little evidence of differentiation interrupted by only occasional zones of largely stromal components, vascular lakes, or lymphocytic infiltrates.

Fragments of tumor judged free of these non-epithelial clusters were used for mRNA

preparation. Frozen tissue (1 - 3 mm x 1 - 3 mm) was submerged in liquid nitrogen in a ceramic mortar and ground to powder. The frozen tissue powder was dissolved and immediately processed for mRNA isolation using a Fast Tract kit for mRNA extraction (Invitrogen, Carlsbad, CA, see above) according to the manufacturers instructions. Affymetrix arrays. The protocol for mRNA quality control and gene [00172] expression analysis was that recommended by the array manufacturer, Affymetrix, Inc. (Santa Clara, CA <a href="http://www.affymetrix.com">http://www.affymetrix.com</a>). In brief, approximately one microgram of mRNA was reverse transcribed with an oligo(dT) primer that has a T7 RNA polymerase promoter at the 5' end. Second strand synthesis was followed by cRNA production incorporating a biotinylated base. Hybridization to Affymetrix Hu6800 arrays representing 7,129 transcripts or Affymetrix U95Av2 array representing 12,626 transcripts overnight for 16 h was followed by washing and labeling using a fluorescently labeled antibody. The arrays were read and data processed using Affymetrix equipment and software (Lockhart, D. J., Dong, H., Byrne, M. C., Follettie, M. T., Gallo, M. V., Chee, M. S., Mittmann, M., Wang, C., Kobayashi, M., Horton, H. and Brown, E. L. Expression monitoring by hybridization to high-density oligonucleotide arrays [see comments]. Nat. Biotechnol. 1996;14:1675-80, incorporated herein by reference). Detailed protocols for data analysis and documentation of the sensitivity, reproducibility and other aspects of the quantitative microarray analysis using Affymetrix technology have been reported (Lockhart, D. J., Dong, H., Byrne, M. C., Follettie, M. T., Gallo, M. V., Chee, M. S., Mittmann, M., Wang, C., Kobayashi, M., Horton, H. and Brown, E. L. Expression monitoring by hybridization to high-density oligonucleotide arrays [see comments]. Nat. Biotechnol. 1996;14:1675-80, incorporated herein by reference).

[00173] To determine the quantitative difference in the mRNA abundance levels between two samples, in each individual sample for each gene the average expression differences were calculated from intensity measurements of perfect match (PM) probes minus corresponding control probes representing a single nucleotide mismatch (MM) oligonucleotides for each gene-specific set of 20 PM/MM pairs of oligonucleotides, after discarding the maximum, the minimum, and any outliers beyond 3 standard deviations (SD) from the average. The averages of pairwise comparisons for each individual gene were made between the samples, and the corresponding expression difference calls (see below) were made with Affymetrix software. Microsoft Access was used for other aspects of data management and storage. For each gene, a matrix-based decision concerning the difference in the mRNA abundance level between two samples was made by the software and reported as a "Difference call" (No change (NC), Increase (I), Decrease (D), Marginal increase (MI), and Marginal decrease (MD)) and the corresponding fold change ratio was calculated. 40-50% of the surveyed genes were called present by the Affymetrix software in these experiments. The concordance analysis of differential gene expression across the data set was performed using Microsoft Access and Affymetrix MicroDB software. For experiments involving study of prostate cancer, three of the normal prostate epithelial (NPE) microarrays are used as controls, and referred to as the NPE expression profile. Thus, when a gene is required to show a 2fold or greater change relative to NPE, this must occur in all three microarrays, for either positive or negative changes. These stringent criteria exclude genes for which one of the three microarrays is in error. The strategy in this study is based on the idea that expression differences will not be called by chance in the same direction in multiple

arrays (see below for statistical justification). Each gene in the final list of the 214 differentially expressed genes was required to be called exclusively as either concordantly up- or down-regulated in 30 separate comparisons (5 prostate cancer cell lines x 2 experimental serum conditions x 3 NPE controls) or 15 separate comparisons (5 prostate cancer cell lines x 1 experimental serum condition x 3 NPE controls). Statistical analysis and quality performance criteria. We used a stringent [00174] analytical approach to test the hypothesis that there are common genes with altered mRNA abundance levels whish appear to be significantly associated with the studied phenotypes. The Affymetrix MicroDB and Affymetrix DMT software was used to identify in any given comparison of two chips only genes that are determined to be expressed at statistically significantly different (p<0.05) levels. These transcripts are called as differentially expressed. To be included in our final differentially regulated gene class the given transcript was required to be determined as differentially regulated in the same direction (up or down) at the statistically significant levels (p<0.05) e.g., in 30 independent comparisons (5 experimental cell lines X 2 experimental conditions X 3 control cell lines). To be recognized as differentially regulated in the orthotopic tumors any given gene of the PC3/LNCap consensus class was required to be determined differentially regulated in the same direction at the statistically significant level (p<0.05) in 18 additional independent comparisons (6 orthotopic tumors X 3 controls). Despite

that identified set of 214 genes is differentially expressed in described experimental

systems with the extremely high level of confidence, we carried out Q-PCR confirmation

analysis for a sub-set of identified genes and confirmed their differential expression in all

instances using an additional independent normal human prostate epithelial cell line as a control.

[00175] Quality performance criteria adopted for the Affymetrix GeneChip system and applied in this study. 40-50% of the surveyed genes were called present by the Affymetrix software in these experiments. This is at the high end of the required standard adopted in many peer-reviewed publications using the same experimental system. Transcripts that are called present by the Affymetrix software in any given experiment were determined to have the signal intensities higher in the perfect match probe sets compared to single-nucleotide mismatch probe sets and background at the statistically significant level. This analysis was performed for each individual transcript using unique set of 20 perfect matches versus 20 single nucleotide mismatch probes. In our final list of 214 genes all transcripts were called present in at least one experimental setting. The inclusion error associated with two mRNA samples from identical cell lines was 2.7% for a difference called by the Affymetrix software. Thus, two independently obtained mRNA from the same cell lines will have 2.7% false positives. When a third independently derived epithelial cell line was included, only 4 genes (0.06%) out of 7,129 were called differentially expressed. The expression profiles of the normal prostate epithelial cell lines used in our experiments were determined to be indistinguishable. Therefore, controls are not likely source of errors in gene expression analysis performed in this study. This is particularly important, since the strategy adopted in this study is based on the idea that expression differences will not be called statistically significant by chance in the same direction in multiple arrays and during multiple independent comparisons of different phenotypes and variable experimental conditions. To impose

additional stringent restrictions on possibility of a gene to be detected as concordantly differentially regulated by chance, we apply the use of multiple experimental models and vastly variable experimental settings such as in vitro and in vivo growth and varying growth conditions. Similar strategy for identification of consistent gene expression changes based on a concordant behavior of the differentially regulated genes using Affymetrix GeneChip system and software was applied and validated in several peerreviewed published papers (see for example, Lee CK, Klopp, RG, Weindruch, R, Prolla, TA. Gene expression profile of aging and its retardation by caloric restriction. Science 1999; 285: 1390-1393; Ishida, S, Huang, E, Zuzan, H, Spang, R, Leone, G, West, M, Nevins, JR. Role for E2F in control of both DNA replication and mitotic function as revealed from DNA microarray analysis. Mol Cell Biol 2001; 21: 4684-4699, incorporated herein by reference). We applied more stringent criteria in our study requiring a concordance in at least 30 of 30 experiments compared to 6 of 6 comparisons in (Lee CK, Klopp, RG, Weindruch, R, Prolla, TA. Gene expression profile of aging and its retardation by caloric restriction. Science 1999; 285: 1390-1393, incorporated herein by reference); and 4 of 6 comparisons in (Ishida, S, Huang, E, Zuzan, H, Spang, R, Leone, G, West, M, Nevins, JR. Role for E2F in control of both DNA replication and mitotic function as revealed from DNA microarray analysis. Mol Cell Biol 2001; 21: 4684-4699, incorporated herein by reference). Ishida, et al. (Ishida, S, Huang, E, Zuzan, H, Spang, R, Leone, G, West, M, Nevins, JR. Role for E2F in control of both DNA replication and mitotic function as revealed from DNA microarray analysis. Mol Cell Biol 2001; 21: 4684-4699, incorporated herein by reference) provided a formal statistical

justification that four or more concordant calls out of six comparisons cannot be explained by chance, with the probability in the range of 1 in 10<sup>-4</sup>.

[00176] Q-PCR confirmation analysis of the differentially regulated genes. To confirm differential regulation of the transcripts comprising a PC3/LNCap-consensus class using an independent method a sample of 14 genes (12 up-regulated and 2 down-regulated) was tested using Q-PCR on an ABI7900 according to the vendor's recommended protocols (available at

http://www.appliedbiosystems.com/support/tutorials/). This PCR experiment used a further new batch of RNA from a third normal human prostate epithelial cell line and human transcript-specific pairs of PCR primers.

### **EXAMPLE 1 - CLASSIFICATION OF HUMAN PROSTATE TUMORS**

## A. General

[00177] A first reference set for human prostate tumors was obtained by obtaining gene expression data from five prostate cancer cell lines (cell lines used were LNCapLN3; LNCapPro5; PC3M; PC3MLN4; PC3Mpro4; see Table 1) and two different normal human prostate epithelial cell lines were obtained from Clonetics/BioWhittaker (San Diego, CA) and grown in complete prostate epithelial growth medium provided by the supplier. An original and a replicate data set was obtained for the first normal cell line, and the second cell line represented an independent data set from an independent epithelial cell line. Each of the tumor cell lines was derived from aggressively metastatic human prostate tumors. Consequently, we expected that these tumor cell lines should have an "invasive" phenotype because had they not been "invasive," they would not have penetrated the prostate capsule, a step pre-requisite to metastasis.

[00178] The expression data were obtained using an Affymetrix Human Genome-U95Av2 ("HG-U95Av2") expression array chip (Affymetrix, Santa Clara, CA). The HG-U95Av2 Array represents approximately 10,000 full-length genes. Data were obtained from the HG-U95Av2 according to the manufacturer's suggested protocols, as outlined in the Materials & Methods Section above

[00179] The original data set thus comprised a total of eight separate sets of gene expression data, five from the set of tumor cell lines and three from the set of epithelial cell lines. Fifteen separate pairwise comparisons were carried out to identify a first reference set of genes that were differentially expressed in the tumor cell lines and the epithelial cell lines. Differential expression was determined using Affymetrix's Microarray Suite software (versions 4.0 and 5.0). To be included in the first reference set, a candidate gene needed to meet two criteria: 1) the candidate gene was shown to be differentially expressed in each of the 15 pairwise comparisons; and 2) the direction of the differential (*i.e.* greater expression in the tumor cell lines *cf.* the epithelial cell lines or *vice-versa*) was consistent in each of the 15 pairwise comparisons. The first reference set comprised of 629 genes.

### B. Recurrence Predictor Cluster and Sample Classification

[00180] The methods of the invention were used to identify gene clusters associated with increased likelihood of tumor recurrence. A second reference set was obtained using expression data obtained from clinical human prostate tumor samples. These data were the supplemental data reported in Singh, D., Febbo, P.G., et al., "Gene Expression Correlates of Clinical Prostate Cancer Behavior," Cancer Cell March 2002 1:203-209, incorporated herein by reference. The clinical human prostate tumor samples were

divided into two groups, recurrent and non-recurrent, as reported in Singh, et al. (2002).

Data from twenty-one patients were evaluable with respect to recurrence following surgery. Recurrence was defined as two successive PSA values > 0.2ng/ml. Of the twenty-one patients, eight had recurrences, and thirteen patients remained relapse-free for at least four years.

[00181] Affymetrix MicroDB (version 3.0) and Affymetrix Data Mining Tools (DMT) (version 3.0) data analysis software were used to identify genes that were differentially regulated in recurrence group compared to relapse-free group of patients at the statistically significant level (p<0.05; Student T-test). Candidate genes were included in the second reference set if they were identified by the DMT software as having p values of 0.05 or less both for up-regulated and down-regulated genes. 316 genes were identified as being members of the second reference set.

[00182] A concordance set of genes was identified from the first and second reference sets. Genes were included in the concordance set if they met the following criteria: 1) the gene was identified as a member of both the first and the second reference sets; and 2) the direction of the differential was consistent in the first and the second reference sets (*i.e.*, the gene transcript was more abundant in the tumor cell lines *cf*. the control cell lines and more abundant in the recurrent *cf*. the non-recurrent samples, or the gene transcript was less abundant in the tumor cell lines *cf*. the control cell lines and less abundant in the recurrent *cf*. the non-recurrent samples). The first criterion provides a way of minimizing the number of genes for which the pairwise comparisons are carried out for the sample data. Only those genes that are members of the first reference set need to be compared for generating the second reference set because the first criterion requires that the

candidate gene be a member of both the first and second reference sets. The concordance set comprises of 19 genes.

The minimum segregation set was obtained as follows. For each gene in the [00183] concordance set, the -fold expression changes (as determined by the ratio of the relative transcript abundance levels) was determined. This was done for the cell line data by computing for each gene in the concordance set the ratio of the average expression in the tumor cell lines to the average expression in the control cell lines, and similarly the ratio of the average expression in the samples obtained from patients who relapsed (recurrent population) from those who did not relapse (non-recurrent population). Using the notation described above, this corresponds to calculating <expression><sub>1</sub>/<expression><sub>2</sub> for the cell line and clinical samples data. For the cell line data, <expression>1 corresponds to the average expression value for gene x over all tumor cell lines and <expression>2 corresponds to the average expression value for gene x over all control cell lines. For the clinical sample data, <expression>1 corresponds to the average expression value for gene x over all samples from patients who relapsed and <expression>2 corresponds to the average expression value for gene x over all samples from patients who did not relapse.

[00184] The –fold expression change data were log<sub>10</sub> transformed and the transformed data were entered as two arrays in a Microsoft Excel spreadsheet. The Excel CORREL function was used to generate a correlation coefficient that characterizes the degree to which the concordance set –fold expression changes were correlated between the cell line and clinical sample data. Typically, we observe correlation coefficients at this stage of the analysis in the range of about 0.7 to about 0.9. A scatter plot showing the relationship

between the log-transformed –fold expression changes in the cell line and clinical sample data is shown in Fig. 1. In the scatter plot, each point represents an individual gene belonging to the concordance set. The correlation coefficient for this concordance set was 0.777.

[00185] A minimum segregation set was selected from the concordance set. This set was chosen by looking at the scatter plot (Fig. 1) and manually selecting sub-sets of genes within the concordance set whose representative points fell closest to an imaginary regression line drawn through the data. Of course, this procedure can be automated. A second correlation coefficient was calculated using the Microsoft Excel CORREL function for several sub-sets of genes within the concordance set to arrive at a highly-correlated sub-set. These genes are members of the minimum segregation set, and represent genes whose −fold expression changes are most highly correlated between the cell line and clinical sample data. Typically, we identified minimum segregation sets that comprised on the order of from about 3 to about 20 genes and that produced correlation coefficients on the order of ≥ 0.98.

[00186] Using this method, a total of nine genes was selected for the recurrence predictor minimum segregation set. This recurrence predictor minimum segregation set had a correlation coefficient of 0.995 for the cell line and sample –fold expression change differences. *See* Fig. 2. Members of this recurrence predictor minimum segregation set are shown in Table 5.

Table 5 – Prostate Tumor Recurrence Predictor Minimum Segregation Set.			
Affymetrix Probe Set ID	LocusLink Identifier <sup>1</sup>	Description <sup>2</sup>	
41435_at	8541	PPFIA3: protein tyrosine	
		phosphatase, receptor type,	
		f polypeptide (PTPRF),	
		interacting protein (liprin),	
		alpha 3	
33228_g_at	3588	IL10RB: interleukin 10	
		receptor, beta	
40522_at	2752	GLUL: glutamate-	
		ammonia ligase (glutamine	
		synthase)	
37026_at	1316	COPEB: core promoter	
		element binding protein	
33436_at	6662	SOX9: SRY (sex	
		determining region Y)-box	
		9 (campomelic dysplasia,	
		autosomal sex-reversal)	
39631_at	2013	EMP2: epithelial	
		membrane protein 2	

-

<sup>&</sup>lt;sup>1</sup> LocusLink provides a single query interface to curated sequence and descriptive information about genetic loci. It presents information on official nomenclature, aliases, sequence accessions, phenotypes, EC numbers, MIM numbers, UniGene clusters, homology, map locations, and related web sites. It may be accessed through the National Center for Biotechnology Information (NCBI) website at http://www.ncbi.nlm.nih.gov/LocusLink/.

<sup>&</sup>lt;sup>2</sup> The first entry in each cell of this column corresponds to the HUGO Gene Nomenclature Committee ("HGNC") Approved Symbol for the gene corresponding to the Affymetrix Probe Set and LocusLink Identifiers within the same row. Information for the subject gene, associated cDNA, mRNA, and protein sequences may be obtained using the LocusLink identifier or the HGNC Approved Symbol by querying the search page at http://www.ncbi.nlm.nih.gov/LocusLink. Note, the footnotes associated with Table 5 apply to every table in this specification that follows the same or similar format as Table 3 (*i.e.*, column 1 contains information on the Affymetrix Probe Set ID, column 2 contains the LocusLink Identifier, and column 3 contains the gene description.

1915_s_at	2353	FOS: v-fos FBJ murine osteosarcoma viral oncogene homolog
37286_at	3726	JUNB: jun B proto- oncogene
40448_at	7538	ZFP36: zinc finger protein 36, C3H type, homolog (mouse)

[00187] The recurrence predictor minimum segregation set was used to calculate a phenotype association indices for each of the twenty-one tumors removed from the patients described in Singh, *et al.* (2002) that were evaluated for recurrence. The phenotype association index was obtained by calculating for each individual tumor sample, the –fold expression change for each of the nine genes in the recurrence predictor minimum segregation set. The –fold expression change was calculated as:

expression/<expression<sub>1</sub> + expression<sub>2</sub>>

[00188] where "expression" is the observed expression level for gene x for the individual tumor, and "<expression<sub>1</sub> + expression<sub>2</sub>>" is the average gene expression level for gene x across the set of 21 tumors used to generate the recurrence predictor minimum segregation set. The –fold expression changes for these nine genes were log<sub>10</sub> transformed, the transformed data entered as an array in a Microsoft Excel spreadsheet, and the Excel CORREL function was used to generate a correlation coefficient between the individual tumor data array and the corresponding log<sub>10</sub> transformed data for the average –fold expression changes in the cell lines for the same nine genes (*i.e.*, log<sub>10</sub>(<expression><sub>1</sub>/<expression><sub>2</sub>). This second correlation coefficient is the phenotype association index. The phenotype association index has the surprising and unexpected

property of allowing the samples to be classified according to the sign of the index. Fig. 3 shows the phenotype association index for each of the twenty-one tumors classified using the recurrence predictor minimum segregation class described above. 7 out of 8 tumors associated with recurrences had positive association indices, while 11 out of 13 tumors associated with no recurrence had negative association indices. Thus, the method correctly classified 18/21 or 86% of the tumors.

# B-1. Prostate Cancer Predictor Clusters and Sample Classification

The methods of the invention were used to identify gene clusters associated [00189] with the presence of prostate carcinoma cells in a tissue sample compared to the adjacent normal tissue samples that were determined to be cancer cell free. The first reference data set was derived as described above in A. A second reference set was obtained using expression data obtained from clinical human prostate tumor samples. These data were two independent sets of the supplemental data reported in Welsh, J.B., et al., "Analysis of gene expression identifies candidate markers and pharmacological targets in prostate cancer," Cancer Research, 2001, 61: 5974-5978; and Singh, D., Febbo, P.G., et al., "Gene Expression Correlates of Clinical Prostate Cancer Behavior," Cancer Cell March 2002 1:203-209, incorporated herein by reference. The clinical human prostate tumor samples were divided into two groups, cancer samples and adjacent normal tissue samples, as reported in Welsh, et al. (2001). Data from twenty-five cancer samples (analysis of one tumor samples was carried out in duplicate) and nine adjacent normal tissue samples were used to identify the concordance gene set with high correlation coefficient and significant sample segregation power thus comprising genes with the properties of the minimum segregation class.

[00190] Genes were included in the concordance set if the direction of the differential was consistent in the first reference set and in the clinical samples (*i.e.*, the gene transcript was more abundant in the tumor cell lines *cf.* the control cell lines and more abundant in the cancer samples *cf.* the adjacent normal tissue (ANT) samples, or the gene transcript was less abundant in the tumor cell lines *cf.* the control cell lines and less abundant in the cancer samples *cf.* the ANT samples. The concordance set comprising 54 genes was identified with correlation coefficient 0.823. Members of this concordance set are shown in Table 6. When applied to individual clinical samples, this gene set yielded sample segregation power of 91%. 30 of 33 clinical samples were classified correctly; 9 of 9 ANT samples displayed negative phenotype association indices while 21 of 24 cancer samples had positive phenotype association indices (Figure 4).

Table 6. 54 genes of the prostate cancer/normal tissue concordant set.				
Affymetrix Probe	Affymetrix	UniGene	LocusLink	Description
Set ID (HuFL6800)	Probe Set ID	Identifier	Identifier	
	(U95Av2)			
U03735_f_at	34575_f_at	Hs.36978	MAGEA3	MAGE-3 antigen
				(MAGE-3) gene
L77701_at	40427_at	Hs.16297	COX17	COX17 mRNA
X70940_s_at	35175_f_at	Hs.2642	EEF1A2	mRNA for elongation
				factor 1 alpha-2
U33053_at	175_s_at	Hs.2499	PRKCL1	lipid-activated protein
				kinase PRK1 mRNA
L18920_f_at	34575_f_at	Hs.36980	MAGEA2	MAGE-2 gene exons 1-
				4
M77140_at	35879_at	Hs.1907	GAL	pro-galanin mRNA
X92896_at	40891_f_at	Hs.18212	DXS9879E	mRNA for ITBA2
				protein

L18877_f_at	34575_f_at	Hs.169246	MAGEA12	MAGE-12 protein gene
M77481_ma1_f_at	36302_f_at	Hs.72879	MAGEA12	antigen (MAGE-1)
				gene
U77413_at	38614_s_at	Hs.100293	OGT	O-linked GlcNAc
				transferase mRNA
U73514_at	40778_at	Hs.171280	HADH2	short-chain alcohol
				dehydrogenase
				(XH98G2) mRNA
U39840_at	37141_at	Hs.299867	HNF3A	hepatocyte nuclear
				factor-3 alpha (HNF-3
				alpha) mRNA
L41559_at	34352_at	Hs.3192	PCBD	pterin-4a-
				carbinolamine
				dehydratase (PCBD)
				mRNA
U90907_at	37961_at	Hs.88051	PIK3R3	clone 23907 mRNA
			•	sequence
D00860_at	36489_at	Hs.56	PRPS1	mRNA for
				phosphoribosyl
	1			pyrophosphate
				synthetase (EC 2.7.6.1)
				subunit I
U81599_at	40327_at	Hs.66731	HOXB13	homeodomain protein
				HOXB13 mRNA
M80254_at	40840_at	Hs.173125	PPIF	cyclophilin isoform
				(hCyP3) mRNA
HG1612-HT1612_at	36174_at	Hs.75061	MACMARCKS	Macmarcks
D85131_s_at	1764_s_at	Hs.7647	MAZ	mRNA for Myc-
				associated zinc-finger
				protein ofislet

U79274_at	31838_at	Hs.150555	HSU79274	clone 23733 mRNA
Z22548_at	39729_at	Hs.146354	PRDX2	thiol-specific
				antioxidant protein
				mRNA
HG4312-	36188_at	Hs.75113	GTF3A	Transcription Factor
HT4582_s_at				Ша
J04444_at	1160_at	Hs.289271	CYC1	cytochrome c-1 gene
X79865_at	39812_at	Hs.109059	MRPL12	Mrp17 mRNA
U37022_rna1_at	1942_s_at	Hs.95577	CDK4	cyclin-dependent
				kinase 4 (CDK4) gene
U07424_at	34291_at	Hs.23111	FARSL	putative tRNA
				synthetase-like protein
-				mRNA
U79287_at	40955_at	Hs.19555	PTOV1	clone 23867 mRNA
				sequence
M34338_s_at	241_g_at	Hs.76244	SRM	spermidine synthase
				mRNA
L37936_at	39659_at	Hs.340959	TSFM	nuclear-encoded
				mitochondrial
				elongation factor Ts
				(EF-Ts) mRNA
X07979_at	32808_at	Hs.287797	ITGB1	mRNA for fibronectin
				receptor beta subunit
X54232_at	33929_at	Hs.2699	GPC1	mRNA for heparan
				sulfate proteaglycan
				(glypican)
M55210_at	232_at	Hs.214982	LAMC1	laminin B2 chain
				(LAMB2) gene

S74017_at	853_at	Hs.155396	NFE2L2	Nrf2=NF-E2-like basic
				leucine zipper
				transcriptional activator
			,	[human
U90913_at	39416_at	Hs.12956	TIP-1	clone 23665 mRNA
				sequence
X52425_at	404_at	Hs.75545	IL4R	IL-4-R mRNA for the
				interleukin 4 receptor
U90878_at	36937_s_at	Hs.75807	PDLIM1	LIM domain protein
				CLP-36 mRNA
X86163_at	39310_at	Hs.250882	BDKRB2	mRNA for B2-
			,	bradykinin receptor
U73377_at	38118_at	Hs.81972	SHC1	p66shc (SHC) mRNA
Z29083_at	368_at	Hs.82128	TPBG	5T4 gene for 5T4
				Oncofetal antigen
M31013_at	39738_at	Hs.146550	МҮН9	nonmuscle myosin
				heavy chain (NMHC)
		;		mRNA
M77349_at	1385_at	Hs.118787	TGFBI	transforming growth
				factor-beta induced
				gene product (BIGH3)
				mRNA
U04636_rna1_at	1069_at	Hs.196384	PTGS2	cyclooxygenase-2
				(hCox-2) gene
X15414_at	36589_at	Hs.75313	AKR1B1	mRNA for aldose
				reductase (EC 1.1.1.2)
M65292_s_at	32249_at	Hs.278568	HFL1	factor H homologue
				mRNA

X07438_s_at	38634_at	Hs.101850	RBP1	DNA for cellular
				retinol binding protein
				(CRBP) exons 3 and 4
				/gb=X07438
				/ntype=DNA
				/annot=exon
X79882_at	38064_at	Hs.80680	MVP	lrp mRNA
M11433_at	38634_at	Hs.101850	RBP1	cellular retinol-binding
	,			protein mRNA
U60060_at	37743_at	Hs.79226	FEZ1	FEZ1 mRNA
X04412_at	32612_at	Hs.290070	GSN	mRNA for plasma
				gelsolin
X93510_at	32610_at	Hs.79691	RIL	mRNA for 37 kDa LIM
				domain protein
M12125_at	32313_at	Hs.300772	TPM2	fibroblast muscle-type
				tropomyosin mRNA
L13210_at	37754_at	Hs.79339	LGALS3BP	Mac-2 binding protein
				mRNA
M21186_at	35807_at	Hs.68877	CYBA	neutrophil cytochrome
				b light chain p22
				phagocyte b-
				cytochrome mRNA
L13720_at	1598_g_at	Hs.78501	GAS6	growth-arrest-specific
				protein (gas) mRNA

[00191] The minimum segregation set was obtained as follows. For each gene in the concordance set, the –fold expression changes (as determined by the ratio of the relative transcript abundance levels) was determined. This was done for the cell line data by computing for each gene in the concordance set the ratio of the average expression in the tumor cell lines to the average expression in the control cell lines, and similarly the ratio

of the average expression values in the samples obtained from cancer samples (malignant population) from those from ANT samples (non-malignant population). Using the notation described above, this corresponds to calculating <expression>1/<expression>2 for the cell line and clinical samples data. For the cell line data, <expression>1 corresponds to the average expression value for gene x over all tumor cell lines and <expression>2 corresponds to the average expression value for gene x over all control cell lines. For the clinical sample data, <expression>1 corresponds to the average expression value for gene x over all cancer samples and <expression>2 corresponds to the average expression value for gene x over all cancer samples and <expression>2 corresponds to the average expression value for gene x over all ANT samples.

[00192] The –fold expression change data were log<sub>10</sub> transformed and the transformed data were entered as two arrays in a Microsoft Excel spreadsheet. The Excel CORREL function was used to generate a correlation coefficient that characterizes the degree to which the concordance set –fold expression changes were correlated between the cell line and clinical sample data. Typically, we observe correlation coefficients at this stage of the analysis in the range of about 0.7 to about 0.9. A scatter plot showing the relationship between the log-transformed –fold expression changes in the cell line and clinical samples data for the 54 genes of a concordance set is shown in Fig. 5. In the scatter plot, each point represents an individual gene belonging to the concordance set. The correlation coefficient for this concordance set was 0.823.

[00193] A minimum segregation set was selected from the concordance set. This set was chosen by looking at the scatter plot (Fig. 5) and manually selecting sub-sets of genes within the concordance set whose representative points fell closest to an imaginary regression line drawn through the data. Of course, this procedure can be automated. A

second correlation coefficient was calculated using the Microsoft Excel CORREL function for several sub-sets of genes within the concordance set to arrive at a highly-correlated sub-set. These genes are members of the minimum segregation cluster, and represent genes whose –fold expression changes are most highly correlated between the cell line and clinical sample data. Typically, we identified minimum segregation clusters that comprised on the order of from about 3 to about 20 genes and that produced correlation coefficients on the order of  $\geq 0.98$ .

[00194] Using this method, a total of ten genes were selected for the prostate cancer/normal tissue predictor minimum segregation set 1 (*i.e.* cluster 1) and a total of five genes was selected for the prostate cancer/normal tissue minimum segregation set 2 (*i.e.*, cluster 2). These prostate cancer predictor minimum segregation clusters had a correlation coefficient of 0.995 (cluster 1) and 0.997 (cluster 2) for the cell line and sample –fold expression change differences. Members of these two prostate cancer minimum segregation clusters are shown in Table 7.

Table 7. The genes comprising prostate cancer minimum segregation set 1 (cluster 1) (ten genes) and minimum segregation set 2 (cluster 2) (five genes).					
10 genes (r =	= 0.995)				
Affymetrix	Affymetrix	Description	Short		
Probe Set	Probe Set ID Description				
ID	(HuFL6800)				
(U95Av2)					
1160_at	J04444_at	J04444 /FEATURE=cds	cytochrome c-1		
		/DEFINITION=HUMCYC1A Human			
		cytochrome c-1 gene, complete cds.			

U77413_at	Cluster Incl. U77413:Human O-linked	O-linked GlcNAc
	GlcNAc transferase mRNA, complete	transferase
	cds /cds=(265,3027) /gb=U77413	
	/gi=2266993 /ug=Hs.100293 /len=3084	
U39840_at	Cluster Incl. U39840:Human hepatocyte	hepatocyte
į	nuclear factor-3 alpha (HNF-3 alpha)	nuclear factor-3
	mRNA, complete cds /cds=(87,1508)	alpha (HNF-3
	/gb=U39840 /gi=1066121	alpha)
	/ug=Hs.105440 /len=2872	
L41559_at	Cluster Incl. AA631698:np79a08.s1	dimerization
	Homo sapiens cDNA /clone=IMAGE-	cofactor of
	1132502 /gb=AA631698 /gi=2554309	hepatocyte
	/ug=Hs.3192 /len=640	nuclear factor 1
		alpha (TCF1)
U81599_at	Cluster Incl. U57052:Human Hoxb-13	homeodomain
	mRNA, complete cds /cds=(54,908)	protein HOXB13
	/gb=U57052 /gi=1519039	
	/ug=Hs.66731 /len=1026	
Z22548_at	Cluster Incl. L19185:Human natural	peroxiredoxin 2
	killer cell enhancing factor (NKEFB)	
	mRNA, complete cds /cds=(124,720)	
	/gb=L19185/gi=440307/ug=Hs.146354	
	/len=980	
U07424_at	Cluster Incl. U07424:Human putative	phenylalanine-
	tRNA synthetase-like protein mRNA,	tRNA synthetase-
	complete cds /cds=(12,1538)	like
	/gb=U07424 /gi=2098578	
	/ug=Hs.23111 /len=1807	
	U39840_at  L41559_at  U81599_at	GlcNAc transferase mRNA, complete cds /cds=(265,3027) /gb=U77413 /gi=2266993 /ug=Hs.100293 /len=3084  U39840_at Cluster Incl. U39840:Human hepatocyte nuclear factor-3 alpha (HNF-3 alpha) mRNA, complete cds /cds=(87,1508) /gb=U39840 /gi=1066121 /ug=Hs.105440 /len=2872  L41559_at Cluster Incl. AA631698:np79a08.s1 Homo sapiens cDNA /clone=IMAGE-1132502 /gb=AA631698 /gi=2554309 /ug=Hs.3192 /len=640  U81599_at Cluster Incl. U57052:Human Hoxb-13 mRNA, complete cds /cds=(54,908) /gb=U57052 /gi=1519039 /ug=Hs.66731 /len=1026  Z22548_at Cluster Incl. L19185:Human natural killer cell enhancing factor (NKEFB) mRNA, complete cds /cds=(124,720) /gb=L19185 /gi=440307 /ug=Hs.146354 /len=980  U07424_at Cluster Incl. U07424:Human putative tRNA synthetase-like protein mRNA, complete cds /cds=(12,1538) /gb=U07424 /gi=2098578

36937_s_at	U90878_at	Cluster Incl. U90878:Homo sapiens	carboxy terminal
		carboxyl terminal LIM domain protein	LIM domain
		(CLIM1) mRNA, complete cds	protein 1
		/cds=(142,1131) /gb=U90878	
		/gi=2957144 /ug=Hs.75807 /len=1480	
38634_at	X07438_s_at	Cluster Incl. M11433:Human cellular	cellular retinol
	-	retinol-binding protein mRNA,	binding protein
		complete cds /cds=(125,532)	(CRBP)
		/gb=M11433 /gi=190947	
		/ug=Hs.101850 /len=716	
32313_at	M12125_at	Cluster Incl. M12125:Human fibroblast	tropomyosin 2
		muscle-type tropomyosin mRNA,	(beta)
		complete cds /cds=(118,972)	
		/gb=M12125 /gi=339951	
		/ug=Hs.180266 /len=1044	
5 genes (r =	0.998)		
36174_at	HG1612-	Cluster Incl. X70326:H.sapiens	Macmarcks
	HT1612_at	MacMarcks mRNA /cds=(13,600)	
		/gb=X70326 /gi=38434 /ug=Hs.75061	
		/len=1334	
39812_at	X79865_at	Cluster Incl. X79865:H.sapiens Mrp17	ribosomal proteir
:		mRNA /cds=(137,733) /gb=X79865	mitochondrial,
		/gi=1313961 /ug=Hs.109059 /len=1008	L12
39310_at	X86163_at	Cluster Incl. X86163:H.sapiens mRNA	bradykinin
		for B2-bradykinin receptor, 3	receptor B2
		/cds=(0,41) /gb=X86163 /gi=1220163	
		/ug=Hs.239809 /len=2582	

38634_at	M11433_at	Cluster Incl. M11433:Human cellular	retinol-binding
	}	retinol-binding protein mRNA,	protein 1, cellular
	<u> </u>	complete cds /cds=(125,532)	
		/gb=M11433 /gi=190947	
	1	/ug=Hs.101850 /len=716	
37743_at	U60060_at	Cluster Incl. U60060:Human FEZ1	fasciculation and
		mRNA, complete cds /cds=(99,1277)	elongation protein
		/gb=U60060/gi=1927201	zeta 1 (zygin I)
		/ug=Hs.79226 /len=1619	

[00195] The prostate cancer/normal tissue minimum segregation clusters were used to calculate phenotype association indices for each of the thirty-three samples from the patients described in Welsh, *et al.* (2001). The phenotype association index was obtained by calculating for each individual clinical sample, the –fold expression change for each of the ten and five genes in the prostate cancer predictor minimum segregation set 1 and 2. The –fold expression change was calculated as:

expression/<expression<sub>1</sub> + expression<sub>2</sub>>

[00196] where "expression" is the observed expression level for gene x for the individual tumor, and "<expression<sub>1</sub> + expression<sub>2</sub>>" is the average gene expression level for gene x across the set of 33 samples used to generate the prostate cancer predictor minimum segregation sets. The –fold expression changes for these ten and five genes were log<sub>10</sub> transformed, the transformed data entered as an array in a Microsoft Excel spreadsheet, and the Excel CORREL function was used to generate a correlation coefficient between the individual tumor data array and the corresponding log<sub>10</sub> transformed data for the average –fold expression changes in the cell lines for the same ten and five genes (*i.e.*, log<sub>10</sub>(<expression><sub>1</sub>/<expression><sub>2</sub>). This second correlation

coefficient is the phenotype association index. The phenotype association indices had the surprising and unexpected property of allowing the samples to be classified according to the sign of the index. Fig. 6 and Fig. 7 show the phenotype association index for each of the thirty-three samples classified using the prostate cancer/normal tissue minimum segregation sets described above. In both instances, using either cluster 1 (ten genes) or cluster 2 (five genes), 9 out of 9 ANT samples had negative association indices, while 21 out of 24 cancer samples had positive association indices. Thus, the method correctly classified 30/33 or 91% of the samples.

[00197] To test the performance of prostate cancer/normal tissue minimum segregation sets or clusters on independent data sets, we applied the method to classify 94 ANT and cancer samples described in Singh, D., Febbo, P.G., *et al.*, "Gene Expression Correlates of Clinical Prostate Cancer Behavior," *Cancer Cell* March 2002 1:203-209, incorporated herein by reference. This set of samples comprises of 47 cancer samples and 47 adjacent normal tissue samples obtained in each instances from the same patients. The phenotype association index was obtained by calculating for each individual clinical sample, the –fold expression change for each of the ten and five genes in the prostate cancer predictor minimum segregation set 1 and 2. The –fold expression change was calculated as:

expression/<expression<sub>1</sub> + expression<sub>2</sub>>

[00198] where "expression" is the observed expression level for gene x for the individual tumor, and "<expression<sub>1</sub> + expression<sub>2</sub>>" is the average gene expression level for gene x across the set of 94 samples. The -fold expression changes for these ten and five genes were log<sub>10</sub> transformed, the transformed data entered as an array in a Microsoft

Excel spreadsheet, and the Excel CORREL function was used to generate a correlation coefficient between the individual tumor data array and the corresponding  $\log_{10}$  transformed data for the average –fold expression changes in the cell lines for the same ten and five genes (i.e.,  $\log_{10}(\langle \text{expression} \rangle_1/\langle \text{expression} \rangle_2)$ .

[00199] Fig. 8 and Fig. 9 show the phenotype association index for each of the ninety-four samples classified using the prostate cancer predictor minimum segregation clusters described above. Using cluster 1 (ten genes), 34 of 47 ANT samples had negative association indices, while 40 of 47 cancer samples had positive association indices.

Thus, the method correctly classified 74/94 or 79% of the samples in independent data set. Using cluster 2 (five genes), 34 of 47 ANT samples had negative association indices, while 42 of 47 cancer samples had positive association indices. Thus, the method correctly classified 76/94 or 81% of the samples in an independent data set.

# C. Invasion Clusters and Sample Classification

[00200] The methods of the invention were used along with the data reported by Singh, et al. (2002) to identify gene clusters associated with an invasive phenotype. Invasive phenotype was assessed by determining the presence or absence of positive surgical margins. The same first reference set described above in part A was used to generate the concordance and minimum segregation sets for invasiveness. The second reference set was obtained following the procedures described above in part B, using the supplemental data reported in Singh, et al. (2002) for fourteen invasive and 38 non-invasive human prostate tumors. Thus, the second reference set was obtained by using the Affymetrix MicroDB (version 3.0) and Affymetrix Data Mining Tools (DMT) (version 3.0) data analysis software to identify genes that were differentially regulated in

invasion group compared to non-invasive group of patients at the statistically significant level (p<0.05; Student T-test). Candidate genes were included in the second reference set if they were identified by the DMT software as having p values of 0.05 or less both for up-regulated and down-regulated genes. 3869 genes were identified as being members of the second reference set.

[00201] The concordance set was obtained by selecting only those genes having a consistent direction of the differential in both the first and the second reference sets (i.e., greater gene expression in the tumor lines cf. the control lines and greater gene expression in the invasive tumor samples cf. the non-invasive tumor samples or viceversa). The concordance set comprised 104 genes with an overall correlation coefficient of 0.755 (Fig. 10).

[00202] A minimum segregation set was selected following the procedures described above in section B. A scatter plot was generated of the log<sub>10</sub> transformed average -fold expression change in the cell line and average –fold expression change in the sample data. For the clinical sample data, <expression><sub>1</sub> corresponds to the average expression value for gene x over all samples from patients who had invasive tumors and <expression><sub>2</sub> corresponds to the average expression value for gene x over all samples from patients who had non-invasive tumors. The overall correlation coefficient for the invasiveness concordance set was 0.755. The invasiveness concordance set is shown in Fig. 10.

[00203] A minimum segregation set was identified by selecting a subset of the highly correlated genes from the invasiveness concordance set. This minimum segregation set (invasion minimum segregation set 1 or invasion cluster 1) included 20 genes listed

below in Table 8. The overall correlation coefficient between the cell lines and clinical samples for invasion cluster 1 was 0.980. Figure 11 shows the scatter plot for invasion cluster 1.

Table 8 – Prostate Cancer Invasion Minimum Segregation Set 1.			
Affymetrix Probe Set ID	LocusLink Identifier	Description	
(U95Av2)			
33904_at	1365	CLDN3: claudin 3	
1842_at	2521	FUS: fusion, derived from	
		t(12;16) malignant	
		liposarcoma	
37741_at	5831	PYCR1: pyrroline-5-	
		carboxylate reductase 1	
36174_at	65108	MACMARCKS:	
	·	macrophage myristoylated	
		alanine-rich C kinase	
		substrate	
1287_at	142	ADPRT: ADP-	
		ribosyltransferase (NAD+;	
		poly (ADP-ribose)	
		polymerase)	
39729_at	7001	PRDX2: peroxiredoxin 2	
39020_at	10572	SIVA: CD27-binding	
		(Siva) protein	
40074_at	10797	MTHFD2: methylene	
		tetrahydrofolate	
		dehydrogenase (NAD+	
		dependent),	
		methenyltetrahydrofolate	
		cyclohydrolaşe	
	<u> </u>		

502_s_at	2709	GJB5: gap junction
- · · · · <u>-   -</u>		protein, beta 5 (connexin
		31.1)
41817_g_at	355	TNFRSF6: tumor necrosis
		factor receptor
		superfamily, member 6
40847_at	3675	ITGA3: integrin, alpha 3
		(antigen CD49C, alpha 3
		subunit of VLA-3
		receptor)
41641_at	578	BAK1: BCL2-
		antagonist/killer 1
40031_at	8626	TP63: tumor protein p63
38608_at	5099	PCDH7: BH-
		protocadherin (brain-heart)
38288_at	N/A [Genbank Accession	KRT6E: keratin 6E
	No. L42611]	
34853_at	2263	FGFR2: fibroblast growth
		factor receptor 2 (bacteria-
		expressed kinase,
		keratinocyte growth factor
		receptor, craniofacial
		dysostosis 1, Crouzon
		syndrome, Pfeiffer
	,	syndrome, Jackson-Weiss
		syndrome)

209_at	2263	FGFR2 fibroblast growth
		factor receptor 2 (bacteria-
		expressed kinase,
		keratinocyte growth factor
		receptor, craniofacial
}		dysostosis 1, Crouzon
		syndrome, Pfeiffer
		syndrome, Jackson-Weiss
		syndrome) 10q26
32719_at	27350	APOBEC3C:
		apolipoprotein B mRNA
		editing enzyme, catalytic
		polypeptide-like 3C
1898_at	3084	NRG1: neuregulin 1
115_at	2263	FGFR2: fibroblast growth
		factor receptor 2 (bacteria-
		expressed kinase,
		keratinocyte growth factor
		receptor, craniofacial
		dysostosis 1, Crouzon
		syndrome, Pfeiffer
·		syndrome, Jackson-Weiss
		syndrome)

[00204] Note that three entries in the table correspond to the same genes, i.e., 34853\_at, 209\_at, and 115\_at. They most likely represent the splice variants of the same gene (Hs.31989). According to Affymetrix annotation, the 34853\_at is an alternative splice 3 variant of the FGFR2.

[00205] Individual phenotype association indices were calculated for each of the 14 invasive and each of the 38 non-invasive human prostate tumors according to the

methods described in section B, above, using data for the 20 genes that make up invasion cluster 1. The phenotype association index for each tumor sample was calculated using the average –fold expression change data for the tumor cell line data and the individual – fold expression change data for the tumor sample. The data were log<sub>10</sub> transformed and a correlation coefficient (phenotype association index) was calculated. The results are shown in Fig. 12. Application of the classification method using invasion cluster 1 resulted in 12/14 invasive tumors having positively signed association indices, and so were correctly classified, while 21/38 of the non-invasive tumors had negative association indices and so were correctly classified. Thus, invasion cluster 1 accurately classified 33/52 = 63% of the tumors in this sample set.

[00206] The greatest percentage of misclassifications obtained using invasion cluster 1 involved false positives, *i.e.*, 17/38 = 44% of the non-invasive tumors were mis-classified as having an expression profile associated with the invasive phenotype. To improve the overall accuracy of the method, the sample set was re-structured so as to include data only from the twelve invasive tumors correctly classified using invasion cluster 1, and from the seventeen tumors mis-classified as false positives. (The false positives were considered to be non-invasive tumors (as, in fact they were) in carrying out the method steps to generate the second reference set, the concordance set, and the minimum segregation set.) Using this set of twenty-nine samples, another second reference set was generated by using the Affymetrix MicroDB (version 3.0) and Affymetrix Data Mining Tools (DMT) (version 3.0) data analysis software to identify genes that were differentially regulated in invasion group compared to non-invasive group of patients at the statistically significant level (p<0.05; Student T-test). Candidate genes were included

in the second reference set if they were identified by the DMT software as having p values of 0.05 or less both for up-regulated and down-regulated genes. 458 genes were identified as being members of the second reference set.

[00207] Once the second reference set was generated, it was used to generate a concordance set by applying the criterion that the direction of the differential was consistent in the cell line and the clinical sample data. That is, the concordance set included only those genes present in the first and second reference sets whose expression was always greater in the tumor cell line cf. the control cell line and always greater in the invasive tumor sample cf. the non-invasive tumor sample, or *vice-versa*. The concordance set comprised 23 genes (r = 0.809).

[00208] Once the concordance set was obtained using the data from the 29-member set of clinical samples, average expression values for genes within the concordance set were generated for the tumor cell lines, the control cell lines, the invasive tumors, and the non-invasive tumors. Average –fold expression changes were obtained, log<sub>10</sub> transformed, and used to generate scatter plots and first correlation coefficients, as described above. A second minimum segregation set (invasion cluster 2) was identified by selecting a subset of genes from the concordance set whose –fold expression changes were highly correlated in the cell line and clinical samples. Invasion cluster 2 included 12 genes, and had an overall correlation coefficient of 0.983. See Fig. 13. The genes that were selected as invasion cluster 2 (invasion minimum segregation set 2) are listed in Table 9.

Table 9 – Prostate Cancer Invasion Minimum Segregation Set 2.		
12 genes ( $r = 0.983$		
Affymetrix Probe	Description	
Set ID (U95Av2)		

1018_at	U81787 /FEATURE= /DEFINITION=HSU81787 Human Wnt10B
	mRNA, complete cds
38336_at	Cluster Incl. AB023230:Homo sapiens mRNA for KIAA1013
	protein, partial cds /cds=(0,3188) /gb=AB023230 /gi=4589675
	/ug=Hs.96427 /len=4783
41619_at	Cluster Incl. AL022398:dJ434O14.4 (Interferon Regulatory Factor 6)
	/cds=(68,1471) /gb=AL022398 /gi=3355547 /ug=Hs.11801
	/len=4077
33369_at	Cluster Incl. AI535653:P9-C4.T3.P9.D4 Homo sapiens cDNA, 3 end
	/clone_end=3 /gb=AI535653/gi=4449788/ug=Hs.223018/len=590
37978_at	Cluster Incl. D78177:Homo sapiens mRNA for quinolinate
	phosphoribosyl transferase, complete cds /cds=(0,893) /gb=D78177
	/gi=1060906 /ug=Hs.8935 /len=894
377_g_at	AB000220 /FEATURE= /DEFINITION=AB000220 Homo sapiens
	mRNA for semaphorin E, complete cds
39411_at	Cluster Incl. AL080156:Homo sapiens mRNA; cDNA
	DKFZp434J214 (from clone DKFZp434J214) /cds=(0,1081)
	/gb=AL080156 /gi=5262614 /ug=Hs.12813 /len=2697
38772_at	Cluster Incl. Y11307:H.sapiens CYR61 mRNA /cds=(223,1368)
	/gb=Y11307 /gi=2791897 /ug=Hs.8867 /len=2052
39248_at	Cluster Incl. N74607:za55a01.s1 Homo sapiens cDNA, 3 end
	/clone=IMAGE-296424 /clone_end=3 /gb=N74607 /gi=1231892
	/ug=Hs.234642 /len=487
41193_at	Cluster Incl. AB013382:Homo sapiens mRNA for DUSP6, complete
	cds /cds=(351,1496) /gb=AB013382 /gi=3869139 /ug=Hs.180383
	/len=2390
672_at-	J03764 /FEATURE=cds /DEFINITION=HUMPAIA Human,
	plasminogen activator inhibitor-1 gene, exons 2 to 9

39052_at	Cluster Incl. J00124:Homo sapiens 50 kDa type I epidermal keratin
	gene, complete cds /cds=(61,1479) /gb=J00124 /gi=186704
	/ug=Hs.117729 /len=1634

[00209] Individual phenotype association indices were calculated for each of the 12 invasive and each of the 17 non-invasive human prostate tumors used to generate invasion cluster 2 according to the methods described in section B, above, using data for the 12 genes that make up invasion cluster 2. The phenotype association index for each tumor sample was calculated using the average –fold expression change data for the tumor cell line data and the individual –fold expression change data for the tumor sample. The data were log<sub>10</sub> transformed and a correlation coefficient (phenotype association index) was calculated. The results are shown in Fig. 14. Application of the classification method using invasion cluster 2 resulted in 11/12 invasive tumors having positively signed association indices, and so were correctly classified, while 10/17 of the non-invasive tumors had negative association indices and so were correctly classified. There thus were 7 false positives identified using invasion cluster 2. Overall, invasion cluster 2 accurately classified 21/29 = 72% of the tumors in this sample set.

[00210] The method was iterated using the 11 properly classified invasive tumors and the 7 non-invasive tumors mis-classified as false positives using invasion cluster 2. Using the expression data from these 18 tumors (11 invasive and 7 non-invasive) and following the identical procedures as outlined above, a new second reference set of 449 genes, concordance set of 16 genes (r = 0.908), and minimum segregation set (minimum segregation set 3 or invasion cluster 3) were generated. Invasion cluster 3 includes the 10 genes listed in Table 10, and had an overall correlation coefficient of 0.998, as shown in Fig. 15.

Table 10	Table 10 - Prostate Cancer Invasion Minimum Segregation Set 3.		
10  genes  (r = 0.998)	3)		
Affymetrix Probe	Description		
Set ID (U95Av2)			
35704_at	Cluster Incl. X92814:H.sapiens mRNA for rat HREV107-like protein		
	/cds=(407,895) /gb=X92814 /gi=1054751 /ug=Hs.37189 /len=1070		
41850_s_at	Cluster Incl. U63825:Human hepatitis delta antigen interacting		
	protein A (dipA) mRNA, complete cds /cds=(28,636) /gb=U63825		
	/gi=1488313 /ug=Hs.66713 /len=879		
39072_at	Cluster Incl. L07648:Human MXI1 mRNA, complete cds		
	/cds=(208,894) /gb=L07648 /gi=506626 /ug=Hs.118630 /len=2400		
38771_at	Cluster Incl. D50405:Human mRNA for RPD3 protein, complete cds		
	/cds=(63,1511) /gb=D50405 /gi=1665722 /ug=Hs.88556 /len=2091		
34987_s_at	Cluster Incl. X79536:H.sapiens mRNA for hnRNPcore protein A1		
	/cds=(26,988) /gb=X79536 /gi=496897 /ug=Hs.151604 /len=1198		
37040_at	Cluster Incl. D42041:Human mRNA for KIAA0088 gene, partial cds		
	/cds=(0,2832) /gb=D42041 /gi=577294 /ug=Hs.76847 /len=3820		
851_s_at	S62539 /FEATURE= /DEFINITION=S62539 insulin receptor		
	substrate-1 [human, skeletal muscle, mRNA, 5828 nt]		
209_at	M94167 /FEATURE= /DEFINITION=HUMHERGC Human		
	heregulin-beta2 gene, complete cds		
936_s_at	Protein Phosphatase Inhibitor Homolog		
115_at	X14787 /FEATURE=cds /DEFINITION=HSTS Human mRNA for		
	thrombospondin		

[00211] As was done with the previous invasion clusters, individual phenotype association indices were calculated for each of the 11 invasive and each of the 7 non-invasive human prostate tumors used to generate invasion cluster 3 according to the methods described in section B, above, using data for the 10 genes that make up invasion cluster 3. The results are shown in Fig. 16. Application of the classification method

using invasion cluster 3 resulted in 10/11 invasive tumors having positively signed association indices, and so were correctly classified, while 7/7 of the non-invasive tumors had negative association indices and so were correctly classified. There thus were 0 false positives identified using invasion cluster 3. Overall, invasion cluster 3 accurately classified 17/18 = 94% of the tumors in this sample set.

[00212] Of the fourteen invasive tumors comprising the original data set, 10/14 = 71% scored positive phenotype association indices in all three invasion clusters, 3/14 = 21% scored positive phenotype association indices in two of the three invasion clusters, and 1/14 = 7% scored a positive phenotype association index in only a single of the three invasion clusters. These data are summarized in Table 11.

Tumor	Invasion Cluster 1	Invasion Cluster 2	Invasion Cluster 3	No. of Correction
T33	0	1	0	1
T46	0	1	1	2
T54	1	1	0	2
T58	1	0	1	2
T01	1	1	1	3
T10	1	1	1	3
T24	1	1	1	3
T29	1	1	1	3
T30	1	1	1	3
T32	1	1	1	3
T47	1	1	1	3
T57	1	1	1	3
T59	1	1	1	3
T62	1	1	1	3

No. Genes in	20	12	10	
Cluster				
Correlation	0.98	0.983	0.998	
Coefficient of				
Cluster				

Note: 1 = Positive phenotype association index;

0 =negative phenotype association index.

[00213] A similar analysis can be carried out for the 38 non-invasive tumors that comprised the original sample set. Of these thirty eight non-invasive tumors, 17/38 = 45% scored a positive phenotype association index in one of the three invasion clusters (one non-invasive tumor (T5) scored negatively in all three invasion clusters and included in this group), and 21/38 = 55% scored a positive phenotype association index in two of the three invasion clusters. These data are summarized in Table 12.

Table 12 - Class	Table 12 – Classification of Non-Invasive Prostate Tumors using Invasion Clusters 1-3.			
Tumor	Invasion	Invasion	Invasion	No. of Correct
	Cluster 1	Cluster 2	Cluster 3	Classifications
T5	0	0	0	3
T3	0	1	0	2
T6	Ö	1	0	2
T11	0	1	0	2
T15	0	1	0	2
T17	0	1	0	2
T18	0	1	0	2
T19	0	1	0	2
T20	0	1	0	2
T21	0	1	0	2
T22	0	1	0	2
T23	0	1	0	2
T26	0	1	0	2

T34	0	1	0	2
T41	0	1	0	2
T49	0	1	0	2
T55	1	0	0	2
T2	0	1	1	1
T4	1	1	0 ·	1
T13	0	1	1	1
T14	0	1	1	1
T16	1	0	1	1
T25	0	1	1	1
T27	1	1	0	1
T28	1	0	1	1
T31	1	0	1	1
T36	1	0	1	1
T37	1	1	0	1
T38	1	1	0	1
T39	0	1	1	1
T40	1	1	0	1
T42	1	1	0	1
T43	1	1	0	1
T45	1	0	1	1
T50	1	0	1	1
T53	1	0	1	1
T56	1	0	1	1
T60	1	0	1	1.
No. Genes in	20	12	10	
Cluster				
Correlation	0.98	0.983	0.998	
Coefficient of				
Cluster				

Note: 1 = Positive phenotype association index;

0 = negative phenotype association index.

[00214] Three of the invasive tumors scored positively in two of the three invasion clusters, and twenty-one of the non-invasive tumors also scored positively in two of the three invasion clusters. We iterated the method, as described above, using this group of three invasive and twenty-one non-invasive tumors to generate another second reference set, concordance set and minimum segregation set (minimum segregation set 4 or invasion cluster 4). The purpose of this experiment was to determine how well invasion cluster 4 could differentiate this set of three invasive and twenty-one non-invasive prostate tumors.

[00215] Invasion cluster 4 includes the 13 genes listed in Table 13, and had an overall correlation coefficient of 0.986, as shown in Fig. 17.

Table 13 – Prostate Cancer Invasion Minimum Segregation Set 4.			
13 genes ( $r = 0.9$	13 genes $(r = 0.986)$		
Affymetrix	Description		
Probe Set ID			
(U95Av2)			
1375_s_at	M32304 /FEATURE= /DEFINITION=HUMMET Human		
	metalloproteinase inhibitor mRNA, complete cds		
41393_at	Cluster Incl. AF003540:Homo sapiens Krueppel family zinc finger		
	protein (znfp104) mRNA, complete cds /cds=(45,1934)		
	/gb=AF003540 /gi=2384652 /ug=Hs.104382 /len=2394		
870_f_at	M93311 /FEATURE=cds /DEFINITION=HUMMETIII Human		
	metallothionein-III gene, complete cds		
39594_f_at	J04152 /FEATURE=mRNA /DEFINITION=HUMGA733A Human		
,	gastrointestinal tumor-associated antigen GA733-1 protein gene,		
	complete cds, clone 05516		

	· · · · · · · · · · · · · · · · · · ·
609_f_at	S62539 /FEATURE= /DEFINITION=S62539 insulin receptor
	substrate-1 [human, skeletal muscle, mRNA, 5828 nt]
40031_at	L33930 /FEATURE= /DEFINITION=HUMCD24B Homo sapiens
	CD24 signal transducer mRNA, complete cds and 3 region
38608_at	Cluster Incl. M10943:Human metallothionein-If gene (hMT-If)
	/cds=(0,185) /gb=M10943 /gi=187540 /ug=Hs.203936 /len=186
38288_at	AB000220 /FEATURE= /DEFINITION=AB000220 Homo sapiens
	mRNA for semaphorin E, complete cds
36883_at	Cluster Incl. L41827:Homo sapiens sensory and motor neuron derived
	factor (SMDF) mRNA, complete cds /cds=(500,1390) /gb=L41827
	/gi=862422 /ug=Hs.172816 /len=1860
36130_f_at	Cluster Incl. M74542:Human aldehyde dehydrogenase type III
	(ALDHIII) mRNA, complete cds /cds=(42,1403) /gb=M74542
	/gi=178401 /ug=Hs.575 /len=1636
35577_at	Cluster Incl. AF027866:Homo sapiens megsin mRNA, complete cds
	/cds=(364,1506) /gb=AF027866 /gi=3769372 /ug=Hs.138202
	/len=2249
32719_at	L20852 /FEATURE= /DEFINITION=HUMGLVR2X Human
	leukemia virus receptor 2 (GLVR2) mRNA, complete cds
291_s_at	Cluster Incl. U40038:Human GTP-binding protein alpha q subunit
	(GNAQ) mRNA, complete cds /cds=(42,1121) /gb=U40038
	/gi=1181670 /ug=Hs.180950 /len=1450
L	

[00216] As shown in Fig. 18, when phenotype association indices were calculated for this set of samples applying genes of the invasion cluster 4, 3/3 invasive and 16/21 non-invasive tumors were correctly classified. Overall, 19 of 24 (79%) samples in this data set were correctly classified. As one skilled in art may determine from the Fig. 18, adjustment of the discrimination threshold (requiring, e.g., a positive association index of at least about 0.4) would yield a more accurate classification close to 100% accuracy.

## D. Gleason Score Clusters and Sample Classifications

The methods of the invention were used along with the data reported by [00217] Singh, et al. (2002) to identify gene clusters capable of distinguishing tumor samples having a Gleason score of 6 or 7 (low grade tumors) from those having a Gleason score of 8 or 9 (high grade tumors). The same first reference set described above in part A was used to generate concordance and minimum segregation sets for Gleason score stratification. The second reference set was obtained following the procedures described above in part B, using the supplemental data reported in Singh, et al. (2002) for 46 low grade tumors and six high-grade tumors. Thus, the second reference set was generated by using the Affymetrix MicroDB (version 3.0) and Affymetrix Data Mining Tools (DMT) (version 3.0) data analysis software to identify genes that were differentially regulated in high grade group compared to low grade group of patients at the statistically significant level (p<0.05; Student T-test). Candidate genes were included in the second reference set if they were identified by the DMT software as having p values of 0.05 or less both for up-regulated and down-regulated genes. 2144 genes were identified as being members of the second reference set.

[00218] The concordance set was obtained by selecting only those genes having a consistent direction of the differential in both the first and the second reference sets (*i.e.*, greater gene expression in the tumor lines *cf.* the control lines and greater gene expression in the high grade *cf.* the low-grade tumor samples or *vice-versa*). The concordance set comprised 58 genes with an overall correlation coefficient equal to 0.823 (*see* Fig. 19).

[00219] A minimum segregation set was selected following the procedures described above in section B. A scatter plot was generated of the log<sub>10</sub> transformed average -fold

expression change in the cell line and average –fold expression change in the sample data. For the clinical sample data, <expression>1 corresponds to the average expression value for gene x over all samples from patients who had tumors with Gleason scores of 8 or 9 (high grade) and <expression>2 corresponds to the average expression value for gene x over all samples from patients who had tumors with Gleason scores of 6 or 7 (low grade). The overall correlation coefficient for the high grade concordance set was 0.823. The high grade concordance set is shown in Fig. 19.

[00220] A minimum segregation set was identified by selecting a subset of the highly correlated genes from the high grade concordance set. This minimum segregation set (Gleason Score 8/9 minimum segregation set 1 or high grade cluster 1) included 17 genes listed below in Table 14. The overall correlation coefficient between the cell lines and clinical samples for high grade cluster 1 was 0.986. Figure 20 shows the scatter plot for high grade cluster 1.

Table 14 – Prostate Cancer Gleason Score 8/9 Minimum Segregation Set 1.			
17 genes ( $r = 0.986$	17 genes $(r = 0.986)$		
Affymetrix Probe	Description		
Set ID (U95Av2)			
34801_at	Cluster Incl. AB014610:Homo sapiens mRNA for KIAA0710		
	protein, complete cds /cds=(203,3550) /gb=AB014610 /gi=3327233		
	/ug=Hs.4198 /len=4607		
35627_at	Cluster Incl. U40571:Human alpha1-syntrophin (SNT A1) mRNA,		
	complete cds /cds=(37,1554) /gb=U40571 /gi=1145727		
	/ug=Hs.31121 /len=2110		
33132_at	Cluster Incl. U37012:Human cleavage and polyadenylation		
	specificity factor mRNA, complete cds /cds=(51,4379) /gb=U37012		
	/gi=1045573 /ug=Hs.83727 /len=4463		

/gb=X79865 /gi=1313961 /ug=Hs.109059 /len=1008  34366_g_at Cluster Incl. AF042386:Homo sapiens cyclophilin-33B (CmRNA, complete cds /cds=(60,950) /gb=AF042386 /gi=28 /ug=Hs.33251 /len=1099  33436_at Cluster Incl. Z46629:Homo sapiens SOX9 mRNA /cds=(3 /gb=Z46629 /gi=758102 /ug=Hs.2316 /len=3923  1143_s_at Fibroblast Growth Factor Receptor K-Sam, Alt. Splice 3, 1 39407_at Cluster Incl. M22488:Human bone morphogenetic protein mRNA /cds=(29,2221) /gb=M22488 /gi=179499 /ug=Hs.1 /len=2487  1343_s_at S66896 /FEATURE= /DEFINITION=S66896 squamous c carcinoma antigen=serine protease inhibitor [human, mRNA]	
mRNA, complete cds /cds=(60,950) /gb=AF042386 /gi=28 /ug=Hs.33251 /len=1099  33436_at Cluster Incl. Z46629:Homo sapiens SOX9 mRNA /cds=(3 /gb=Z46629 /gi=758102 /ug=Hs.2316 /len=3923  1143_s_at Fibroblast Growth Factor Receptor K-Sam, Alt. Splice 3, I  39407_at Cluster Incl. M22488:Human bone morphogenetic protein mRNA /cds=(29,2221) /gb=M22488 /gi=179499 /ug=Hs.1 /len=2487  1343_s_at S66896 /FEATURE= /DEFINITION=S66896 squamous c	
/ug=Hs.33251 /len=1099  33436_at Cluster Incl. Z46629:Homo sapiens SOX9 mRNA /cds=(3 /gb=Z46629 /gi=758102 /ug=Hs.2316 /len=3923  1143_s_at Fibroblast Growth Factor Receptor K-Sam, Alt. Splice 3, I  39407_at Cluster Incl. M22488:Human bone morphogenetic protein mRNA /cds=(29,2221) /gb=M22488 /gi=179499 /ug=Hs.1 /len=2487  1343_s_at S66896 /FEATURE= /DEFINITION=S66896 squamous c	CYP-33)
Cluster Incl. Z46629:Homo sapiens SOX9 mRNA /cds=(3 /gb=Z46629 /gi=758102 /ug=Hs.2316 /len=3923  1143_s_at Fibroblast Growth Factor Receptor K-Sam, Alt. Splice 3, I  39407_at Cluster Incl. M22488:Human bone morphogenetic protein mRNA /cds=(29,2221) /gb=M22488 /gi=179499 /ug=Hs.1 /len=2487  1343_s_at S66896 /FEATURE= /DEFINITION=S66896 squamous c	828150
/gb=Z46629 /gi=758102 /ug=Hs.2316 /len=3923  1143_s_at Fibroblast Growth Factor Receptor K-Sam, Alt. Splice 3, I 39407_at Cluster Incl. M22488:Human bone morphogenetic protein mRNA /cds=(29,2221) /gb=M22488 /gi=179499 /ug=Hs.1 /len=2487  1343_s_at S66896 /FEATURE= /DEFINITION=S66896 squamous c	
Fibroblast Growth Factor Receptor K-Sam, Alt. Splice 3, I  Gluster Incl. M22488:Human bone morphogenetic protein mRNA /cds=(29,2221) /gb=M22488 /gi=179499 /ug=Hs.1 /len=2487  S66896 /FEATURE= /DEFINITION=S66896 squamous c	59,1888)
39407_at Cluster Incl. M22488:Human bone morphogenetic protein mRNA /cds=(29,2221) /gb=M22488 /gi=179499 /ug=Hs.1 /len=2487  S66896 /FEATURE= /DEFINITION=S66896 squamous c	
mRNA /cds=(29,2221) /gb=M22488 /gi=179499 /ug=Hs.1 /len=2487 1343_s_at S66896 /FEATURE= /DEFINITION=S66896 squamous c	K-Sam III
/len=2487  1343_s_at S66896 /FEATURE= /DEFINITION=S66896 squamous c	1 (BMP-1)
1343_s_at S66896 /FEATURE= /DEFINITION=S66896 squamous c	1274
·	
carcinoma antigen=serine protease inhibitor [human, mRN	ell
	IA, 1711
nt]	
2073_s_at L34058 /FEATURE= /DEFINITION=HUMCA13A Homo	sapiens
cadherin-13 mRNA, complete cds	
33272_at Cluster Incl. AA829286:of08a01.s1 Homo sapiens cDNA,	3 end
/clone=IMAGE-1420488 /clone_end=3 /gb=AA829286 /g	gi=2902385
/ug=Hs.181062 /len=559	
1440_s_at X83490 /FEATURE=exon /DEFINITION=HSFAS34 H.sa	apiens
mRNA for Fas/Apo-1 (clone pCRTM11-Fasdelta(3,4))	
32382_at Cluster Incl. AB015234:Homo sapiens mRNA for uroplak	in 1b,
complete cds /cds=(0,782) /gb=AB015234 /gi=3721857	
/ug=Hs.198650 /len=783	
988_at X16354 /FEATURE= /DEFINITION=HSTM1CEA Huma	n mRNA
for transmembrane carcinoembryonic antigen BGPa (form	erly TM1-
CEA)	
779_at D21337 /FEATURE= /DEFINITION=HUMCO Human m	
collagen	RNA for

39721_at	Cluster Incl. U09303:Human T cell leukemia LERK-2 (EPLG2)
	mRNA, complete cds /cds=(701,1741) /gb=U09303 /gi=1783360
	/ug=Hs.144700 /len=2895
37989_at	Cluster Incl. J03802:Human renal carcinoma parathgrad hormone-
	like peptide mRNA, complete cds /cds=(303,830) /gb=J03802
	/gi=190717 /ug=Hs.89626 /len=1595

[00221] Individual phenotype association indices were calculated for each of the six high grade and each of the 46 low grade human prostate tumors used to generate high grade cluster 1 according to the methods described in section B, above, using data for the 17 genes that make up high grade cluster 1 (data not shown). Application of the classification method using high grade cluster 1 resulted in 6/6 high grade tumors having positively signed association indices, and so were correctly classified, while 26/46 of the low grade tumors had negative association indices and so were correctly classified.

There thus were 20 false positives (*i.e.*, low grade tumors improperly classified as high grade tumors) identified using high grade cluster 1. Overall, high grade cluster 1 accurately classified 32/52 = 62% of the tumors in this sample set.

[00222] To improve the accuracy of the method, we selected from the concordance set of 58 genes additional minimum segregation sets and tested their ability to classify tumor samples. A second minimum segregation set was identified by selecting a smaller subset of the highly correlated genes from the high grade minimum segregation cluster 1. This minimum segregation set (Gleason Score 8/9 minimum segregation set 2 or high grade cluster 2) included 12 genes listed below in Table 15. The overall correlation coefficient between the cell lines and clinical samples for high grade cluster 2 was 0.994. Figure 21 shows the scatter plot for high grade cluster 2.

ostate Cancer Gleason Score 8/9 Minimum Segregation Set 2.
Description
Cluster Incl. AB014610:Homo sapiens mRNA for KIAA0710
protein, complete cds /cds=(203,3550) /gb=AB014610 /gi=3327233
/ug=Hs.4198 /len=4607
Cluster Incl. U40571:Human alpha1-syntrophin (SNT A1) mRNA,
complete cds /cds=(37,1554) /gb=U40571 /gi=1145727
/ug=Hs.31121 /len=2110
Cluster Incl. U37012:Human cleavage and polyadenylation
specificity factor mRNA, complete cds /cds=(51,4379) /gb=U37012
/gi=1045573 /ug=Hs.83727 /len=4463
Cluster Incl. X79865:H.sapiens Mrp17 mRNA /cds=(137,733)
/gb=X79865 /gi=1313961 /ug=Hs.109059 /len=1008
Cluster Incl. AF042386:Homo sapiens cyclophilin-33B (CYP-33)
mRNA, complete cds /cds=(60,950) /gb=AF042386 /gi=2828150
/ug=Hs.33251 /len=1099
Cluster Incl. D26579:Homo sapiens mRNA for transmembrane
protein, complete cds /cds=(9,2483) /gb=D26579 /gi=1864004
/ug=Hs.86947 /len=3236
Cluster Incl. AF099731:Homo sapiens connexin 31.1 (GJB5) gene,
complete cds /cds=(27,848) /gb=AF099731 /gi=4009521
/ug=Hs.198249 /len=1370
X84213 /FEATURE=cds /DEFINITION=HSCEBP1 H.sapiens BAK
mRNA for BCl-2 homologue
Cluster Incl. M92843:H.sapiens zinc finger transcriptional regulator
mRNA, complete cds /cds=(59,1039) /gb=M92843 /gi=183442
/ug=Hs.1665 /len=1746

39721_at	Cluster Incl. U09303:Human T cell leukemia LERK-2 (EPLG2)
	mRNA, complete cds /cds=(701,1741) /gb=U09303 /gi=1783360
, :	/ug=Hs.144700 /len=2895
36543_at	Cluster Incl. J02931:Human placental tissue factor (two forms)
}	mRNA, complete cds /cds=(111,998) /gb=J02931 /gi=339501
	/ug=Hs.62192 /len=2141
37989_at	Cluster Incl. J03802:Human renal carcinoma parathgrad hormone-
	like peptide mRNA, complete cds /cds=(303,830) /gb=J03802
,	/gi=190717 /ug=Hs.89626 /len=1595

[00223] Individual phenotype association indices were calculated for each of the six high grade and each of the 46 low grade human prostate tumors according to the methods described in section B, above, using data for the 12 genes that make up high grade cluster 2 (data not shown). Application of the classification method using high grade cluster 2 resulted in 6/6 high grade tumors having positively signed association indices, and so were correctly classified, while 30/46 of the low grade tumors had negative association indices and so were correctly classified. There thus were 16 false positives (*i.e.*, low grade tumors improperly classified as high grade tumors) identified using high grade cluster 2. Overall, high grade cluster 2 accurately classified 36/52 = 69% of the tumors in this sample set.

[00224] A third minimum segregation set was identified by selecting a smaller subset of the highly correlated genes from the high grade minimum segregation cluster 2. This minimum segregation set (Gleason Score 8/9 minimum segregation set 3 or high grade cluster 3) included the 7 genes listed below in Table 16. The overall correlation coefficient between the cell lines and clinical samples for high grade cluster 3 was 0.970 (Fig. 22).

ostate Cancer Gleason Score 8/9 Minimum Segregation Set 3.
Description
·
Cluster Incl. D26579:Homo sapiens mRNA for transmembrane
protein, complete cds /cds=(9,2483) /gb=D26579 /gi=1864004
/ug=Hs.86947 /len=3236
Cluster Incl. AF099731:Homo sapiens connexin 31.1 (GJB5) gene,
complete cds /cds=(27,848) /gb=AF099731 /gi=4009521
/ug=Hs.198249 /len=1370
X84213 /FEATURE=cds /DEFINITION=HSCEBP1 H.sapiens BAK
mRNA for BCl-2 homologue
Cluster Incl. M92843:H.sapiens zinc finger transcriptional regulator
mRNA, complete cds /cds=(59,1039) /gb=M92843 /gi=183442
/ug=Hs.1665 /len=1746
Cluster Incl. U09303:Human T cell leukemia LERK-2 (EPLG2)
mRNA, complete cds /cds=(701,1741) /gb=U09303 /gi=1783360
/ug=Hs.144700 /len=2895
Cluster Incl. J02931:Human placental tissue factor (two forms)
mRNA, complete cds /cds=(111,998) /gb=J02931 /gi=339501
/ug=Hs.62192 /len=2141
Cluster Incl. J03802:Human renal carcinoma parathgrad hormone-
like peptide mRNA, complete cds /cds=(303,830) /gb=J03802
/gi=190717 /ug=Hs.89626 /len=1595

[00225] Individual phenotype association indices were calculated for each of the six high grade and each of the 46 low grade human prostate tumors according to the methods described in section B, above, using data for the 7 genes that make up high grade cluster 3 (data not shown). Application of the classification method using high grade cluster 3 again resulted in 6/6 high grade tumors having positively signed association indices, and

so were correctly classified, while 17/46 of the low grade tumors had negative association indices and so were correctly classified. There thus were 29 false positives (*i.e.*, low grade tumors improperly classified as high grade tumors) identified using high grade cluster 3. Overall, high grade cluster 3 accurately classified 23/52 = 44% of the tumors in this sample set.

[00226] A summary of the accuracy with which the first three high grade clusters distinguished high grade (Gleason score 8 or 9) from low grade (Gleason score 6 or 7) tumors is provided in Table 17.

Table 17 – Cl	Table 17 - Classification of High Grade & Low Grade Prostate Tumors using			
	High Grade Clusters 1-3.			
Tumor	High Grade	High Grade	High Grade	No. of Correct
	Cluster 1	Cluster 2	Cluster 3	Classifications
	Gleason Sco	re 8 or 9 (high gr	ade) Tumors	
T26	1	1	1	3
T31	1	1	1	3
T45	1	1	1	3
T57	1	1	1	3
T58	1	1	1	3
T59	1	1	1	3
	Gleason Sco	re 6 or 7 (low gra	ade) Tumors	
T01	1	1	1	0
T02	0	0	1	2
T03	0	0	0	3
T04	0	0	0	3
T05	0	0	1	2
T06	0	0 .	0	3
T10	1	1	0	1

T13	T11	0	0	1	2
T14       0       0       1       2         T15       0       0       0       3         T16       1       0       0       2         T17       0       0       1       2         T18       0       0       1       2         T19       0       0       0       3         T20       0       0       0       3         T21       0       0       1       2         T22       0       0       0       3         T23       0       0       1       2         T24       0       0       1       2         T25       1       0       1       1         T27       0       0       0       3         T28       1       1       1       0         T29       1       1       1       0         T30       1       0       0       2         T32       0       0       0       3         T33       0       0       1       2         T34       0       0       1       2         T	<b>}</b>				
T15         0         0         0         3           T16         1         0         0         2           T17         0         0         1         2           T18         0         0         1         2           T19         0         0         0         3           T20         0         0         0         3           T21         0         0         1         2           T22         0         0         0         3           T23         0         0         1         2           T24         0         0         1         2           T25         1         0         1         1           T27         0         0         0         3           T28         1         1         1         0           T30         1         0         0         2           T32         0         0         0         3           T33         0         0         1         2           T34         0         0         1         2           T38         0         0	]				
T16         1         0         0         2           T17         0         0         1         2           T18         0         0         1         2           T19         0         0         0         3           T20         0         0         0         3           T21         0         0         1         2           T22         0         0         0         3           T23         0         0         1         2           T24         0         0         1         2           T25         1         0         1         1           T27         0         0         0         3           T28         1         1         1         0           T30         1         0         0         2           T30         1         0         0         3           T33         0         0         1         2           T34         0         0         1         2           T38         0         0         1         2           T39         0         0	T14	0	0	1	
T17       0       0       1       2         T18       0       0       1       2         T19       0       0       0       3         T20       0       0       0       3         T21       0       0       1       2         T22       0       0       0       3         T23       0       0       1       2         T24       0       0       1       2         T25       1       0       1       1         T27       0       0       0       3         T28       1       1       1       0         T29       1       1       1       0         T30       1       0       0       2         T32       0       0       0       3         T33       0       0       1       2         T34       0       0       1       2         T34       0       0       1       2         T38       0       0       1       2         T38       0       0       1       2         T	T15	0	0	0	
T18       0       0       1       2         T19       0       0       0       3         T20       0       0       0       3         T21       0       0       1       2         T22       0       0       0       3         T23       0       0       1       2         T24       0       0       1       2         T25       1       0       1       1         T27       0       0       0       3         T28       1       1       1       0         T29       1       1       1       0         T30       1       0       0       2         T32       0       0       0       3         T33       0       0       1       2         T34       0       0       1       2         T36       1       1       1       0         T37       0       0       1       2         T38       0       0       1       2         T39       0       0       1       2         T	T16	1	0	0	2
T19         0         0         0         3           T20         0         0         0         3           T21         0         0         1         2           T22         0         0         0         3           T23         0         0         1         2           T24         0         0         1         2           T25         1         0         1         1           T27         0         0         0         3           T28         1         1         1         0           T29         1         1         1         0           T30         1         0         0         2           T32         0         0         0         3           T33         0         0         1         2           T34         0         0         1         2           T36         1         1         1         0           T37         0         0         1         2           T38         0         0         1         2           T40         1         1	T17	0	0	1	2
T20       0       0       0       3         T21       0       0       1       2         T22       0       0       0       3         T23       0       0       1       2         T24       0       0       1       2         T25       1       0       1       1         T27       0       0       0       3         T28       1       1       1       0         T29       1       1       1       0         T30       1       0       0       2         T32       0       0       0       3         T33       0       0       1       2         T34       0       0       1       2         T34       0       0       1       2         T36       1       1       1       0         T37       0       0       1       2         T38       0       0       1       2         T39       0       0       1       2         T40       1       1       1       0         T	T18	0	0	1	2
T21       0       0       1       2         T22       0       0       0       3         T23       0       0       1       2         T24       0       0       1       2         T25       1       0       1       1         T27       0       0       0       3         T28       1       1       1       0         T29       1       1       1       0         T30       1       0       0       2         T32       0       0       0       3         T33       0       0       1       2         T34       0       0       1       2         T34       0       0       1       2         T36       1       1       1       0         T37       0       0       1       2         T38       0       0       1       2         T39       0       0       1       2         T40       1       1       1       0         T41       1       0       0       2         T	T19	0	0	0	3
T22       0       0       0       3         T23       0       0       1       2         T24       0       0       1       2         T25       1       0       1       1         T27       0       0       0       3         T28       1       1       1       0         T29       1       1       1       0         T30       1       0       0       2         T32       0       0       0       3         T33       0       0       1       2         T34       0       0       1       2         T34       0       0       1       2         T36       1       1       1       0         T37       0       0       1       2         T38       0       0       1       2         T39       0       0       1       2         T40       1       1       1       0         T41       1       0       0       2         T42       1       1       1       0         0	T20	0	0	0	3
T23       0       0       1       2         T24       0       0       1       2         T25       1       0       1       1         T27       0       0       0       3         T28       1       1       1       0         T29       1       1       1       0         T30       1       0       0       2         T32       0       0       0       3         T33       0       0       1       2         T34       0       0       1       2         T36       1       1       1       0         T37       0       0       1       2         T38       0       0       1       2         T39       0       0       1       2         T40       1       1       1       0         T41       1       0       0       2         T42       1       1       1       0         T43       1       1       1       0	T21	0	0	1	2
T24       0       0       1       2         T25       1       0       1       1         T27       0       0       0       3         T28       1       1       1       0         T29       1       1       1       0         T30       1       0       0       2         T32       0       0       0       3         T33       0       0       1       2         T34       0       0       1       2         T36       1       1       1       0         T37       0       0       1       2         T38       0       0       1       2         T39       0       0       1       2         T40       1       1       1       0         T41       1       0       0       2         T42       1       1       1       0         T43       1       1       1       0	T22	0	0	0	3
T25         1         0         1         1           T27         0         0         0         3           T28         1         1         1         0           T29         1         1         1         0           T30         1         0         0         2           T32         0         0         0         3           T33         0         0         1         2           T34         0         0         1         2           T36         1         1         1         0           T37         0         0         1         2           T38         0         0         1         2           T40         1         1         1         0           T41         1         0         0         2           T42         1         1         1         0           T43         1         1         1         0	T23	0	0	1	2
T27       0       0       0       3         T28       1       1       1       0         T29       1       1       1       0         T30       1       0       0       2         T32       0       0       0       3         T33       0       0       1       2         T34       0       0       1       2         T36       1       1       1       0         T37       0       0       1       2         T38       0       0       1       2         T39       0       0       1       2         T40       1       1       1       0         T41       1       0       0       2         T42       1       1       1       0         T43       1       1       1       0	T24	0	0	1	2
T28       1       1       1       0         T29       1       1       1       0         T30       1       0       0       2         T32       0       0       0       3         T33       0       0       1       2         T34       0       0       1       2         T36       1       1       1       0         T37       0       0       1       2         T38       0       0       1       2         T39       0       0       1       2         T40       1       1       1       0         T41       1       0       0       2         T42       1       1       1       1       0         T43       1       1       1       0       0	T25	1	0	1	1
T29       1       1       1       0         T30       1       0       0       2         T32       0       0       0       3         T33       0       0       1       2         T34       0       0       1       2         T36       1       1       1       0         T37       0       0       1       2         T38       0       0       1       2         T39       0       0       1       2         T40       1       1       1       0         T41       1       0       0       2         T42       1       1       1       0         T43       1       1       1       0	T27	0	0	0	3
T30       1       0       0       2         T32       0       0       0       3         T33       0       0       1       2         T34       0       0       1       2         T36       1       1       1       0         T37       0       0       1       2         T38       0       0       1       2         T39       0       0       1       2         T40       1       1       1       0         T41       1       0       0       2         T42       1       1       1       0         T43       1       1       1       0	T28	1	1	1	0
T32       0       0       0       3         T33       0       0       1       2         T34       0       0       1       2         T36       1       1       1       0         T37       0       0       1       2         T38       0       0       1       2         T39       0       0       1       2         T40       1       1       1       0         T41       1       0       0       2         T42       1       1       1       0         T43       1       1       1       0	T29	1	1	1	0
T33       0       0       1       2         T34       0       0       1       2         T36       1       1       1       0         T37       0       0       1       2         T38       0       0       1       2         T39       0       0       1       2         T40       1       1       1       0         T41       1       0       0       2         T42       1       1       1       0         T43       1       1       1       0	T30	1	0	0	2
T34       0       0       1       2         T36       1       1       1       0         T37       0       0       1       2         T38       0       0       1       2         T39       0       0       1       2         T40       1       1       1       0         T41       1       0       0       2         T42       1       1       1       0         T43       1       1       1       0	T32	0	0	0	3
T36       1       1       1       0         T37       0       0       1       2         T38       0       0       1       2         T39       0       0       1       2         T40       1       1       1       0         T41       1       0       0       2         T42       1       1       1       0         T43       1       1       1       0	T33	0	0	1	2
T37       0       0       1       2         T38       0       0       1       2         T39       0       0       1       2         T40       1       1       1       0         T41       1       0       0       2         T42       1       1       1       0         T43       1       1       1       0	T34	0	0	1	2
T38       0       0       1       2         T39       0       0       1       2         T40       1       1       1       0         T41       1       0       0       2         T42       1       1       1       0         T43       1       1       1       0	T36	1	1	1	0
T39       0       0       1       2         T40       1       1       1       0         T41       1       0       0       2         T42       1       1       1       0         T43       1       1       1       0	T37	0	0	1	2
T40     1     1     1     0       T41     1     0     0     2       T42     1     1     1     0       T43     1     1     1     0	T38	0	0	1	2
T41     1     0     0     2       T42     1     1     1     0       T43     1     1     1     0	T39	0	0	1	2
T42     1     1     1     0       T43     1     1     1     0	T40	1	1	1	0
T43 1 1 0	T41	1	0	0	2
	T42	1	1	1	0
T46 1 1 0 1	T43	1	1	1	0
1 · · · · · · · · · · · · · · · · · · ·	T46	1	1	0	1

T47	1	1	1	0
T49	0	0	1	2
T50	0	0	0	3
. T53	1	1	1	0
T54	1	1	1	0
T55	1	1	1	0
T56	1	1	0	1
T60	1	1	1	0
T62	1	1	0	1
No. Genes in	17	12	7	
Cluster				
Correlation	0.986	0.994	0.97	
Coefficient of				
Cluster				

Note: 1 = Positive phenotype association index;

0 = negative phenotype association index.

[00227] Since the overall classification accuracy of high grade cluster 3 was lower than that of high grade cluster 1 and 2, additional high grade clusters were generated from a high grade concordance set of 58 genes. The resulting alternative minimum segregation set (ALT high grade cluster) included a total of 38 genes listed below in Table 18. The overall correlation coefficient between the cell line and clinical samples for this high grade cluster (Gleason Score 8/9 ALT high grade cluster) was 0.929 (Fig. 23).

Phenotype association indices were calculated for each of the 6 high grade and each of the 46 low grade tumors to determine how well this high grade cluster would classify the samples. All six of the high grade tumors were correctly classified, while 26/46 of the low grade tumors were correctly classified. Thus overall, this minimum segregation set correctly classified 32/52 = 62% of the samples.

Table 18 – Prostate Cancer Gleason Score 8/9			
A	ALT High Grade Minimum Segregation Set (38 genes).		
38  genes  (r = 0.929)			
Affymetrix	Description		
Probe Set ID	· ·		
(U95Av2)			
34801_at	Cluster Incl. AB014610:Homo sapiens mRNA for KIAA0710 protein,		
	complete cds /cds=(203,3550) /gb=AB014610 /gi=3327233		
,	/ug=Hs.4198 /len=4607		
35627_at	Cluster Incl. U40571:Human alpha1-syntrophin (SNT A1) mRNA,		
	complete cds /cds=(37,1554) /gb=U40571 /gi=1145727 /ug=Hs.31121		
	/len=2110		
33132_at	Cluster Incl. U37012:Human cleavage and polyadenylation specificity		
	factor mRNA, complete cds /cds=(51,4379) /gb=U37012 /gi=1045573		
	/ug=Hs.83727 /len=4463		
39812_at	Cluster Incl. X79865:H.sapiens Mrp17 mRNA /cds=(137,733)		
	/gb=X79865 /gi=1313961 /ug=Hs.109059 /len=1008		
34366_g_at	Cluster Incl. AF042386:Homo sapiens cyclophilin-33B (CYP-33)		
	mRNA, complete cds /cds=(60,950) /gb=AF042386 /gi=2828150		
	/ug=Hs.33251 /len=1099		
32545_r_at	Cluster Incl. L12535:Human RSU-1/RSP-1 mRNA, complete cds		
	/cds=(827,1660) /gb=L12535 /gi=434050 /ug=Hs.75551 /len=2194		
35899_at	Cluster Incl. AF109401:Homo sapiens neurotrophic factor artemin		
	precursor (ARTN) mRNA, complete cds /cds=(298,960)		
	/gb=AF109401 /gi=4071352 /ug=Hs.194689 /len=1003		
32855_at	Cluster Incl. L00352:Human low density lipoprotein receptor gene		
	/cds=(93,2675) /gb=L00352 /gi=460289 /ug=Hs.213289 /len=5175		
41817_g_at	Cluster Incl. AL049851:Human DNA sequence from clone 889J22B		
	on chromosome 22q13.1 /cds=(0,1000) /gb=AL049851 /gi=4826526		
	/ug=Hs.57973 /len=1798		
<del></del>			

22426	Chater Incl. 746620 Home coming COVO mDNA (ada-(250 1999)
33436_at	Cluster Incl. Z46629:Homo sapiens SOX9 mRNA /cds=(359,1888)
	/gb=Z46629 /gi=758102 /ug=Hs.2316 /len=3923
41663_at	Cluster Incl. AF038202:Homo sapiens clone 23570 mRNA sequence
	/cds=UNKNOWN /gb=AF038202 /gi=2795923 /ug=Hs.12311
1	/len=1742
188_at	U09303 /FEATURE= /DEFINITION=HSU09303 Human T cell
	leukemia LERK-2 (EPLG2) mRNA, complete cds
38822_at	Cluster Incl. AB011420:Homo sapiens mRNA for DRAK1, complete
	cds /cds=(117,1361) /gb=AB011420 /gi=3834353 /ug=Hs.9075
	/len=2641
38913_at	Cluster Incl. U60319:Homo sapiens haemochromatosis protein (HLA-
	H) mRNA, complete cds /cds=(221,1267) /gb=U60319 /gi=1469789
	/ug=Hs.20019 /len=2716
1143_s_at	Fibroblast Growth Factor Receptor K-Sam, Alt. Splice 3, K-Sam III
40712_at	Cluster Incl. D26579:Homo sapiens mRNA for transmembrane
	protein, complete cds /cds=(9,2483) /gb=D26579 /gi=1864004
	/ug=Hs.86947 /len=3236
39407_at	Cluster Incl. M22488:Human bone morphogenetic protein 1 (BMP-1)
	mRNA /cds=(29,2221) /gb=M22488 /gi=179499 /ug=Hs.1274
	/len=2487
34044_at	Cluster Incl. AB007131:Homo sapiens mRNA for HSF2BP, complete
	cds /cds=(332,1336) /gb=AB007131 /gi=3345673 /ug=Hs.97624
	/len=1898
39320_at	Cluster Incl. U13697:Human interleukin 1-beta converting enzyme
	isoform beta (IL1BCE) mRNA, complete cds /cds=(0,1151)
	/gb=U13697 /gi=717039 /ug=Hs.2490 /len=1185
38608_at	Cluster Incl. AA010777:ze22f06.rl Homo sapiens cDNA, 5 end
	/clone=IMAGE-359747 /clone_end=5 /gb=AA010777 /gi=1471804
	/ug=Hs.99923 /len=521
L	<u></u>

35194_at	Cluster Incl. X53463:Human mRNA for glutathione peroxidase-like
	protein /cds=(51,623) /gb=X53463 /gi=31894 /ug=Hs.2704 /len=951
1343_s_at	S66896 /FEATURE= /DEFINITION=S66896 squamous cell
	carcinoma antigen=serine protease inhibitor [human, mRNA, 1711 nt]
2073_s_at	L34058 /FEATURE= /DEFINITION=HUMCA13A Homo sapiens
	cadherin-13 mRNA, complete cds
38903_at	Cluster Incl. AF099731:Homo sapiens connexin 31.1 (GJB5) gene,
	complete cds /cds=(27,848) /gb=AF099731 /gi=4009521
	/ug=Hs.198249 /len=1370
33272_at	Cluster Incl. AA829286:of08a01.s1 Homo sapiens cDNA, 3 end
	/clone=IMAGE-1420488 /clone_end=3 /gb=AA829286 /gi=2902385
	/ug=Hs.181062 /len=559
1687_s_at	X84213 /FEATURE=cds /DEFINITION=HSCEBP1 H.sapiens BAK
	mRNA for BCl-2 homologue
1440_s_at	X83490 /FEATURE=exon /DEFINITION=HSFAS34 H.sapiens
	mRNA for Fas/Apo-1 (clone pCRTM11-Fasdelta(3,4))
32382_at	Cluster Incl. AB015234:Homo sapiens mRNA for uroplakin 1b,
	complete cds /cds=(0,782) /gb=AB015234 /gi=3721857
	/ug=Hs.198650 /len=783
40448_at	Cluster Incl. M92843:H.sapiens zinc finger transcriptional regulator
	mRNA, complete cds /cds=(59,1039) /gb=M92843 /gi=183442
	/ug=Hs.1665 /len=1746
988_at	X16354 /FEATURE= /DEFINITION=HSTM1CEA Human mRNA
	for transmembrane carcinoembryonic antigen BGPa (formerly TM1-
,	CEA)
41481_at	Cluster Incl. X17033:Human mRNA for integrin alpha-2 subunit
	/cds=(48,3593) /gb=X17033 /gi=33906 /ug=Hs.1142 /len=5373
35444_at	Cluster Incl. AC004030:Homo sapiens DNA from chromosome 19,
	cosmid F21856 /cds=(0,2039) /gb=AC004030 /gi=2804590
	/ug=Hs.169508 /len=2040

779_at	D21337 /FEATURE= /DEFINITION=HUMCO Human mRNA for
	collagen
38746_at	Cluster Incl. AF011375:Homo sapiens integrin variant beta4E
	(ITGB4) mRNA, complete cds /cds=(0,2894) /gb=AF011375
	/gi=2293520 /ug=Hs.85266 /len=2895
32821_at	Cluster Incl. AI762213:wi54d04.x1 Homo sapiens cDNA, 3 end
	/clone=IMAGE-2394055 /clone_end=3 /gb=AI762213 /gi=5177880
	/ug=Hs.204238 /len=677
39721_at	Cluster Incl. U09303:Human T cell leukemia LERK-2 (EPLG2)
	mRNA, complete cds /cds=(701,1741) /gb=U09303 /gi=1783360
	/ug=Hs.144700 /len=2895
36543_at	Cluster Incl. J02931:Human placental tissue factor (two forms)
	mRNA, complete cds /cds=(111,998) /gb=J02931 /gi=339501
	/ug=Hs.62192 /len=2141
37989_at	Cluster Incl. J03802:Human renal carcinoma parathgrad hormone-like
	peptide mRNA, complete cds /cds=(303,830) /gb=J03802 /gi=190717
	/ug=Hs.89626 /len=1595

[00228] To further improve the overall classification accuracy, additional high grade clusters were generated by culling a subset of sample data made up of all the true positives (*i.e.*, the 6 high grade tumors correctly classified using each of the first three high grade clusters) and the set of 12 low grade tumors that scored as false positives in 3/3 of the first 3 high grade clusters (*i.e.*, all the Gleason score 6&7 tumors that had a "0" in the "No. of Correct Classifications" column in Table 15). This subset was used to generate another second reference set, and concordance set using the same procedures outlined above. From this concordance set of 33 genes (r = 0.731), a fourth minimum segregation set was identified by selecting a subset of the highly correlated genes from the new high grade concordance set. This minimum segregation set (Gleason Score 8/9)

minimum segregation set 4 or high grade cluster 4) included 5 genes listed below in Table 19. The overall correlation coefficient between the cell lines and clinical samples for high grade cluster 4 was 0.995. Figure 24 shows the scatter plot for high grade cluster 4.

Table 19 – Prostate Cancer Gleason Score 8/9 Minimum Segregation Set 4.			
5  genes  (r = 0.995)	5 genes $(r = 0.995)$		
Affymetrix Probe	Description		
Set ID (U95Av2)			
1733_at	M60315 /FEATURE= /DEFINITION=HUMTGFBC Human		
	transforming growth factor-beta (tgf-beta) mRNA, complete cds		
41850_s_at	Cluster Incl. U63825: Human hepatitis delta antigen interacting		
	protein A (dipA) mRNA, complete cds /cds=(28,636) /gb=U63825		
	/gi=1488313 /ug=Hs.66713 /len=879		
39020_at	Cluster Incl. U82938:Human CD27BP (Siva) mRNA, complete cds		
	/cds=(252,821) /gb=U82938 /gi=2228596 /ug=Hs.112058 /len=1034		
33436_at	Cluster Incl. Z46629:Homo sapiens SOX9 mRNA /cds=(359,1888)		
	/gb=Z46629 /gi=758102 /ug=Hs.2316 /len=3923		
988_at	X16354 /FEATURE= /DEFINITION=HSTM1CEA Human mRNA		
	for transmembrane carcinoembryonic antigen BGPa (formerly TM1-		
	CEA)		

[00229] Phenotype association indices were calculated using the average cell line and individual sample –fold change expression data for the genes in high grade cluster 4. The sample included the 6 high grade tumors and the set of 17 low grade tumors that scored as false positives in 2/3 or 3/3 of the first three high grade clusters (i.e., all the Gleason score 6&7 tumors that had a "0" or "1" in the "No. of Correct Classifications" column in Table 17).

[00230] High grade cluster 4 correctly classified 6/6 high grade tumors, and 12/17 low grade tumors. Overall, high grade cluster 4 accurately characterized 18/23 = 78% of the tumors in this set.

[00231] To improve the accuracy of the classification, several additional minimum segregation sets of highly correlated genes were selected. Gleason Score 8/9 minimum segregation set 5, or high grade cluster 5, was used to generate phenotype association indices for the 6 high grade tumors (true positives) and the set of 17 low grade tumors that scored as false positives in 2/3 or 3/3 of the first three high grade clusters (i.e., all the Gleason score 6&7 tumors that had a "0" or "1" in the "No. of Correct Classifications" column in Table 17). High grade cluster 5 correctly classified 6/6 high grade tumors and 9/17 low grade tumors. Overall, high grade cluster 5 correctly classified 15/23 = 65% of the samples in this set.

[00232] High grade cluster 5 included 4 genes listed below in Table 20. The overall correlation coefficient between the cell lines and clinical samples for high grade cluster 5 was 0.998. Figure 25 shows the scatter plot for high grade cluster 5.

Table 20 – Prostate Cancer Gleason Score 8/9 Minimum Segregation Set 5. 4 genes (r = 0.998)		
Cluster Incl. U63825:Human hepatitis delta antigen interacting		
protein A (dipA) mRNA, complete cds /cds=(28,636) /gb=U63825		
/gi=1488313 /ug=Hs.66713 /len=879		
Cluster Incl. U82938:Human CD27BP (Siva) mRNA, complete cds		
/cds=(252,821) /gb=U82938 /gi=2228596 /ug=Hs.112058 /len=1034		
Cluster Incl. Z46629:Homo sapiens SOX9 mRNA /cds=(359,1888)		
/gb=Z46629 /gi=758102 /ug=Hs.2316 /len=3923		

988_at	X16354 /FEATURE= /DEFINITION=HSTM1CEA Human mRNA
	for transmembrane carcinoembryonic antigen BGPa (formerly TM1-
	CEA)

[00233] High grade cluster 6 included 7 genes and had an overall correlation coefficient of 0.995 (Fig. 26). High grade cluster 7 included 13 genes and had an overall correlation coefficient of 0.992 (Fig. 27). High grade cluster 6 correctly classified 6/6 of the high grade tumors, and 13/17 of the low grade tumors. Overall, high grade cluster 6 correctly classified 19/23 = 83% of the samples in this set. High grade cluster 7 correctly classified 6/6 of the high grade tumors and 14/17 of the low grade tumors. Overall, high grade cluster 7 correctly classified 20/23 = 87% of the samples in this set. Tables 21 and 22 list the genes that make up high grade cluster 6 and high grade cluster 7. A summary of the accuracy with which high grade clusters 4 – 7 distinguished high grade (Gleason score 8 or 9) from the "false positive" subset of seventeen low grade (Gleason score 6 or 7) tumors is provided in Table 23.

Table 21 – Prostate Cancer Gleason Score 8/9 Minimum Segregation Set 6.					
7  genes  (r = 0.995)					
Affymetrix Probe Set ID (U95Av2)	Description				
1733_at	M60315 /FEATURE= /DEFINITION=HUMTGFBC Human transforming growth factor-beta (tgf-beta) mRNA, complete cds				
41850_s_at	Cluster Incl. U63825:Human hepatitis delta antigen interacting protein A (dipA) mRNA, complete cds /cds=(28,636) /gb=U63825 /gi=1488313 /ug=Hs.66713 /len=879				
39020_at	Cluster Incl. U82938:Human CD27BP (Siva) mRNA, complete cds /cds=(252,821) /gb=U82938 /gi=2228596 /ug=Hs.112058 /len=1034				

37026_at	Cluster Incl. AF001461:Homo sapiens Kruppel-like zinc finger protein Zf9 mRNA, complete cds /cds=(30,881) /gb=AF001461
	/gi=3378030 /ug=Hs.76526 /len=1354
32587_at	Cluster Incl. U07802:Human Tis11d gene, complete cds
	/cds=(291,1739) /gb=U07802 /gi=984508 /ug=Hs.78909 /len=3655
40448_at	Cluster Incl. M92843:H.sapiens zinc finger transcriptional regulator
	mRNA, complete cds /cds=(59,1039) /gb=M92843 /gi=183442
	/ug=Hs.1665 /len=1746
779_at	D21337 /FEATURE= /DEFINITION=HUMCO Human mRNA for
	collagen

Table 22 – Prostate Cancer Gleason Score 8/9 Minimum Segregation Set 7.						
13 genes $(r = 0.992)$						
Affymetrix Probe	Description					
Set ID (U95Av2)						
1733_at	M60315 /FEATURE= /DEFINITION=HUMTGFBC Human					
	transforming growth factor-beta (tgf-beta) mRNA, complete cds					
41850_s_at	Cluster Incl. U63825:Human hepatitis delta antigen interacting					
	protein A (dipA) mRNA, complete cds /cds=(28,636) /gb=U63825					
	/gi=1488313 /ug=Hs.66713 /len=879					
39020_at	Cluster Incl. U82938:Human CD27BP (Siva) mRNA, complete cds					
	/cds=(252,821) /gb=U82938 /gi=2228596 /ug=Hs.112058 /len=1034					
33936_at	Cluster Incl. D86181:Homo sapiens DNA for galactocerebrosidase					
	/cds=(146,2155) /gb=D86181 /gi=2897770 /ug=Hs.273 /len=3869					
39631_at	Cluster Incl. U52100:Human XMP mRNA, complete cds					
	/cds=(63,566) /gb=U52100 /gi=2474095 /ug=Hs.29191 /len=690					
38617_at	Cluster Incl. D45906:Homo sapiens mRNA for LIMK-2, complete					
	cds /cds=(114,2030) /gb=D45906 /gi=1805593 /ug=Hs.100623					
	/len=3668					

35703_at	Cluster Incl. X06374:Human mRNA for platelet-derived growth
	factor PDGF-A /cds=(403,993) /gb=X06374 /gi=35363 /ug=Hs.37040
	/len=2305
41257_at	Cluster Incl. D16217:Human mRNA for calpastatin, complete cds
	/cds=(162,2288) /gb=D16217 /gi=303598 /ug=Hs.226067 /len=2493
32786_at	Cluster Incl. X51345:Human jun-B mRNA for JUN-B protein
	/cds=(253,1296) /gb=X51345 /gi=34014 /ug=Hs.198951 /len=1797
1052_s_at	M83667 /FEATURE=mRNA /DEFINITION=HUMNFIL6BA
	Human NF-IL6-beta protein mRNA, complete cds
231_at	M55153 /FEATURE= /DEFINITION=HUMTGASE Human
	transglutaminase (TGase) mRNA, complete cds
31792_at	Cluster Incl. M20560:Human lipocortin-III mRNA, complete cds
	/cds=(46,1017) /gb=M20560 /gi=186967 /ug=Hs.1378 /len=1339
36543_at	Cluster Incl. J02931:Human placental tissue factor (two forms)
	mRNA, complete cds /cds=(111,998) /gb=J02931 /gi=339501
	/ug=Hs.62192 /len=2141

Table 23 – Cl	Table 23 – Classification of High Grade & "False Positive" Low Grade Prostate  Tumors using High Grade Clusters 4-7.							
Tumor	High Grade Cluster 4	High Grade Cluster 5	High Grade Cluster 6	High Grade Cluster 7	No. of Correct Classifications			
	Gleason Score 8 or 9 (high grade) Tumors							
T26	1	1	1	1	4			
T31	1	1	1	1	4			
T45	1	1	1	1	4			
T57	1	1	1	1	4			
T58	1	1	1	1	4			
T59	1	1	1	1	4			
	Gleason Score 6 or 7 (low grade) Tumors							

T01	1	0	0	0	3	
T10	1	1	1	0	1	
T25	0	0	0	1	3	
T28	0	0	0	0	4	
T29	0	0	1	1	2	
T36	0	0	0	0	4	
T40	0	0	1	0	3	
			l	<u> </u>		
T42	0	1	0	0	3	
T43	1	0	0	1	2	
T46	1	1	0	0	2	
T47	. 0	1	0	0	3	
T53	1	1	0	0	2	
T54	0	0	0	0	4	
T55	0	0	0	0	4	
T56	0	1	0	0	3	
T60	0	1	0	0	3	
T62	0	1	0	0	3	
No. Genes in	5	4	7	13		
Cluster						
Correlation	0.995	0.998	0.995	0.992		
Coefficient of						
Cluster						
Note: 1 = Positive phenotype association index; 0 = negative phenotype association index.						

[00234] Application of the methods of present invention to classification of human prostate tumors according to Gleason grade revealed that high grade tumors can be readily distinguished from the majority of low grade prostate cancers based on gene

expression analysis of small discrete clusters of genes. However, there is a significant fraction of low grade tumors that closely resemble transcriptional profiles of more advanced and aggressive high grade tumors suggesting that these low grade tumors may represent a precursor of aggressive metastatic disease.

## D. Benign Prostatic Hyperplasia (BPH) Sample Classification

[00235] Applying method of present invention we identified a BPH vs. prostate cancer discrimination cluster comprising 14 genes listed in Table 22. In this example we utilized human prostate carcinoma cell line gene expression data to develop a first reference set and clinical sample data set presented in Stamey TA, Warrington JA, Caldwell MC, Chen Z, Fan Z, Mahadevappa M, McNeal JE,Nolley R, Zhang Z. Molecular genetic profiling of Gleason grade 4/5 prostate cancers compared to benign prostatic hyperplasia. J Urol 2001 166(6):2171-2177, 2001; incorporate herein by reference. The clinical data set consists of 17 samples obtained from 8 patients with BPH and 9 patients with prostate cancer (Stamey, T.A., et al., 2001).

[00236] We identified a concordance set of 54 genes (r = 0.842) exhibiting concordant gene expression changes between prostate cancer cell lines vs. normal prostate epithelial cells and clinical samples of prostate cancer vs. BPH. As shown in Figure 28, 7 of 8 samples from the BPH group had negative phenotype association indices, whereas 9 of 9 samples from the prostate cancer group had positive phenotype association indices yielding overall accuracy of 94% in sample classification.

[00237] Applying the methods of the present invention, we next identified a minimum segregation set of genes (BPH minimum segregation set 1 or BPH cluster 1 (MAGE-1 cluster) – Table 24) that is able accurately discriminates between BPH and prostate

cancer in clinical tissue samples derived from human prostate. This BPH vs. prostate cancer discrimination cluster comprises 14 genes displaying a high correlation coefficient of -fold expression changes in prostate cancer cell lines vs. normal prostate epithelial cells and clinical samples of prostate cancer vs. BPH (r = 0.990) and high accuracy of sample classification. As shown in Figure 29, of 8 samples from the BPH group had negative phenotype association indices, whereas 9 of 9 samples from the prostate cancer group had positive phenotype association indices yielding overall accuracy of 100% in sample classification.

Table 24 – BPH Minimum Segregation Set 1.				
14 genes (r = 0.990) [BPH segregation cluster (MAGE-1 cluster)]				
Affymetrix Probe Set ID	Description			
(U95Av2)	•			
M77481_rna1_f_at	MAGE-1			
U73514_at	hydroxyacyl-Coenzyme A dehydrogenase, type II			
U39840_at	hepatocyte nuclear factor-3 alpha (HNF-3 alpha)			
L41559_at	dimerization cofactor of hepatocyte nuclear factor 1 alpha			
	(TCF1)			
U90907_at	clone 23907			
D00860_at	phosphoribosyl pyrophosphate synthetase subunit I			
U81599_at	homeodomain protein HOXB13			
X91247_at	thioredoxin reductase 1			
U79274_at	clone 23733			
J03473_at	poly(ADP-ribose) synthetase			
HG4312-HT4582_s_at	Transcription Factor IIIa			
M55593_at	matrix metalloproteinase 2 (gelatinase A, 72kD gelatinase,			
	72kD type IV collagenase)			
M11433_at	retinol-binding protein 1, cellular			
X93510_at	LIM domain protein			

## E. Metastatic Prostate Cancer Sample Classification

[00238]Applying method of present invention we identified two gene clusters comprising 17 and 19 genes useful for classifying prostate cancer metastases. In this example we utilized human prostate carcinoma cell line gene expression data and clinical sample data set presented in Dhanasekaran, S.M., Barrette, T.R., Ghosh, D., Shah, R., Varambally, S., Kurachi, K., Pienta, K.J., Rubin, M.A., Chinnalyan, A.M. Delineation of prognostic biomarkers in prostate cancer. Nature, 412:822-826, 2001, incorporated herein by reference. As a starting gene set we utilized a set of 242 genes that was identified using a combination of statistical and clustering analyses approach in Dhanasekaran, S.M., et al., 2001 and was found to be useful in classification of various clinical samples using hierarchical clustering algorithm. Our initial analysis applying the methods of the present invention was performed on a small training data set comprising three human prostate cancer cell lines (LNCap; PC3; DU145), three samples of adjacent to cancer normal prostate, one sample of prostatitis, five samples of BPH, ten samples of hormone dependent localized prostate cancer, and seven samples of hormone refractory metastatic prostate cancer.

[00239] The original gene expression data were presented as log transformed -fold expression changes of a gene in a sample compared to normal human prostate. For the set of 242 genes we calculated average gene expression values for three prostate cancer cell lines (first reference set) and average expression values for group of metastatic prostate tumors vs. localized prostate tumors (second reference set). The initial set of 242 genes displayed only a weak correlation coefficient of the –fold expression changes in

prostate cancer cell lines and clinical samples of metastatic prostate cancer vs. localized prostate cancer (r = 0.323).

[00240] Applying the methods of the present invention, we identified a concordance set of 72 genes (r = 0.866) exhibiting concordant gene expression changes between prostate cancer cell lines and clinical samples of metastatic prostate cancer vs. localized prostate cancer. When we utilized genes of this concordance set to calculate the phenotype association indices in individual clinical samples, 3 of 3 samples from ANP group, 5 of 5 samples from the BPH group, one sample of prostatitis, and five of ten samples of localized prostate cancer had negative phenotype association indices, whereas 7 of 7 samples from the metastatic prostate cancer group had positive phenotype association indices yielding overall accuracy of 84% in sample classification.

[00241] Applying the methods of the present invention, we next identified two minimum segregation sets of genes capable of accurately discriminating between metastatic prostate cancer and localized prostate cancer in clinical tissue samples derived from human prostate. The first metastatic prostate cancer (MPC) vs. localized prostate cancer (LPC) minimum segregation set or cluster (metastasis minimum segregation set 1) comprises 17 genes displaying a high correlation coefficient of fold expression changes in prostate cancer cell lines and clinical samples of metastatic prostate cancer prostate cancer vs. localized prostate cancer (r = 0.988) and is highly accurate in discriminating among these different types of samples. As shown in Figure 30, 3 of 3 samples from ANP group, 5 of 5 samples from the BPH group, one sample of prostatitis, and nine of ten samples of localized prostate cancer had negative phenotype association indices,

whereas 7 of 7 samples from the metastatic prostate cancer group had positive phenotype association indices yielding overall accuracy of 96% in sample classification.

[00242] The second metastatic prostate cancer vs. localized prostate cancer discrimination cluster (metastasis minimum segregation set 2) comprises 19 genes displaying a high correlation coefficient of –fold expression changes in prostate cancer cell lines and clinical samples of metastatic prostate cancer prostate cancer vs. localized prostate cancer (r = 0.988) and also is highly accurate in discriminating among these different types of samples. As shown in Figure 31, 3 of 3 samples from ANP group, 5 of 5 samples from the BPH group, one sample of prostatitis, and nine of ten samples of localized prostate cancer had negative phenotype association indices, whereas 7 of 7 samples from the metastatic prostate cancer group had positive phenotype association indices yielding overall accuracy of 96% in sample classification.

[00243] To further validate the sample classification accuracy using an independent data set, we tested the performance of the two metastatic prostate cancer discrimination clusters on a larger set of clinical samples consisting of four samples of adjacent to cancer normal prostate (ANP), one sample of prostatitis, fourteen samples of BPH, fourteen samples of hormone dependent localized prostate cancer (LPC), and twenty samples of hormone refractory metastatic prostate cancer. As shown in Figure 32, when metastasis minimum segregation set 1 (*i.e.*, the cluster of 17 genes) was utilized, 4 of 4 samples from ANP group, 14 of 14 samples from the BPH group, one sample of prostatitis, and 10 of 14 samples of localized prostate cancer had negative phenotype association indices, whereas 20 of 20 samples from the metastatic prostate cancer group

had positive phenotype association indices yielding overall accuracy of 92% in sample classification.

[00244] As shown in Figure 33, when metastasis minimum segregation set 2 (*i.e.*, the cluster of 19 genes) was utilized, 4 of 4 samples from ANP group, 13 of 14 samples from the BPH group, one sample of prostatitis, and 12 of 14 samples of localized prostate cancer had negative phenotype association indices, whereas 20 of 20 samples from the metastatic prostate cancer group had positive phenotype association indices yielding overall accuracy of 94% in sample classification. The genes comprising prostate cancer metastasis minimum segregation sets 1 and 2 are set forth in Tables 25 and 26.

	Table 25. Prostate Cancer Metastasis Minimum Segregation Set 1.						
17 genes $(r = 0.988)$							
Clone	UniGene	Accession	NID	Gene	NAME		
ID	Cluster			Symbol			
469954	Hs.169449	AA030029	g1496255	PRKCA	protein kinase C, alpha		
308041	Hs.3847	W24429	g1301379	PNUTL1	peanut (Drosophila)-like 1		
83605	Hs.50966	T61078	g664115	CPS1	carbamoyl-phosphate		
				·	synthetase 1, mitochondrial		
123755	Hs.45514	R01304	g751040	ERG	v-ets avian erythroblastosis		
i.	1				virus E26 oncogene related		
810512	Hs.87409	AA464630	g2189514	THBS1	thrombospondin 1		
811028	Hs.9946	AA485373	g2214592		ESTs		
767828	Hs.83951	AA418773	g2080583	HPS	Hermansky-Pudlak syndrome		
417711	Hs.180255	W88967	g1404003	HLA-	major histocompatibility		
			}	DRB1	complex, class II, DR beta 1		
727251	Hs.1244	AA412053	g2070642	CD9	CD9 antigen (p24)		
214990	Hs.80562	H72027	g1043843	GSN	gelsolin (amyloidosis, Finnish		
:					type)		

788566	Hs.80296	AA452966	g2166635	PCP4	Purkinje cell protein 4
205049	Hs.111676	H57494	g1010326		ESTs, Weakly similar to heat
					shock protein 27 [H.sapiens]
81289	Hs.77443	T60048	g661885	ACTG2	actin, gamma 2, smooth
					muscle, enteric
77915	Hs.76422	T61323	g664360	PLA2G2A	phospholipase A2, group IIA
					(platelets, synovial fluid)
898092	Hs.75511	AA598794		CTGF	connective tissue growth factor
343646	Hs.2969	W69471		SKI	v-ski avian sarcoma viral
					oncogene homolog
134422	Hs.200499	R31679	g787522		ESTs

	Table 26. Prostate Cancer Metastasis Minimum Segregation Set 2.							
19 genes $(r = 0.988)$								
Clone	UniGene	Accession	NID	Gene	NAME			
ID	Cluster			Symbol				
469954	Hs.169449	AA030029	g1496255	PRKCA	protein kinase C, alpha			
308041	Hs.3847	W24429	g1301379	PNUTL1	peanut (Drosophila)-like 1			
83605	Hs.50966	T61078	g664115	CPS1	carbamoyl-phosphate synthetase			
					1, mitochondrial			
123755	Hs.45514	R01304	g751040	ERG	v-ets avian erythroblastosis virus			
					E26 oncogene related			
784959	Hs.90408	AA447658	g2161328	NEO1	neogenin (chicken) homolog 1			
130977	Hs.23437	R22926	g777814		Homo sapiens mRNA; cDNA			
ı					DKFZp586G0623 (from clone			
					DKFZp586G0623)			
80109	Hs.198253	T63324	g667189	HLA-	major histocompatibility complex,			
		,		DQA1	class II, DQ alpha 1			
768370	Hs.204354	AA495846	g2229167	ARHB	ras homolog gene family, member			
					В			

795758	Hs.179972	AA460304	g2185120	G1P3	interferon, alpha-inducible protein
					(clone IFI-6-16)
839736	Hs.1940	AA504943	g2241103	CRYAB	crystallin, alpha B
783696	Hs.75485	AA446819	g2159484	OAT	ornithine aminotransferase (gyrate
					atrophy)
50506	Hs.75465	H17504	g883744	MAPK6	mitogen-activated protein kinase
					6
773771	Hs.85050	AA427940	g2112058	PLN	phospholamban
813712	Hs.181101	AA453849	g2167518	ATP5F1	ATP synthase, H+ transporting,
					mitochondrial F0 complex,
			j		subunit b, isoform 1
502326	Hs.184567	AA156674	g1728353		ESTs
188036	Hs.620	H44784	g920836	BPAG1	bullous pemphigoid antigen 1
					(230/240kD)
840942	Hs.814	AA486627	g2216791	HLA-	major histocompatibility complex,
				DPB1	class II, DP beta 1
208718	Hs.78225	H63077	g1017878	ANXA1	annexin A1
753104	Hs.240217	AA478553	g2207187	DCT	dopachrome tautomerase
				i	(dopachrome delta-isomerase,
					tyrosine-related protein 2)

## EXAMPLE 2 - CLASSIFICATION OF HUMAN BREAST CANCERS

[00245] A recent study on gene expression profiling of breast cancer identifies 70 genes whose expression pattern is strongly predictive of a short post-diagnosis and treatment interval to distant metastases (van't Veer, L.J., et al., "Gene expression profiling predicts clinical outcome of breast cancer," Nature, 415: 530-536, 2002, incorporated herein by reference). The expression pattern of these 70 genes discriminates with 81% (optimized sensitivity threshold) or 83% (optimal accuracy threshold) accuracy the patient's prognosis in the group of 78 young women diagnosed with sporadic lymph-

node-negative breast cancer. This group comprises 34 patients who developed distant metastases within 5 years and 44 patients who continued to be disease-free after a period of at least 5 years; they constitute a poor prognosis and good prognosis group, correspondingly.

We applied the methods of the present invention to further reduce the number [00246] of genes whose expression patterns represent genetic signatures of breast cancers with "poor prognosis" or "good prognosis." Measurements of mRNA expression levels of 70 genes in established human breast carcinoma cell lines (MCF7; MDA-MB-435; MDA-MB-468; MDA-MB-231; MDA-MB-435Br1; MDA-MB-435BL3) and primary cultures of normal human breast epithelial cells were performed utilizing Q-PCR method, which generally is accepted as the current most reliable method of gene expression analysis and unambiguous confirmation of gene identity. Applying the methods of the present invention, for each breast cancer cell line, concordant sets of genes were identified exhibiting both positive and negative correlation between –fold expression changes in cancer cell lines versus control cell line and the poor prognosis group versus the good prognosis group. Minimum segregation sets were selected from corresponding concordance sets and individual phenotype association indices were calculated. Three top-performing breast cancer metastasis predictor gene clusters are listed in Tables 27-29, and corresponding phenotype association indices are presented in Figures 34-36. [00247] A breast cancer poor prognosis predictor cluster comprising 6 genes was identified (r = 0.981) using MDA-MB-468 cell line gene expression profile as a reference standard (Figure 34). 32 of 34 samples from the poor prognosis group had positive

phenotype association indices, whereas 29 of 44 samples from the good prognosis group

had negative phenotype association indices yielding an overall sample classification accuracy of 78%.

Table	Table 27. Breast Cancer Poor Prognosis Minimum Segregation Set 1.		
6 genes (MDA-MB-468; Q-PCR) (r = 0.981)			
Systematic	Gene	Sequence description	
name	name		
NM_002019	FLT1	fms-related tyrosine kinase 1 (vascular endothelial growth factor/vascular permeability factor receptor)	
U82987	BBC3	Bcl-2 binding component 3	
NM_003239	TGFB3	transforming growth factor, beta 3	
AF201951	MS4A7	high affinity immunoglobulin epsilon receptor beta subunit	
NM_000849	GSTM3	glutathione S-transferase M3 (brain)	
NM_003862	FGF18	fibroblast growth factor 18	

[00248] A breast cancer good prognosis predictor cluster comprising 14 genes was identified (r = -0.952) using MDA-MB-435Br1 cell line gene expression profile as a reference standard (Figure 35). 30 of 34 samples from the poor prognosis group had negative phenotype association indices, whereas 34 of 44 samples from the good prognosis group had positive phenotype association indices yielding an overall sample classification accuracy of 82%.

Table 28. Br	east Cancer Goo	od Prognosis Minimum Segregation Set 1.	
MDA-MB-435Br1 (	MDA-MB-435Br1 (14 genes; Q-PCR) (r = -0.952)		
Systematic name	Gene name	Sequence description	
AF201951	MS4A7	high affinity immunoglobulin epsilon receptor beta subunit	
NM_003239	TGFB3	transforming growth factor, beta 3	
U82987	BBC3	Bcl-2 binding component 3	
NM_001282	AP2B1	adaptor-related protein complex 2, beta 1 subunit	

NM_003748	ALDH4A1	aldehyde dehydrogenase 4 (glutamate gamma- semialdehyde dehydrogenase; pyrroline-5- carboxylate dehydrogenase)
NM_018354	FLJ11190	hypothetical protein FLJ11190
NM_020188	DC13	DC13 protein
NM_003875	GMPS	guanine monphosphate synthetase
Contig57258_RC	AKAP2	ESTs
NM_000788	DCK	deoxycytidine kinase
Contig25991	ECT2	epithelial cell transforming sequence 2 oncogene
Contig38288_RC		ESTs, Weakly similar to
NM_000436	OXCT	3-oxoacid CoA transferase
NM_000127	EXT1	exostoses (multiple) 1

[00249] Another breast cancer good prognosis minimum segregation set 2 comprising 13 genes (r = -0.992) was identified using MCF7 cell line gene expression profile as a reference standard (Figure 36). 30 of 34 samples from the poor prognosis group had negative phenotype association indices, whereas 32 of 44 samples from the good prognosis group had positive phenotype association indices yielding overall sample classification accuracy of 79%.

Table 29. Breast Cancer Good Prognosis Minimum Segregation Set 2.					
r = -0.992	System 1	System 1 (MCF7)			
Locus Link	GenBank	UniGene	Systematic	Gene	Gene Description
Symbol			name	name	
CEGP1		Hs.222399	NM_020974	CEGP1	Homo sapiens CEGP1 protein (CEGP1), mRNA.
FGF18		Hs.49585	NM_003862	FGF18	fibroblast growth factor 18
GSTM3		Hs.2006	NM_000849	GSTM3	glutathione S-transferase M3 (brain)

TGFB3		Hs.2025	NM_003239	TGFB3	transforming growth
					factor, beta 3
CFFM4 or		Hs.11090	AF201951	MS4A7	high affinity
MS4A7					immunoglobulin epsilon
(   				:	receptor beta subunit
	AI918032	Hs.5521	Contig55377_	RC	ESTs
AP2B1		Hs.74626	NM_001282	AP2B1	adaptor-related protein
}		<u> </u>			complex 2, beta 1 subunit
CCNE2		Hs.30464	NM_004702	CCNE2	cyclin E2
KIAA0175		Hs.184339	NM_014791	KIAA0175	KIAA0175 gene product
EXT1		Hs.184161	NM_000127	EXT1	exostoses (multiple) 1
	AI813331	Hs.283127	Contig46218_	RC	ESTs
PK428		Hs.44708	NM_003607	PK428	Ser-Thr protein kinase
		i		}	related to the myotonic
					dystrophy protein kinase
	AI554061	Hs.309165	Contig38288_	RC	ESTs, Weakly similar to
					quiescin [H.sapiens]

[00250] To validate the classification accuracy using an independent data set, we tested performance of the 13 genes good prognosis predictor cluster (good prognosis minimum segregation set 2) on a set of 19 samples obtained from 11 breast cancer patients who developed distant metastases within five years after diagnosis and treatment and 8 patients who remained disease free for at least five years (van't Veer et al., 2002). As shown in Figure 37, 9 of 11 samples from the poor prognosis group had negative phenotype association indices, whereas 6 of 8 samples from the good prognosis group had positive phenotype association indices yielding overall sample classification accuracy of 79%.

## **EXAMPLE 3 – CLASSIFICATION OF HUMAN OVARIAN CANCER**

[00251] Lack of effective diagnostic and prognostic markers is generally considered a major problem in the clinical management of ovarian cancer – an epithelial neoplasm that has one of the worst prognoses among epithelial malignancies in women and is the leading cause of death from gynecologic cancer. The clinical utility of the most widely used biomarker of ovarian cancer, CA125, is largely limited to follow-up the response to therapy and progression of the disease and considered to be less efficient in diagnostic and prognostic applications (Meyer, T., Rustin, G.J. Br. J. Cancer, 82: 1535-1538, 2000, incorporated herein by reference).

We applied the methods of the present invention to identify gene expression [00252] profiles distinguishing poorly differentiated ovarian epithelial tumors, often exhibiting invasive, highly malignant phenotype, from less aggressive, well and moderately differentiated ovarian epithelial malignancies. Both clinical and cell line data sets utilized in this example were published in Welsh, J.B., et al., "Analysis of gene expression profiles in normal and neoplastic ovarian tissue samples identifies candidate molecular markers of epithelial ovarian cancer," PNAS, 98: 1176-1181, 2001, incorporated herein by reference. As a starting point for identification of the concordant set of genes for established ovarian cancer cell lines and ovarian tumor tissue samples we utilized a set of the top 501 genes selected by a multidimensional statistical metric that was devised to identify genes with an expression pattern considered ideal for the molecular detection of epithelial ovarian cancer (Welsh et al., 2001). There determined that there was no significant correlation between the -fold changes in the expression levels of these 501 genes in the three cancer cell lines (SKOV8; MDA2774; CAOV3) compared to a control sample (HuOVR) and three poorly differentiated tumors

(OVR\_11; OVR\_12; OVR\_27) compared to eleven moderately and well differentiated tumors (OVR\_1; \_2; \_5; \_8; \_10; \_13; \_16; \_19; \_22; \_26; \_28), (r = 0.101).

[00253] According to the methods of present invention, we selected from the set of 501 genes two concordant sets of genes: concordant set 1 comprising 251 genes and exhibiting positive correlation (r = 0.504) between cell lines and tissue samples data sets and concordant set 2, comprising 248 genes and exhibiting negative correlation (r = -0.296) between cell lines and clinical samples. We selected from concordance set 1 a set of 11 genes (ovarian cancer poor prognosis minimum segregation set 1) (ovarian cancer poor prognosis cluster – *see* Table 30) displaying a high positive correlation (r = 0.988) between the cell lines and tissue samples data sets and exhibiting a 93% success rate in clinical sample classification based on individual phenotype association indices. As shown in Figure 38, all three poorly differentiated tumors had positive phenotype association indices, whereas 10/11 well and moderately differentiated tumors displayed negative phenotype association indices.

Table 30. Ovarian Cancer Poor Prognosis Minimum Segregation Set 1.			
Poor Prognosis Predic	Poor Prognosis Predictor Performance: 93% (13/14)		
Performance: 93% (1			
r = 0.988	r = 0.988		
Affymetrix Probe Set	Affymetrix Probe Set Description		
ID (HuFL6800)			
L22524_s_at	L22524, class B, 18 probes, 15 in L22524cds 462-734: 3 in		
U47077 at	reverseSequence, 46-197, Human matrilysin gene U47077, class A, 20 probes, 20 in U47077 13025-13463, Human		
047077_at	DNA-dependent protein kinase catalytic subunit (DNA-PKcs)  mRNA, complete cds		

U46006_s_at	U46006, class A, 20 probes, 20 in U46006 140-620, Human
	smooth muscle LIM protein (h-SmLIM) mRNA, complete cds.
	/gb=U46006 /ntype=RNA
L40357_at	L40357, class A, 20 probes, 20 in L40357mRNA 7-463, Homo
	sapiens thyroid receptor interactor (TRIP7) mRNA, 3' end of cds
M64098_at	M64098, class A, 20 probes, 20 in M64098 3873-4305, Human
	high density lipoprotein binding protein (HBP) mRNA, complete
	cds
D79993_at	D79993, class A, 20 probes, 20 in D79993 2741-3167, Human
	mRNA for KIAA0171 gene, complete cds
U15085_at	U15085, class A, 20 probes, 20 in U15085 821-1289, Human
	HLA-DMB mRNA, complete cds
U60975_at	U60975, class A, 20 probes, 20 in U60975 6398-6824, Human
	hybrid receptor gp250 precursor mRNA, complete cds
M79462_at	M79462, class A, 20 probes, 20 in M79462 3853-4333, Human
	PML-1 mRNA, complete CDS
Z23090_at	Z23090, class A, 20 probes, 17 in Z23090cds 277-589: 3 in
	reverseSequence, 1086-1098, H.sapiens mRNA for 28 kDa heat
	shock protein
X03635_at	X03635, class C, 20 probes, 20 in all_X03635 5885-6402,
	Human mRNA for oestrogen receptor

[00254] Applying the methods of the present invention, we selected from concordance set 2 a set of 10 genes (ovarian cancer good prognosis minimum segregation set 1) (ovarian cancer good prognosis cluster – see Table 31) displaying a high negative correlation (r = -0.964) between the tumor cell lines and clinical samples data sets and exhibiting a 93% success rate in clinical sample classification based on individual phenotype association indices. As shown in Figure 39, all three poorly differentiated

tumors had negative phenotype association indices, whereas 10/11 well and moderately differentiated tumors displayed positive phenotype association indices.

Table 31. Ovarian Can	cer Good Prognosis Minimum Segregation Set 1
Good Prognosis Predictor	
Performance: 93% (13/14)	
r = - 0.964	
Affymetrix Probe Set ID	Description
(HuFL6800)	
U90551_at	U90551, class A, 20 probes, 20 in U90551 1071-
	1623, Human histone 2A-like protein (H2A/l)
	mRNA, complete cds
L19779_at	L19779, class A, 20 probes, 20 in L19779 7-496,
	Homo sapiens histone H2A.2 mRNA, complete
	cds
M90657_at	M90657, class A, 20 probes, 20 in M90657 581-
	1163, Human tumor antigen (L6) mRNA, complete
	cds
M13755_at	M13755, class A, 20 probes, 20 in M13755mRNA
	33-591, Human interferon-induced 17-kDa/15-kDa
	protein mRNA, complete cds
U90915_at	U90915, class A, 20 probes, 20 in U90915 122-
	674, Human clone 23600 cytochrome c oxidase
	subunit IV mRNA, complete cds
Z74792_s_at	Z74792, class A, 20 probes, 20 in Z74792mRNA
	1470-1917, H.sapiens mRNA for CCAAT
	transcription binding factor subunit gamma.
X99325_at	X99325, class C, 20 probes, 20 in all_X99325
	1482-1927, H.sapiens mRNA for Ste20-like kinase
HG2614-HT2710_at	Collagen, Type Viii, Alpha 1

J03242_s_at	J03242, class A, 20 probes, 20 in J03242 1155-
	1324, Human insulin-like growth factor II mRNA,
	complete cds
D86983_at	D86983, class A, 20 probes, 20 in D86983 5131-
	5485, Human mRNA for KIAA0230 gene, partial
	cds

## **EXAMPLE 4 - CLASSIFICATION OF HUMAN LUNG CANCER**

[00255] Lung cancer accounts for more than 150,000 cancer-related deaths every year in the United States, thus exceeding the combined mortality caused by breast, prostate, and colorectal cancers (Greenlee, R.T., Hill-Harmon, M.B., Murray, T., Thun, M. CA Cancer J. Clin. 51: 15-36, 2001, incorporated herein by reference). Late stage of cancer at diagnosis and lack of efficient diagnostic and prognostic biomarkers are significant factors that adversely affect the clinical management of lung cancer (Mountain, C.F. Revisions in the international system for staging lung cancer. Chest, 111:1710-1717, 1997; Ihde, D.C. Chemotherapy of lung cancer. N.Engl.J.Med., 327:1434-1441, 1992; Sugita, M., Geraci, M., Gao, B., Powell, R.L., Hirsch, F.R., Johnson, G., Lapadat, R., Gabrielson, E., Bremnes, R., Bunn, P.A., Franklin, W.A. Combined use of oligonucleotide and tissue microarrays identifies cancer/testis antigens as biomarkers in lung cancer. Cancer Res., 62:3971-3979, 2002). Non-small-cell lung carcinoma (NSCLC) is a clinically and histopathologically distinct major form of lung cancer and is further classified as adenocarcinoma (most common form of NSCLC), squamous cell carcinoma, and large-cell carcinoma (Travis, W.D., Travis, L.B., Devesa, S.S. Cancer, 75:191-202, 1995).

[00256] We applied the methods of the present invention to identify gene expression profiles distinguishing lung adenoracinoma samples from normal lung specimens as well

as a highly malignant phenotype of lung adenocarcinoma, associated with short survival after diagnosis and therapy, from less aggressive lung cancers, associated with longer patient survival. Both clinical and cell line data sets utilized in this example were published (Clinical data: Bhattacharjee, A., Richards, W.G., Staunton, J., Li, C., Monti, S., Vasa, P., Ladd, C., Beheshti, J., Bueno, R., Gillette, M., Loda, M., Weber, G., Mark, E.J., Lander, E.S., Wong, W., Johnson, B.E., Golub, T.R., Sugarbaker, D.J., Meyerson, M. Classification of human lung carcinomas by mRNA expression profiling reveals distinct adenocarcinoma subclasses. PNAS, 98: 13790-13795, 2001; incorporated herein by reference; Cell line data: Sugita, M., Geraci, M., Gao, B., Powell, R.L., Hirsch, F.R., Johnson, G., Lapadat, R., Gabrielson, E., Bremnes, R., Bunn, P.A., Franklin, W.A. Combined use of oligonucleotide and tissue microarrays identifies cancer/testis antigens as biomarkers in lung cancer. Cancer Res., 62:3971-3979, 2002; incorporated herein by reference. As a starting point for identification of the concordant set of genes for established lung cancer cell lines and lung cancer tissue samples we utilized a set of the 675 transcripts selected based on a statistical analysis of the quality of the dataset and variability of gene expression across dataset (Bhattacharje et al., 2001). Initial analysis showed that there was no significant correlation between the -fold changes in the expression levels of these 675 genes in the two NSCLC cancer cell lines (H647 and A549 cell lines) compared to a control sample (normal bronchial epithelial cell cultures obtained from a healthy 48-year-old donor) and 139 samples of lung adenoracinomas compared to the 17 normal lung specimens (r = 0.163).

[00257] According to the methods of present invention, we selected from the set of 675 genes a concordant set of transcripts comprising 355 genes and exhibiting positive

correlation (r = 0.523) between cell lines and tissue samples data sets. Next we selected from the concordant set of 355 genes two minimum segregation sets of genes: a set of 13 genes (lung adenoracinoma minimum segregation set 1, also referred to as lung adenocarcinoma cluster 1 – see Table 32) and a set of 26 genes (lung adenoracinoma minimum segregation set 2, also referred to as lung adenocarcinoma cluster 2 – see Table 33) both displaying high positive correlation (r = 0.979 and r = 0.966, respectively) between the cell lines and tissue samples data sets (Figures 40 and 41). For each minimum segregation set we calculated the individual phenotype association indices for 17 normal lung samples and 139 lung adenocarcinoma samples. After adjustment of the dataset by subtracting 0.52 from all the phenotype association indices, both gene clusters exhibited a 96% success rate in clinical sample classification based on individual phenotype association indices (Figures 42 and 43). The adjustment was made following visual inspection of the raw data indicating that 0.52 was a useful threshold for discriminating normal lung samples from lung adenocarcinoma samples, and had the added benefit of allowing classification to be carried out according to the sign of the phenotype association index. Without wishing to be bound by theory, it appears likely that the adjustment was necessary because the published datasets used for constructing this example were derived from different groups using non-identical data reduction methods. As shown in Figures 42 and 43, 16/17 normal lung samples had negative phenotype association indices, whereas 134/139 of lung adenocarcinoma specimens displayed positive phenotype association indices. When scores from the two clusters were considered and a criterion of at least one positive phenotype association index was adopted for assigning a lung adenocarcinoma classification, the classification success rate

was 99%. 16/17 (94%) normal lung samples had two negative phenotype association indices, whereas 131/139 of lung adenocarcinoma specimens displayed two positive phenotype association indices, seven of 139 had at least one positive phenotype association index, and only a single lung adenocarcinoma specimen had two negative phenotype association indices. Thus, 154/156 (99%) of clinical lung adenocarcinima samples were correctly classified using this strategy.

Table :	Table 32. Lung adenocarcinoma minimum segregation set 1.		
13 genes (r = 0.979	)		
Affymetrix Probe	Description		
Set ID (U95Av2)			
34342_s_at	secreted phosphoprotein 1 (osteopontin, bone sialoprotein I, early T-		
	lymphocyte activation 1)		
2092_s_at	secreted phosphoprotein 1 (osteopontin, bone sialoprotein I, early T-		
	lymphocyte activation 1)		
31798_at	Cluster Incl AA314825:EST186646 Homo sapiens cDNA, 5 end		
	/clone=ATCC-111986 /clone_end=5" /gb=AA314825 /gi=1967154		
	/ug=Hs.1406 /len=574"		
668_s_at	matrix metalloproteinase 7 (matrilysin, uterine)		
31599_f_at	melanoma antigen, family A, 6		
39008_at	ceruloplasmin (ferroxidase)		
31844_at	homogentisate 1,2-dioxygenase (homogentisate oxidase)		
31477_at	trefoil factor 3 (intestinal)		
38825_at	fibrinogen, A alpha polypeptide		
32306_g_at	collagen, type I, alpha 2		
32773_at	Cluster Incl AA868382:ak41e04.s1 Homo sapiens cDNA, 3 end		
	/clone=IMAGE-1408542 /clone_end=3" /gb=AA868382		
	/gi=2963827 /ug=Hs.198253 /len=936"		

36623_at	Cluster Incl AB011406:Homo sapiens mRNA for alkalin
	phosphatase, complete cds /cds=(176,1750) /gb=AB011406
	/gi=3401944 /ug=Hs.75431 /len=2510
31870_at	CD37 antigen

Table 33. Lung adenocarcinoma minimum segregation set 2.		
26 genes (r = 0.966)		
Affymetrix Probe	Description	
Set ID (U95Av2)		
33904_at	claudin 3	
1481_at	matrix metalloproteinase 12 (macrophage elastase)	
38261_at	ATP-binding cassette, sub-family C (CFTR/MRP), member 3	
1586_at	insulin-like growth factor binding protein 3	
38066_at	diaphorase (NADH/NADPH) (cytochrome b-5 reductase)	
34575_f_at	melanoma antigen, family A, 5	
41583_at	flap structure-specific endonuclease 1	
32787_at	v-erb-b2 avian erythroblastic leukemia viral oncogene homolog 3	
1788_s_at	dual specificity phosphatase 4	
32805_at	aldo-keto reductase family 1, member C1 (dihydrodiol	
l İ	dehydrogenase 1; 20-alpha (3-alpha)-hydroxysteroid dehydrogenase)	
39260_at	solute carrier family 16 (monocarboxylic acid transporters), member	
	4	
41748_at	Cluster Incl AA196476:zp99g10.r1 Homo sapiens cDNA, 5 end	
	/clone=IMAGE-628386 /clone_end=5" /gb=AA196476 /gi=1792058	
	/ug=Hs.182421 /len=697"	
38656_s_at	Cluster Incl W27939:39g3 Homo sapiens cDNA /gb=W27939	
	/gi=1307887 /ug=Hs.103834 /len=862	
823_at	small inducible cytokine subfamily D (Cys-X3-Cys), member 1	
	(fractalkine, neurotactin)	
32052_at	hemoglobin, beta	
36979_at	solute carrier family 2 (facilitated glucose transporter), member 3	
40367_at	bone morphogenetic protein 2	
36937_s_at	PDZ and LIM domain 1 (elfin)	
40567_at	Tubulin, alpha, brain-specific	
33900_at	follistatin-like 3 (secreted glycoprotein)	

34320_at	Cluster Incl AL050224:Homo sapiens mRNA; cDNA				
	DKFZp586L2123 (from clone DKFZp586L2123) /cds=UNKNOWN				
	/gb=AL050224 /gi=4884466 /ug=Hs.29759 /len=1250				
37027_at	AHNAK nucleoprotein (desmoyokin)				
31622_f_at	metallothionein 1F (functional)				
609_f_at	metallothionein 1B (functional)				
37951_at	deleted in liver cancer 1				
31687_f_at	hemoglobin, beta				

[00258] Next we applied the methods of the present invention to identify gene expression profiles distinguishing highly malignant phenotype of lung adenocarcinoma, associated with short patient survival after diagnosis and therapy, from less aggressive lung cancers, associated with longer patient survival. Using the clinical data set and associated clinical history published in Bhattacharje et al., 2001, we selected two groups of adenocarcinoma patients having markedly distinct survival after diagnosis and therapy: poor prognosis group 1 comprising 34 patients with median survival of 8.5 months (range 0.1-17.3 months) and good prognosis group 2 comprising 16 patients with median survival of 84 months (range 75.4-106.1 months).

[00259] Applying the methods of the present invention, we selected from the set of 675 genes a concordant set of transcripts comprising 302 genes and exhibiting positive correlation (r = 0.444) between cell lines data (NSCLC cell lines versus normal bronchial epithelial cells) and tissue samples data sets (poor prognosis samples versus good prognosis samples). We selected from the concordant set of 302 genes a set of 38 genes (lung adenocarcinoma poor prognosis predictor cluster 1 - see Table 34) displaying high positive correlation (r = 0.881) between the cell lines and tissue samples data sets (Figure

44). This gene cluster exhibited a 64% success rate in clinical sample classification based on individual phenotype association indices (Figure 45). As shown in Figure 45, 16/16 of the lung adenocarcinoma samples of the good prognosis group had negative phenotype association indices, whereas 16/34 of lung adenocarcinoma specimens of the poor prognosis group displayed positive phenotype association indices.

Table 34. Lung adenocarcinoma poor prognosis predictor cluster 1.						
38  genes  (r = 0.881)	)					
Affymetrix Probe	Description					
Set ID (U95Av2)	·					
36990_at	ubiquitin carboxyl-terminal esterase L1 (ubiquitin thiolesterase)					
33998_at	neurotensin					
1481_at	matrix metalloproteinase 12 (macrophage elastase)					
36555_at	synuclein, gamma (breast cancer-specific protein 1)					
38389_at	2',5'-oligoadenylate synthetase 1 (40-46 kD)					
33128_s_at	Cluster Incl W68521:zd36f07.r1 Homo sapiens cDNA, 5 end					
	/clone=IMAGE-342757 /clone_end=5" /gb=W68521 /gi=1377410					
	/ug=Hs.83393 /len=579"					
40297_at	six transmembrane epithelial antigen of the prostate					
41531_at	Cluster Incl AI445461:tj34g07.x1 Homo sapiens cDNA, 3 end					
	/clone=IMAGE-2143452 /clone_end=3" /gb=AI445461 /gi=4288374					
	/ug=Hs.3337 /len=775"					
892_at	transmembrane 4 superfamily member 1					
32821_at	Cluster Incl AI762213:wi54d04.x1 Homo sapiens cDNA, 3 end					
	/clone=IMAGE-2394055 /clone_end=3" /gb=AI762213 /gi=5177880					
	/ug=Hs.204238 /len=677"					
1651_at	ubiquitin carrier protein E2-C					
37921_at	neuronal pentraxin I					
36302_f_at	melanoma antigen, family A, 4					

32426_f_at	melanoma antigen, family A, 1 (directs expression of antigen M					
	E)					
32607_at	brain acid-soluble protein 1					
41471_at	Cluster Incl W72424:zd66a09.s1 Homo sapiens cDNA, 3 end					
	/clone=IMAGE-345592 /clone_end=3" /gb=W72424 /gi=1382379					
	/ug=Hs.112405 /len=604"					
41758_at	chromosome 22 open reading frame 5					
38354_at	CCAAT/enhancer binding protein (C/EBP), beta					
195_s_at	caspase 4, apoptosis-related cysteine protease					
33267_at	Cluster Incl AF035315:Homo sapiens clone 23664 and 23905					
	mRNA sequence /cds=UNKNOWN /gb=AF035315 /gi=2661077					
i	/ug=Hs.180737 /len=1331					
39341_at	Cluster Incl AJ001902:Homo sapiens mRNA for TRIP6 (thyroid					
	receptor interacting protein) /cds=(72,1502) /gb=AJ001902					
	/gi=2558591 /ug=Hs.119498 /len=1653					
34445_at	KIAA0471 gene product					
36201_at	glyoxalase I					
36736_f_at	phosphoserine phosphatase					
1057_at	cellular retinoic acid-binding protein 2					
32072_at	mesothelin					
37811_at	calcium channel, voltage-dependent, alpha 2/delta subunit 2					
41771_g_at	Cluster Incl AA420624:nc61c12.r1 Homo sapiens cDNA					
	/clone=IMAGE-745750 /gb=AA420624 /gi=2094502					
i	/ug=Hs.183109 /len=533					
41770_at	Cluster Incl AA420624:nc61c12.r1 Homo sapiens cDNA					
	/clone=IMAGE-745750 /gb=AA420624 /gi=2094502					
	/ug=Hs.183109 /len=533					
41772_at	monoamine oxidase A					
40004_at	sine oculis homeobox (Drosophila) homolog 1					
40367_at	bone morphogenetic protein 2					
40367_at	bone morphogenetic protein 2					

40508_at	glutathione S-transferase A4			
33754_at	thyroid transcription factor 1			
32154_at	transcription factor AP-2 alpha (activating enhancer-binding protein 2 alpha)			
37600_at	extracellular matrix protein 1			
37874_at	flavin containing monooxygenase 5			
37208_at	phosphoserine phosphatase-like			

[00260] Using the sample iteration and cluster reduction strategies described in the previous examples, we selected four additional sets of genes displaying high positive correlation between the cell lines (NSCLC cell lines versus normal bronchial epithelial cells) and tissue samples data sets (poor prognosis samples versus good prognosis samples) (see Tables 35-38) and thus having potential discriminating power in classification of lung adenocarcinoma samples.

Table 35. Lung adenocarcinoma poor prognosis predictor cluster 2.				
19 genes $(r = 0.938)$				
Affymetrix Probe Set ID (U95Av2)	Description			
36555_at	synuclein, gamma (breast cancer-specific protein 1)			
41531_at	Cluster Incl AI445461:tj34g07.x1 Homo sapiens cDNA, 3 end /clone=IMAGE-2143452 /clone_end=3" /gb=AI445461 /gi=4288374 /ug=Hs.3337 /len=775"			
1868_g_at	CASP8 and FADD-like apoptosis regulator			
37921_at	neuronal pentraxin I			
37918_at	integrin, beta 2 (antigen CD18 (p95), lymphocyte function- associated antigen 1; macrophage antigen 1 (mac-1) beta subunit)			
38422_s_at	four and a half LIM domains 2			
39114_at	decidual protein induced by progesterone			

34375_at small inducible cytokine A2 (monocyte chemotactic prote						
	homologous to mouse Sig-je)					
36495_at	fructose-1,6-bisphosphatase 1					
37187_at	GRO2 oncogene					
37014_at	myxovirus (influenza) resistance 1, homolog of murine (interferon-					
	inducible protein p78)					
925_at	interferon, gamma-inducible protein 30					
39372_at	Cluster Incl W26480:30b8 Homo sapiens cDNA /gb=W26480					
	/gi=1307179 /ug=Hs.12214 /len=854					
32072_at	mesothelin					
41771_g_at	Cluster Incl AA420624:nc61c12.r1 Homo sapiens cDNA					
	/clone=IMAGE-745750 /gb=AA420624 /gi=2094502					
	/ug=Hs.183109 /len=533					
40508_at	glutathione S-transferase A4					
41772_at	monoamine oxidase A					
40004_at	sine oculis homeobox (Drosophila) homolog 1					
37600_at	extracellular matrix protein 1					

Table 36. Lung adenocarcinoma poor prognosis predictor cluster 3.						
23 genes (r = 0.891)						
Affymetrix Probe	Description					
Set ID (U95Av2)						
41106_at	potassium intermediate/small conductance calcium-activated					
·	channel, subfamily N, member 4					
1868_g_at	CASP8 and FADD-like apoptosis regulator					
41471_at	Cluster Incl W72424:zd66a09.s1 Homo sapiens cDNA, 3 end					
	/clone=IMAGE-345592 /clone_end=3" /gb=W72424 /gi=1382379					
·	/ug=Hs.112405 /len=604"					
37921_at	neuronal pentraxin I					
38422_s_at	four and a half LIM domains 2					

39114_at	decidual protein induced by progesterone					
34375_at	small inducible cytokine A2 (monocyte chemotactic protein 1,					
:	homologous to mouse Sig-je)					
36495_at	fructose-1,6-bisphosphatase 1					
37187_at	GRO2 oncogene					
37014_at	myxovirus (influenza) resistance 1, homolog of murine (interferon-					
	inducible protein p78)					
925_at	interferon, gamma-inducible protein 30					
35766_at	keratin 18					
39372_at	Cluster Incl W26480:30b8 Homo sapiens cDNA /gb=W26480					
	/gi=1307179 /ug=Hs.12214 /len=854					
32072_at	mesothelin					
40422_at	insulin-like growth factor binding protein 2 (36kD)					
41771_g_at	Cluster Incl AA420624:nc61c12.r1 Homo sapiens cDNA					
	/clone=IMAGE-745750 /gb=AA420624 /gi=2094502					
	/ug=Hs.183109 /len=533					
40508_at	glutathione S-transferase A4					
1741_s_at	S37730 /FEATURE=cds /DEFINITION=S37712S4 insulin-like					
	growth factor binding protein-2 [human, placenta, Genomic, 1342					
	nt, segment 4 of 4]					
41772_at	monoamine oxidase A					
37874_at	flavin containing monooxygenase 5					
37811_at	calcium channel, voltage-dependent, alpha 2/delta subunit 2					
40004_at	sine oculis homeobox (Drosophila) homolog 1					
37600_at	extracellular matrix protein 1					

Table 37. Lung adenocarcinoma poor prognosis predictor cluster 4.				
10 genes $(r = 0.872)$				
Affymetrix Probe Set ID	Affymetrix Probe Set ID Description			
(U95Av2)				

34342_s_at	secreted phosphoprotein 1 (osteopontin, bone sialoprotein I,
	early T-lymphocyte activation 1)
2092_s_at	secreted phosphoprotein 1 (osteopontin, bone sialoprotein I,
	early T-lymphocyte activation 1)
37019_at	fibrinogen, B beta polypeptide
38825_at	fibrinogen, A alpha polypeptide
37233_at	oxidised low density lipoprotein (lectin-like) receptor 1
31512_at	immunoglobulin kappa variable 1-13
36736_f_at	phosphoserine phosphatase
37811_at	calcium channel, voltage-dependent, alpha 2/delta subunit 2
40004_at	sine oculis homeobox (Drosophila) homolog 1
37874_at	flavin containing monooxygenase 5

Table 38. Lung adenocarcinoma poor prognosis predictor cluster 5.  6 genes (r = 0.918)				
				Affymetrix Probe Description
Set ID				
34342_s_at	secreted phosphoprotein 1 (osteopontin, bone sialoprotein I, early			
	T-lymphocyte activation 1)			
38825_at	fibrinogen, A alpha polypeptide			
31512_at	immunoglobulin kappa variable 1-13			
37811_at	calcium channel, voltage-dependent, alpha 2/delta subunit 2			
40004_at	sine oculis homeobox (Drosophila) homolog 1			
37874_at	flavin containing monooxygenase 5			

[00261] The scoring summary of the individual phenotype association indices calculated for each of the five poor prognosis predictor clusters are presented in Table 39 for the good prognosis patients and in Table 40 for the poor prognosis patients. Only a single patient in the good prognosis group had one positive association index. All the

remaining 15 good prognosis patients had negative phenotype association indices for each of the five poor prognosis gene clusters (Table 39). In contrast, 30 of 34 poor prognosis patients had at least one positive association index and 27 of 34 poor prognosis patients scored at least two positive phenotype association indices (Table 40). Thus, applying the methods of the present invention and applying a criterion requiring at least 1 positive phenotype association index for poor prognosis classification, 45 of 50 (90%) adenocarcinoma patients in this data set could be correctly classified as having a good or a poor prognosis.

Table 39. Scoring summary of the lung adenocarcinoma poor prognosis gene clusters for good prognosis patients.						
	T	<del></del>	T.		T	Number of false
Sample	38 genes	19 genes	23 genes	10 genes	6 genes	classifications
		Phenoty	pe Associat	ion Indices	<del>- L</del> .	
AD187	-0.06452	-0.04784	0.452696	-0.00941	-0.23775	1
AD119	-0.29927	-0.33723	-0.1148	-0.28902	-0.23916	0
AD131	-0.17964	-0.48139	-0.33392	-0.401	-0.17498	0
AD163	-0.12353	-0.28925	-0.0734	-0.15033	-0.01296	0
AD170	-0.17682	-0.49435	-0.34161	-0.32239	-0.64159	0
AD186	-0.34093	-0.61548	-0.28551	-0.37547	-0.19218	0
AD203	-0.50111	-0.52408	-0.06856	-0.14395	-0.21014	0
AD250	-0.27238	-0.25103	-0.12624	-0.68264	-0.68955	0
AD305	-0.17459	-0.36628	-0.29005	-0.11941	-0.39534	0
AD308	-0.6101	-0.03024	-0.02817	-0.40192	-0.34151	0
AD317	-0.276	-0.56248	-0.16234	-0.57284	-0.51591	0
AD318	-0.08142	-0.60361	-0.52572	-0.30083	-0.54905	0
AD320	-0.09336	-0.40628	-0.09197	-0.16229	-0.29432	0

AD327	-0.05072	-0.11578	-0.1069	-0.11479	-0.49102	0
AD338	-0.49705	-0.45102	-0.26864	-0.803	-0.84779	0
AD367	-0.03213	-0.22574	-0.30494	-0.5605	-0.39852	0

Table	Table 40. Scoring summary of the lung adenocarcinoma poor prognosis					
	gene clusters for poor prognosis patients.					
						Number of correct
Sample	38 genes	19 genes	23 genes	10 genes	6 genes	classification
	P	henotype	Associat	ion Indice	es	
AD277	0.234435	0.410067	0.736989	0.574246	0.712075	5
AD330	0.413889	0.175061	0.101943	0.382497	0.242026	5
AD374	0.055386	0.455203	0.549645	0.002916	0.052327	5
AD177	0.304326	0.55951	0.423434	-0.08411	0.479041	. 4
AD258	0.43388	-0.05816	0.293763	0.558311	0.70477	4
AD276	0.171625	-0.53343	0.415923	0.713297	0.80945	4
AD287	0.233826	-0.14383	0.281022	0.069933	0.221046	4
AD323	-0.1194	0.267964	0.027922	0.140244	0.399934	4
AD352	0.115964	0.041747	0.196362	0.622718	0.802551	4
AD157	-0.08334	0.179166	0.102028	-0.1272	0.294908	3
AD164	0.281754	0.608169	0.31086	-0.10786	-0.4293	3
AD208	0.236001	0.310463	0.230929	-0.23772	-0.70165	3
AD221	-0.23875	-0.42763	0.261846	0.292941	0.749037	3
AD236	0.172613	-0.4351	0.155221	-0.05824	0.650534	. 3
AD275	-0.04808	0.203627	0.111381	0.050702	-0.17309	3
AD296	0.438626	0.52086	0.084982	-0.57093	-0.9214	3
AD301	0.048676	-0.41297	-0.27021	0.15905	0.049724	3
AD043	0.047335	-0.00851	0.357719	-0.15053	-0.23508	2
AD127	-0.07916	-0.3513	0.273233	-0.03922	0.184294	2
AD262	-0.05662	0.287899	0.423555	-0.23891	-0.12164	2

AD304	-0.21516	0.186401	0.076621	-0.25509	-0.18305	2
AD332	0.241748	0.198359	-0.20156	-0.22034	-0.06101	2
AD334	0.234121	-0.32246	-0.47165	0.357084	-0.03519	2
AD346	-0.54482	-0.40513	0.228292	-0.22006	0.355989	2
AD361	-0.46304	0.368086	0.071209	-0.455	-0.48077	2
AD363	-0.33631	-0.1249	-0.12018	0.161188	0.075687	2
AD384	-0.20144	-0.3584	0.451957	-0.13904	0.870275	2
AD130	-0.17359	-0.26894	0.414704	-0.2768	-0.41716	1
AD225	-0.14786	-0.2287	0.072267	-0.0685	-0.35463	1
AD353	-0.61406	-0.52593	0.187469	-0.89949	-0.97919	1
AD201	-0.08499	-0.4772	-0.47199	-0.23861	-0.54777	0
AD252	-0.07534	-0.4901	-0.35684	-0.23247	-0.15586	0
AD347	-0.5658	-0.52075	-0.31889	-0.60543	-0.92335	0
AD366	-0.34494	-0.56913	-0.24398	-0.14348	-0.43697	0

## EXAMPLE 5 – ORTHOTOPIC XENOGRAFT GENE EXPRESSION PROFILE AS PREDICTIVE REFERENCE OF EXPECTED TRANSCRIPT ABUNDANCE BEHAVIOR IN CLINICAL SAMPLES AND USE TO IDENTIFY GENE CLUSTERS WITH CLINICALLY USEFUL PROPERTIES.

[00262] When human cancer cells derived from the metastatic tumors are injected into ectopic sites in nude mice most do not metastasize (1, 2). The host tissue environment influences metastatic ability of cancer cells in such a way that many human and animal tumors transplanted into nude mice metastasize only if placed in the orthotopic organ (3-8). Several orthotopic models of human cancer metastasis have been developed (9-15). The orthotopic model of human cancer metastasis in nude mice was utilized for in vivo selection of highly and poorly metastatic cell variants (6, 13-15). This approach was successfully applied for development of human prostate cancer cell variants with distinct metastatic potential (15). Experimental evidence indicates that enhancement of metastatic

capability of human cancer cells transplanted orthotopically is associated with differential expression of several metastasis-associated genes that have been implicated earlier in certain key features of the metastatic phenotype (16). It is well established that even highly metastatic cells, when implanted ectopically, are not able to consistently produce metastasis.

Here we identified metastasis-associated gene expression signatures based on [00263] expression profiling human prostate carcinoma xenografts derived from the same highly metastatic variant implanted at orthotopic (metastasis promoting setting) and ectopic (metastasis suppressing setting) sites, demonstrating that distinct malignant behavior of highly metastatic cells associated with the site of inoculation in a nude mouse is dependent upon differential gene expression in prostate cancer cells implanted either orthotopically or ectopically. We utilized the Affymetrix GeneChip system to compare the expression profiles of 12,625 transcripts in highly metastatic variant PC-3MLN4 implanted at orthotopic (metastasis promoting setting) ("PC3MLN4OR") and ectopic (metastasis suppressing setting) ("PC3MLN4SC") sites. PC-3MLN4 tumors growing in orthotopic metastasis-promoting setting appear to dramatically over-express a set of genes with well-established invasion-activation functions (Figure 46). Changes in expression for each transcript are plotted as Log10Fold Change Average expression level in PC-3MLN4OR versus Average expression level in less metastatic parental PC3OR and PC3MOR (recurrence signatures) (Fig. 47A) or versus Average expression level in PC3PC-3MLN4SC (invasion signatures) (Fig. 47B) and Log10Fold Change Average expression level in aggressive (recurrent or invasive) versus Average expression level in corresponding non-aggressive (non-recurrent or non-invasive) clinical phenotypes.

Expression profiling of the 12,625 transcripts in the orthotopic and s.c. xenografts derived from the cell variants of the PC-3 lineage was carried out. Transcripts differentially expressed at the statistically significant level (p<0.05; T-test) in the orthotopic PC-3M-LN4 tumors compared to the s.c. tumors of the same lineage as well as orthotopic tumors derived from the less metastatic parental PC-3M and PC-3 cell lines were identified using the Affymetrix MicroDB and Affymetrix DMT software. Similarly, transcripts differentially regulated in the 8 recurrent versus 13 non-recurrent (Fig. 47A) or 26 invasive versus 26 non-invasive (Fig. 47B) human prostate tumors at the statistically significant level (p<0.05; T-test) were identified. The small clusters of genes exhibiting highly concordant gene expression patterns in the xenograft model and clinical setting were identified using the methods of the invention. In the first example (Fig. 47A), comparisons of the average fold expression changes in highly metastatic PC3MLN4 orthotopic xenografts versus less metastatic parental PC3 and PC3M orthotopic xenografts and 8 recurrent versus 13 non-recurrent primary carcinomas were carried out and a Pearson correlation coefficient was calculated for set of transcripts exhibiting concordant expression changes (Fig. 47A). In the second example (Fig. 47B), comparisons of the average fold expression changes in orthotopic versus s.c. PC3MLN4 xenografts and 26 invasive versus 26 non-invasive primary carcinomas were carried out and a Pearson correlation coefficient was calculated for set of transcripts exhibiting concordant expression changes (Fig. 47B). The transcript abundance levels of several genes encoding matrix metalloproteinases (MMP9; MMP10; MMP1; MMP14 [Fig. 46A1-Fig. 46A4]) as well as components of plasminogen activator (PA) / PA receptor & plasminogen receptor system (uPA; tPA; uPA receptor; plasminogen receptor; PAI-

1[Figs. 46B1-B4]) are substantially higher in PC-3MLN4 orthotopic tumors versus PC-3MLN4 s.c. (ectopic) tumors, reflecting a plausible mechanistic association of the induction of multiple invasion-activating enzymes with enhanced metastatic potential of PC-3MLN4 tumors in orthotopic setting. Consistent with this idea, the transcript abundance levels for these genes were uniformly lower in orthotopic tumors derived from less metastatic parental PC-3 ("PC3OR") and PC-3M ("PC3MOR") cells compared to the PC-3MLN4 orthotopic tumors (Figures 46A & 46B). Decreased level of expression of protease and angiogenesis inhibitor Maspin in PC-3MLN4 orthotopic tumors (Fig. 46C4) provides an additional clinically relevant example of potential metastasis-promoting molecular alterations in this model since diminished level of Maspin was recently reported in clinical specimens of human prostate cancer (23, 24). Second, a functionally intriguing set of genes highlighted in this model is potentially relevant to metastatic affinity of human prostate carcinoma cells to the bone and represented by a constellation of adhesion molecules (Fig. 46D). Documented in this model is an increase in expression (in a metastasis-promoting setting) of non-epithelial cadherins such as osteoblast cadherins (OB-cadherin-1 and -2) as well as vascular endothelial cadherin (VE-cadherin) along with a concomitantly diminished level of expression of epithelial cadherin (Ecadherin) (Fig. 46D). These molecular aberrations identified in our model correlate with the clinical phenomenon described as a cadherin switching in human prostate carcinoma (25, 26). Interestingly, increased expression of the osteoblast cadherins in clinical prostate cancer specimens was associated with progression and metastasis of human prostate cancer (25, 26), supporting the notion that metastasis-associated molecular alterations identified in the model system are clinically relevant. Two other adhesion

shown), share some common properties: they mediate both homotypic and heterotypic cell-cell adhesion crucial for metastasis of melanoma cells (27-30); they are expressed on activated leukocytes and on human endothelium (31-35). In addition, ALCAM expression was identified on bone marrow stromal and mesenchymal stem cells and implicated in bone marrow formation and hematopoiesis (31; 36-39). Interestingly, similarly to cadherins, ALCAM is capable to mediate cell-cell adhesion through homophilic ALCAM-ALCAM interactions (31, 40), thus, expression of ALCAM on human prostate carcinoma cells makes this molecule a viable candidate mediator of human prostate carcinoma homing to the bone. MCAM (MUC18) protein overexpression was reported recently in human prostate cancer cell lines, high-grade prostatic intraepithelial neoplasia (PIN), prostate carcinomas, and lymph node metastasis (41, 42). [00264] Expression profiling experiments imply that human prostate carcinoma cells growing in orthotopic metastasis-promoting setting display many clinically relevant gene expression features. Highly aggressive clinically relevant biological behavior of human prostate cancer cells growing in the prostate of nude mice is particularly evident in a fluorescent orthotopic bone metastasis model recapitulating to a significant degree the clinical pattern of metastatic spread of advanced prostate cancer in men (12). Recent gene expression analysis experiments showed that molecular signatures of metastasis could be identified in primary solid tumors (43). We sought to determine whether human prostate carcinoma xenografts growing in the prostate of nude mice would carry the clinically relevant gene-expression signatures of metastasis. We compared the gene expression profiles of 9 metastatic and 23 primary human prostate tumors (the original clinical data

molecules expressed in PC-3MLN4 orthotopic tumors, MCAM and ALCAM (data not

were published in LaTulippe, E., Satagopan, J., Smith, A., Scher, H., Scardino, P., Reuter, V., Gerald, W.L. Comprehensive gene expression analysis of prostate cancer reveals distinct transcriptional programs associated with metastatic disease. Cancer Res., 62: 4499-4506, 2002) to identify a broad spectrum of transcripts differentially regulated at the statistically significant level (p<0.05) in metastatic human prostate cancer. Next, we compared a set of transcripts differentially regulated in clinical metastatic human prostate tumors with transcripts differentially regulated in orthotopic human prostate carcinoma xenografts versus subcutaneous ("s.c.")(i.e., ectopic) tumors of the same lineage. This comparison identified a set of 131 genes that exhibited highly concordant behavior in clinical metastatic samples and orthotopic metastasis-promoting tumors (Pearson correlation coefficient, r = 0.799; Figure 48A; Table 41.0).

Table 41.0	Table 41.0. Prostate cancer metastasis segregation cluster comprising 131 genes			
Affymetrix	Change	Description		
Probe ID	direction in			
(U95Av2)	metastasis			
		Cluster Incl. X89426:H.sapiens mRNA for ESM-1		
		protein /cds=(55,609) /gb=X89426 /gi=1150418		
33534_at	Up	/ug=Hs.41716 /len=2006		
		Cluster Incl. AI017574:ou23f10.x1 Homo sapiens cDNA,		
		3 end /clone=IMAGE-1627147 /clone_end=3		
33232_at	Up	/gb=AI017574 /gi=3231910 /ug=Hs.17409 /len=501		
		Cluster Incl. D50920:Human mRNA for KIAA0130		
		gene, complete cds /cds=(73,3042) /gb=D50920		
34289_f_at	Up	/gi=1469182 /ug=Hs.23106 /len=3468		
		Cluster Incl. D79987:Human mRNA for KIAA0165		
		gene, complete cds /cds=(1113,6500) /gb=D79987		
38158_at	Up	/gi=1136391 /ug=Hs.153479 /len=6662		

		X00737 /FEATURE=cds /DEFINITION=HSPNP Human
		mRNA for purine nucleoside phosphorylase (PNP; EC
430_at	Up	2.4.2.1)
		M13792 /FEATURE=cds /DEFINITION=HUMADAG
907_at	Up	Human adenosine deaminase (ADA) gene, complete cds
	<del> </del>	Cluster Incl. Z23115:H.sapiens bcl-xL mRNA
		/cds=(134,835) /gb=Z23115 /gi=510900 /ug=Hs.239744
34742_at	Up	/len=926
	<del> </del>	Z23115 /FEATURE=cds /DEFINITION=HSBCLXL
1615_at	Up	H.sapiens bcl-xL mRNA
	<del> </del>	Cluster Incl. AF000652:Homo sapiens syntenin (sycl)
		mRNA, complete cds /cds=(148,1044) /gb=AF000652
38110_at	Up	/gi=2795862 /ug=Hs.8180 /len=2162
		Cluster Incl. AF037195:Homo sapiens regulator of G
		protein signaling RGS14 mRNA, complete cds
,		/cds=(73,1398) /gb=AF037195 /gi=2708809
38290_at	Up	/ug=Hs.9347 /len=1531
		Cluster Incl. U28964:Homo sapiens 14-3-3 protein
		mRNA, complete cds /cds=(126,863) /gb=U28964
34642_at	Up	/gi=899458 /ug=Hs.75103 /len=1030
		Cluster Incl. AB007925:Homo sapiens mRNA for
		KIAA0456 protein, partial cds /cds=(0,3287)
36069_at	Up	/gb=AB007925 /gi=3413873 /ug=Hs.5003 /len=6305
		M31303 /FEATURE=mRNA
		/DEFINITION=HUMOP18A Human oncoprotein 18
1782_s_at	Up	(Op18) gene, complete cds
		U14518 /FEATURE= /DEFINITION=HSU14518 Human
527_at	Up	centromere protein-A (CENP-A) mRNA, complete cds
		X13293 /FEATURE=cds /DEFINITION=HSBMYB
1854_at	Up	Human mRNA for B-myb gene

	T	Cluster Incl. U28386:Human nuclear localization
-		sequence receptor hSRP1alpha mRNA, complete cds
		/cds=(132,1721) /gb=U28386 /gi=899538 /ug=Hs.159557
40407_at	Up	/len=1976
		Cluster Incl. AB018347:Homo sapiens mRNA for
		KIAA0804 protein, partial cds /cds=(0,3636)
36870_at	Up	/gb=AB018347 /gi=3882328 /ug=Hs.7316 /len=4216
		U40343 /FEATURE= /DEFINITION=HSU40343 Human
1797_at	Up	CDK inhibitor p19INK4d mRNA, complete cds
		M87339 /FEATURE= /DEFINITION=HUMACT1A
		Human replication factor C, 37-kDa subunit mRNA,
1054_at	Up	complete cds
<del></del>	<del></del>	Cluster Incl. X59618:H.sapiens RR2 mRNA for small
		subunit ribonucleotide reductase /cds=(194,1363)
36922_at	Up	/gb=X59618 /gi=36154 /ug=Hs.75319 /len=2475
	<del> </del>	Cluster Incl. U37426:Human kinesin-like spindle protein
		HKSP (HKSP) mRNA, complete cds /cds=(90,3260)
40726_at	Up	/gb=U37426 /gi=1171152 /ug=Hs.8878 /len=4858
		Cluster Incl. AF007875:Homo sapiens dolichol
}		monophosphate mannose synthase (DPM1) mRNA,
		partial cds /cds=(0,761) /gb=AF007875 /gi=2258417
34879_at	Up	/ug=Hs.5085 /len=1054
		Cluster Incl. AF006010:Human progestin induced protein
		(DD5) mRNA, complete cds /cds=(33,8423)
39035_at	Up	/gb=AF006010 /gi=4101694 /ug=Hs.11469 /len=8493
		Stimulatory Gdp/Gtp Exchange Protein For C-Ki-Ras
1624_at	Up	P21 And Smg P21
<b> </b>	1	Cluster Incl. U74612:Human hepatocyte nuclear factor-
		3/fork head homolog 11A (HFH-11A) mRNA complete
		cds /cds=(114,2519) /gb=U74612 /gi=1842252
34715_at	Up	/ug=Hs.239 /len=3474

		M86400 /FEATURE= /DEFINITION=HUMPHPLA2
1235_at	Up	Human phospholipase A2 mRNA, complete cds
		Cluster Incl. U18271:Human thymopoietin (TMPO) gene
		/cds=(313,2397) /gb=U18271 /gi=2182141
32683_at	Up	/ug=Hs.170225 /len=2796
	<del> </del>	Cluster Incl. AF030424:Homo sapiens histone
		acetyltransferase 1 mRNA, complete cds /cds=(36,1295)
41855_at	Up	/gb=AF030424 /gi=2623155 /ug=Hs.13340 /len=1568
}	<del> </del>	X74794 /FEATURE=cds /DEFINITION=HSP1CDC21
981_at	Up	H.sapiens P1-Cdc21 mRNA
		Cluster Incl. X93921:H.sapiens mRNA for protein-
		tyrosine-phosphatase (tissue type- testis) /cds=(0,968)
39933_at	Up	/gb=X93921 /gi=1418935 /ug=Hs.3843 /len=1471
		Cluster Incl. X76770:H.sapiens PAP mRNA
		/cds=UNKNOWN /gb=X76770 /gi=556782
34855_at	Up	/ug=Hs.49007 /len=1956
		Cluster Incl. L36055:Human 4E-binding protein 1
·		mRNA, complete cds /cds=(0,356) /gb=L36055
31597_r_at	Up	/gi=561629 /ug=Hs.198144 /len=357
		U01062 /FEATURE=mRNA
		/DEFINITION=HUMIP3R3 Human type 3 inositol 1,4,5-
182_at	Up	trisphosphate receptor (ITPR3) mRNA, complete cds
		Cluster Incl. D31762:Human mRNA for KIAA0057
		gene, complete cds /cds=(75,1187) /gb=D31762
40051_at	Up	/gi=498149 /ug=Hs.153954 /len=6974
1906_at	Up	Ras Inhibitor Inf
		Cluster Incl. U66867:Human ubiquitin conjugating
		enzyme 9 (hUBC9) mRNA, complete cds
		/cds=(806,1282)/gb=U66867/gi=1561758/ug=Hs.84285
38480_s_at	Up	/len=1823

	Ţ	Cluster Incl. U37352:Human protein phosphatase 2A
		Balpha1 regulatory subunit mRNA, complete cds
		/cds=(88,1632)/gb=U37352/gi=1203811/ug=Hs.171734
40786_at	Up	/len=4064
		Cluster Incl. Y08614:Homo sapiens mRNA for CRM1
		protein /cds=(38,3253) /gb=Y08614 /gi=5541866
37729_at	Up	/ug=Hs.79090 /len=4148
<del></del>		Cluster Incl. AF070640:Homo sapiens clone 24781
		mRNA sequence /cds=UNKNOWN /gb=AF070640
38702_at	Up	/gi=3283913 /ug=Hs.108112 /len=1583
,		Cluster Incl. AW005997:wz91c01.x1 Homo sapiens
		cDNA, 3 end /clone=IMAGE-2566176 /clone_end=3
32578_at	Up	/gb=AW005997 /gi=5854775 /ug=Hs.78185 /len=702
		M74524 /FEATURE= /DEFINITION=HUMHHR6A
		Human HHR6A (yeast RAD 6 homologue) mRNA,
890_at	Up	complete cds
		Cluster Incl. M37583:Human histone (H2A.Z) mRNA,
		complete cds /cds=(106,492) /gb=M37583 /gi=184059
39337_at	Up	/ug=Hs.119192 /len=873
		Cluster Incl. AI961669:wt65e11.x1 Homo sapiens
		cDNA, 3 end /clone=IMAGE-2512364 /clone_end=3
34484_at	Up	/gb=AI961669 /gi=5754382 /ug=Hs.118249 /len=565
<del></del>		Cluster Incl. AF025840:Homo sapiens DNA polymerase
		epsilon subunit B (DPE2) mRNA, complete cds
		/cds=(130,1710)/gb=AF025840/gi=2697122
41085_at	Up	/ug=Hs.99185 /len=1807
		Cluster Incl. X54942:H.sapiens ckshs2 mRNA for Cks1
		protein homologue /cds=(95,334) /gb=X54942 /gi=29978
40690_at	Up	/ug=Hs.83758 /len=612

	T	Cluster Incl. Y08685:H.sapiens mRNA for serine
		palmitoyltransferase, subunit I /cds=(0,1421)
38818_at	Up	/gb=Y08685 /gi=2564246 /ug=Hs.90458 /len=1621
	<del> </del>	Cluster Incl. U84573:Homo sapiens lysyl hydroxylase
		isoform 2 (PLOD2) mRNA, complete cds /cds=(0,2213)
34795_at	Up	/gb=U84573 /gi=2138313 /ug=Hs.41270 /len=3480
		M30938 /FEATURE=mRNA#1
		/DEFINITION=HUMKUP Human Ku (p70/p80) subunit
584_s_at	Up	mRNA, complete cds
		Cluster Incl. AJ132258:Homo sapiens mRNA for staufen
		protein, partial /cds=(35,1525) /gb=AJ132258
41823_at	Up	/gi=4572587 /ug=Hs.6113 /len=3066
		Cluster Incl. AB015633:Homo sapiens mRNA for type II
		membrane protein, complete cds, clone-HP10481
		/cds=(104,1435)/gb=AB015633/gi=4586843
37445_at	Up	/ug=Hs.112986 /len=1451
		Cluster Incl. AI680675:tx40a08.x1 Homo sapiens cDNA,
}		3 end /clone=IMAGE-2272022 /clone_end=3
41569_at	Up	/gb=AI680675 /gi=4890857 /ug=Hs.44131 /len=554
1515_at	Up	Rad2
		Cluster Incl. U58087:Human Hs-cul-1 mRNA, complete
		cds /cds=(124,2382) /gb=U58087 /gi=1381141
39724_s_at	Up	/ug=Hs.14541 /len=2511
		Cluster Incl. AI347155:tc04c11.x1 Homo sapiens cDNA,
		3 end/clone=IMAGE-2062868/clone_end=3
36492_at	Up	/gb=AI347155 /gi=4084361 /ug=Hs.5648 /len=750
		Cluster Incl. AB028990:Homo sapiens mRNA for
		KIAA1067 protein, partial cds /cds=(0,2072)
33877_s_at	Up	/gb=AB028990 /gi=5689470 /ug=Hs.24375 /len=4704

	<del>,                                    </del>	Chater Incl. A1525202.DT1 1 07 A11 - Home coniens
		Cluster Incl. AI525393:PT1.1_07_A11.r Homo sapiens
		cDNA, 5 end /clone_end=5 /gb=AI525393 /gi=4439528
35810_at	Up	/ug=Hs.6895 /len=811
		K03460 /FEATURE=cds /DEFINITION=HUMTUBA2H
685_f_at	Up	Human alpha-tubulin isotype H2-alpha gene, last exon
		Cluster Incl. AF070582:Homo sapiens clone 24766
		mRNA sequence /cds=UNKNOWN /gb=AF070582
35165_at	Up	/gi=3387954 /ug=Hs.26118 /len=1744
		Cluster Incl. U23143:Human mitochondrial serine
	<u> </u>	hydroxymethyltransferase gene, nuclear encoded
	, ,	mitochondrion protein, complete cds /cds=(0,1451)
36178_at	Up	/gb=U23143 /gi=746435 /ug=Hs.75069 /len=1452
		Cluster Incl. D25278:Human mRNA for KIAA0036
		gene, complete cds /cds=(156,1952) /gb=D25278
32657_at	Up	/gi=434780 /ug=Hs.169387 /len=2535
<del></del>		Cluster Incl. AL096719:Homo sapiens mRNA; cDNA
		DKFZp566N043 (from clone DKFZp566N043)
		/cds=UNKNOWN/gb=AL096719/gi=5419854
38839_at	Up	/ug=Hs.91747 /len=2185
		U56816 /FEATURE= /DEFINITION=HSU56816 Human
480_at	Up	kinase Myt1 (Myt1) mRNA, complete cds
	<u> </u>	X74795 /FEATURE=cds /DEFINITION=HSP1CDC46
982_at	Up	H.sapiens P1-Cdc46 mRNA
		Cluster Incl. M65028:Human hnRNP type A/B protein
		mRNA, complete cds /cds=(142,996) /gb=M65028
38094_at	Up	/gi=337450 /ug=Hs.81361 /len=1537
		Cluster Incl. L03532:Human M4 protein mRNA,
		complete cds /cds=(11,2200) /gb=L03532 /gi=187280
37717_at	Up	/ug=Hs.79024 /len=2457

	Ţ ·	Cluster Incl. M62762:Human vacuolar H+ ATPase
}		proton channel subunit mRNA, complete cds
	1	/cds=(230,697) /gb=M62762 /gi=189675 /ug=Hs.76159
36994_at	Up	/len=1162
		Cluster Incl. AL021546:Human DNA sequence from
		BAC 15E1 on chromosome 12. Contains Cytochrome C
		Oxidase Polypeptide VIa-liver precursor gene, 60S
		ribosomal protein L31 pseudogene, pre-mRNA splicing
		factor SRp30c gene, two putative genes, ESTs, STSs and
32573_at	Up	pu
·		Cluster Incl. AF032456:Homo sapiens ubiquitin
		conjugating enzyme G2 (UBE2G2) mRNA, complete cds
		/cds=(55,552) /gb=AF032456 /gi=3004908
32236_at	Up	/ug=Hs.192853 /len=2890
		Cluster Incl. S65738:actin depolymerizing factor [human,
		fetal brain, mRNA, 1452 nt] /cds=(72,569) /gb=S65738
38385_at	Down	/gi=415586 /ug=Hs.82306 /len=1452
		Cluster Incl. W28865:53g9 Homo sapiens cDNA
38982_at	Down	/gb=W28865 /gi=1308876 /ug=Hs.109875 /len=926
		Cluster Incl. X58199:Human mRNA for beta adducin
		/cds=(322,2502) /gb=X58199 /gi=29368 /ug=Hs.4852
36051_s_at	Down	/len=2597
		Cluster Incl. AF044671:Homo sapiens MM46 mRNA,
		complete cds /cds=(78,431) /gb=AF044671 /gi=4105274
37298_at	Down	/ug=Hs.7719 /len=859
		Cluster Incl. M58458:Human ribosomal protein S4
		(RPS4X) isoform mRNA, complete cds /cds=(35,826)
34643_at	Down	/gb=M58458 /gi=337509 /ug=Hs.75344 /len=888
		Cluster Incl. U37230:Human ribosomal protein L23a
		mRNA, complete cds /cds=(23,493) /gb=U37230
32341_f_at	Down	/gi=1574941 /ug=Hs.184776 /len=548

		Cluster Incl. M17886:Human acidic ribosomal
		phosphoprotein P1 mRNA, complete cds /cds=(129,473)
31956_f_at	Down	/gb=M17886 /gi=190233 /ug=Hs.177592 /len=512
		Cluster Incl. M17886:Human acidic ribosomal
		phosphoprotein P1 mRNA, complete cds /cds=(129,473)
31957_r_at	Down	/gb=M17886 /gi=190233 /ug=Hs.177592 /len=512
		L77886 /FEATURE= /DEFINITION=HUMPTPC
		Human protein tyrosine phosphatase mRNA, complete
1488_at	Down	cds
		Cluster Incl. L14754:Human DNA-binding protein
		(SMBP2) mRNA, complete cds /cds=(49,3030)
31861_at	Down	/gb=L14754 /gi=401775 /ug=Hs.1521 /len=3892
		Cluster Incl. L06499:Homo sapiens ribosomal protein
		L37a (RPL37A) mRNA, complete cds /cds=(17,295)
31962_at	Down	/gb=L06499 /gi=292438 /ug=Hs.184109 /len=357
		Cluster Incl. AF070638:Homo sapiens clone 24448
		unknown mRNA, partial cds /cds=(0,659) /gb=AF070638
34864_at	Down	/gi=3283909 /ug=Hs.4973 /len=1348
		Cluster Incl. M13934:Human ribosomal protein S14
		gene, complete cds /cds=(2,457) /gb=M13934
32412_at	Down	/gi=337498 /ug=Hs.3491 /len=503
	<u> </u>	Cluster Incl. U03105:Human B4-2 protein mRNA,
		complete_cds /cds=(113,1096) /gb=U03105 /gi=476094
36980_at	Down	/ug=Hs.75969 /len=2061
		Cluster Incl. AA977163:oq25a04.s1 Homo sapiens
		cDNA, 3 end/clone=IMAGE-1587342/clone_end=3
33116_f_at	Down	/gb=AA977163 /gi=3154609 /ug=Hs.82148 /len=524
		Cluster Incl. X56932:H.sapiens mRNA for 23 kD highly
		basic protein /cds=(17,628) /gb=X56932 /gi=23690
35119_at	Down	/ug=Hs.119122 /len=672

		Cluster Incl. X64707:H.sapiens BBC1 mRNA	
		/cds=(51,686) /gb=X64707 /gi=29382 /ug=Hs.180842	
31509_at	Down	/len=942	
}		Cluster Incl. U14971:Human ribosomal protein S9	
		mRNA, complete cds /cds=(35,619) /gb=U14971	
31511_at	Down	/gi=550022 /ug=Hs.180920 /len=692	
		Cluster Incl. M16279:Human MIC2 mRNA, complete	
		cds /cds=(177,734) /gb=M16279 /gi=188542	
41138_at	Down	/ug=Hs.177543 /len=1238	
		Cluster Incl. X15940:Human mRNA for ribosomal	
! !		protein L31 /cds=(7,384) /gb=X15940 /gi=36129	
33676_at	Down	/ug=Hs.184014 /len=414	
		Cluster Incl. M13932:Human ribosomal protein S17	
		mRNA, complete cds /cds=(25,432) /gb=M13932	
34592_at	Down	/gi=337500 /ug=Hs.5174 /len=477	
		Cluster Incl. AI541336:pec1.2-7.A07.r Homo sapiens	
		cDNA, 5 end /clone_end=5 /gb=AI541336 /gi=4458709	
38060_at	Down	/ug=Hs.80595 /len=717	
		Cluster Incl. AI557852:P6test.G05.r Homo sapiens	
		cDNA, 5 end /clone_end=5 /gb=AI557852 /gi=4490215	
32748_at	Down	/ug=Hs.195453 /len=693	
		M54915 /FEATURE= /DEFINITION=HUMPIMILE	
883_s_at	Down	Human h-pim-1 protein (h-pim-1) mRNA, complete cds	
		U21689 /FEATURE=cds /DEFINITION=HSU21689	
829_s_at	Down	Human glutathione S-transferase-P1c gene, complete cds	
		Cluster Incl. AL050006:Homo sapiens mRNA; cDNA	
		DKFZp564A033 (from clone DKFZp564A033)	
		/cds=(0,957)/gb=AL050006/gi=4884074/ug=Hs.7627	
37197_s_at	Down	/len=1252	

		Cluster Incl. X17206:Human mRNA for LLRep3	
		/cds=(240,905) /gb=X17206 /gi=34391 /ug=Hs.182426	
31527_at	Down	/len=934	
		Cluster Incl. X03342:Human mRNA for ribosomal	
<u> </u> 		protein L32 /cds=(34,441) /gb=X03342 /gi=36131	
32276_at	Down	/ug=Hs.169793 /len=505	
		K02100 /FEATURE=mRNA /DEFINITION=HUMOTC	
		Human ornithine transcarbamylase (OTC) mRNA,	
683_at	Down	complete coding sequence .	
		U02570 /FEATURE= /DEFINITION=HSU02570 Human	
552_at	Down	CDC42 GTPase-activating protein mRNA, partial cds	
1173_g_at	Down	Spermidine/Spermine N1-Acetyltransferase, Alt. Splice 2	
		Cluster Incl. Z80776:H.sapiens H2A/g gene /cds=(0,392)	
31693_f_at	Down	/gb=Z80776/gi=1568542/ug=Hs.239458/len=393	
		Cluster Incl. J02984:Human insulinoma rig-analog	
		mRNA encoding DNA-binding protein, complete cds	
		/cds=(29,466) /gb=J02984 /gi=184553 /ug=Hs.133230	
39916_r_at	Down	/len=498	
		Cluster Incl. AB014558:Homo sapiens mRNA for	
		KIAA0658 protein, partial cds /cds=(0,1770)	
35852_at	Down	/gb=AB014558 /gi=3327129 /ug=Hs.7278 /len=4103	
		Cluster Incl. L01124:Human ribosomal protein S13	
		(RPS13) mRNA, complete cds /cds=(32,487)	
33619_at	Down	/gb=L01124 /gi=307390 /ug=Hs.165590 /len=530	
		Cluster Incl. M13903:Human involucrin mRNA	
		/cds=(0,1757) /gb=M13903 /gi=186520 /ug=Hs.157091	
36355_at	Down	/len=1758	
		Cluster Incl. U14968:Human ribosomal protein L27a	
		mRNA, complete cds /cds=(16,462) /gb=U14968	
32436_at	Down	/gi=550016 /ug=Hs.76064 /len=507	

	ļ	Cluster Incl. AF040963:Homo sapiens Mad4 homolog	
		(Mad4) mRNA, complete cds /cds=(13,642)	
38639_at	Down	/gb=AF040963 /gi=2792361 /ug=Hs.102402 /len=879	
		Cluster Incl. AL035079:dJ53C18.1 (Catalase)	
		/cds=(74,1657)/gb=AL035079/gi=4775614	
37009_at	Down	/ug=Hs.76359 /len=2287	
		Cluster Incl. M80899:Human novel protein AHNAK	
		mRNA, partial sequence /cds=(0,3835) /gb=M80899	
37027_at	Down	/gi=178282 /ug=Hs.76549 /len=4051	
		Cluster Incl. X16155:Human mRNA for chicken	
		ovalbumin upstream promoter transcription factor	
		(COUP-TF) /cds=(0,1256) /gb=X16155 /gi=30139	
39294_at	Down	/ug=Hs.239468 /len=1513	
		Cluster Incl. AJ132440:Homo sapiens mRNA for PLU-1	
		protein /cds=(89,4723) /gb=AJ132440 /gi=4902723	
39713_at	Down	/ug=Hs.143323 /len=6355	
		Cluster Incl. U07802:Human Tis11d gene, complete cds	
		/cds=(291,1739) /gb=U07802 /gi=984508 /ug=Hs.78909	
32587_at	Down	/len=3655	
		Cluster Incl. AL080121:Homo sapiens mRNA; cDNA	
		DKFZp564O0823 (from clone DKFZp564O0823)	
		/cds=(170,904) /gb=AL080121 /gi=5262554	
41402_at	Down	/ug=Hs.105460 /len=2135	
		Cluster Incl. M97287:Human MAR/SAR DNA binding	
		protein (SATB1) mRNA, complete cds /cds=(214,2505)	
36899_at	Down	/gb=M97287 /gi=337810 /ug=Hs.74592 /len=2928	
		Cluster Incl. X93498:H.sapiens mRNA for 21-Glutamic	
		Acid-Rich Protein (21-GARP) /cds=UNKNOWN	
36039_s_at	Down	/gb=X93498/gi=1673496/ug=Hs.47438/len=1160	

	Cluster Incl. L38941:Homo sapiens ribosomal protein	
	N I I I I I I I I I I I I I I I I I I I	
	L34 (RPL34) mRNA, complete cds /cds=(20,373)	
Down	/gb=L38941 /gi=1008855 /ug=Hs.179779 /len=392	
	Cluster Incl. AA658877:nt84c12.s1 Homo sapiens cDNA	
	/clone=IMAGE-1205206 /gb=AA658877 /gi=2595031	
Down	/ug=Hs.181350 /len=897	
	Cluster Incl. AF065388:Homo sapiens tetraspan NET-1	
	mRNA, complete cds /cds=(121,846) /gb=AF065388	
Down -	/gi=3152700 /ug=Hs.38972 /len=1278	
	V00542 /FEATURE=mRNA /DEFINITION=HSIFR14	
Down	Messenger RNA for human leukocyte (alpha) interferon	
	Cluster Incl. AL050381:Homo sapiens mRNA; cDNA	
	DKFZp586B2023 (from clone DKFZp586B2023)	
	/cds=UNKNOWN /gb=AL050381 /gi=4914611	
Down	/ug=Hs.172639 /len=1485	
Down	V-Erba Related Ear-3 Protein	
	Cluster Incl. AF042386:Homo sapiens cyclophilin-33B	
	(CYP-33) mRNA, complete cds /cds=(60,950)	
Down	/gb=AF042386 /gi=2828150 /ug=Hs.33251 /len=1099	
	Cluster Incl. AL022718:dJ1052M9.3 (mouse DOC4	
	LIKE protein) /cds=(0,4094) /gb=AL022718	
Down	/gi=3763969 /ug=Hs.23796 /len=8728	
	Cluster Incl. AL035305:H.sapiens gene from PAC	
	102G20 /cds=(117,803) /gb=AL035305 /gi=4200223	
Down	/ug=Hs.27258 /len=2435	
	Cluster Incl. AI337192:qx88h10.x1 Homo sapiens	
	cDNA, 3 end/clone=IMAGE-2009635/clone_end=3	
Down	/gb=AI337192 /gi=4074119 /ug=Hs.47438 /len=925	
	Cluster Incl. U81523:Human endometrial bleeding	
	associated factor mRNA, complete cds /cds=(33,1145)	
Down	/gb=U81523 /gi=2058537 /ug=Hs.25195 /len=1961	
	Down Down Down Down Down Down Down Down	

		Cluster Incl. W28428:49d8 Homo sapiens cDNA	
35546_at	Down	/gb=W28428 /gi=1308583 /ug=Hs.132153 /len=812	
		Cluster Incl. AL038340:DKFZp566K192_s1 Homo	
		sapiens cDNA, 3 end /clone=DKFZp566K192	
		/clone_end=3 /gb=AL038340/gi=5407591/ug=Hs.1940	
32242_at	Down	/len=746	
		AB000905 /FEATURE=cds /DEFINITION=AB000905	
762_f_at	Down	Homo sapiens DNA for H4 histone, complete cds	
:		Cluster Incl. AF022797:Homo sapiens intermediate	
		conductance calcium-activated potassium channel	
		(hKCa4) mRNA, complete cds /cds=(396,1679)	
41106_at	Down	/gb=AF022797 /gi=2674355 /ug=Hs.10082 /len=2238	
		Cluster Incl. D90150:Human Gx-alpha gene	
		/cds=(619,1686) /gb=D90150 /gi=219668 /ug=Hs.92002	
38279_at	Down	/len=3289	
		J03242 /FEATURE= /DEFINITION=HUMGFIL2	
1591_s_at	Down	Human insulin-lke growth factor II mRNA, complete cds	

[00265] Remarkably, when we compared the expression profiles of these 131 transcripts in orthotopic xenografts and individual clinical samples, we found that all metastatic prostate carcinomas have expression patterns highly similar to orthotopic xenografts as reflected in positive correlation of expression profiles, whereas all primary tumors displayed a negative correlation of expression profiles (Figure 49A). We next attempted to refine the gene-expression signature associated with human prostate cancer metastasis to a small set of transcripts that would exhibit similar discrimination accuracy between metastatic and primary tumors. To achieve this we used the increase in correlation coefficient of gene expression profiles between orthotopic xenografts and clinical samples as a guide for reduction of transcripts number in a cluster (Figures 48B,

C, and D). Using this strategy we were able to identify several smaller clusters of coregulated genes exhibiting highly concordant behavior in the model system and clinical samples (Figures 48 A-D and Tables 41.1, 41.2, 41 & 42) and demonstrating highly accurate discrimination (at least 94%) between clinical samples of metastatic and primary human prostate carcinomas (Figures 49A-D and Table 42).

Table 41.1 Prostate cancer metastasis segregation cluster comprising 37 genes			
Affymetrix	Change	Description	
ID (U95Av2)	direction in		
	metastasis	·	
		Cluster Incl. X89426:H.sapiens mRNA for ESM-1	
		protein /cds=(55,609) /gb=X89426 /gi=1150418	
33534_at	Up	/ug=Hs.41716 /len=2006	
		Cluster Incl. AI017574:ou23f10.x1 Homo sapiens	
		cDNA, 3 end/clone=IMAGE-1627147/clone_end=3	
33232_at	Up	/gb=AI017574 /gi=3231910 /ug=Hs.17409 /len=501	
		Cluster Incl. D50920:Human mRNA for KIAA0130	
		gene, complete cds /cds=(73,3042) /gb=D50920	
34289_f_at	Up	/gi=1469182 /ug=Hs.23106 /len=3468	
}		X00737 /FEATURE=cds /DEFINITION=HSPNP	
		Human mRNA for purine nucleoside phosphorylase	
430_at	Up	(PNP; EC 2.4.2.1)	
		M13792 /FEATURE=cds /DEFINITION=HUMADAG	
907_at	Up	Human adenosine deaminase (ADA) gene, complete cds	
		Cluster Incl. Z23115:H.sapiens bcl-xL mRNA	
		/cds=(134,835)/gb=Z23115/gi=510900/ug=Hs.239744	
34742_at	Up	/len=926	
		Cluster Incl. AF000652:Homo sapiens syntenin (sycl)	
ı		mRNA, complete cds /cds=(148,1044) /gb=AF000652	
38110_at	Up	/gi=2795862 /ug=Hs.8180 /len=2162	

		Cluster Incl. AF037195:Homo sapiens regulator of G	
		protein signaling RGS14 mRNA, complete cds	
		/cds=(73,1398)/gb=AF037195/gi=2708809	
38290_at	Up	/ug=Hs.9347 /len=1531	
<del></del>		Cluster Incl. AB018347:Homo sapiens mRNA for	
		KIAA0804 protein, partial cds /cds=(0,3636)	
36870_at	Up	/gb=AB018347 /gi=3882328 /ug=Hs.7316 /len=4216	
		Stimulatory Gdp/Gtp Exchange Protein For C-Ki-Ras	
1624_at	Up	P21 And Smg P21	
		Cluster Incl. AF030424:Homo sapiens histone	
		acetyltransferase 1 mRNA, complete cds /cds=(36,1295)	
41855_at	Up	/gb=AF030424 /gi=2623155 /ug=Hs.13340 /len=1568	
		Cluster Incl. M13903:Human involucrin mRNA	
		/cds=(0,1757) /gb=M13903 /gi=186520 /ug=Hs.157091	
36355_at	Down	/len=1758	
		Cluster Incl. U14968:Human ribosomal protein L27a	
		mRNA, complete cds /cds=(16,462) /gb=U14968	
32436_at	Down	/gi=550016 /ug=Hs.76064 /len=507	
		Cluster Incl. AF040963:Homo sapiens Mad4 homolog	
		(Mad4) mRNA, complete cds /cds=(13,642)	
38639_at	Down	/gb=AF040963 /gi=2792361 /ug=Hs.102402 /len=879	
		Cluster Incl. AL035079:dJ53C18.1 (Catalase)	
		/cds=(74,1657)/gb=AL035079/gi=4775614	
37009_at	Down	/ug=Hs.76359 /len=2287	
		Cluster Incl. M80899:Human novel protein AHNAK	
		mRNA, partial sequence /cds=(0,3835) /gb=M80899	
37027_at	Down	/gi=178282 /ug=Hs.76549 /len=4051	
		Cluster Incl. X16155:Human mRNA for chicken	
		ovalbumin upstream promoter transcription factor	
		(COUP-TF) /cds=(0,1256) /gb=X16155 /gi=30139	
39294_at	Down	/ug=Hs.239468 /len=1513	

	T	Cluster Incl. AJ132440:Homo sapiens mRNA for PLU-1	
		protein /cds=(89,4723) /gb=AJ132440 /gi=4902723	
39713_at	Down	/ug=Hs.143323 /len=6355	
	<u> </u>	Cluster Incl. U07802:Human Tis11d gene, complete cds	
		/cds=(291,1739) /gb=U07802 /gi=984508 /ug=Hs.78909	
32587_at	Down	/len=3655	
<u> </u>		Cluster Incl. AL080121:Homo sapiens mRNA; cDNA	
		DKFZp564O0823 (from clone DKFZp564O0823)	
		/cds=(170,904)/gb=AL080121/gi=5262554	
41402_at	Down	/ug=Hs.105460 /len=2135	
		Cluster Incl. X93498:H.sapiens mRNA for 21-Glutamic	
		Acid-Rich Protein (21-GARP) /cds=UNKNOWN	
36039_s_at	Down	/gb=X93498 /gi=1673496 /ug=Hs.47438 /len=1160	
		Cluster Incl. L38941:Homo sapiens ribosomal protein	
		L34 (RPL34) mRNA, complete cds /cds=(20,373)	
33657_at	Down	/gb=L38941 /gi=1008855 /ug=Hs.179779 /len=392	
		Cluster Incl. AA658877:nt84c12.s1 Homo sapiens	
		cDNA /clone=IMAGE-1205206 /gb=AA658877	
41721_at	Down	/gi=2595031 /ug=Hs.181350 /len=897	
		Cluster Incl. AF065388:Homo sapiens tetraspan NET-1	
		mRNA, complete cds /cds=(121,846) /gb=AF065388	
34775_at	. Down	/gi=3152700 /ug=Hs.38972 /len=1278	
		V00542 /FEATURE=mRNA /DEFINITION=HSIFR14	
1022_f_at	Down	Messenger RNA for human leukocyte (alpha) interferon	
		Cluster Incl. AL050381:Homo sapiens mRNA; cDNA	
		DKFZp586B2023 (from clone DKFZp586B2023)	
		/cds=UNKNOWN/gb=AL050381/gi=4914611	
35468_at	Down	/ug=Hs.172639 /len=1485	
1147_at	Down	V-Erba Related Ear-3 Protein	

		Cluster Incl. AF042386:Homo sapiens cyclophilin-33B	
		(CYP-33) mRNA, complete cds /cds=(60,950)	
34365_at	Down	/gb=AF042386 /gi=2828150 /ug=Hs.33251 /len=1099	
		Cluster Incl. AL035305:H.sapiens gene from PAC	
		102G20 /cds=(117,803) /gb=AL035305 /gi=4200223	
33935_at	Down	/ug=Hs.27258 /len=2435	
		Cluster Incl. AI337192:qx88h10.x1 Homo sapiens	
		cDNA, 3 end /clone=IMAGE-2009635 /clone_end=3	
36040_at	Down	/gb=AI337192 /gi=4074119 /ug=Hs.47438 /len=925	
		Cluster Incl. U81523:Human endometrial bleeding	
		associated factor mRNA, complete cds /cds=(33,1145)	
39325_at	Down	/gb=U81523 /gi=2058537 /ug=Hs.25195 /len=1961	
		Cluster Incl. W28428:49d8 Homo sapiens cDNA	
35546_at	Down	/gb=W28428 /gi=1308583 /ug=Hs.132153 /len=812.	
		Cluster Incl. AL038340:DKFZp566K192_s1 Homo	
		sapiens cDNA, 3 end /clone=DKFZp566K192	
		/clone_end=3 /gb=AL038340/gi=5407591/ug=Hs.1940	
32242_at	Down	/len=746	
		AB000905 /FEATURE=cds /DEFINITION=AB000905	
762_f_at	Down	Homo sapiens DNA for H4 histone, complete cds	
		Cluster Incl. AF022797:Homo sapiens intermediate	
		conductance calcium-activated potassium channel	
	·	(hKCa4) mRNA, complete cds /cds=(396,1679)	
41106_at	Down	/gb=AF022797 /gi=2674355 /ug=Hs.10082 /len=2238	
		Cluster Incl. D90150:Human Gx-alpha gene	
		/cds=(619,1686)/gb=D90150/gi=219668/ug=Hs.92002	
38279_at	Down	/len=3289	
		J03242 /FEATURE= /DEFINITION=HUMGFIL2	
1591_s_at	Down	Human insulin-lke growth factor II mRNA, complete cds	

Table 41.2. Prostate cancer metastasis segregation cluster comprising 12 genes				
Affymetrix	Change	Description		
ID (U95Av2)	direction in			
	metastasis			
<del></del>		Cluster Incl. X89426:H.sapiens mRNA for ESM-1		
		protein /cds=(55,609) /gb=X89426 /gi=1150418		
33534_at	Up	/ug=Hs.41716 /len=2006		
		Cluster Incl. AI017574:ou23f10.x1 Homo sapiens		
		cDNA, 3 end /clone=IMAGE-1627147 /clone_end=3		
33232_at	Up	/gb=AI017574 /gi=3231910 /ug=Hs.17409 /len=501		
		Cluster Incl. D50920:Human mRNA for KIAA0130		
		gene, complete cds /cds=(73,3042) /gb=D50920		
34289_f_at	Up	/gi=1469182 /ug=Hs.23106 /len=3468		
		X00737 /FEATURE=cds /DEFINITION=HSPNP		
		Human mRNA for purine nucleoside phosphorylase		
430_at	Up	(PNP; EC 2.4.2.1)		
		M13792 /FEATURE=cds /DEFINITION=HUMADAG		
907_at	Up	Human adenosine deaminase (ADA) gene, complete cds		
		Cluster Incl. Z23115:H.sapiens bcl-xL mRNA		
		/cds=(134,835) /gb=Z23115 /gi=510900 /ug=Hs.239744		
34742_at	Up	/len=926		
		Cluster Incl. AI337192:qx88h10.x1 Homo sapiens		
		cDNA, 3 end/clone=IMAGE-2009635/clone_end=3		
36040_at	Down	/gb=AI337192 /gi=4074119 /ug=Hs.47438 /len=925		
<u> </u>		Cluster Incl. W28428:49d8 Homo sapiens cDNA		
35546_at	Down	/gb=W28428 /gi=1308583 /ug=Hs.132153 /len=812		
		AB000905 /FEATURE=cds /DEFINITION=AB000905		
762_f_at	Down	Homo sapiens DNA for H4 histone, complete cds		

		Cluster Incl. AF022797:Homo sapiens intermediate	
		conductance calcium-activated potassium channel	
		(hKCa4) mRNA, complete cds /cds=(396,1679)	
41106_at	Down	/gb=AF022797 /gi=2674355 /ug=Hs.10082 /len=2238	
		Cluster Incl. D90150:Human Gx-alpha gene	
		/cds=(619,1686) /gb=D90150 /gi=219668 /ug=Hs.92002	
38279_at	Down	/len=3289	
		J03242 /FEATURE= /DEFINITION=HUMGFIL2	
		Human insulin-lke growth factor II mRNA, complete	
1591_s_at	Down	cds	

[00266] Interestingly, the 9-gene molecular signature cluster (Fig. 48D; Tables 41& 42) associated with human prostate cancer metastasis has several candidate markers and targets for mechanistic studies and/or drug development such as secreted proteins (*ESM-1* and *EBAF*), transcription regulators (*CRIP1*, *TRAP100*, *NRF2F1*), two enzymes playing a key role in the purine salvage pathway (*NP* and *ADA*), an apoptosis inhibitor (*BCL-X<sub>L</sub>*), and a molecular chaperone (*CRYAB*).

Table 41.	Table 41. The 9-gene molecular signature associated with metastatic prostate cancer				
Gene	Gene name	GenBank	UniGene		
-		ID	ID		
ESM1	Endothelial cell-specific molecule 1	X89426	Hs.41716		
CRIP1	Cysteine-rich protein 1	AI0175174	Hs.17409		
TRAP100	Thyroid hormone receptor-associated protein	D50920	Hs.23106		
NP	Nucleoside phosphorylase	X00737	Hs.75514		
ADA	Adenosine deaminase	M13792	Hs.1217		
BCL2L1	BCL2-like 1	Z23115	Hs.305890		
NRF2F1	Nuclear receptor subfamily 2, group F, member 1	X16155	Hs.421993		
EBAF	Endometrial bleeding associated factor	U81523	Hs.25195		

CRYAB Crystallin, alpha B	AL038340	Hs.391270
---------------------------	----------	-----------

Table 42. Classification accuracy of metastasis segregation clusters				
Number of genes in cluster	Correlation coefficient	Performance (metastases)	Performance (primary tumors)	Overall performance
131 genes	r = 0.799	9 of 9 (100%)	23 of 23 (100%)	32 of 32 (100%)
37 genes	r = 0.938	9 of 9 (100%)	21 of 23 (91%)	30 of 32 (94%)
15 genes	r = 0.958	9 of 9 (100%)	21 of 23 (91%)	30 of 32 (94%)
12 genes	r = 0.990	9 of 9 (100%)	21 of 23 (91%)	30 of 32 (94%)
9 genes	r = 0.973	9 of 9 (100%)	21 of 23 (91%)	30 of 32 (94%)
14 genes	r = 0.937	9 of 9 (100%)	22 of 23 (96%)	31 Of 32 (97%)

[00267] To further test the potential clinical relevance of the models, we attempted to utilize expression profiling of highly metastatic orthotopic human prostate carcinoma xenografts for identification of gene expression correlates of clinically significant phenotypes such as invasive behavior and recurrence propensity of human prostate tumors (the original clinical data utilized in these examples were recently published in Singh, D., Febbo, P.G., Ross, K., Jackson, D.G., Manola, C.L., Tamayo, P., Renshaw, A.A., D'Amico, A.V., Richie, J.P., Lander, E.S., Loda, M., Kantoff, P.W., Golub, T.R., Sellers, W.R. Gene expression correlates of clinical prostate cancer behavior. Cancer Cell, 1: 203-209, 2002). Using gene expression profiles of metastasis-promoting orthotopic xenografts as a predictive reference of expected transcript abundance behavior in clinical samples, we identified a five-gene cluster (Table 43) of co-regulated transcripts discriminating with 75% accuracy invasive versus non-invasive human prostate tumors (Fig. 47B and 50A).

Table 43. The 5-gene molecular fingerprint associated with invasive phenotype of human prostate cancer			
Gene	Gene name	GenBank ID	UniGene ID
HRASLS3	HRAS-like suppressor 3	X92814	Hs.37189
	EST	AI986201	Hs.355812
KIAA0962	KIAA0962 protein	AB023179	Hs.9059
SLC29A2	Solute carrier family 29	AF034102	Hs.32951
KIAA0557	KIAA0557 protein	AB011129	Hs.101414

[00268] 20 of 26 samples (77%) obtained from the patients with invasive prostate cancer defined by histology as having positive surgical margins ("PSM") and/or extracapsular penetration ("PCP") exhibited a positive correlation coefficient of expression of the five-gene cluster (Table 43) compared to orthotopic xenografts. In contrast, 19 of 26 samples (73%) from the patients with organ-confined disease showed a negative correlation coefficient of expression of the five-gene cluster (Table 43) compared to orthotopic xenografts (Fig. 50A). Furthermore, using this strategy we identified an eightgene cluster (Table 44) of co-regulated transcripts discriminating with 90% accuracy human prostate tumors exhibiting recurrent or non-recurrent clinical behavior (Figures 47A& 50B).

Table 44. The 8-gene molecular fingerprint predicting recurrent phenotype of			
	human prostate cancer		
Gene	Gene name	GenBank ID	UniGene ID
MGC5466	Hypothetical protein MGC5466	U90904	Hs.83724
CHAF1A	Chromatin assembly factor 1, subunit	U20979	Hs.79018
	A		
CDS2	CDP-diacylglycerol synthase 2	Y16521	Hs.24812
STX7	Syntaxin 7	U77942	Hs.427065
IER3	Immediate early response 3	S81914	Hs.76095

GLUL	Glutamate-ammonia ligase	X59834	Hs.170171
MYBPC1	Myosin binding protein C	X73114	Hs.169849
SOX9	SRY-box 9	Z46629	Hs.2316

[00269] In this example we compared a set of transcripts differentially regulated in recurrent versus non-recurrent human prostate tumors with transcripts differentially regulated in orthotopic human prostate carcinoma xenografts derived from highly metastatic PC3MLN4 cell variant versus orthotopic tumors of the less metastatic parental lineages, PC3 and PC3M. Figure 50B illustrates application of the eight-gene cluster (Table 44) to characterize clinical prostate cancer samples according to their propensity for recurrence after therapy. The expression pattern of the genes in the recurrence predictor cluster was analyzed in each of twenty-one separate clinical samples. The analysis produces a quantitative phenotype association index (plotted on the Y-axis) for each of the twenty-one clinical prostate cancer samples. Tumors that are likely to recur are expected to have positive phenotype association indices reflecting positive correlation of gene expression with metastasis-promoting orthotopic xenografts, while those that are unlikely to recur are expected to have negative association indices.

[00270] Figure 50B shows the phenotype association indices for eight samples from patients who later had recurrence as bars 1 through 8, while the association indices for thirteen samples from patients whose tumors did not recur is shown as bars 12 through 24. Eight of the eight samples (or 100%) from patients who later experienced recurrence had positive phenotype association indices and so were properly classified. Eleven of the thirteen samples (or 84.6%) from patients whose tumors did not recur had negative phenotype association indices and so were properly classified as non-recurrent tumors.

Thus, overall, nineteen of the twenty-one samples (or 90.5%) were properly classified using an eight-gene recurrence predictor cluster.

[00271] Next we compared a set of transcripts differentially regulated in recurrent versus non-recurrent human prostate tumors with transcripts differentially regulated in orthotopic human prostate carcinoma xenografts derived from highly metastatic PC3MLN4 cell variant versus subcutaneous ("s.c.") ectopic tumors of the same lineage. This comparison identified a set of 25 genes (Figures 52A & B & Table 45) that exhibited highly concordant behavior in clinical recurrent samples and orthotopic metastasis-promoting tumors (Pearson correlation coefficient, r = 0.862; Figure 52B).

Table 45. The 25-gene molecular signature predicting recurrent prostate cancer			
Gene	Gene name	GenBank ID	UniGene ID
ETS1	v-ets erythroblastosis virus E26 oncogene	X14798	Hs.18063
	homolog 1		
MGC5466	Hypothetical protein MGC5466	U90904	Hs.83724
CA2	carbonic anhydrase II	J03037	Hs.155097
LRP2	Megalin	U33837	Hs.153595
ЕРНА3	receptor tyrosine kinase HEK	M83941	Hs.123642
Wnt5A	proto-oncogene Wnt5A	L20861	Hs.152213
ADRA1A	adrenergic, alpha-1A-, receptor	D32202	Hs.52931
	EST	R38263	Hs.375190
CDS2	CDP-diacylglycerol synthase	Y16521	Hs.24812
	EST	AL050002	Hs.94795
STX7	syntaxin 7	U77942	Hs.427065
RANBP3	RAN binding protein 3	Y08698	Hs.176657
FSTL1	follistatin-like 1	U06863	Hs.433622
ZFP36L2	zinc finger protein 36	U07802	Hs.78909
GGT2	gamma-glutamyltransferase 2	M30474	Hs.289098

KIAA0476	KIAA0476 protein	AB007945	Hs.6684
ITPR1	inositol 1,4,5-trisphosphate receptor, type	D26070	Hs.198443
(	1		
ITCH	Itchy homolog E3 ubiquitin protein ligase	AF038564	Hs.98074
CD44	CD44 antigen	L05424	Hs.169610
TNRC15	Trinucleotide repeat containing 15	AB014542	Hs.323317
MXI1	MAX interacting protein 1	L07648	Hs.118630
TCF2	transcription factor 2, hepatic	X58840	Hs.169853
KCNN4	intermediate conductance calcium-	AF022797	Hs.10082
	activated potassium channel		
APS	Adaptor protein	AB000520	Hs.105052
SOX9	SRY-box 9	Z46629	Hs.2316

[00272] When we compared the expression profiles of these 25 transcripts in orthotopic xenografts and individual clinical samples, we found that all recurrent prostate carcinomas have expression patterns highly similar to orthotopic xenografts as reflected in positive correlation of expression profiles, whereas 12 of 13 non-recurrent tumors displayed a negative correlation of expression profiles (Figure 53). We next attempted to refine the gene-expression signature associated with human prostate cancer metastasis to a smaller set of transcripts that would exhibit similar discrimination accuracy between recurrent and non-recurrent tumors. To achieve this we used the increase in correlation coefficient of gene expression profiles between orthotopic xenografts and clinical samples as a guide for reducing the number of genes in the cluster (cf. Figures 52 B & 55). Using this strategy we identified a smaller cluster of 12 co-regulated genes (Figure 54 & Table 46) exhibiting highly concordant behavior in the model system and clinical samples (r = 0.992; Figure 55) and demonstrating highly accurate discrimination (20 of

21 samples, or 95% were correctly classified) between clinical samples of recurrent and non-recurrent human prostate carcinomas (Figure 56).

	The 12-gene molecular signature predicting		
Gene	Gene name	GenBank	UniGene
		ID	ID
MGC5466	Hypothetical protein MGC5466	U90904	Hs.83724
ЕРНА3	Receptor tyrosine kinase HEK	M83941	Hs.123642
Wnt5A	Proto-oncogene Wnt5A	L20861	Hs.152213
CDS2	CDP-diacylglycerol synthase	Y16521	Hs.24812
	EST	AL050002	Hs.94795
STX7	Syntaxin 7	U77942	Hs.427065
RANBP3	RAN binding protein 3	Y08698	Hs.176657
KIAA0476	KIAA0476 protein	AB007945	Hs.6684
ITPR1	Inositol 1,4,5-trisphosphate receptor, type 1	D26070	Hs.198443
MXI1	MAX interacting protein 1	L07648	Hs.118630
TCF2	Transcription factor 2, hepatic	X58840	Hs.169853
KCNN4	Intermediate conductance calcium-activated	AF022797	Hs.10082
	potassium channel		

[00273] In conclusion, using gene expression profiles of metastasis-promoting orthotopic xenografts as a predictive reference of expected transcript abundance behavior in clinical samples, we identified clusters of co-regulated genes discriminating with 75-100% accuracy among metastatic versus primary, invasive versus non-invasive, and recurrent versus non-recurrent human prostate tumors. Our data indicate that human prostate cancer cells derived from metastatic lesions have stable "genetic memory" of metastatic behavior and that genetic signatures associated with metastatic phenotype could be revived by growth in a metastasis-promoting orthotopic environment. The genetic signatures of metastatic prostate cancer have the ability to be used as nucleic

acid-based and/or protein-based clinical prognostic and diagnostic tests useful in clinical management of prostate cancer patients, and as a source of targets for novel therapeutic approaches for disease management.

EXAMPLE 6 – SELECTION OF THE GENE CLUSTERS WITH CLINICALLY USEFUL PROPERTIES USING THE BEST-FIT SAMPLE(S) AS A REFERENCE STANDARD.

[00274] Application of the present invention for identification of gene clusters with useful clinical properties was not limited by the availability of the suitable reference standard such as the appropriate cell lines and/or in vivo model systems. When a suitable reference standard was not readily available an algorithm utilizing the expression profile(s) of the best-fit sample(s) as a reference standard was applied for selection of the minimum segregation set of genes. As the first step of such analysis we compared the gene expression profiles of two distinct sets of samples that are subjects of classification (for example, metastatic and non-metastatic human breast tumors) to identify a broad spectrum of transcripts differentially regulated at a statistically significant level (p<0.05) in metastatic human breast cancer. If desirable, further criteria such as a particular cut-off based on fold expression changes (e.g., 2-fold, 3-fold, etc.) can be applied for selecting differentially expressed genes. Next, we calculated the average expression values for each transcript of the differentially expressed genes in the metastatic and non-metastatic tumors and determined the average fold expression change in metastatic versus nonmetastatic tumors ("average" metastatic expression profile). We then determined the individual expression profiles for each sample within the two classification groups by calculating fold expression change for each transcript of the differentially expressed class of genes in a given sample by dividing an individual expression value of a gene by the average expression value for a particular gene across the entire data set. At the next step,

we determined the individual phenotype association indices across the entire data set by calculating the Pearson correlation coefficient between the "average" metastatic expression profile and individual expression profiles. Next, the selection of the best-fit sample(s) was performed based on a highest positive and/or negative value(s) of the individual phenotype association index. The expression profile(s) of the best-fit sample(s) was utilized to refine the gene-expression signature associated with a particular phenotype to a small set of transcripts that would exhibit high discrimination accuracy between metastatic and non-metastatic tumors. To achieve this we used the increase in correlation coefficient of gene expression profiles between the "average" metastatic expression profile and an expression profile(s) of the best-fit sample(s) as a guide for reducing the number of members within a cluster.

BETWEEN INVASIVE AND NON-INVASIVE HUMAN PROSTATE CANCER. [00275] The methods of the invention were used along with the data reported by Singh, et al. (2002) to identify gene clusters associated with an invasive phenotype. These data were the supplemental data reported in Singh, D., Febbo, P.G., et al., "Gene Expression Correlates of Clinical Prostate Cancer Behavior," Cancer Cell March 2002 1:203-209, incorporated herein by reference. The clinical human prostate tumor samples were divided into two groups, invasive and non-invasive, as reported in Singh, et al. (2002). Invasive phenotype was assessed by determining the presence or absence of positive surgical margins ("PSM") and positive or negative capsular penetration ("PCP"). The reference set was obtained following the procedures described above in part B, using

EXAMPLE 7 – SELECTION OF THE GENE CLUSTERS DISCRIMINATING

the supplemental data reported in Singh, et al. (2002) for 26 invasive (identified as

having positive surgical margins and/or positive capsular penetration) and 26 non-

invasive (identified as having no evidence of positive surgical margins and/or positive capsular penetration) human prostate tumors. Thus, the first reference set was obtained by using the Affymetrix MicroDB (version 3.0) and Affymetrix Data Mining Tools (DMT) (version 3.0) data analysis software to identify genes that were differentially regulated in invasive group compared to non-invasive group of patients at the statistically significant level (p<0.05; Student T-test). Candidate genes were included in the first reference set if they were identified by the DMT software as having p values of 0.05 or less both for upregulated and down-regulated genes. 114 genes were identified as being members of the reference set (Table 47).

Table 47. 114 genes differentially regulated in 26 invasive		
	versus 26 non-invasive human prostate tumors.	
Affymetrix	Description	
Probe Set ID		
(U95Av2)		
40635_at	Cluster Incl. AF089750:Homo sapiens flotillin-1 mRNA, complete cds	
	/cds=(164,1447)/gb=AF089750/gi=3599572/ug=Hs.179986	
	/len=1796	
36993_at	Cluster Incl. M33210:Human colony stimulating factor 1 receptor	
	(CSF1R) gene /cds=(0,283) /gb=M33210 /gi=532592 /ug=Hs.76144	
	/len=2206	
38682_at	Cluster Incl. AF045581:Homo sapiens BRCA1 associated protein 1	
	(BAP1) mRNA, complete cds /cds=(39,2228) /gb=AF045581	
	/gi=2854120 /ug=Hs.106674 /len=3506	
38260_at	Cluster Incl. AL050306:Human DNA sequence from clone 475B7 on	
	chromosome Xq12.1-13. Contains the 3 part of the gene for a novel	
	KIAA0615 and KIAA0323 LIKE protein, the gene for a novel protein,	
•	ESTs, STSs, GSSs and two putative CpG islands /cds=(48,2201)	
	/gb=AL050306 /gi=5419784 /ug=Hs.90625 /len=2395	

41725_at	Cluster Incl. U89896:Homo sapiens casein kinase I gamma 2 mRNA,
	complete cds /cds=(239,1486) /gb=U89896 /gi=1890117
	/ug=Hs.181390 /len=1749
34880_at	Cluster Incl. AC002115:Human DNA from overlapping chromosome
	19 cosmids R31396, F25451, and R31076 containing COX6B and
	UPKA, genomic sequence /cds=(336,1355) /gb=AC002115
	/gi=2098573 /ug=Hs.5086 /len=1473
32140_at	Cluster Incl. Y08110:H.sapiens mRNA for mosaic protein LR11
	/cds=(80,6724) /gb=Y08110 /gi=1552323 /ug=Hs.166294 /len=6840
35704_at	Cluster Incl. X92814:H.sapiens mRNA for rat HREV107-like protein
	/cds=(407,895) /gb=X92814 /gi=1054751 /ug=Hs.37189 /len=1070
32212_at	Cluster Incl. AL049703:Human gene from PAC 179D3, chromosome
	X, isoform of mitochondrial apoptosis inducing factor, AIF, AF100928
	/cds=(96,1925) /gb=AL049703 /gi=4678806 /ug=Hs.18720 /len=2121
1385_at	M77349 /FEATURE= /DEFINITION=HUMTGFBIG Human
	transforming growth factor-beta induced gene product (BIGH3)
	mRNA, complete cds
37585_at	Cluster Incl. X13482:Human mRNA for U2 snRNP-specific A protein
	/cds=(56,823) /gb=X13482 /gi=37546 /ug=Hs.80506 /len=1033
41869_at	Cluster Incl. U78310:Homo sapiens pescadillo mRNA, complete cds
	/cds=(58,1824) /gb=U78310 /gi=2194202 /ug=Hs.13501 /len=2235
33833_at	Cluster Incl. J05243:Human nonerythroid alpha-spectrin (SPTAN1)
	mRNA, complete cds /cds=(102,7520) /gb=J05243 /gi=179105
	/ug=Hs.237180 /len=7787
38794_at	Cluster Incl. X53390:Human mRNA for upstream binding factor
·	(hUBF) /cds=(147,2441) /gb=X53390 /gi=509240 /ug=Hs.89781
	/len=3097
33915_at	Cluster Incl. W22655:71B9 Homo sapiens cDNA /clone=(not-
	directional) /gb=W22655 /gi=1299488 /ug=Hs.26070 /len=761
<u> </u>	

35905_s_at	Cluster Incl. U34995:Human normal keratinocyte subtraction library
	mRNA, clone H22a, complete sequence /cds=UNKNOWN
	/gb=U34995 /gi=1497857 /ug=Hs.195188 /len=1626
39798_at	Cluster Incl. R87876:yo45h01.r1 Homo sapiens cDNA, 5 end
	/clone=IMAGE-180913 /clone_end=5 /gb=R87876 /gi=946689
	/ug=Hs.153177 /len=483
1878_g_at	M13194 /FEATURE=mRNA /DEFINITION=HUMERCC1 Human
	excision repair protein (ERCC1) mRNA, complete cds, clone pcDE
41116_at	Cluster Incl. AI799802:wc43d09.x1 Homo sapiens cDNA, 3 end
,	/clone=IMAGE-2321393 /clone_end=3 /gb=AI799802 /gi=5365274
	/ug=Hs.101516 /len=688
35961_at	Cluster Incl. AL049390:Homo sapiens mRNA; cDNA
	DKFZp586O1318 (from clone DKFZp586O1318) /cds=UNKNOWN
	/gb=AL049390 /gi=4500184 /ug=Hs.22689 /len=2322
37390_at	Cluster Incl. D86977:Human mRNA for KIAA0224 gene, complete cds
	/cds=(136,3819) /gb=D86977 /gi=1504027 /ug=Hs.78054 /len=4226
38841_at	Cluster Incl. AF068195:Homo sapiens putative glialblastoma cell
	differentiation-related protein (GBDR1) mRNA, complete cds
	/cds=(58,1062) /gb=AF068195 /gi=3192872 /ug=Hs.9194 /len=1493
35787_at	Cluster Incl. AI986201:wr81a01.x1 Homo sapiens cDNA, 3 end
	/clone=IMAGE-2494056 /clone_end=3 /gb=AI986201 /gi=5813478
	/ug=Hs.66881 /len=814
39379_at	Cluster Incl. AL049397:Homo sapiens mRNA; cDNA
!	DKFZp586C1019 (from clone DKFZp586C1019) /cds=UNKNOWN
	/gb=AL049397 /gi=4500188 /ug=Hs.12314 /len=1720
928_at	L02785 /FEATURE= /DEFINITION=HUMDRA Homo sapiens colon
	mucosa-associated (DRA) mRNA, complete cds
37349_r_at	Cluster Incl. AI817618:wk39f01.x1 Homo sapiens cDNA, 3 end
	/clone=IMAGE-2417785 /clone_end=3 /gb=AI817618 /gi=5436697
	/ug=Hs.77558 /len=734
37349_r_at	/clone=IMAGE-2417785 /clone_end=3 /gb=AI817618 /gi=5436697

32933_r_at	Cluster Incl. AL050122:Homo sapiens mRNA; cDNA DKFZp586E121
	(from clone DKFZp586E121) /cds=UNKNOWN /gb=AL050122
	/gi=4884330 /ug=Hs.227742 /len=1843
34909_at	Cluster Incl. AC004990:Homo sapiens PAC clone DJ1185I07 from
	7q11.23-q21 /cds=(0,1766) /gb=AC004990 /gi=3924668
	/ug=Hs.128653 /len=1767
AFFX-	U18530 SGD:YEL018W Yeast S. cerevisiae Protein of unknown
YEL018w/_at	function
37054_at	Cluster Incl. J04739: Human bactericidal permeability increasing
37034_ <b>u</b> t	protein (BPI) mRNA, complete cds /cds=(30,1493) /gb=J04739
	/gi=179528 /ug=Hs.89535 /len=1813
38871_at	Cluster Incl. AJ006288:Homo sapiens mRNA for bcl-10 protein
300/1_at	/cds=(690,1391) /gb=AJ006288 /gi=4049459 /ug=Hs.193516
	//cds=(090,1391)/g0=AJ000288/g1=4049439/dg=Hs.193310 //len=1877
07000	
37800_r_at	Cluster Incl. AI263099:qz35b09.x1 Homo sapiens cDNA, 3 end
	/clone=IMAGE-2028857 /clone_end=3 /gb=AI263099 /gi=3871302
	/ug=Hs.126261 /len=838
37236_at	Cluster Incl. M11437:Human kininogen gene /cds=(0,1934)
	/gb=M11437 /gi=186752 /ug=Hs.77741 /len=1935
38198_at	Cluster Incl. AL079275:Homo sapiens mRNA full length insert cDNA
	clone EUROIMAGE 566443 /cds=UNKNOWN /gb=AL079275
	/gi=5102578 /ug=Hs.157078 /len=2082
35640_at	Cluster Incl. D14822:Human chimeric mRNA derived from AML1
	gene and MTG8(ETO) gene, partial sequence /cds=(0,597)
	/gb=D14822 /gi=467498 /ug=Hs.31551 /len=799
39828_at	Cluster Incl. AA477714:zu44e09.s1 Homo sapiens cDNA, 3 end
	/clone=IMAGE-740872 /clone_end=3 /gb=AA477714 /gi=2206348
	/ug=Hs.111554 /len=588
38938_at	Cluster Incl. AI816413:au47f05.x1 Homo sapiens cDNA, 3 end
	/clone=IMAGE-2517921 /clone_end=3 /gb=AI816413 /gi=5431959
	/ug=Hs.210862 /len=586
<u></u>	<u> </u>

39654_at	Cluster Incl. S67156:ASP=aspartoacylase [human, kidney, mRNA,
	1435 nt] /cds=(158,1099) /gb=S67156 /gi=455833 /ug=Hs.32042
	/len=1417
1393_at	L20348 /FEATURE=expanded_cds /DEFINITION=HUMOMDLN04
	Homo sapiens oncomodulin gene, exon 5
35920_at	Cluster Incl. N55205:yv44g05.s1 Homo sapiens cDNA, 3 end
	/clone=IMAGE-245624 /clone_end=3 /gb=N55205 /gi=1198084
	/ug=Hs.20205 /len=458
31368_at	Cluster Incl. W27967:40b10 Homo sapiens cDNA /gb=W27967
	/gi=1307915 /ug=Hs.136154 /len=755
39912_at	Cluster Incl. AB006179:Homo sapiens mRNA for heparin-sulfate 6-
	sulfotransferase, complete cds /cds=(111,1343) /gb=AB006179
	/gi=3073774 /ug=Hs.132884 /len=2051
35489_at	Cluster Incl. M82962:Human N-benzoyl-L-tyrosyl-p-amino-benzoic
	acid hydrolase alpha subunit (PPH alpha) mRNA, complete cds
	/cds=(9,2249) /gb=M82962 /gi=535474 /ug=Hs.179704 /len=2902
34486_at	Cluster Incl. U88897:Human endogenous retroviral H D2 leader region,
	protease region, and integrase/envelope region mRNA sequence
:	/cds=UNKNOWN /gb=U88897 /gi=2104917 /ug=Hs.11828 /len=1004
32596_at	Cluster Incl. W25828:13g2 Homo sapiens cDNA /gb=W25828
	/gi=1305951 /ug=Hs.79362 /len=744
34057_at	Cluster Incl. U84392:Human Na+-dependent purine specific transporter
	mRNA, complete cds /cds=(59,2035) /gb=U84392 /gi=2731438
	/ug=Hs.193665 /len=2459
31759_at	Cluster Incl. W26220:22d9 Homo sapiens cDNA /gb=W26220
	/gi=1306631 /ug=Hs.136089 /len=687
1485_at	L36642 /FEATURE=mRNA /DEFINITION=HUMRPTK Homo
	sapiens receptor protein-tyrosine kinase (HEK11) mRNA, complete cds

9475_at	Cluster Incl. L37199:Homo sapiens (clone cD24-1) Huntingtons
> 1.10 <u> </u>	disease candidate region mRNA fragment /cds=UNKNOWN
	/gb=L37199 /gi=600520 /ug=Hs.117487 /len=1356
3012_at	Cluster Incl. L09753:Homo sapiens CD30 ligand mRNA, complete cds
	/cds=(114,818) /gb=L09753 /gi=349277 /ug=Hs.1313 /len=1906
321_s_at	U43916 /FEATURE= /DEFINITION=HSU43916 Human tumor-
	associated membrane protein homolog (TMP) mRNA, complete cds
32387_at	Cluster Incl. AB017494:Homo sapiens mRNA for LCAT-like
	lysophospholipase (LLPL), complete cds /cds=(32,1270)
	/gb=AB017494 /gi=4589719 /ug=Hs.227221 /len=1400
35565_at	Cluster Incl. U79301:Human clone 23842 mRNA sequence
35500	/cds=UNKNOWN /gb=U79301 /gi=1710286 /ug=Hs.135617
	/len=1582
1832_at	M62397 /FEATURE= /DEFINITION=HUMCRCMUT Human
_	colorectal mutant cancer protein mRNA, complete cds
39924_at	Cluster Incl. AB020660:Homo sapiens mRNA for KIAA0853 protein,
	partial cds /cds=(0,2905) /gb=AB020660 /gi=4240194 /ug=Hs.136102
	/len=4363
39281_at	Cluster Incl. AB002378:Human mRNA for KIAA0380 gene, complete
_	cds /cds=(745,5313) /gb=AB002378 /gi=2224700 /ug=Hs.239022
	/len=5790
34976_at	Cluster Incl. M60052:Human histidine-rich calcium binding protein
	(HRC) mRNA, complete cds /cds=(170,2269) /gb=M60052 /gi=18391
	/ug=Hs.1480 /len=2365
39642_at	Cluster Incl. AL080199:Homo sapiens mRNA; cDNA DKFZp434E08
	(from clone DKFZp434E082) /cds=UNKNOWN /gb=AL080199
	/gi=5262682 /ug=Hs.30504 /len=1034
33615_at	Cluster Incl. X64994:H.sapiens HGMP07I gene for olfactory receptor
_	/cds=(0,944) /gb=X64994 /gi=32085 /ug=Hs.163670 /len=945

32054_at	Cluster Incl. AF048732: Homo sapiens cyclin T2b mRNA, complete cds
	/cds=(0,2192) /gb=AF048732 /gi=2981199 /ug=Hs.155478 /len=2193
36383_at	Cluster Incl. M17254:Human erg2 gene encoding erg2 protein,
	complete cds /cds=(0,1388) /gb=M17254 /gi=182186 /ug=Hs.159432
	/len=1389
154_at	X07024 /FEATURE=cds /DEFINITION=HSCCG1 Human X
	chromosome mRNA for CCG1 protein inv. in cell proliferation
39882_at	Cluster Incl. U66035:Human X-linked deafness dystonia protein (DDP)
	mRNA, complete cds /cds=(35,328) /gb=U66035 /gi=3123842
1	/ug=Hs.125565 /len=1169
35452_at	Cluster Incl. AL109690:Homo sapiens mRNA full length insert cDNA
	clone EUROIMAGE 190711 /cds=UNKNOWN /gb=AL109690
	/gi=5689787 /ug=Hs.169950 /len=2031
39926_at	Cluster Incl. U59913:Human chromosome 5 Mad homolog Smad5
	mRNA, complete cds /cds=(130,1527) /gb=U59913 /gi=1654324
	/ug=Hs.37501 /len=2205
39246_at	Cluster Incl. Z75330:H.sapiens mRNA for nuclear protein SA-1
	/cds=(400,4176) /gb=Z75330 /gi=2204212 /ug=Hs.234435 /len=4337
40248_at	Cluster Incl. AL022165:dJ71L16.5 (KIAA0267 LIKE putative
	Na(+)/H(+) exchanger) /cds=(0,1852) /gb=AL022165 /gi=3281985
	/ug=Hs.154353 /len=3487
31446_s_at	Cluster Incl. D89501:Human PBI gene, complete cds /cds=(14,418)
	/gb=D89501 /gi=1854451 /ug=Hs.166099 /len=576
37937_at	Cluster Incl. AJ005257:Homo sapiens partial mRNA for beta-
	transducin family protein (putative) /cds=(0,262) /gb=AJ005257
	/gi=3043442 /ug=Hs.85570 /len=1349
39914_r_at	Cluster Incl. W28976:54e5 Homo sapiens cDNA /gb=W28976
	/gi=1308924 /ug=Hs.133151 /len=903
L	<del></del>

NA for
NA for
NA for
ning
uence
repeat
nd
9121
nd
97509
orotein,
101414
HML6)
es,
protein
SSTR2)

677_s_at	J04430 /FEATURE=mRNA /DEFINITION=HUMACP5 Human
	tartrate-resistant acid phosphatase type 5 mRNA, complete cds
41291_at	Cluster Incl. AC004528:Homo sapiens chromosome 19, cosmid
	R32184 /cds=(0,1589) /gb=AC004528 /gi=3025444 /ug=Hs.238519
	/len=1590
32746_at	Cluster Incl. AF015451:Homo sapiens Usurpin-beta mRNA, complete
	cds /cds=(0,1388) /gb=AF015451 /gi=3133282 /ug=Hs.195175
•	/len=1389
39364_s_at	Cluster Incl. Y18207:Homo sapiens mRNA for protein phosphatase 1
	(PPP1R5) /cds=(91,1044) /gb=Y18207 /gi=3805818 /ug=Hs.12112
	/len=1158
135_g_at	X95632 /FEATURE=cds /DEFINITION=HSARGBPIA H.sapiens
	mRNA for Arg protein tyrosine kinase-binding protein
37785_at	Cluster Incl. U69563:U69563 Homo sapiens cDNA /clone=25050
	/gb=U69563 /gi=2731394 /ug=Hs.124940 /len=1657
39190_s_at	Cluster Incl. AC002126:Homo sapiens DNA from chromosome 19-
	cosmids R30102-R29350-R27740 containing MEF2B, genomic
	sequence /cds=(0,307) /gb=AC002126 /gi=2329908 /ug=Hs.125220
	/len=308
41550_at	Cluster Incl. AF091071:Homo sapiens clone 192 Rer1 mRNA,
	complete cds /cds=(76,696) /gb=AF091071 /gi=3859979 /ug=Hs.40500
	/len=1400
40240_at	Cluster Incl. AC004131:Homo sapiens Chromosome 16 BAC clone
	CIT987SK-A-69G12 /cds=(0,1211) /gb=AC004131 /gi=3342217
	/ug=Hs.154050 /len=1887
38224_at	Cluster Incl. U71300:Human snRNA activating protein complex 50kD
	subunit (SNAP50) mRNA, complete cds /cds=(14,1249) /gb=U71300
	/gi=1619945 /ug=Hs.164915 /len=1848
41534_at	Cluster Incl. AB006755:Homo sapiens mRNA for PCDH7 (BH-Pcdh)a,
	complete cds /cds=(1010,4219) /gb=AB006755 /gi=2979417
	/ug=Hs.34073 /len=4648

complete cds /cds=(0,2270) /gb=AF031416 /gi=3213216 //ug=Hs.226573 /len=2271  Cluster Incl. AA532495:nj54a10.s1 Homo sapiens cDNA //clone=IMAGE-996282 /gb=AA532495 /gi=2276749 /ug=Hs.183752 //len=549  1668_s_at  L15409 /FEATURE= /DEFINITION=HUMHIPLIND Homo sapiens (clone g7) von Hippel-Lindau disease tumor suppressor mRNA sequence  Cluster Incl. AA524802:nh33h11.s1 Homo sapiens cDNA //clone=IMAGE-954213 /gb=AA524802 /gi=2265730 /ug=Hs.203907 //len=500  Cluster Incl. L07592:Human peroxisome proliferator activated receptor mRNA, complete cds /cds=(337,1662) /gb=L07592 /gi=190229 //ug=Hs.106415 /len=3301  Cluster Incl. M95740:Human alpha-L-iduronidase gene /cds=(0,1961) //gb=M95740 /gi=178412 /ug=Hs.89560 /len=2234  Cluster Incl. U90268:Human Krit1 mRNA, complete cds //cds=(25,1614) /gb=U90268 /gi=2149601 /ug=Hs.93810 /len=1986  Cluster Incl. AF014643:Homo sapiens connexin46.6 (Cx46.6) gene, complete cds /cds=(28,1338) /gb=AF014643 /gi=2738576 //ug=Hs.100072 /len=2087  Cluster Incl. AL050258:Novel human mRNA similar to mouse tuftelin- interacting protein 10 mRNA, AF097181 /cds=(263,2776) //gb=AL050258 /gi=4886426 /ug=Hs.20225 /len=3565  Cluster Incl. U09850:Human zinc finger protein (ZNF143) mRNA,	1569_r_at	L42243 /FEATURE=exon#3 /DEFINITION=HUMIFNAM08 Homo
Cluster Incl. AF031416:Homo sapiens IkB kinase beta subunit mRNA, complete cds /cds=(0,2270) /gb=AF031416 /gi=3213216 /ug=Hs.226573 /len=2271		sapiens (clone 51H8) alternatively spliced interferon receptor
complete cds /cds=(0,2270) /gb=AF031416 /gi=3213216 //ug=Hs.226573 /len=2271  Cluster Incl. AA532495:nj54a10.s1 Homo sapiens cDNA //clone=IMAGE-996282 /gb=AA532495 /gi=2276749 /ug=Hs.183752 //len=549  1668_s_at  L15409 /FEATURE= /DEFINITION=HUMHIPLIND Homo sapiens (clone g7) von Hippel-Lindau disease tumor suppressor mRNA sequence  Cluster Incl. AA524802:nh33h11.s1 Homo sapiens cDNA //clone=IMAGE-954213 /gb=AA524802 /gi=2265730 /ug=Hs.203907 //len=500  Cluster Incl. L07592:Human peroxisome proliferator activated receptor mRNA, complete cds /cds=(337,1662) /gb=L07592 /gi=190229 //ug=Hs.106415 /len=3301  Cluster Incl. M95740:Human alpha-L-iduronidase gene /cds=(0,1961) //gb=M95740 /gi=178412 /ug=Hs.89560 /len=2234  Cluster Incl. U90268:Human Krit1 mRNA, complete cds //cds=(25,1614) /gb=U90268 /gi=2149601 /ug=Hs.93810 /len=1986  Cluster Incl. AF014643:Homo sapiens connexin46.6 (Cx46.6) gene, complete cds /cds=(28,1338) /gb=AF014643 /gi=2738576 //ug=Hs.100072 /len=2087  Cluster Incl. AL050258:Novel human mRNA similar to mouse tuftelin- interacting protein 10 mRNA, AF097181 /cds=(263,2776) //gb=AL050258 /gi=4886426 /ug=Hs.20225 /len=3565  Cluster Incl. U09850:Human zinc finger protein (ZNF143) mRNA,		(IFNAR2) gene, exon 9 and complete cds s
/ug=Hs.226573 /len=2271  Cluster Incl. AA532495:nj54a10.s1 Homo sapiens cDNA /clone=IMAGE-996282 /gb=AA532495 /gi=2276749 /ug=Hs.183752 /len=549  1668_s_at  L15409 /FEATURE= /DEFINITION=HUMHIPLIND Homo sapiens (clone g7) von Hippel-Lindau disease tumor suppressor mRNA sequence  32877_i_at  Cluster Incl. AA524802:nh33h11.s1 Homo sapiens cDNA /clone=IMAGE-954213 /gb=AA524802 /gi=2265730 /ug=Hs.203907 /len=500  37152_at  Cluster Incl. L07592:Human peroxisome proliferator activated receptor mRNA, complete cds /cds=(337,1662) /gb=L07592 /gi=190229 /ug=Hs.106415 /len=3301  Cluster Incl. M95740:Human alpha-L-iduronidase gene /cds=(0,1961) /gb=M95740 /gi=178412 /ug=Hs.89560 /len=2234  34031_i_at  Cluster Incl. U90268:Human Krit1 mRNA, complete cds /cds=(25,1614) /gb=U90268 /gi=2149601 /ug=Hs.93810 /len=1986  39504_at  Cluster Incl. AF014643:Homo sapiens connexin46.6 (Cx46.6) gene, complete cds /cds=(28,1338) /gb=AF014643 /gi=2738576 /ug=Hs.100072 /len=2087  Cluster Incl. AL050258:Novel human mRNA similar to mouse tuftelin- interacting protein 10 mRNA, AF097181 /cds=(263,2776) /gb=AL050258 /gi=4886426 /ug=Hs.20225 /len=3565  Cluster Incl. U09850:Human zinc finger protein (ZNF143) mRNA,	35960_at	Cluster Incl. AF031416:Homo sapiens IkB kinase beta subunit mRNA,
Cluster Incl. AA532495:nj54a10.s1 Homo sapiens cDNA		complete cds /cds=(0,2270) /gb=AF031416 /gi=3213216
/clone=IMAGE-996282 /gb=AA532495 /gi=2276749 /ug=Hs.183752 /len=549  1668_s_at  L15409 /FEATURE= /DEFINITION=HUMHIPLIND Homo sapiens (clone g7) von Hippel-Lindau disease tumor suppressor mRNA sequence  32877_i_at  Cluster Incl. AA524802:nh33h11.s1 Homo sapiens cDNA /clone=IMAGE-954213 /gb=AA524802 /gi=2265730 /ug=Hs.203907 /len=500  37152_at  Cluster Incl. L07592:Human peroxisome proliferator activated receptor mRNA, complete cds /cds=(337,1662) /gb=L07592 /gi=190229 /ug=Hs.106415 /len=3301  33155_at  Cluster Incl. M95740:Human alpha-L-iduronidase gene /cds=(0,1961) /gb=M95740 /gi=178412 /ug=Hs.89560 /len=2234  34031_i_at  Cluster Incl. U90268:Human Krit1 mRNA, complete cds /cds=(25,1614) /gb=U90268 /gi=2149601 /ug=Hs.93810 /len=1986  39504_at  Cluster Incl. AF014643:Homo sapiens connexin46.6 (Cx46.6) gene, complete cds /cds=(28,1338) /gb=AF014643 /gi=2738576 /ug=Hs.100072 /len=2087  Cluster Incl. AL050258:Novel human mRNA similar to mouse tuftelininteracting protein 10 mRNA, AF097181 /cds=(263,2776) /gb=AL050258 /gi=4886426 /ug=Hs.20225 /len=3565  Cluster Incl. U09850:Human zinc finger protein (ZNF143) mRNA,		/ug=Hs.226573 /len=2271
	32149_at	Cluster Incl. AA532495:nj54a10.s1 Homo sapiens cDNA
L15409 /FEATURE= /DEFINITION=HUMHIPLIND Homo sapiens (clone g7) von Hippel-Lindau disease tumor suppressor mRNA sequence     32877_i_at   Cluster Incl. AA524802:nh33h11.s1 Homo sapiens cDNA /clone=IMAGE-954213 /gb=AA524802 /gi=2265730 /ug=Hs.203907 /len=500     37152_at   Cluster Incl. L07592:Human peroxisome proliferator activated receptor mRNA, complete cds /cds=(337,1662) /gb=L07592 /gi=190229 /ug=Hs.106415 /len=3301     33155_at   Cluster Incl. M95740:Human alpha-L-iduronidase gene /cds=(0,1961) /gb=M95740 /gi=178412 /ug=Hs.89560 /len=2234     34031_i_at   Cluster Incl. U90268:Human Krit1 mRNA, complete cds /cds=(25,1614) /gb=U90268 /gi=2149601 /ug=Hs.93810 /len=1986     39504_at   Cluster Incl. AF014643:Homo sapiens connexin46.6 (Cx46.6) gene, complete cds /cds=(28,1338) /gb=AF014643 /gi=2738576 /ug=Hs.100072 /len=2087     40975_s_at   Cluster Incl. AL050258:Novel human mRNA similar to mouse tuftelininteracting protein 10 mRNA, AF097181 /cds=(263,2776) /gb=AL050258 /gi=4886426 /ug=Hs.20225 /len=3565     40241_at   Cluster Incl. U09850:Human zinc finger protein (ZNF143) mRNA,		/clone=IMAGE-996282 /gb=AA532495 /gi=2276749 /ug=Hs.183752
(clone g7) von Hippel-Lindau disease tumor suppressor mRNA sequence  32877_i_at  Cluster Incl. AA524802:nh33h11.s1 Homo sapiens cDNA /clone=IMAGE-954213 /gb=AA524802 /gi=2265730 /ug=Hs.203907 /len=500  37152_at  Cluster Incl. L07592:Human peroxisome proliferator activated receptor mRNA, complete cds /cds=(337,1662) /gb=L07592 /gi=190229 /ug=Hs.106415 /len=3301  Cluster Incl. M95740:Human alpha-L-iduronidase gene /cds=(0,1961) /gb=M95740 /gi=178412 /ug=Hs.89560 /len=2234  Cluster Incl. U90268:Human Krit1 mRNA, complete cds /cds=(25,1614) /gb=U90268 /gi=2149601 /ug=Hs.93810 /len=1986  Cluster Incl. AF014643:Homo sapiens connexin46.6 (Cx46.6) gene, complete cds /cds=(28,1338) /gb=AF014643 /gi=2738576 /ug=Hs.100072 /len=2087  Cluster Incl. AL050258:Novel human mRNA similar to mouse tuftelin-interacting protein 10 mRNA, AF097181 /cds=(263,2776) /gb=AL050258 /gi=4886426 /ug=Hs.20225 /len=3565  Cluster Incl. U09850:Human zinc finger protein (ZNF143) mRNA,		/len=549
Sequence   Sequence   Cluster Incl. AA524802:nh33h11.s1 Homo sapiens cDNA   /clone=IMAGE-954213 /gb=AA524802 /gi=2265730 /ug=Hs.203907 /len=500   Cluster Incl. L07592:Human peroxisome proliferator activated receptor mRNA, complete cds /cds=(337,1662) /gb=L07592 /gi=190229 /ug=Hs.106415 /len=3301   Cluster Incl. M95740:Human alpha-L-iduronidase gene /cds=(0,1961) /gb=M95740 /gi=178412 /ug=Hs.89560 /len=2234   Cluster Incl. U90268:Human Krit1 mRNA, complete cds /cds=(25,1614) /gb=U90268 /gi=2149601 /ug=Hs.93810 /len=1986   Cluster Incl. AF014643:Homo sapiens connexin46.6 (Cx46.6) gene, complete cds /cds=(28,1338) /gb=AF014643 /gi=2738576 /ug=Hs.100072 /len=2087   Cluster Incl. AL050258:Novel human mRNA similar to mouse tuftelin-interacting protein 10 mRNA, AF097181 /cds=(263,2776)   /gb=AL050258 /gi=4886426 /ug=Hs.20225 /len=3565   Cluster Incl. U09850:Human zinc finger protein (ZNF143) mRNA,	1668_s_at	L15409 /FEATURE= /DEFINITION=HUMHIPLIND Homo sapiens
Cluster Incl. AA524802:nh33h11.s1 Homo sapiens cDNA //clone=IMAGE-954213 /gb=AA524802 /gi=2265730 /ug=Hs.203907 //len=500  Cluster Incl. L07592:Human peroxisome proliferator activated receptor mRNA, complete cds /cds=(337,1662) /gb=L07592 /gi=190229 //ug=Hs.106415 /len=3301  Cluster Incl. M95740:Human alpha-L-iduronidase gene /cds=(0,1961) //gb=M95740 /gi=178412 /ug=Hs.89560 /len=2234  Cluster Incl. U90268:Human Krit1 mRNA, complete cds //cds=(25,1614) /gb=U90268 /gi=2149601 /ug=Hs.93810 /len=1986  Cluster Incl. AF014643:Homo sapiens connexin46.6 (Cx46.6) gene, complete cds /cds=(28,1338) /gb=AF014643 /gi=2738576 //ug=Hs.100072 /len=2087  Cluster Incl. AL050258:Novel human mRNA similar to mouse tuftelin-interacting protein 10 mRNA, AF097181 /cds=(263,2776) //gb=AL050258 /gi=4886426 /ug=Hs.20225 /len=3565  Cluster Incl. U09850:Human zinc finger protein (ZNF143) mRNA,	}	(clone g7) von Hippel-Lindau disease tumor suppressor mRNA
/clone=IMAGE-954213 /gb=AA524802 /gi=2265730 /ug=Hs.203907 /len=500  37152_at Cluster Incl. L07592:Human peroxisome proliferator activated receptor mRNA, complete cds /cds=(337,1662) /gb=L07592 /gi=190229 /ug=Hs.106415 /len=3301  Cluster Incl. M95740:Human alpha-L-iduronidase gene /cds=(0,1961) /gb=M95740 /gi=178412 /ug=Hs.89560 /len=2234  Cluster Incl. U90268:Human Krit1 mRNA, complete cds /cds=(25,1614) /gb=U90268 /gi=2149601 /ug=Hs.93810 /len=1986  Cluster Incl. AF014643:Homo sapiens connexin46.6 (Cx46.6) gene, complete cds /cds=(28,1338) /gb=AF014643 /gi=2738576 /ug=Hs.100072 /len=2087  Cluster Incl. AL050258:Novel human mRNA similar to mouse tuftelin-interacting protein 10 mRNA, AF097181 /cds=(263,2776) /gb=AL050258 /gi=4886426 /ug=Hs.20225 /len=3565  Cluster Incl. U09850:Human zinc finger protein (ZNF143) mRNA,		sequence
Cluster Incl. L07592:Human peroxisome proliferator activated receptor mRNA, complete cds /cds=(337,1662) /gb=L07592 /gi=190229 /ug=Hs.106415 /len=3301     Cluster Incl. M95740:Human alpha-L-iduronidase gene /cds=(0,1961) /gb=M95740 /gi=178412 /ug=Hs.89560 /len=2234     Cluster Incl. U90268:Human Krit1 mRNA, complete cds /cds=(25,1614) /gb=U90268 /gi=2149601 /ug=Hs.93810 /len=1986     Cluster Incl. AF014643:Homo sapiens connexin46.6 (Cx46.6) gene, complete cds /cds=(28,1338) /gb=AF014643 /gi=2738576 /ug=Hs.100072 /len=2087     Cluster Incl. AL050258:Novel human mRNA similar to mouse tuftelin-interacting protein 10 mRNA, AF097181 /cds=(263,2776) /gb=AL050258 /gi=4886426 /ug=Hs.20225 /len=3565     Cluster Incl. U09850:Human zinc finger protein (ZNF143) mRNA,	32877_i_at	Cluster Incl. AA524802:nh33h11.s1 Homo sapiens cDNA
Cluster Incl. L07592:Human peroxisome proliferator activated receptor mRNA, complete cds /cds=(337,1662) /gb=L07592 /gi=190229 /ug=Hs.106415 /len=3301  Cluster Incl. M95740:Human alpha-L-iduronidase gene /cds=(0,1961) /gb=M95740 /gi=178412 /ug=Hs.89560 /len=2234  Cluster Incl. U90268:Human Krit1 mRNA, complete cds /cds=(25,1614) /gb=U90268 /gi=2149601 /ug=Hs.93810 /len=1986  Cluster Incl. AF014643:Homo sapiens connexin46.6 (Cx46.6) gene, complete cds /cds=(28,1338) /gb=AF014643 /gi=2738576 /ug=Hs.100072 /len=2087  Cluster Incl. AL050258:Novel human mRNA similar to mouse tuftelin-interacting protein 10 mRNA, AF097181 /cds=(263,2776) /gb=AL050258 /gi=4886426 /ug=Hs.20225 /len=3565  Cluster Incl. U09850:Human zinc finger protein (ZNF143) mRNA,		/clone=IMAGE-954213 /gb=AA524802 /gi=2265730 /ug=Hs.203907
mRNA, complete cds /cds=(337,1662) /gb=L07592 /gi=190229 /ug=Hs.106415 /len=3301  Cluster Incl. M95740:Human alpha-L-iduronidase gene /cds=(0,1961) /gb=M95740 /gi=178412 /ug=Hs.89560 /len=2234  Cluster Incl. U90268:Human Krit1 mRNA, complete cds /cds=(25,1614) /gb=U90268 /gi=2149601 /ug=Hs.93810 /len=1986  Cluster Incl. AF014643:Homo sapiens connexin46.6 (Cx46.6) gene, complete cds /cds=(28,1338) /gb=AF014643 /gi=2738576 /ug=Hs.100072 /len=2087  Cluster Incl. AL050258:Novel human mRNA similar to mouse tuftelin- interacting protein 10 mRNA, AF097181 /cds=(263,2776) /gb=AL050258 /gi=4886426 /ug=Hs.20225 /len=3565  Cluster Incl. U09850:Human zinc finger protein (ZNF143) mRNA,		/len=500
/ug=Hs.106415 /len=3301  Cluster Incl. M95740:Human alpha-L-iduronidase gene /cds=(0,1961) /gb=M95740 /gi=178412 /ug=Hs.89560 /len=2234  Cluster Incl. U90268:Human Krit1 mRNA, complete cds /cds=(25,1614) /gb=U90268 /gi=2149601 /ug=Hs.93810 /len=1986  Cluster Incl. AF014643:Homo sapiens connexin46.6 (Cx46.6) gene, complete cds /cds=(28,1338) /gb=AF014643 /gi=2738576 /ug=Hs.100072 /len=2087  Cluster Incl. AL050258:Novel human mRNA similar to mouse tuftelin- interacting protein 10 mRNA, AF097181 /cds=(263,2776) /gb=AL050258 /gi=4886426 /ug=Hs.20225 /len=3565  Cluster Incl. U09850:Human zinc finger protein (ZNF143) mRNA,	37152_at	Cluster Incl. L07592:Human peroxisome proliferator activated receptor
Cluster Incl. M95740:Human alpha-L-iduronidase gene /cds=(0,1961) /gb=M95740 /gi=178412 /ug=Hs.89560 /len=2234  Cluster Incl. U90268:Human Krit1 mRNA, complete cds /cds=(25,1614) /gb=U90268 /gi=2149601 /ug=Hs.93810 /len=1986  Cluster Incl. AF014643:Homo sapiens connexin46.6 (Cx46.6) gene, complete cds /cds=(28,1338) /gb=AF014643 /gi=2738576 /ug=Hs.100072 /len=2087  Cluster Incl. AL050258:Novel human mRNA similar to mouse tuftelin- interacting protein 10 mRNA, AF097181 /cds=(263,2776) /gb=AL050258 /gi=4886426 /ug=Hs.20225 /len=3565  Cluster Incl. U09850:Human zinc finger protein (ZNF143) mRNA,		mRNA, complete cds /cds=(337,1662) /gb=L07592 /gi=190229
/gb=M95740 /gi=178412 /ug=Hs.89560 /len=2234  Cluster Incl. U90268:Human Krit1 mRNA, complete cds /cds=(25,1614) /gb=U90268 /gi=2149601 /ug=Hs.93810 /len=1986  Cluster Incl. AF014643:Homo sapiens connexin46.6 (Cx46.6) gene, complete cds /cds=(28,1338) /gb=AF014643 /gi=2738576 /ug=Hs.100072 /len=2087  Cluster Incl. AL050258:Novel human mRNA similar to mouse tuftelin- interacting protein 10 mRNA, AF097181 /cds=(263,2776) /gb=AL050258 /gi=4886426 /ug=Hs.20225 /len=3565  Cluster Incl. U09850:Human zinc finger protein (ZNF143) mRNA,		/ug=Hs.106415 /len=3301
Cluster Incl. U90268:Human Krit1 mRNA, complete cds /cds=(25,1614) /gb=U90268 /gi=2149601 /ug=Hs.93810 /len=1986  Cluster Incl. AF014643:Homo sapiens connexin46.6 (Cx46.6) gene, complete cds /cds=(28,1338) /gb=AF014643 /gi=2738576 /ug=Hs.100072 /len=2087  Cluster Incl. AL050258:Novel human mRNA similar to mouse tuftelin- interacting protein 10 mRNA, AF097181 /cds=(263,2776) /gb=AL050258 /gi=4886426 /ug=Hs.20225 /len=3565  Cluster Incl. U09850:Human zinc finger protein (ZNF143) mRNA,	33155_at	Cluster Incl. M95740:Human alpha-L-iduronidase gene /cds=(0,1961)
/cds=(25,1614) /gb=U90268 /gi=2149601 /ug=Hs.93810 /len=1986  Cluster Incl. AF014643:Homo sapiens connexin46.6 (Cx46.6) gene, complete cds /cds=(28,1338) /gb=AF014643 /gi=2738576 /ug=Hs.100072 /len=2087  Cluster Incl. AL050258:Novel human mRNA similar to mouse tuftelin-interacting protein 10 mRNA, AF097181 /cds=(263,2776) /gb=AL050258 /gi=4886426 /ug=Hs.20225 /len=3565  Cluster Incl. U09850:Human zinc finger protein (ZNF143) mRNA,		/gb=M95740 /gi=178412 /ug=Hs.89560 /len=2234
Cluster Incl. AF014643:Homo sapiens connexin46.6 (Cx46.6) gene, complete cds /cds=(28,1338) /gb=AF014643 /gi=2738576 /ug=Hs.100072 /len=2087  Cluster Incl. AL050258:Novel human mRNA similar to mouse tuftelin-interacting protein 10 mRNA, AF097181 /cds=(263,2776) /gb=AL050258 /gi=4886426 /ug=Hs.20225 /len=3565  Cluster Incl. U09850:Human zinc finger protein (ZNF143) mRNA,	34031_i_at	Cluster Incl. U90268:Human Krit1 mRNA, complete cds
complete cds /cds=(28,1338) /gb=AF014643 /gi=2738576 /ug=Hs.100072 /len=2087  Cluster Incl. AL050258:Novel human mRNA similar to mouse tuftelin- interacting protein 10 mRNA, AF097181 /cds=(263,2776) /gb=AL050258 /gi=4886426 /ug=Hs.20225 /len=3565  Cluster Incl. U09850:Human zinc finger protein (ZNF143) mRNA,		/cds=(25,1614) /gb=U90268 /gi=2149601 /ug=Hs.93810 /len=1986
/ug=Hs.100072 /len=2087  Cluster Incl. AL050258:Novel human mRNA similar to mouse tuftelin-interacting protein 10 mRNA, AF097181 /cds=(263,2776) /gb=AL050258 /gi=4886426 /ug=Hs.20225 /len=3565  Cluster Incl. U09850:Human zinc finger protein (ZNF143) mRNA,	39504_at	Cluster Incl. AF014643:Homo sapiens connexin46.6 (Cx46.6) gene,
Cluster Incl. AL050258:Novel human mRNA similar to mouse tuftelin- interacting protein 10 mRNA, AF097181 /cds=(263,2776) /gb=AL050258 /gi=4886426 /ug=Hs.20225 /len=3565  Cluster Incl. U09850:Human zinc finger protein (ZNF143) mRNA,		complete cds /cds=(28,1338) /gb=AF014643 /gi=2738576
interacting protein 10 mRNA, AF097181 /cds=(263,2776) /gb=AL050258 /gi=4886426 /ug=Hs.20225 /len=3565  Cluster Incl. U09850:Human zinc finger protein (ZNF143) mRNA,		/ug=Hs.100072 /len=2087
/gb=AL050258 /gi=4886426 /ug=Hs.20225 /len=3565  Cluster Incl. U09850:Human zinc finger protein (ZNF143) mRNA,	40975_s_at	Cluster Incl. AL050258:Novel human mRNA similar to mouse tuftelin-
40241_at Cluster Incl. U09850:Human zinc finger protein (ZNF143) mRNA,		interacting protein 10 mRNA, AF097181 /cds=(263,2776)
		/gb=AL050258 /gi=4886426 /ug=Hs.20225 /len=3565
complete cds /cds=(37 1917) /gh=IJ09850 /gi=495571 /ug=Hs 154095	40241_at	Cluster Incl. U09850:Human zinc finger protein (ZNF143) mRNA,
John Profession 201, 1711, 180 - 00, 000 (81 - 1700) 1 (48 - 18.15 + 1700)		complete cds /cds=(37,1917) /gb=U09850 /gi=495571 /ug=Hs.154095
/len=3908		/len=3908

33723_at	Cluster Incl. AL049346:Homo sapiens mRNA; cDNA DKFZp566B213
	(from clone DKFZp566B213) /cds=UNKNOWN /gb=AL049346
	/gi=4500130 /ug=Hs.194051 /len=1554
1459_at	M68941 /FEATURE=mRNA /DEFINITION=HUMPTYPH Human
	protein-tyrosine phosphatase mRNA, complete cds
40033_at	Cluster Incl. AL022328:Human DNA sequence from clone 402G11 on
	chromosome 22q13.31-13.33 Contains genes for SAPK3 (stress-
	activated protein kinase 3), PRKM11 (protein kinase mitogen-activated
	11), KIAA0315, ESTs, GSSs and CpG islands /cds=(11,1105)
	/gb=AL022328 /gi=5263010 /ug=Hs.57732 /len=2341
39661_s_at	Cluster Incl. AF034102:Homo sapiens NBMPR-insensitive nucleoside
	transporter ei (ENT2) mRNA, complete cds /cds=(237,1607)
•	/gb=AF034102 /gi=2811136 /ug=Hs.32951 /len=2522
37629_at	Cluster Incl. M55268:Human casein kinase II alpha subunit mRNA,
	complete cds /cds=(163,1215) /gb=M55268 /gi=177837 /ug=Hs.82201
	/len=1677
1624_at	Stimulatory Gdp/Gtp Exchange Protein For C-Ki-Ras P21 And Smg
,	P21
1903_at	Ras-Related Protein Rap1b
33170_at	Cluster Incl. AB023179:Homo sapiens mRNA for KIAA0962 protein,
	partial cds /cds=(0,1893) /gb=AB023179 /gi=4589567 /ug=Hs.9059
	/len=5460
33175_at	Cluster Incl. AA156237:zl50c09.s1 Homo sapiens cDNA, 3 end
	/clone=IMAGE-505360 /clone_end=3 /gb=AA156237 /gi=1727855
	/ug=Hs.90804 /len=644
38044_at	Cluster Incl. AF035283:Homo sapiens clone 23916 mRNA sequence
	/cds=UNKNOWN /gb=AF035283 /gi=2661034 /ug=Hs.8022
	/len=2022
40440_at	Cluster Incl. AL080119:Homo sapiens mRNA; cDNA
	DKFZp564M2423 (from clone DKFZp564M2423) /cds=(85,1248)
	/gb=AL080119 /gi=5262550 /ug=Hs.165998 /len=2183
<u> </u>	

35254_at	Cluster Incl. AB007447:Homo sapiens mRNA for Fln29, complete cds
}	/cds=(54,1802) /gb=AB007447 /gi=2463530 /ug=Hs.5148 /len=2618

[00276] Next, we calculated phenotype association indices for all 52 samples and determined that this gene cluster exhibited a 77% success rate in clinical sample classification based on individual phenotype association indices (Table 48). As shown in Table 48, 22/26 (or 85%) of the invasive prostate cancer samples had positive phenotype association indices, whereas 18/26 (or 69%) of non-invasive prostate cancer samples displayed negative phenotype association indices. Overall, 40 of 52 samples (or 77%) were correctly classified.

Table 48. Classification accuracy of the prostate cancer invasion clusters				
Cluster	r value (Phenotype Association	Invasive tumors	Non-invasive tumors	Overall
1	Index)			
114	0.704	22/26 (85%)	18/26 (69%)	40/52
genes				(77%)
53 genes	0.893	22/26 (85%)	17/26 (65%)	39/52
				(75%)
39 genes	0.972	22/26 (85%)	18/26 (69%)	40/52
				(77%)
26 genes	0.994	23/26 (88%)	17/26 (65%)	40/52
				(77%)
24 genes	0.997	21/26 (81%)	17/26 (65%)	38/52
				(73%)
22 genes	0.995	21/26 (81%)	18/26 (69%)	39/52
.				(75%)

[00277] Next, we identified a single best-fit invasive prostate cancer sample displaying the correlation coefficient of 0.704 to the average expression profile of the 26 invasive

prostate cancer samples. The expression profile of this single best-fit invasive prostate cancer sample was utilized as a second reference set.

[00278] The concordance set was obtained by selecting only those genes having a consistent direction of the differential expression in both the first and the second reference sets (i.e., greater gene expression difference in the invasive cf. the non-invasive samples and greater gene expression in the best-fit tumor sample cf. the average expression value across the entire data set or vice-versa). The concordance set comprised of 107 genes (r = 0.721). A minimum segregation set was selected following the procedures described in above. Scatter plots were generated of the log<sub>10</sub> transformed average -fold expression change in the first reference set and average -fold expression change in the second reference set (in case of a single best-fit tumor it was the log<sub>10</sub> transformed ratio of the expression value for a gene to the average expression value across the entire data set). For the samples of the first reference set, <expression>1 corresponds to the average expression value for gene x over all samples from patients who had invasive tumors and <expression>2 corresponds to the average expression value for gene x over all samples from patients who had non-invasive tumors. A minimum segregation set was identified by selecting a subset of the highly correlated genes between two reference sets from the invasiveness concordance set. Using this approach we identified five gene clusters discriminating with high accuracy between invasive and non-invasive human prostate tumors. The members of these invasion predictors or invasion minimum segregation sets (invasion minimum segregation gene clusters) are listed in Tables 49-54. The classification performance for each of these gene clusters is presented in the Table 48.

	Table 49. 53-gene signature of invasive prostate cancer		
Affymetrix	Description		
Probe Set ID			
(U95Av2)			
1878_g_at	M13194 /FEATURE=mRNA /DEFINITION=HUMERCC1 Human		
	excision repair protein (ERCC1) mRNA, complete cds, clone pcDE		
33833_at	Cluster Incl. J05243:Human nonerythroid alpha-spectrin (SPTAN1)		
	mRNA, complete cds /cds=(102,7520) /gb=J05243 /gi=179105		
	/ug=Hs.237180 /len=7787		
33915_at	Cluster Incl. W22655:71B9 Homo sapiens cDNA /clone=(not-		
	directional) /gb=W22655 /gi=1299488 /ug=Hs.26070 /len=761		
35787_at	Cluster Incl. AI986201:wr81a01.x1 Homo sapiens cDNA, 3 end		
	/clone=IMAGE-2494056 /clone_end=3 /gb=AI986201 /gi=5813478		
	/ug=Hs.66881 /len=814		
37390_at	Cluster Incl. D86977:Human mRNA for KIAA0224 gene, complete cds		
	/cds=(136,3819) /gb=D86977 /gi=1504027 /ug=Hs.78054 /len=4226		
38260_at	Cluster Incl. AL050306:Human DNA sequence from clone 475B7 on		
	chromosome Xq12.1-13. Contains the 3 part of the gene for a novel		
	KIAA0615 and KIAA0323 LIKE protein, the gene for a novel protein,		
	ESTs, STSs, GSSs and two putative CpG islands /cds=(48,2201)		
	/gb=AL050306 /gi=5419784 /ug=Hs.90625 /len=2395		
38794_at	Cluster Incl. X53390:Human mRNA for upstream binding factor (hUBF)		
	/cds=(147,2441) /gb=X53390 /gi=509240 /ug=Hs.89781 /len=3097		
38841_at	Cluster Incl. AF068195:Homo sapiens putative glialblastoma cell		
	differentiation-related protein (GBDR1) mRNA, complete cds		
	/cds=(58,1062) /gb=AF068195 /gi=3192872 /ug=Hs.9194 /len=1493		
39379_at	Cluster Incl. AL049397:Homo sapiens mRNA; cDNA DKFZp586C1019		
	(from clone DKFZp586C1019) /cds=UNKNOWN /gb=AL049397		
	/gi=4500188 /ug=Hs.12314 /len=1720		

/cds=(164,1447) /gb=AF089750 /gi=3599572 /ug=Hs.179986 /len=17 41116_at
/clone=IMAGE-2321393 /clone_end=3 /gb=AI799802 /gi=5365274 /ug=Hs.101516 /len=688  41869_at Cluster Incl. U78310:Homo sapiens pescadillo mRNA, complete cds /cds=(58,1824) /gb=U78310 /gi=2194202 /ug=Hs.13501 /len=2235  1321_s_at U43916 /FEATURE= /DEFINITION=HSU43916 Human tumor- associated membrane protein homolog (TMP) mRNA, complete cds  154_at X07024 /FEATURE=cds /DEFINITION=HSCCG1 Human X chromosome mRNA for CCG1 protein inv. in cell proliferation  1569_r_at L42243 /FEATURE=exon#3 /DEFINITION=HUMIFNAM08 Homo sapiens (clone 51H8) alternatively spliced interferon receptor (IFNAR gene, exon 9 and complete cds s
/ug=Hs.101516 /len=688  Cluster Incl. U78310:Homo sapiens pescadillo mRNA, complete cds /cds=(58,1824) /gb=U78310 /gi=2194202 /ug=Hs.13501 /len=2235  1321_s_at U43916 /FEATURE= /DEFINITION=HSU43916 Human tumor- associated membrane protein homolog (TMP) mRNA, complete cds  X07024 /FEATURE=cds /DEFINITION=HSCCG1 Human X chromosome mRNA for CCG1 protein inv. in cell proliferation  L42243 /FEATURE=exon#3 /DEFINITION=HUMIFNAM08 Homo sapiens (clone 51H8) alternatively spliced interferon receptor (IFNAR gene, exon 9 and complete cds s
Cluster Incl. U78310:Homo sapiens pescadillo mRNA, complete cds /cds=(58,1824) /gb=U78310 /gi=2194202 /ug=Hs.13501 /len=2235  1321_s_at  U43916 /FEATURE= /DEFINITION=HSU43916 Human tumor- associated membrane protein homolog (TMP) mRNA, complete cds  X07024 /FEATURE=cds /DEFINITION=HSCCG1 Human X chromosome mRNA for CCG1 protein inv. in cell proliferation  L42243 /FEATURE=exon#3 /DEFINITION=HUMIFNAM08 Homo sapiens (clone 51H8) alternatively spliced interferon receptor (IFNAR gene, exon 9 and complete cds s
/cds=(58,1824) /gb=U78310 /gi=2194202 /ug=Hs.13501 /len=2235  1321_s_at U43916 /FEATURE= /DEFINITION=HSU43916 Human tumor- associated membrane protein homolog (TMP) mRNA, complete cds  154_at X07024 /FEATURE=cds /DEFINITION=HSCCG1 Human X chromosome mRNA for CCG1 protein inv. in cell proliferation  1569_r_at L42243 /FEATURE=exon#3 /DEFINITION=HUMIFNAM08 Homo sapiens (clone 51H8) alternatively spliced interferon receptor (IFNAR gene, exon 9 and complete cds s
1321_s_at  U43916 /FEATURE= /DEFINITION=HSU43916 Human tumor- associated membrane protein homolog (TMP) mRNA, complete cds  X07024 /FEATURE=cds /DEFINITION=HSCCG1 Human X chromosome mRNA for CCG1 protein inv. in cell proliferation  L42243 /FEATURE=exon#3 /DEFINITION=HUMIFNAM08 Homo sapiens (clone 51H8) alternatively spliced interferon receptor (IFNAR gene, exon 9 and complete cds s
associated membrane protein homolog (TMP) mRNA, complete cds  154_at X07024 /FEATURE=cds /DEFINITION=HSCCG1 Human X chromosome mRNA for CCG1 protein inv. in cell proliferation  1569_r_at L42243 /FEATURE=exon#3 /DEFINITION=HUMIFNAM08 Homo sapiens (clone 51H8) alternatively spliced interferon receptor (IFNAR gene, exon 9 and complete cds s
154_at X07024 /FEATURE=cds /DEFINITION=HSCCG1 Human X chromosome mRNA for CCG1 protein inv. in cell proliferation  1569_r_at L42243 /FEATURE=exon#3 /DEFINITION=HUMIFNAM08 Homo sapiens (clone 51H8) alternatively spliced interferon receptor (IFNAR gene, exon 9 and complete cds s
chromosome mRNA for CCG1 protein inv. in cell proliferation  1569_r_at
1569_r_at L42243 /FEATURE=exon#3 /DEFINITION=HUMIFNAM08 Homo sapiens (clone 51H8) alternatively spliced interferon receptor (IFNAR gene, exon 9 and complete cds s
sapiens (clone 51H8) alternatively spliced interferon receptor (IFNAR gene, exon 9 and complete cds s
gene, exon 9 and complete cds s
1668_s_at L15409 /FEATURE= /DEFINITION=HUMHIPLIND Homo sapiens
(clone g7) von Hippel-Lindau disease tumor suppressor mRNA sequen
1832_at M62397 /FEATURE= /DEFINITION=HUMCRCMUT Human
colorectal mutant cancer protein mRNA, complete cds
1903_at Ras-Related Protein Rap1b
Cluster Incl. W27967:40b10 Homo sapiens cDNA /gb=W27967
/gi=1307915 /ug=Hs.136154 /len=755
31446_s_at Cluster Incl. D89501:Human PBI gene, complete cds /cds=(14,418)
/gb=D89501 /gi=1854451 /ug=Hs.166099 /len=576
31922_i_at Cluster Incl. U60269:Human endogenous retrovirus HERV-K(HML6)
proviral clone HML6.17 putative polymerase and envelope genes, part
cds, and 3LTR /cds=(0,491) /gb=U60269 /gi=1408208 /ug=Hs.159902
/len=492
32054_at Cluster Incl. AF048732:Homo sapiens cyclin T2b mRNA, complete co
/cds=(0,2192) /gb=AF048732 /gi=2981199 /ug=Hs.155478 /len=2193

32149_at	Cluster Incl. AA532495:nj54a10.s1 Homo sapiens cDNA
	/clone=IMAGE-996282 /gb=AA532495 /gi=2276749 /ug=Hs.183752
	/len=549
32596_at	Cluster Incl. W25828:13g2 Homo sapiens cDNA /gb=W25828
	/gi=1305951 /ug=Hs.79362 /len=744
33615_at	Cluster Incl. X64994:H.sapiens HGMP07I gene for olfactory receptor
	/cds=(0,944) /gb=X64994 /gi=32085 /ug=Hs.163670 /len=945
33723_at	Cluster Incl. AL049346:Homo sapiens mRNA; cDNA DKFZp566B213
	(from clone DKFZp566B213) /cds=UNKNOWN /gb=AL049346
	/gi=4500130 /ug=Hs.194051 /len=1554
34057_at	Cluster Incl. U84392:Human Na+-dependent purine specific transporter
	mRNA, complete cds /cds=(59,2035) /gb=U84392 /gi=2731438
	/ug=Hs.193665 /len=2459
34059_at	Cluster Incl. AA586695:nn42h06.s1 Homo sapiens cDNA, 3 end
	/clone=IMAGE-1086587 /clone_end=3 /gb=AA586695 /gi=2397509
	/ug=Hs.193956 /len=522
34486_at	Cluster Incl. U88897:Human endogenous retroviral H D2 leader region,
	protease region, and integrase/envelope region mRNA sequence
	/cds=UNKNOWN /gb=U88897 /gi=2104917 /ug=Hs.11828 /len=1004
34909_at	Cluster Incl. AC004990:Homo sapiens PAC clone DJ1185I07 from
	7q11.23-q21 /cds=(0,1766) /gb=AC004990 /gi=3924668 /ug=Hs.128653
	/len=1767
35489_at	Cluster Incl. M82962:Human N-benzoyl-L-tyrosyl-p-amino-benzoic acid
	hydrolase alpha subunit (PPH alpha) mRNA, complete cds /cds=(9,2249)
	/gb=M82962 /gi=535474 /ug=Hs.179704 /len=2902
35565_at	Cluster Incl. U79301:Human clone 23842 mRNA sequence
	/cds=UNKNOWN /gb=U79301 /gi=1710286 /ug=Hs.135617 /len=1582
35640_at	Cluster Incl. D14822:Human chimeric mRNA derived from AML1 gene
	and MTG8(ETO) gene, partial sequence /cds=(0,597) /gb=D14822
	/gi=467498 /ug=Hs.31551 /len=799
L	

35960_at	Cluster Incl. AF031416:Homo sapiens IkB kinase beta subunit mRNA,
33900_at	
	complete cds /cds=(0,2270) /gb=AF031416 /gi=3213216 /ug=Hs.226573
	/len=2271
37054_at	Cluster Incl. J04739: Human bactericidal permeability increasing protein
	(BPI) mRNA, complete cds /cds=(30,1493) /gb=J04739 /gi=179528
	/ug=Hs.89535 /len=1813
37785_at	Cluster Incl. U69563:U69563 Homo sapiens cDNA /clone=25050
	/gb=U69563 /gi=2731394 /ug=Hs.124940 /len=1657
38198_at	Cluster Incl. AL079275:Homo sapiens mRNA full length insert cDNA
	clone EUROIMAGE 566443 /cds=UNKNOWN /gb=AL079275
	/gi=5102578 /ug=Hs.157078 /len=2082
38871_at	Cluster Incl. AJ006288:Homo sapiens mRNA for bcl-10 protein
	/cds=(690,1391) /gb=AJ006288 /gi=4049459 /ug=Hs.193516 /len=1877
38938_at	Cluster Incl. AI816413:au47f05.x1 Homo sapiens cDNA, 3 end
	/clone=IMAGE-2517921 /clone_end=3 /gb=AI816413 /gi=5431959
	/ug=Hs.210862 /len=586
39304_g_at	Cluster Incl. Y14153:Homo sapiens mRNA for beta-transducin repeat
	containing protein /cds=(69,1778) /gb=Y14153 /gi=2995193
	/ug=Hs.239742 /len=2141
39364_s_at	Cluster Incl. Y18207:Homo sapiens mRNA for protein phosphatase 1
	(PPP1R5) /cds=(91,1044) /gb=Y18207 /gi=3805818 /ug=Hs.12112
	/len=1158
39475_at	Cluster Incl. L37199:Homo sapiens (clone cD24-1) Huntingtons disease
	candidate region mRNA fragment /cds=UNKNOWN /gb=L37199
	/gi=600520 /ug=Hs.117487 /len=1356
39661_s_at	Cluster Incl. AF034102:Homo sapiens NBMPR-insensitive nucleoside
	transporter ei (ENT2) mRNA, complete cds /cds=(237,1607)
	/gb=AF034102 /gi=2811136 /ug=Hs.32951 /len=2522
39882_at	Cluster Incl. U66035:Human X-linked deafness dystonia protein (DDP)
3700 <b>2_</b> at	mRNA, complete cds /cds=(35,328) /gb=U66035 /gi=3123842
	/ug=Hs.125565 /len=1169
	/ ug-115.123303 /1011-1109

39912_at	Cluster Incl. AB006179:Homo sapiens mRNA for heparan-sulfate 6-
	sulfotransferase, complete cds /cds=(111,1343) /gb=AB006179
	/gi=3073774 /ug=Hs.132884 /len=2051
39924_at	Cluster Incl. AB020660:Homo sapiens mRNA for KIAA0853 protein,
	partial cds /cds=(0,2905) /gb=AB020660 /gi=4240194 /ug=Hs.136102
	/len=4363
39926_at	Cluster Incl. U59913:Human chromosome 5 Mad homolog Smad5
	mRNA, complete cds /cds=(130,1527) /gb=U59913 /gi=1654324
	/ug=Hs.37501 /len=2205
40241_at	· Cluster Incl. U09850:Human zinc finger protein (ZNF143) mRNA,
	complete cds /cds=(37,1917) /gb=U09850 /gi=495571 /ug=Hs.154095
	/len=3908
40975_s_at	Cluster Incl. AL050258:Novel human mRNA similar to mouse tuftelin-
	interacting protein 10 mRNA, AF097181 /cds=(263,2776)
	/gb=AL050258 /gi=4886426 /ug=Hs.20225 /len=3565
41112_at	Cluster Incl. AB011129:Homo sapiens mRNA for KIAA0557 protein,
	partial cds /cds=(0,1482) /gb=AB011129 /gi=3043637 /ug=Hs.101414
	/len=5627
41550_at	Cluster Incl. AF091071:Homo sapiens clone 192 Rer1 mRNA, complete
	cds /cds=(76,696) /gb=AF091071 /gi=3859979 /ug=Hs.40500 /len=1400
677_s_at	J04430 /FEATURE=mRNA /DEFINITION=HUMACP5 Human tartrate-
	resistant acid phosphatase type 5 mRNA, complete cds
971_s_at	Y00083 /FEATURE=cds /DEFINITION=HSGTSF Human mRNA for
	glioblastoma-derived T-cell suppressor factor G-TsF (transforming
	growth factor-beta2, TGF-beta2)
L	<del></del>

Table 50. 39-gene signature of invasive prostate cancer	
Affymetrix	Description
Probe Set ID	
(U95Av2)	

1878_g_at	M13194 /FEATURE=mRNA /DEFINITION=HUMERCC1 Human
	excision repair protein (ERCC1) mRNA, complete cds, clone pcDE
33833_at	Cluster Incl. J05243:Human nonerythroid alpha-spectrin (SPTAN1)
	mRNA, complete cds /cds=(102,7520) /gb=J05243 /gi=179105
	/ug=Hs.237180 /len=7787
33915_at	Cluster Incl. W22655:71B9 Homo sapiens cDNA /clone=(not-directional)
	/gb=W22655 /gi=1299488 /ug=Hs.26070 /len=761
35787_at	Cluster Incl. AI986201:wr81a01.x1 Homo sapiens cDNA, 3 end
į	/clone=IMAGE-2494056 /clone_end=3 /gb=AI986201 /gi=5813478
	/ug=Hs.66881 /len=814
37390_at	Cluster Incl. D86977:Human mRNA for KIAA0224 gene, complete cds
	/cds=(136,3819) /gb=D86977 /gi=1504027 /ug=Hs.78054 /len=4226
38260_at	Cluster Incl. AL050306:Human DNA sequence from clone 475B7 on
}	chromosome Xq12.1-13. Contains the 3 part of the gene for a novel
	KIAA0615 and KIAA0323 LIKE protein, the gene for a novel protein,
	ESTs, STSs, GSSs and two putative CpG islands /cds=(48,2201)
	/gb=AL050306 /gi=5419784 /ug=Hs.90625 /len=2395
38794_at	Cluster Incl. X53390:Human mRNA for upstream binding factor (hUBF)
	/cds=(147,2441) /gb=X53390 /gi=509240 /ug=Hs.89781 /len=3097
38841_at	Cluster Incl. AF068195:Homo sapiens putative glialblastoma cell
	differentiation-related protein (GBDR1) mRNA, complete cds
	/cds=(58,1062) /gb=AF068195 /gi=3192872 /ug=Hs.9194 /len=1493
39379_at	Cluster Incl. AL049397:Homo sapiens mRNA; cDNA DKFZp586C1019
	(from clone DKFZp586C1019) /cds=UNKNOWN /gb=AL049397
	/gi=4500188 /ug=Hs.12314 /len=1720
40635_at	Cluster Incl. AF089750:Homo sapiens flotillin-1 mRNA, complete cds
	/cds=(164,1447) /gb=AF089750 /gi=3599572 /ug=Hs.179986 /len=1796
41116_at	Cluster Incl. AI799802:wc43d09.x1 Homo sapiens cDNA, 3 end
	/clone=IMAGE-2321393 /clone_end=3 /gb=AI799802 /gi=5365274
	/ug=Hs.101516 /len=688
L	4

41869_at	Cluster Incl. U78310:Homo sapiens pescadillo mRNA, complete cds
	/cds=(58,1824) /gb=U78310 /gi=2194202 /ug=Hs.13501 /len=2235
1321_s_at	U43916 /FEATURE= /DEFINITION=HSU43916 Human tumor-
	associated membrane protein homolog (TMP) mRNA, complete cds
1668_s_at	L15409 /FEATURE= /DEFINITION=HUMHIPLIND Homo sapiens
	(clone g7) von Hippel-Lindau disease tumor suppressor mRNA sequence
1832_at	M62397 /FEATURE= /DEFINITION=HUMCRCMUT Human colorectal
	mutant cancer protein mRNA, complete cds
1903_at	Ras-Related Protein Rap1b
31368_at	Cluster Incl. W27967:40b10 Homo sapiens cDNA /gb=W27967
ļ	/gi=1307915 /ug=Hs.136154 /len=755
31446_s_at	Cluster Incl. D89501:Human PBI gene, complete cds /cds=(14,418)
	/gb=D89501 /gi=1854451 /ug=Hs.166099 /len=576
31922_i_at	Cluster Incl. U60269:Human endogenous retrovirus HERV-K(HML6)
	proviral clone HML6.17 putative polymerase and envelope genes, partial
	cds, and 3LTR /cds=(0,491) /gb=U60269 /gi=1408208 /ug=Hs.159902
	/len=492
32054_at	Cluster Incl. AF048732:Homo sapiens cyclin T2b mRNA, complete cds
	/cds=(0,2192) /gb=AF048732 /gi=2981199 /ug=Hs.155478 /len=2193
32149_at	Cluster Incl. AA532495:nj54a10.s1 Homo sapiens cDNA /clone=IMAGE-
	996282 /gb=AA532495 /gi=2276749 /ug=Hs.183752 /len=549
33723_at	Cluster Incl. AL049346:Homo sapiens mRNA; cDNA DKFZp566B213
	(from clone DKFZp566B213) /cds=UNKNOWN /gb=AL049346
	/gi=4500130 /ug=Hs.194051 /len=1554
34059_at	Cluster Incl. AA586695:nn42h06.s1 Homo sapiens cDNA, 3 end
	/clone=IMAGE-1086587 /clone_end=3 /gb=AA586695 /gi=2397509
	/ug=Hs.193956 /len=522
34909_at	Cluster Incl. AC004990:Homo sapiens PAC clone DJ1185I07 from
	7q11.23-q21 /cds=(0,1766) /gb=AC004990 /gi=3924668 /ug=Hs.128653
	/len=1767
L	<u></u>

35489_at	Cluster Incl. M82962:Human N-benzoyl-L-tyrosyl-p-amino-benzoic acid
<u> </u> 	hydrolase alpha subunit (PPH alpha) mRNA, complete cds /cds=(9,2249)
i i	/gb=M82962 /gi=535474 /ug=Hs.179704 /len=2902
35640_at	Cluster Incl. D14822:Human chimeric mRNA derived from AML1 gene
	and MTG8(ETO) gene, partial sequence /cds=(0,597) /gb=D14822
	/gi=467498 /ug=Hs.31551 /len=799
37054_at	Cluster Incl. J04739:Human bactericidal permeability increasing protein
	(BPI) mRNA, complete cds /cds=(30,1493) /gb=J04739 /gi=179528
	/ug=Hs.89535 /len=1813
37785_at	Cluster Incl. U69563:U69563 Homo sapiens cDNA /clone=25050
	/gb=U69563 /gi=2731394 /ug=Hs.124940 /len=1657
38198_at	Cluster Incl. AL079275:Homo sapiens mRNA full length insert cDNA
}	clone EUROIMAGE 566443 /cds=UNKNOWN /gb=AL079275
	/gi=5102578 /ug=Hs.157078 /len=2082
38871_at	Cluster Incl. AJ006288:Homo sapiens mRNA for bcl-10 protein
	/cds=(690,1391) /gb=AJ006288 /gi=4049459 /ug=Hs.193516 /len=1877
39475_at	Cluster Incl. L37199:Homo sapiens (clone cD24-1) Huntingtons disease
	candidate region mRNA fragment /cds=UNKNOWN /gb=L37199
	/gi=600520 /ug=Hs.117487 /len=1356
39661_s_at	Cluster Incl. AF034102:Homo sapiens NBMPR-insensitive nucleoside
	transporter ei (ENT2) mRNA, complete cds /cds=(237,1607)
ļ	/gb=AF034102 /gi=2811136 /ug=Hs.32951 /len=2522
39882_at	Cluster Incl. U66035:Human X-linked deafness dystonia protein (DDP)
į	mRNA, complete cds /cds=(35,328) /gb=U66035 /gi=3123842
	/ug=Hs.125565 /len=1169
39912_at	Cluster Incl. AB006179:Homo sapiens mRNA for heparan-sulfate 6-
	sulfotransferase, complete cds /cds=(111,1343) /gb=AB006179
	/gi=3073774 /ug=Hs.132884 /len=2051
40241_at	Cluster Incl. U09850:Human zinc finger protein (ZNF143) mRNA,
	complete cds /cds=(37,1917) /gb=U09850 /gi=495571 /ug=Hs.154095
	/len=3908
L	

40975_s_at	Cluster Incl. AL050258:Novel human mRNA similar to mouse tuftelin-
	interacting protein 10 mRNA, AF097181 /cds=(263,2776) /gb=AL050258
<u> </u> 	/gi=4886426 /ug=Hs.20225 /len=3565
41550_at	Cluster Incl. AF091071:Homo sapiens clone 192 Rer1 mRNA, complete
;	cds /cds=(76,696) /gb=AF091071 /gi=3859979 /ug=Hs.40500 /len=1400
677_s_at	J04430 /FEATURE=mRNA /DEFINITION=HUMACP5 Human tartrate-
	resistant acid phosphatase type 5 mRNA, complete cds
971_s_at	Y00083 /FEATURE=cds /DEFINITION=HSGTSF Human mRNA for
	glioblastoma-derived T-cell suppressor factor G-TsF (transforming growth
	factor-beta2, TGF-beta2)

Table 51. 26-gene signature of invasive prostate cancer	
Affymetrix	Description
Probe Set ID	
(U95Av2)	
36993_at	Cluster Incl. M33210:Human colony stimulating factor 1 receptor
	(CSF1R) gene /cds=(0,283) /gb=M33210 /gi=532592 /ug=Hs.76144
	/len=2206
38682_at	Cluster Incl. AF045581:Homo sapiens BRCA1 associated protein 1
	(BAP1) mRNA, complete cds /cds=(39,2228) /gb=AF045581
	/gi=2854120 /ug=Hs.106674 /len=3506
41725_at	Cluster Incl. U89896:Homo sapiens casein kinase I gamma 2 mRNA,
	complete cds /cds=(239,1486) /gb=U89896 /gi=1890117
	/ug=Hs.181390 /len=1749
32212_at	Cluster Incl. AL049703:Human gene from PAC 179D3, chromosome
	X, isoform of mitochondrial apoptosis inducing factor, AIF, AF100928
	/cds=(96,1925) /gb=AL049703 /gi=4678806 /ug=Hs.18720 /len=2121
1385_at	M77349 /FEATURE= /DEFINITION=HUMTGFBIG Human
	transforming growth factor-beta induced gene product (BIGH3)
	mRNA, complete cds

Cluster Incl. X13482:Human mRNA for U2 snRNP-specific A protein
/cds=(56,823) /gb=X13482 /gi=37546 /ug=Hs.80506 /len=1033
Ras-Related Protein Rap1b
Cluster Incl. AF034102:Homo sapiens NBMPR-insensitive nucleoside
transporter ei (ENT2) mRNA, complete cds /cds=(237,1607)
/gb=AF034102 /gi=2811136 /ug=Hs.32951 /len=2522
Cluster Incl. U09850:Human zinc finger protein (ZNF143) mRNA,
complete cds /cds=(37,1917) /gb=U09850 /gi=495571 /ug=Hs.154095
/len=3908
Cluster Incl. AL050258:Novel human mRNA similar to mouse tuftelin-
interacting protein 10 mRNA, AF097181 /cds=(263,2776)
/gb=AL050258 /gi=4886426 /ug=Hs.20225 /len=3565
Cluster Incl. AA532495:nj54a10.s1 Homo sapiens cDNA
/clone=IMAGE-996282 /gb=AA532495 /gi=2276749 /ug=Hs.183752
/len=549
Cluster Incl. AC002126:Homo sapiens DNA from chromosome 19-
cosmids R30102-R29350-R27740 containing MEF2B, genomic
sequence /cds=(0,307) /gb=AC002126 /gi=2329908 /ug=Hs.125220
/len=308
Cluster Incl. AF015451:Homo sapiens Usurpin-beta mRNA, complete
cds /cds=(0,1388) /gb=AF015451 /gi=3133282 /ug=Hs.195175
/len=1389
Cluster Incl. AA586695:nn42h06.s1 Homo sapiens cDNA, 3 end
/clone=IMAGE-1086587 /clone_end=3 /gb=AA586695 /gi=2397509
/ug=Hs.193956 /len=522
Cluster Incl. W28976:54e5 Homo sapiens cDNA /gb=W28976
/gi=1308924 /ug=Hs.133151 /len=903
Cluster Incl. AF048732:Homo sapiens cyclin T2b mRNA, complete
cds /cds=(0,2192) /gb=AF048732 /gi=2981199 /ug=Hs.155478
/len=2193

M62397 /FEATURE= /DEFINITION=HUMCRCMUT Human
colorectal mutant cancer protein mRNA, complete cds
U43916 /FEATURE= /DEFINITION=HSU43916 Human tumor-
associated membrane protein homolog (TMP) mRNA, complete cds
Cluster Incl. M82962:Human N-benzoyl-L-tyrosyl-p-amino-benzoic
acid hydrolase alpha subunit (PPH alpha) mRNA, complete cds
/cds=(9,2249) /gb=M82962 /gi=535474 /ug=Hs.179704 /len=2902
Cluster Incl. AB006179:Homo sapiens mRNA for heparan-sulfate 6-
sulfotransferase, complete cds /cds=(111,1343) /gb=AB006179
/gi=3073774 /ug=Hs.132884 /len=2051
Cluster Incl. W27967:40b10 Homo sapiens cDNA /gb=W27967
/gi=1307915 /ug=Hs.136154 /len=755
Cluster Incl. D14822:Human chimeric mRNA derived from AML1
gene and MTG8(ETO) gene, partial sequence /cds=(0,597)
/gb=D14822 /gi=467498 /ug=Hs.31551 /len=799
Cluster Incl. AL079275:Homo sapiens mRNA full length insert cDNA
clone EUROIMAGE 566443 /cds=UNKNOWN /gb=AL079275
/gi=5102578 /ug=Hs.157078 /len=2082
Cluster Incl. AJ006288:Homo sapiens mRNA for bcl-10 protein
/cds=(690,1391) /gb=AJ006288 /gi=4049459 /ug=Hs.193516
/len=1877
Cluster Incl. J04739:Human bactericidal permeability increasing
protein (BPI) mRNA, complete cds /cds=(30,1493) /gb=J04739
/gi=179528 /ug=Hs.89535 /len=1813
Cluster Incl. AC004990:Homo sapiens PAC clone DJ1185I07 from
7q11.23-q21 /cds=(0,1766) /gb=AC004990 /gi=3924668
/ug=Hs.128653 /len=1767

Table 52. 24-gene signature of invasive prostate cancer
Description
Cluster Incl. AF089750:Homo sapiens flotillin-1 mRNA, complete cds
/cds=(164,1447) /gb=AF089750 /gi=3599572 /ug=Hs.179986 /len=1796
Cluster Incl. AL050306:Human DNA sequence from clone 475B7 on
chromosome Xq12.1-13. Contains the 3 part of the gene for a novel
KIAA0615 and KIAA0323 LIKE protein, the gene for a novel protein,
ESTs, STSs, GSSs and two putative CpG islands /cds=(48,2201)
/gb=AL050306 /gi=5419784 /ug=Hs.90625 /len=2395
Cluster Incl. U78310:Homo sapiens pescadillo mRNA, complete cds
/cds=(58,1824) /gb=U78310 /gi=2194202 /ug=Hs.13501 /len=2235
M13194 /FEATURE=mRNA /DEFINITION=HUMERCC1 Human
excision repair protein (ERCC1) mRNA, complete cds, clone pcDE
Cluster Incl. AI799802:wc43d09.x1 Homo sapiens cDNA, 3 end
/clone=IMAGE-2321393 /clone_end=3 /gb=AI799802 /gi=5365274
/ug=Hs.101516 /len=688
Cluster Incl. D86977:Human mRNA for KIAA0224 gene, complete cds
/cds=(136,3819) /gb=D86977 /gi=1504027 /ug=Hs.78054 /len=4226
Cluster Incl. AF068195:Homo sapiens putative glialblastoma cell
differentiation-related protein (GBDR1) mRNA, complete cds
/cds=(58,1062) /gb=AF068195 /gi=3192872 /ug=Hs.9194 /len=1493
Cluster Incl. AI986201:wr81a01.x1 Homo sapiens cDNA, 3 end
/clone=IMAGE-2494056 /clone_end=3 /gb=AI986201 /gi=5813478
/ug=Hs.66881 /len=814
Ras-Related Protein Rap1b
Cluster Incl. AF034102:Homo sapiens NBMPR-insensitive nucleoside
transporter ei (ENT2) mRNA, complete cds /cds=(237,1607)
/gb=AF034102 /gi=2811136 /ug=Hs.32951 /len=2522

40241_at	Cluster Incl. U09850:Human zinc finger protein (ZNF143) mRNA,
	complete cds /cds=(37,1917) /gb=U09850 /gi=495571 /ug=Hs.154095
	/len=3908
40975_s_at	Cluster Incl. AL050258:Novel human mRNA similar to mouse tuftelin-
	interacting protein 10 mRNA, AF097181 /cds=(263,2776)
	/gb=AL050258 /gi=4886426 /ug=Hs.20225 /len=3565
32149_at	Cluster Incl. AA532495;nj54a10.s1 Homo sapiens cDNA
•	/clone=IMAGE-996282 /gb=AA532495 /gi=2276749 /ug=Hs.183752
	/len=549
34059_at	Cluster Incl. AA586695:nn42h06.s1 Homo sapiens cDNA, 3 end
	/clone=IMAGE-1086587 /clone_end=3 /gb=AA586695 /gi=2397509
	/ug=Hs.193956 /len=522
1832_at	M62397 /FEATURE= /DEFINITION=HUMCRCMUT Human
	colorectal mutant cancer protein mRNA, complete cds
1321_s_at	U43916 /FEATURE= /DEFINITION=HSU43916 Human tumor-
	associated membrane protein homolog (TMP) mRNA, complete cds
35489_at	Cluster Incl. M82962:Human N-benzoyl-L-tyrosyl-p-amino-benzoic acid
	hydrolase alpha subunit (PPH alpha) mRNA, complete cds /cds=(9,2249)
	/gb=M82962 /gi=535474 /ug=Hs.179704 /len=2902
39912_at	Cluster Incl. AB006179:Homo sapiens mRNA for heparan-sulfate 6-
:	sulfotransferase, complete cds /cds=(111,1343) /gb=AB006179
	/gi=3073774 /ug=Hs.132884 /len=2051
31368_at	Cluster Incl. W27967:40b10 Homo sapiens cDNA /gb=W27967
,	/gi=1307915 /ug=Hs.136154 /len=755
35640_at	Cluster Incl. D14822:Human chimeric mRNA derived from AML1 gene
	and MTG8(ETO) gene, partial sequence /cds=(0,597) /gb=D14822
	/gi=467498 /ug=Hs.31551 /len=799
38198_at	Cluster Incl. AL079275:Homo sapiens mRNA full length insert cDNA
	clone EUROIMAGE 566443 /cds=UNKNOWN /gb=AL079275
	/gi=5102578 /ug=Hs.157078 /len=2082
L	<u>- Longo en la companya de  companya del companya de la companya d</u>

38871_at	Cluster Incl. AJ006288:Homo sapiens mRNA for bcl-10 protein
	/cds=(690,1391) /gb=AJ006288 /gi=4049459 /ug=Hs.193516 /len=1877
37054_at	Cluster Incl. J04739:Human bactericidal permeability increasing protein
	(BPI) mRNA, complete cds /cds=(30,1493) /gb=J04739 /gi=179528
	/ug=Hs.89535 /len=1813
34909_at	Cluster Incl. AC004990:Homo sapiens PAC clone DJ1185I07 from
	7q11.23-q21 /cds=(0,1766) /gb=AC004990 /gi=3924668 /ug=Hs.128653
	/len=1767

	Table 53. 22-gene-signature of invasive prostate cancer
Affymetrix	Description
Probe Set ID	
(U95Av2)	
40635_at	Cluster Incl. AF089750:Homo sapiens flotillin-1 mRNA, complete cds
	/cds=(164,1447) /gb=AF089750 /gi=3599572 /ug=Hs.179986 /len=1796
38260_at	Cluster Incl. AL050306:Human DNA sequence from clone 475B7 on
	chromosome Xq12.1-13. Contains the 3 part of the gene for a novel
<u> </u>	KIAA0615 and KIAA0323 LIKE protein, the gene for a novel protein,
	ESTs, STSs, GSSs and two putative CpG islands /cds=(48,2201)
j :	/gb=AL050306 /gi=5419784 /ug=Hs.90625 /len=2395
33833_at	Cluster Incl. J05243:Human nonerythroid alpha-spectrin (SPTAN1)
	mRNA, complete cds /cds=(102,7520) /gb=J05243 /gi=179105
	/ug=Hs.237180 /len=7787
38794_at	Cluster Incl. X53390:Human mRNA for upstream binding factor (hUBF)
	/cds=(147,2441) /gb=X53390 /gi=509240 /ug=Hs.89781 /len=3097
33915_at	Cluster Incl. W22655:71B9 Homo sapiens cDNA /clone=(not-
<u>.</u> 1	directional) /gb=W22655 /gi=1299488 /ug=Hs.26070 /len=761
39379_at	Cluster Incl. AL049397:Homo sapiens mRNA; cDNA DKFZp586C1019
,	(from clone DKFZp586C1019) /cds=UNKNOWN /gb=AL049397
	/gi=4500188 /ug=Hs.12314 /len=1720

1903_at	Ras-Related Protein Rap1b
39661_s_at	Cluster Incl. AF034102:Homo sapiens NBMPR-insensitive nucleoside
	transporter ei (ENT2) mRNA, complete cds /cds=(237,1607)
	/gb=AF034102 /gi=2811136 /ug=Hs.32951 /len=2522
40241_at	Cluster Incl. U09850:Human zinc finger protein (ZNF143) mRNA,
	complete cds /cds=(37,1917) /gb=U09850 /gi=495571 /ug=Hs.154095
·	/len=3908
40975_s_at	Cluster Incl. AL050258:Novel human mRNA similar to mouse tuftelin-
	interacting protein 10 mRNA, AF097181 /cds=(263,2776)
	/gb=AL050258 /gi=4886426 /ug=Hs.20225 /len=3565
32149_at	Cluster Incl. AA532495:nj54a10.s1 Homo sapiens cDNA
	/clone=IMAGE-996282 /gb=AA532495 /gi=2276749 /ug=Hs.183752
	/len=549
34059_at	Cluster Incl. AA586695:nn42h06.s1 Homo sapiens cDNA, 3 end
	/clone=IMAGE-1086587 /clone_end=3 /gb=AA586695 /gi=2397509
	/ug=Hs.193956 /len=522
1832_at	M62397 /FEATURE= /DEFINITION=HUMCRCMUT Human
	colorectal mutant cancer protein mRNA, complete cds
1321_s_at	U43916 /FEATURE= /DEFINITION=HSU43916 Human tumor-
	associated membrane protein homolog (TMP) mRNA, complete cds
35489_at	Cluster Incl. M82962:Human N-benzoyl-L-tyrosyl-p-amino-benzoic acid
	hydrolase alpha subunit (PPH alpha) mRNA, complete cds /cds=(9,2249)
	/gb=M82962 /gi=535474 /ug=Hs.179704 /len=2902
39912_at	Cluster Incl. AB006179:Homo sapiens mRNA for heparan-sulfate 6-
	sulfotransferase, complete cds /cds=(111,1343) /gb=AB006179
	/gi=3073774 /ug=Hs.132884 /len=2051
31368_at	Cluster Incl. W27967:40b10 Homo sapiens cDNA /gb=W27967
	/gi=1307915 /ug=Hs.136154 /len=755
L	

35640_at	Cluster Incl. D14822:Human chimeric mRNA derived from AML1 gene
	and MTG8(ETO) gene, partial sequence /cds=(0,597) /gb=D14822
	/gi=467498 /ug=Hs.31551 /len=799
38198_at	Cluster Incl. AL079275:Homo sapiens mRNA full length insert cDNA
	clone EUROIMAGE 566443 /cds=UNKNOWN /gb=AL079275
	/gi=5102578 /ug=Hs.157078 /len=2082
38871_at	Cluster Incl. AJ006288:Homo sapiens mRNA for bcl-10 protein
	/cds=(690,1391) /gb=AJ006288 /gi=4049459 /ug=Hs.193516 /len=1877
37054_at	Cluster Incl. J04739:Human bactericidal permeability increasing protein
	(BPI) mRNA, complete cds /cds=(30,1493) /gb=J04739 /gi=179528
	/ug=Hs.89535 /len=1813
34909_at	Cluster Incl. AC004990:Homo sapiens PAC clone DJ1185I07 from
	7q11.23-q21 /cds=(0,1766) /gb=AC004990 /gi=3924668 /ug=Hs.128653
	/len=1767

# EXAMPLE 8 – SELECTION OF THE GENE CLUSTERS DISCRIMINATING BETWEEN METASTATIC AND NON-METASTATIC HUMAN BREAST CANCER.

[00279] In this example we utilized gene expression data and associated clinical information published in the recent study on gene expression profiling of breast cancer (van't Veer, L.J., et al., "Gene expression profiling predicts clinical outcome of breast cancer," Nature, 415: 530-536, 2002, incorporated herein by reference). This study identifies 70 genes whose expression pattern is strongly predictive of a short post-diagnosis and treatment interval to distant metastases (van't Veer, L.J., et al.,2002). The expression pattern of these 70 genes discriminate with 81% (optimized sensitivity threshold) or 83% (optimal accuracy threshold) accuracy the patient's prognosis in the group of 78 young women diagnosed with sporadic lymph-node-negative breast cancer (this group comprises of 34 patients who developed distant metastases within 5 years and

44 patients who continued to be disease-free after a period of at least 5 years; they constitute a poor prognosis and good prognosis group, correspondingly). The authors described in this paper the second independent groups of breast cancer patients comprising 11 patients who developed distant metastases within 5 years and 8 patients who continued to be disease-free after a period of at least 5 years. We applied the method of the present invention to further reduce the number of genes whose expression patterns represent genetic signatures of breast cancer with "poor prognosis" or "good prognosis." In our example we utilized the data derived from a group of 19 patients as a training set of samples, and the data derived from a group of 78 patients as a test set of samples. [00280] Using the methods of present invention, we calculated the phenotype association indices for 19 samples of the training set and determined that this gene cluster exhibited a 84% success rate in clinical sample classification based on individual phenotype association indices (Table 54). As shown in Table 54, 7/8 (or 88%) of the good prognosis breast cancer samples had negative phenotype association indices, whereas 9/11 (or 82%) of poor prognosis breast cancer samples displayed negative phenotype association indices. Overall, 16 of 19 samples (or 84%) were correctly classified.

Table 54. Classification accuracy of the breast cancer prognosis predictor gene				
	clusters			
Cluster	r value	Good prognosis	Poor prognosis	Overall
70 genes		7/8 (88%)	9/11 (82%)	16/19 (84%)
19 genes	0.984	7/8 (88%)	9/11 (82%)	16/19 (84%)
19 genes	0.984	29/44 (66%)	28/34 (82%)	57/78 (73%)
9 genes	0.984	7/8 (88%)	10/11 (91%)	17/19 (89%)
9 genes	0.984	32/44 (73%)	28/34 (82%)	60/78 (77%)

22 genes	0.975	7/8 (88%)	10/11 (91%)	17/19 (89%)
22 genes	0.975	29/44 (66%)	29/34 (85%)	58/78 (74%)
12 genes	0.989	7/8 (88%)	10/11 (91%)	17/19 (89%)
12 genes	0.989	31/44 (70%)	28/34 (82%)	59/78 (76%)

[00281] Next, we identified two best-fit poor prognosis breast cancer samples displaying the correlation coefficient of 0.751 and 0.832 to the average expression profile of the 11 poor prognosis breast cancer samples. The average expression profile of the 11 poor prognosis breast cancer samples was utilized as a first reference set. The average expression profile of these two best-fit poor prognosis breast cancer samples was utilized as a second reference set.

[00282] The concordance set was obtained by selecting only those genes having a consistent direction of the differential expression in both the first and the second reference sets (i.e., greater gene expression difference in the poor prognosis *cf.* the good prognosis samples and greater gene expression in the best-fit tumor sample *cf.* the average expression value across the entire data set or *vice-versa*). The concordance set comprised of 44 genes (r = 0.950). A minimum segregation set was selected following the procedures described above. Scatter plots were generated of the log<sub>10</sub> transformed average -fold expression change in the first reference set and average –fold expression change in the second reference set (in case of a single best-fit tumor it was the log<sub>10</sub> transformed ratio of the expression value for a gene to the average expression value across the entire data set). For the samples of the first reference set, <expression><sub>1</sub> corresponds to the average expression value for gene x over all samples from patients who had invasive tumors and <expression><sub>2</sub> corresponds to the average expression value for gene x over all samples from patients

segregation set was identified by selecting a subset of the highly correlated genes between two reference sets from the concordance set. Using this approach we identified two gene clusters (19-gene cluster and 9-gene cluster) discriminating with high accuracy between poor prognosis and good prognosis human breast tumors in both training and test sets of clinical samples. These two breast cancer metastasis predictors or poor prognosis minimum segregation sets are listed in Tables 55 & 56. The classification performance for each of these gene clusters is presented in the Table 54.

Table 55. 19-gene signature of breast cancer prognosis predictor $(r = 0.984)$	
Gene ID (Chip identified in van't Veer, L.J., et al.,2002)	Sequence Name
Contig55725_RC	EST
NM_005915	МСМ6
Contig46218_RC	EST
NM_001809	CENPA
NM_016359	LOC51203
NM_002073	GNAZ
NM_014321	ORC6L
NM_016448	L2DTL
NM_002916	RFC4
NM_003875	GMPS
NM_014791	KIAA0175
Contig28552_RC	EST
NM_003981	PRC1
AL137718	DIAPH3
NM_000849	GSTM3
NM_003862	FGF18
NM_004994	MMP9
NM_003239	TGFB3

5.77		CECP1	
N	M_020974	CEGP1	
		1	

Table 56. 9-gene signature of breast cancer prognosis predictor $(r = 0.984)$	
Gene ID (Chip identified in van't Veer, L.J., et al.,2002)	Sequence Name
Contig55725_RC	EST
NM_005915	MCM6
Contig46218_RC	EST
NM_003875	GMPS
NM_000849	GSTM3
NM_003862	FGF18
NM_004994	MMP9
NM_003239	TGFB3
NM_020974	CEGP1

[00283] In the next example, the average expression profile of all 19 breast cancer samples obtained from 11 patients with poor prognosis and 8 patients with good prognosis was utilized as a first reference set. Next, we calculated the individual phenotype association indices and identified a single best-fit poor prognosis breast cancer sample displaying the correlation coefficient of 0.677 to the average expression profile of the 19 breast cancer samples. The average expression profile of this single best-fit poor prognosis breast cancer sample was utilized as a second reference set.

[00284] The concordance set was obtained by selecting only those genes having a consistent direction of the differential expression in both the first and the second reference sets (*i.e.*, greater gene expression difference in the poor prognosis *cf.* the good prognosis samples and greater gene expression in the best-fit tumor sample *cf.* the average expression value across the entire data set or *vice-versa*). The concordance set comprised of 47 genes (r=0.822). A minimum segregation set was selected following the

procedures described in the introduction to the Detailed Description of the Preferred Embodiments and the Materials & Methods sections. Scatter plots were generated of the log<sub>10</sub> transformed average -fold expression change in the first reference set and average fold expression change in the second reference set (in case of a single best-fit tumor it was the log<sub>10</sub> transformed ratio of the expression value for a gene to the average expression value across the entire data set). For the samples of the first reference set, <expression>1 corresponds to the average expression value for gene x over all samples from patients who had invasive tumors and <expression>2 corresponds to the average expression value for gene x over all samples from patients who had non-invasive tumors. A minimum segregation set was identified by selecting a subset of the highly correlated genes between two reference sets from the concordance set. Using this approach we identified two gene clusters (22-gene cluster and 12-gene cluster) discriminating with high accuracy between poor prognosis and good prognosis human breast tumors in both training and test sets of clinical samples. These two breast cancer metastasis predictors or poor prognosis minimum segregation sets are listed in Tables 57 & 58. The classification performance for each of these gene clusters is presented in the Table 54.

Table 57. 22-gene signature of breast cancer prognosis predictor $(r = 0.975)$	
Gene ID (Chip identified in van't Veer, L.J., et al.,2002) Sequence Nam	
NM_005915	MCM6
Contig46218_RC	EST
AA555029_RC	EST
NM_016359	LOC51203
Contig56457_RC	TMEFF1
NM_007036	ESM1
NM_007203	AKAP2

AF073519	SERF1A
NM_015984	UCH37
NM_014321	ORC6L
U82987	BBC3
Contig2399_RC	SM-20
NM_003882	WISP1
AB037863	KIAA1442
Contig63649_RC	EST
Contig20217_RC	EST
AF055033	IGFBP5
NM_003862	FGF18
NM_003239	TGFB3
NM_000849	GSTM3
NM_000599	IGFBP5
NM_020974	CEGP1

Table 58. 12-gene signature of breast cancer prognosis predictor $(r = 0.989)$	
Gene ID (Chip identified in van't Veer, L.J., et al.,2002)	Sequence Name
NM_005915	МСМ6
NM_007036	ESM1
NM_007203	AKAP2
AF073519	SERF1A
NM_015984	UCH37
NM_014321	ORC6L
AF055033	IGFBP5
NM_003862	FGF18
NM_003239	TGFB3
NM_000849	GSTM3
NM_000599	IGFBP5
NM_020974	CEGP1

### EXAMPLE 9. – SELECTION OF THE GENE CLUSTERS PREDICTING GOOD AND POOR PROGNOSIS OF HUMAN LUNG CARCINOMA.

We applied the methods of the present invention to identify gene expression [00285] profiles distinguishing lung adenocarcinoma samples from normal lung specimens as well as highly malignant phenotype of lung adenocarcinoma, associated with short survival after diagnosis and therapy, from less aggressive lung cancers, associated with longer patient's survival. Clinical data set utilized in this example was published (Bhattacharjee, A., Richards, W.G., Staunton, J., Li, C., Monti, S., Vasa, P., Ladd, C., Beheshti, J., Bueno, R., Gillette, M., Loda, M., Weber, G., Mark, E.J., Lander, E.S., Wong, W., Johnson, B.E., Golub, T.R., Sugarbaker, D.J., Meyerson, M. Classification of human lung carcinomas by mRNA expression profiling reveals distinct adenocarcinoma subclasses. PNAS, 98: 13790-13795, 2001; incorporated herein by reference). [00286] Using the clinical data set and associated clinical history (Bhattacharje et al., 2001), we selected two groups of adenocarcinoma patients having markedly distinct survival after diagnosis and therapy: poor prognosis group 1 comprising 34 patients with the median survival of 8.5 month (range 0.1-17.3 month) and good prognosis group 2 comprising 16 patients with the median survival of 84 month (range 75.4-106.1 month). As a starting point, we utilized a set of the 675 transcripts selected based on a statistical analysis of the quality of the dataset and variability of gene expression across the dataset (Bhattacharje et al., 2001). Applying methods of the present invention, we identified a set of 38 genes displaying at least a 2-fold difference in the average values of the mRNA expression levels between 34 poor prognosis samples versus 16 good prognosis samples (Table 59).

Table 59. 38 genes differentially regulated in human lung adenocarcinomas		
exhibiting poor and good clinical outcomes after the therapy.		
Affymetrix Probe Description		
Set ID (U95Av2)		
1665_s_at	Endothelial Cell Growth Factor 1	
38428_at	matrix metalloproteinase 1 (interstitial collagenase)	
40544_g_at	achaete-scute complex (Drosophila) homolog-like 1	
34898_at	amphiregulin (schwannoma-derived growth factor)	
1482_g_at	matrix metalloproteinase 12 (macrophage elastase)	
35175_f_at	eukaryotic translation elongation factor 1 alpha 2	
1481_at	matrix metalloproteinase 12 (macrophage elastase)	
38389_at	2',5'-oligoadenylate synthetase 1 (40-46 kD)	
40543_at	achaete-scute complex (Drosophila) homolog-like 1	
408_at	GRO1 oncogene (melanoma growth stimulating activity, alpha)	
40004_at	sine oculis homeobox (Drosophila) homolog 1	
35938_at	phospholipase A2, group IVA (cytosolic, calcium-dependent)	
37874_at	flavin containing monooxygenase 5	
33754_at	thyroid transcription factor 1	
38790_at	epoxide hydrolase 1, microsomal (xenobiotic)	
32275_at	secretory leukocyte protease inhibitor (antileukoproteinase)	
32081_at	citron (rho-interacting, serine/threonine kinase 21)	
32154_at	transcription factor AP-2 alpha (activating enhancer-binding protein	
	2 alpha)	
206_at	cathepsin E	
36623_at	Cluster Incl AB011406:Homo sapiens mRNA for alkalin	
	phosphatase, complete cds /cds=(176,1750) /gb=AB011406	
	/gi=3401944 /ug=Hs.75431 /len=2510	
37576_at	Purkinje cell protein 4	
37811_at	calcium channel, voltage-dependent, alpha 2/delta subunit 2	

39681_at	zinc finger protein 145 (Kruppel-like, expressed in promyelocytic
	leukemia)
1270_at	RAP1, GTPase activating protein 1
32570_at	hydroxyprostaglandin dehydrogenase 15-(NAD)
37600_at	extracellular matrix protein 1
31844_at	homogentisate 1,2-dioxygenase (homogentisate oxidase)
35834_at	alpha-2-glycoprotein 1, zinc
36681_at	apolipoprotein D
37430_at	arachidonate 15-lipoxygenase, second type
36680_at	amylase, alpha 2B; pancreatic
40031_at	aldehyde dehydrogenase 3
38773_at	carbonyl reductase 1
765_s_at	lectin, galactoside-binding, soluble, 4 (galectin 4)
37209_g_at	phosphoserine phosphatase-like
36736_f_at	phosphoserine phosphatase
41069_at	chondromodulin I precursor
37208_at	phosphoserine phosphatase-like

[00287] Next, we calculated the phenotype association indices for all 50 samples and determined that this gene cluster exhibited a 72% success rate in clinical sample classification based on individual phenotype association indices (Table 60). As shown in Table 60, 12/16 (or 75%) of the lung adenocarcinoma samples of the good prognosis group had negative phenotype association indices, whereas 24/34 (or 71%) of lung adenocarcinoma specimens of the poor prognosis group displayed positive phenotype association indices. Overall, 36 of 50 samples (or 72%) were correctly classified.

Table 60. Classification accuracy of lung adenocarcinoma prognosis predictor										
	clusters									
Cluster r value Poor prognosis Good Prognosis Overall										

38 genes	0.771	24/34 (71%)	12/16 (75%)	36/50 (72%)
26 genes	0.938	13/34 (38%)	15/16 (94%)	28/50 (56%)
15 genes	0.942	28/34 (82%)	11/16 (69%)	39/50 (78%)

[00288] Next, we identified 8 best-fit poor prognosis samples displaying the correlation coefficient of 0.3 or higher to the average expression profile of the 34 poor prognosis samples. We calculated the average expression profile for these 8 best-fit poor prognosis samples by dividing the average expression value for each gene in the 8 samples of the best-fir set by the average expression value across the entire data set. [00289] Next, we selected from an initial set of 38 genes a set of 26 genes (lung adenocarcinoma poor prognosis predictor cluster 1 – see Table 61) displaying high positive correlation (r = 0.938) between the best-fit tumors and poor prognosis samples data sets. This gene cluster exhibited a 56% success rate in clinical sample classification based on individual phenotype association indices (Table 60). As shown in Table 60, 15/16 (or 94%) of the lung adenocarcinoma samples of the good prognosis group had negative phenotype association indices, whereas 13/34 of lung adenocarcinoma specimens of the poor prognosis group displayed positive phenotype association indices. Overall, 28 of 50 samples (or 56%) were correctly classified.

Table 61. 26 genes of the lung adenocarcinoma poor prognosis predictor cluster 1.

Affymetrix Probe Set ID (U95Av2)

Description

Endothelial Cell Growth Factor 1

38428\_at matrix metalloproteinase 1 (interstitial collagenase)

40544\_g\_at achaete-scute complex (Drosophila) homolog-like 1

1482\_g\_at matrix metalloproteinase 12 (macrophage elastase)

1481\_at matrix metalloproteinase 12 (macrophage elastase)

2',5'-oligoadenylate synthetase 1 (40-46 kD)  40543_at achaete-scute complex (Drosophila) homolog-like 1  408_at GRO1 oncogene (melanoma growth stimulating activity, alpha)  35938_at phospholipase A2, group IVA (cytosolic, calcium-dependent)  37874_at flavin containing monooxygenase 5  33754_at thyroid transcription factor 1  38790_at epoxide hydrolase 1, microsomal (xenobiotic)  32275_at secretory leukocyte protease inhibitor (antileukoproteinase)  32081_at citron (rho-interacting, serine/threonine kinase 21)  206_at cathepsin E
GRO1 oncogene (melanoma growth stimulating activity, alpha)  35938_at phospholipase A2, group IVA (cytosolic, calcium-dependent)  37874_at flavin containing monooxygenase 5  33754_at thyroid transcription factor 1  38790_at epoxide hydrolase 1, microsomal (xenobiotic)  32275_at secretory leukocyte protease inhibitor (antileukoproteinase)  32081_at citron (rho-interacting, serine/threonine kinase 21)
phospholipase A2, group IVA (cytosolic, calcium-dependent)  flavin containing monooxygenase 5  thyroid transcription factor 1  epoxide hydrolase 1, microsomal (xenobiotic)  secretory leukocyte protease inhibitor (antileukoproteinase)  citron (rho-interacting, serine/threonine kinase 21)
37874_at flavin containing monooxygenase 5  33754_at thyroid transcription factor 1  38790_at epoxide hydrolase 1, microsomal (xenobiotic)  32275_at secretory leukocyte protease inhibitor (antileukoproteinase)  32081_at citron (rho-interacting, serine/threonine kinase 21)
thyroid transcription factor 1  series 1  series 1  thyroid transcription factor 1  epoxide hydrolase 1, microsomal (xenobiotic)  secretory leukocyte protease inhibitor (antileukoproteinase)  citron (rho-interacting, serine/threonine kinase 21)
38790_at epoxide hydrolase 1, microsomal (xenobiotic)  32275_at secretory leukocyte protease inhibitor (antileukoproteinase)  32081_at citron (rho-interacting, serine/threonine kinase 21)
32275_at secretory leukocyte protease inhibitor (antileukoproteinase) 32081_at citron (rho-interacting, serine/threonine kinase 21)
32081_at citron (rho-interacting, serine/threonine kinase 21)
L
206_at cathepsin E
36623_at Cluster Incl AB011406:Homo sapiens mRNA for alkalin
phosphatase, complete cds /cds=(176,1750) /gb=AB011406
/gi=3401944 /ug=Hs.75431 /len=2510
37576_at Purkinje cell protein 4
37811_at calcium channel, voltage-dependent, alpha 2/delta subunit 2
32570_at hydroxyprostaglandin dehydrogenase 15-(NAD)
37600_at extracellular matrix protein 1
31844_at homogentisate 1,2-dioxygenase (homogentisate oxidase)
36681_at apolipoprotein D
36680_at amylase, alpha 2B; pancreatic
38773_at carbonyl reductase 1
37209_g_at phosphoserine phosphatase-like
36736_f_at phosphoserine phosphatase

[00290] To improve the classification accuracy, we selected from an initial set of 38 genes a set of 15 genes (lung adenocarcinoma poor prognosis predictor cluster 2 - see Table 62) displaying high positive correlation (r = 0.942) between the best-fit tumors and poor prognosis samples data sets.

Affymetrix	Description
Probe Set ID	
(U95Av2)	•
1665_s_at	Endothelial Cell Growth Factor 1
38428_at	matrix metalloproteinase 1 (interstitial collagenase)
40544_g_at	achaete-scute complex (Drosophila) homolog-like 1
1482_g_at	matrix metalloproteinase 12 (macrophage elastase)
1481_at	matrix metalloproteinase 12 (macrophage elastase)
38389_at	2',5'-oligoadenylate synthetase 1 (40-46 kD)
40543_at	achaete-scute complex (Drosophila) homolog-like 1
408_at	GRO1 oncogene (melanoma growth stimulating activity, alpha)
35938_at	phospholipase A2, group IVA (cytosolic, calcium-dependent)
39681_at	zinc finger protein 145 (Kruppel-like, expressed in promyelocytic
	leukemia)
35834_at	alpha-2-glycoprotein 1, zinc
40031_at	aldehyde dehydrogenase 3
765_s_at	lectin, galactoside-binding, soluble, 4 (galectin 4)
41069_at	chondromodulin I precursor
37208_at	phosphoserine phosphatase-like

[00291] This gene cluster exhibited a 78% success rate in clinical sample classification based on individual phenotype association indices (Table 60). As shown in Table 60, 11/16 (or 69%) of the lung adenocarcinoma samples of the good prognosis group had negative phenotype association indices, whereas 28/34 (or 82%) of lung adenocarcinoma specimens of the poor prognosis group displayed positive phenotype association indices. Overall, 39 of 50 samples (or 78%) were correctly classified.

## EXAMPLE 10 – SELECTION OF THE GENE CLUSTERS ASSOCIATED WITH METASTATIC CANCER.

[00292] The methods of the present invention were used along with the data reported by Ramaswamy et al. (2003) to identify gene clusters distinguishing between the human primary adenocarcinomas of diverse origin and metastatic adenocarcinoma lesions. These data were the supplemental data reported in Ramaswamy, S., Ross, K.N., Lander, E.S., Golub, T.R. "A molecular signature of metastasis in primary solid tumors," Nature Genetics, January 2003, 33: 49-54, incorporated herein by reference. Ramaswamy et al. (2003) identified the 17-gene cluster expression profile of which distinguishes 12 metastatic adenocarcinoma nodules of diverse origin and 64 human primary adenocarcinomas of diverse origin (lung, breast, prostate, colorectal, uterus, ovary). Both metastatic lesions and primary adenocarcinomas were representing the same diverse spectrum of tumor types obtained from different individuals (Ramaswamy et al., 2003).

[00293] The expression profile of the 17-gene cluster in metastatic versus primary

[00294] Next, we calculated the phenotype association indices for all 76 samples and determined that this gene cluster exhibited a 45% success rate in clinical sample classification based on individual phenotype association indices (Table 63). As shown in Table 63, 12/12 (or 100%) of the metastatic samples had positive phenotype association indices, whereas 22/64 (or 34%) of primary tumor samples displayed negative phenotype association indices. Overall, 34 of 76 samples (or 45%) were correctly classified.

tumors was utilized as a first reference set.

Tal	Table 63. Classification accuracy of the metastases segregation gene clusters											
			(r :	= 0.00	0 discrim	ination	thresh	old)				
			Primary tumors									
Cluster	r	Breast	Colon	Lung	Prostate	Uterus	Ovary	Primary	Metastases	Overall		
	value		İ					tumors				
17	0.964	2 of	4 of	3 of	8 of 10	5 of 10	0 of	22/64	12/12	34/76		
genes		11	11	11			11	(34%)	(100%)	(45%)		
12	0.991	3 of	5 of	0 of	8 of 10	6 of 10	0 of	22/64	12/12	34/76		
genes		11	11	11			11	(34%)	(100%)	(45%)		
11	0.992	8 of	6 of	6 of	4 of 10	6 of 10	2 of	32/64	12/12	44/76		
genes		11	11	11			11	(50%)	(100%)	(58%)		
8 genes	0.989	3 of	7 of	1 of	8 of 10	6 of 10	1 of	26/64	12/12	38/76		
		11	11	11			11	(41%)	(100%)	(50%)		
7 genes	0.993	7 of	6 of	7 of	6 of 10	7 of 10	2 of	35/64	12/12	47/76		
		11	11	11		<u> </u>	11	(55%)	(100%)	(62%)		

[00295] The classification accuracy of the 17-gene cluster was much improved when the discrimination threshold was set at the level of 0.400 of a correlation coefficient. As shown in Table 64, 12/12 (or 100%) of the metastatic samples had phenotype association indices higher than 0.400, whereas 48/64 (or 75%) of primary tumor samples displayed phenotype association indices lower than 0.400. Overall, 60 of 76 samples (or 79%) were correctly classified.

Table 64. Classification accuracy of the metastases segregation gene clusters (r = 0.400 discrimination threshold)											
Primary tumors											
Cluster	r	Breast	Colon	Lung	Prostate	Uterus	Ovary	Primary	Metastases	Overall	
	value							tumors			
17	0.964	9 of	7 of	8 of	8 of 10	8 of 10	8 of	48/64	12/12	60/76	
genes		11	11	11			11	(75%)	(100%)	(79%)	

12	0.991	10 of	7 of	7 of	8 of 10	8 of 10	3 of	43/64	12/12	55/76
genes		11	11	11			11	(67%)	(100%)	(72%)
11	0.992	11 of	7 of	8 of	8 of 10	8 of 10	8 of	50/64	12/12	62/76
genes		11	11	11			11	(78%)	(100%)	(82%)
8 genes	0.989	8 of	7 of	7 of	8 of 10	7 of 10	5 of	42/64	12/12	54/76
		11	11	11			11 .	(66%)	(100%)	(71%)
7 genes	0.993	11 of	7 of	8 of	8 of 10	7 of 10	7 of	49/64	12/12	61/76
		11	11	11			11	(77%)	(100%)	(80%)

[00296] Next, we identified three best-fit metastatic samples displaying the correlation coefficient of 0.870, 0.923, and 0.874 to the average expression profile of the 12 metastatic samples. The average expression profile of these three best-fit metastatic samples was utilized as a second reference set.

[00297] The expression profile of the best-fit samples was utilized to refine the gene-expression signature associated with a metastatic phenotype to a small set of transcripts that would exhibit high discrimination accuracy between metastatic lesions and primary tumors. Thus, selecting a subset of the highly correlated genes between two reference sets identified a minimum segregation set suitable for clinical samples classification. Using this approach we identified four gene clusters discriminating with high accuracy between metastatic lesions and primary tumors. The members of these metastases minimum segregation sets (metastases minimum segregation gene clusters) are listed in Tables 65-68. The classification performance for each of these gene clusters is presented in the Tables 63 and 64.

Table 65. 12-gene signature of metastase						
	Affymetrix Probe ID (U95Av2)					
J034	164_s_at					

L37747_s_at
RC_AA430032_at
X85372_at
RC_AA608850_at
HG110-HT110_s_at
Z74615_at
U23946_at
D43968_at
U48959_at
D17408_s_at
D00654_at

Affymetrix Probe ID (U95Av2)
J03464_s_at
L37747_s_at
RC_AA430032_at
X85372_at
RC_AA608850_at
HG110-HT110_s_at
Z74615_at
U23946_at
D43968_at
M83664_at
AF001548_rna1_at

Table 67. 8-gene signature of metast	ases
Affymetrix Probe ID (U95Av2)	
J03464_s_at	
L37747_s_at	

RC_AA430032_at	
U23946_at	
D43968_at	
U48959_at	
D17408_s_at	
D00654_at	

Table 68. 7-gene signature of metastases Gene ID (Chip identified in van't Veer	
L37747_s_at	
RC_AA430032_at	
U23946_at	
D43968_at	
M83664_at	
AF001548_rna1_at	

### REFERENCES

- Fidler, I.J. The nude mouse model for studies of human cancer metastasis.
   In: V. Schirrmacher and R. Schwartz-Abliez (eds.). pp. 11-17. Berlin: Springer-Verlag, 1989.
- Fidler, I.J. Critical factors in the biology of human cancer metastasis.
   Cancer Res., 50, 6130-6138, 1990.
- 3. Fidler, I.J., Naito, S., Pathak, S. Orhtotopic implantation is essential for the selection, growth and metastasis of human renal cell cancer in nude mice.

  Cancer Metastasis Rev., 9, 149-165, 1990.

- 4. Giavazzi, R., Campbell, D.E., Jessup, J.M., Cleary, K., and Fidler, I.J. Metastatic behavior of tumor cells isolated from primary and metastatic human colorectal carcinomas implanted into different sites in nude mice. Cancer Res., 46: 1928-1948, 1986.
- 5. Naito, S., von Eschenbach, A.C., Giavazzi, R., and Fidler, I.J. Growth and metastasis of tumor cells isolated from a renal cell carcinoma implanted into different organs of nude mice. Cancer Res., 46: 4109-4115, 1986.
- 6. McLemore, T.L., et al. Novel intrapulmonary model for orthotopic propagation of human lung cancer in athymic nude mice. Cancer Res., 47: 5132-5140, 1987.
- 7. Fu, X., Herrera, H., and Hoffman, R.M. Orthotopic growth and metastasis of human prostate carcinoma in nude mice after transplantation of histologically intact tissue. Int. J.Cancer, 52: 987-990, 1992.
- 8. Stephenson, R.A., Dinney, C.P.N., Gohji, K., Ordonez, N.G., Killion, J.J., and Fidler, I.J. Metastatic model for human prostate cancer using orthotopic implantation in nude mice. J. Natl. Cancer Inst., 84: 951-957, 1992.
- 9. Pettaway, C.A., Stephenson, R.A., and Fidler, I.J. Development of orthotopic models of metastatic human prostate cancer. Cancer Bull. (Houst.), 45: 424-429, 1993.
- 10. An, Z., Wang, X., Geller, J., Moossa, A.R., and Hoffman, R.M. Surgical orthotopic implantation allows high lung and lymph node metastasis expression of human prostate carcinoma cell line PC-3 in nude mice. The Prostate, 34: 169-174, 1998.

- 11. Wang, X., An, Z., Geller, J., and Hoffman, R.M. High-malignancy orthotopic mouse model of human prostate cancer LNCaP. The Prostate, 39: 182-186, 1999.
- 12. Yang, M., Jiang, P., Sun, F.-X., Hasegawa, S., Baranov, E., Chishima, T., Shimada, H., Moosa, A.R., and Hofman, R.M. A fluorescent orthotopic bone metastasis model of human prostate cancer. Cancer Res., 59: 781-786, 1999.
- 13. Morikawa, K., Walker, S.M., Jessup, J.M., Cleary, K., and Fidler, I.J. In vivo selection of highly metastatic cells from surgical specimens of different primary human colon carcinoma implanted in nude mice. Cancer Res., 48: 1943-1948, 1988.
- 14. Dinney, C.P.N. et al. Isolation and characterization of metastatic variants from human transitional cell carcinoma passaged by orthotopic implantation in athymic nude mice. J. Urol., 154: 1532-1538, 1995.
- 15. Pettaway, C.A., Pathak, S., Greene, G., Ramirez, E., Wilson, M.R., Killion, J.J., and Fidler, I.J. Selection of highly metastatic variants of different human prostatic carcinomas using orthotopic implantation in nude mice. Clinical Cancer Res., 2: 1627-1636, 1996.
- 16. Greene, G.F., Kitadai, Y., Pettaway, C.A., von Eschenbach, A.C., Bucana, C.D., Fidler, I.J. Correlation of metastasis-related gene expression with metastatic potential in human prostate carcinoma cells implanted in nude mice using an in situ messenger RNA hybridization technique. American J. Pathology, 150: 1571-1582, 1997.

- 17. Glinsky, G. V. and Glinsky, V. V. Apoptosis and metastasis: a superior resistance of metastatic cancer cells to programmed cell death. Cancer Lett. *101*:43-51, 1996.
- 18. Glinsky, G. V., Price, J. E., Glinsky, V. V., Mossine, V. V., Kiriakova, G. and Metcalf, J. B. Inhibition of human breast cancer metastasis in nude mice by synthetic glycoamines. Cancer Res. *56*:5319-24, 1996.
- 19. Glinsky, G. V., Glinsky, V. V., Ivanova, A. B. and Hueser, C. J. Apoptosis and metastasis: increased apoptosis resistance of metastatic cancer cells is associated with the profound deficiency of apoptosis execution mechanisms.

  Cancer Lett. 115:185-93, 1997.
- 20. Lockhart, D. J., Dong, H., Byrne, M. C., Follettie, M. T., Gallo, M. V., Chee, M. S., Mittmann, M., Wang, C., Kobayashi, M., Horton, H. and Brown, E. L. Expression monitoring by hybridization to high-density oligonucleotide arrays [see comments]. Nat. Biotechnol., *14*:1675-80, 1996.
- 21. Singh, D., Febbo, P.G., Ross, K., Jackson, D.G., Manola, C.L., Tamayo, P., Renshaw, A.A., D'Amico, A.V., Richie, J.P., Lander, E.S., Loda, M., Kantoff, P.W., Golub, T.R., Sellers, W.R. Gene expression correlates of clinical prostate cancer behavior. Cancer Cell, 1: 203-209, 2002.
- 22. Gorgani, N.N., Smith, B.A., Kono, D.H., Theofilopoulos, A.N. Histidinerich glycoprotein binds DNA and Fc□RI and potentiates the ingestion of apoptotic cells by macrophages. J. Immunol., 169: 4745-4751, 2002.
- 23. Machtens, S., Serth, J., Bokemeyer, C., Bathke, W., Minssen, A., Kollmannsberger, C., Hartmann, J., Knuchel, R., Kondo, M., Jonas, U., Kuczyk,

- M. Expression of the p53 and Maspin protein in primary prostate cancer: correlation with clinical features. Int J Cancer, 95: 337-342, 2001.
- 24. Zou, Z., Zhang, W., Young, D., Gleave, M.G., Rennie, P., Connell, T., Connelly, R., Moul, J., Srivastava, S., Sesterhenn, I. Maspin expression profile in human prostate cancer (CaP) and in vitro induction of Maspin expression by androgen ablation. Clin Cancer Res, 8: 1172-1177, 2002.
- 25. Bussemakers, MJ, Van Bokhoven, A, Tomita, K, Jansen, CF, Schalken, JA. Complex cadherin expression in human prostate cancer cells. Int. J. Cancer, 85: 446-450, 2000.
- 26. Tomita, K, Van Bokhoven, A, Van Leenders, GJ, Ruijter, ET, Jansen, CF, Bussemakers, MJ, Schalken, JA. Cadherin switching in human prostate cancer progression. Cancer Res., 60: 3650-3654, 2000.
- 27. Mills L, Tellez C, Huang S, Baker C, McCarty M, Green L, Gudas JM, Feng X, Bar-Eli M. Fully human antibodies to MCAM/MUC18 inhibit tumor growth and metastasis of human melanoma. Cancer Res., 62:5106-5114, 2002.
- 28. Johnson JP, Bar-Eli M, Jansen B, Markhof E. Melanoma progression-associated glycoprotein MUC18/MCAM mediates homotypic cell adhesion through interaction with a heterophilic ligand. Int J Cancer, 73:769-774, 1997.
- 29. Van Kempen LC, van den Oord JJ, Van Muijen GN, Weidle UH, Bloemers HP, Swart GW. Activated leukocyte cell adhesion molecule/CD 166, a marker of tumor progression in primary malignant melanoma of the skin. Am J Pathol., 156:769-774, 2000.

- 30. Degen WG, Van Kempen LC, Gijzen EG, Van Groningen JJ, Can Kooyk Y, Bloemers HO, Swart GW. MEMD, a new cell adhesion molecule in metastasizing human melanoma cell lines, is identical to ALCAM (activated leukocyte cell adhesion molecule). Am J Pathol., 152:805-813, 1998.
- 31. Swart GW. Activated leukocyte cell adhesion molecule (CD166/ALCAM): developmental and mechanistic aspects of cell clustering and cell migration. Eur J Cell Biol., 81:313-321, 2002.
- 32. Ohneda O, Ohneda K, Arai F, Lee J, Miyamoto T, Fukushima Y, Dowbenko D, Lasky LA, Suda T. ALCAM (CD166): its role in hematopoietic and endothelial development. Blood, 98:2134-2142, 2001.
- 33. Bowen MA, Patel DD, Li X, Modrell B, Malacko AR, Wang WC, Marquardt H, Neubauer M, Pesando JM, Francke U, et al. Cloning, mapping, and characterization of activated leukocyte-cell adhesion molecule (ALCAM), a CD6 ligand. J Exp Med., 181:2213-2220, 1995.
- 34. Bardin N, Anfossa F, Masse JM, Cramer E, Sabatier F, Le Bivic A, Sampol J, Dignat-George F. Identification of CD146 as a component of the endothelial junction involved in the control of cell-cell cohesion. Blood, 98:3677-3736, 2001.
- 35. Pickl WF, Majdic O, Fischer GF, Petzelbauer P, Fae I, Waclavicek M, Stockl J, Scheinecker C, Vidicki T, Aschauer H, Johnson JP, Knapp W. MUC18/MCAM (CD146), an activation antigen of human T lymphocytes. J Immunol., 158:2107-2115, 1997.

- 36. Arai F, Ohneda O, Miyamoto T, Zhang XQ, Suda T. Mesenchymal stem cells in perichondrium express activated leukocyte cell adhesion molecule and participate in bone marrow formation. J Exp Med., 195:1549-1563, 2002.
- 37. Seshi B, Kumar S, Sellers D. Human bone marrow stromal cell: coexpression of markers specific for multiple mesenchymal cell lineages. Blood Cells Mol Dis., 26:234-246, 2000.
- 38. Guo Z, Yang J, Liu X, Li X, Hou C, Tang PH, Mao N. Biological features of mesenchymal stem cells from human bone marrow. Chin Med J (Engl), 114:950-953, 2001.
- 39. Bruder SP, Ricalton NS, Boynton RE, Connolly TJ, Jaiswal N, Zaia J, Barry FP. Mesenchymal stem cell surface antigen SB-10 corresponds to activated leukocyte cell adhesion molecule and is involved in osteogenic differentiation. J Bone Miner Res., 13:655-663, 1998.
- 40. Léon C. L. T. van Kempen, Judith M. D. T. Nelissen, Winfried G. J. Degen, Ruurd Torensma, Ulrich H. Weidle, Henri P. J. Bloemers, Carl G. Figdor, and Guido W. M. Molecular Basis for the Homophilic Activated Leukocyte Cell Adhesion Molecule (ALCAM)-ALCAM Interaction. J. Biol. Chem., 276: 25783-25790, 2001.
- 41. Wu GJ, Wu MW, Wang SW, Liu Z, Qu P, Peng Q, Yang H, Varma VA, Sun QC, Petros JA, Lim SD, Amin MB. Isolation and characterization of the major-form of h uman MUC18 cDNA gene and correlation of MUC18 over-expression in prostate cancer cell lines and tissues with malignant progression.

  Gene, 279:17-31, 2001.

- 42. Wu GJ, Varma VA, Wu MW, Wang SW, Qu P, Yang H, Petros JA, Lim SD, Amin MB. Expression of a human cell adhesion molecule, MUC18, in prostate cancer cell lines and tissues. Prostate, 48:305-315, 2001.
- 43. Ramaswamy, S., Ross, K.N., Lander, E.S., Golub, T.R. A molecular signature of metastasis in primary solid tumors. Nature Genetics, 33: 49-54, 2003.
- 44. LaTulippe, E., Satagopan, J., Smith, A., Scher, H., Scardino, P., Reuter, V., Gerald, W.L. Comprehensive gene expression analysis of prostate cancer reveals distinct transcriptional programs associated with metastatic disease.

  Cancer Res., 62: 4499-4506, 2002.

### EXAMPLE 11 – USE OF EXPRESSION DATA WITH OTHER METRICS TO PREDICT PROSTATE CANCER PATIENT SURVIVAL

#### Introduction

[00298] Critical clinical need in development of reliable prognostic markers suitable for stratification of prostate cancer patients is clearly demonstrated by the results of a recent randomized study of the therapeutic efficacy of surgery versus watch and wait strategy demonstrating only modest 6.6% absolute reduction in mortality after prostatectomy compared to observation, despite the association of surgery with a 50% reduction in hazard ration of death from prostate cancer (1). It appears that a measurable clinical benefit of surgery is limited to poorly defined sub-population of prostate cancer patients. Therefore, an improved ability to identify a sub-group of prostate cancer patients who would benefit from therapy should have a significant immediate positive clinical and socio-economic impact.

[00299] Widely used biochemical, histopathological, and clinical criteria such as PSA level, Gleason score, the clinical tumor stage and molecular genetic approaches assaying

loss of tumor suppressors or gain of oncogenes (2) had only limited success with respect to prostate cancer patients stratification and demonstrated a significant variability in predictive value among different clinical laboratories and hospitals. Furthermore, best existing markers cannot reliably identify at the time of diagnosis a poor prognosis group of prostate cancer patients that ultimately would fail therapy (3). Classification nomograms that incorporate measurements of several individual pre- and postoperative parameters are generally recognized as most efficient clinically useful models currently available for prediction of the probability of relapse-free survival after therapy of individual prostate cancer patients (4-7). However, one of the significant deficiencies of these classification systems is that they have only limited utility in predicting the differences in outcomes readily observed between patients diagnosed with prostate cancers exhibiting similar clinical, histopathological, and biochemical features.

Therefore, a critical clinical need exists to improve the classification accuracy of prostate

[00300] Expression profiling of prostate tumor samples using oligonucleotide or cDNA microarray technology revealed gene expression signatures associated with human prostate cancer (8-19), including potential prostate cancer prognosis markers (9, 14, 16, 17). However, one of the major limitations of these studies was that the same clinical data set was utilized for both signature discovery and validation. Furthermore, usually only a single or few hits were validated using independent methods and independent clinical data sets, thus diminishing the potential advantage of the use of a panel of markers over a single marker in diagnostic and/or prognostic applications.

cancer patients with respect to clinical outcome after therapy.

[00301] Here we applied a microarray-based gene expression profiling approach to identify molecular signatures distinguishing sub-groups of patients with differing outcome and develop a stratification algorithm demonstrating high discrimination accuracy between sub-groups of prostate cancer patients with distinct clinical outcome after therapy in a training set of 21 prostate cancer patients. To validate a potential clinical utility of discovered genetic signatures, we confirmed the discrimination power of proposed prostate cancer prognosis stratification algorithm using an independent set of 79 clinical tumor samples.

[00302] Our data indicate that identified molecular signatures provide the bases for developing clinical prognostic tests suitable for stratification of prostate cancer patients at the time of diagnosis with respect to likelihood of negative or positive clinical outcome after therapy. Our results provide experimental evidence of a transcriptional resemblance between metastatic human prostate carcinoma xenografts in nude mice and primary prostate tumors from patients subsequently developing relapse after therapy. These data suggest that genetically defined metastasis-promoting features of primary tumors are one of the major contributing factors of aggressive clinical behavior and unfavorable prognosis in prostate cancer patients.

## Materials and Methods

[00303] Clinical Samples. We utilized in our experiments two independent sets of clinical samples for signature discovery (training outcome set of 21 samples) and validation (validation outcome set of 79 samples). Original gene expression profiles of the training set of 21 clinical samples analyzed in this study were recently reported (14). Primary gene expression data files of clinical samples as well as associated clinical

information were provided by Dr. W. Sellers and can be found at <a href="http://www-genome.wi.mit.edu/cancer/">http://www-genome.wi.mit.edu/cancer/</a>.

[00304] Prostate tumor tissues comprising validation data set were obtained from 79 prostate cancer patients undergoing therapeutic or diagnostic procedures performed as part routine clinical management at MSKCC. Clinical and pathological features of 79 prostate cancer cases comprising validation outcome set are presented in the Table 70. Median follow-up after therapy in this cohort of patients was 70 months. Samples were snap-frozen in liquid nitrogen and stored at – 80°C. Each sample was examined histologically using H&E-stained cryostat sections. Care was taken to remove nonneoplastic tissues from tumor samples. Cells of interest were manually dissected from the frozen block, trimming away other tissues. All of the studies were conducted under MSKCC Institutional Review Board-approved protocols.

[00305] Cell Culture. Cell lines used in this study were previously described (19). The LNCap- and PC-3-derived cell lines were developed by consecutive serial orthotopic implantation, either from metastases to the lymph node (for the LN series), or reimplanted from the prostate (Pro series). This procedure generated cell variants with differing tumorigenicity, frequency and latency of regional lymph node metastasis (19). Except where noted, cell lines were grown in RPMI1640 supplemented with 10% FBS and gentamycin (Gibco BRL) to 70-80% confluence and subjected to serum starvation as described (19), or maintained in fresh complete media, supplemented with 10% FBS.

[00306] Orthotopic Xenografts. Orthotopic xenografts of human prostate PC-3 cells and sublines used in this study were developed by surgical orthotopic implantation as previously described (19). Briefly, 2 x 10<sup>6</sup> cultured PC3 cells, PC3M or PC3MLN4

sublines were injected subcutaneously into male athymic mice, and allowed to develop into firm palpable and visible tumors over the course of 2 - 4 weeks. Intact tissue was harvested from a single subcutaneous tumor and surgically implanted in the ventral lateral lobes of the prostate gland in a series of six athymic mice per cell line subtype. The mice were examined periodically for suprapubic masses, which appeared for all subline cell types, in the order PC3MLN4 >PC3M>>PC3. Tumor-bearing mice were sacrificed by  $CO_2$  inhalation over dry ice and necropsy was carried out in a  $2-4^{\circ}C$  cold room. Typically, bilaterally symmetric prostate gland tumors in the shape of greatly distended prostate glands were apparent. Prostate tumor tissue was excised and snap frozen in liquid nitrogen. The elapsed time from sacrifice to snap freezing was < 5 min. A systematic gross and microscopic post mortem examination was carried out.

[00307] Tissue Processing for mRNA and RNA Isolation. Fresh frozen orthotopic tumor was examined by use of hematoxylin and eosin stained frozen sections. Orthotopic tumors of all sublines exhibited similar morphology consisting of sheets of monotonous closely packed tumor cells with little evidence of differentiation interrupted by only occasional zones of largely stromal components, vascular lakes, or lymphocytic infiltrates. Fragments of tumor judged free of these non-epithelial clusters were used for mRNA preparation. Frozen tissue (1 - 3 mm x 1 - 3 mm) was submerged in liquid nitrogen in a ceramic mortar and ground to powder. The frozen tissue powder was dissolved and immediately processed for mRNA isolation using a Fast Tract kit for mRNA extraction (Invitrogen, Carlsbad, CA, see above) according to the manufacturers instructions.

[00308] RNA and mRNA Extraction. For gene expression analysis, cells were harvested in lysis buffer 2 hrs after the last media change at 70-80% confluence and total RNA or mRNA was extracted using the RNeasy (Qiagen, Chatsworth, CA) or FastTract kits (Invitrogen, Carlsbad, CA). Cell lines were not split more than 5 times prior to RNA extraction, except where noted.

[00309] Affymetrix Arrays. The protocol for mRNA quality control and gene expression analysis was that recommended by Affymetrix (<a href="http://www.affymetrix.com">http://www.affymetrix.com</a>). In brief, approximately one microgram of mRNA was reverse transcribed with an oligo(dT) primer that has a T7 RNA polymerase promoter at the 5' end. Second strand synthesis was followed by cRNA production incorporating a biotinylated base. Hybridization to Affymetrix U95Av2 arrays representing 12,625 transcripts overnight for 16 h was followed by washing and labeling using a fluorescently labeled antibody. The arrays were read and data processed using Affymetrix equipment and software as reported previously (18, 19).

[00310] Data Analysis. Detailed protocols for data analysis and documentation of the sensitivity, reproducibility and other aspects of the quantitative statistical microarray analysis using Affymetrix technology have been reported (18, 19). 40-50% of the surveyed genes were called present by the Affymetrix Microarray Suite 5.0 software in these experiments. The concordance analysis of differential gene expression across the data sets was performed using Affymetrix MicroDB v. 3.0 and DMT v.3.0 software as described earlier (18, 19). We processed the microarray data using the Affymetrix Microarray Suite v.5.0 software and performed statistical analysis of expression data set using the Affymetrix MicroDB and Affymetrix DMT software. This analysis identified a

set of 218 genes (91 up-regulated and 127 down-regulated transcripts) differentially regulated in tumors from patients with recurrent versus non-recurrent prostate cancer at the statistically significant level (p<0.05) defined by both T-test and Mann-Whitney test (Table 69). The concordance analysis of differential gene expression across the clinical and experimental data sets was performed using Affymetrix MicroDB v. 3.0 and DMT v.3.0 software as described earlier (19). The Pearson correlation coefficient for individual test samples and appropriate reference standard was determined using the Microsoft Excel software as described in the signature discovery protocol.

[00311] Survival Analysis. The Kaplan-Meier survival analysis was carried out using the Prism 4.0 software. Statistical significance of the difference between the survival curves for different groups of patients was assessed using Chi square and Logrank tests.

[00312] Discovery and validation of the prostate cancer recurrence predictor algorithm. According to the present invention, clinically relevant genetic signatures can be found by searching for clusters of co-regulated genes that display highly concordant transcript abundance behavior across multiple experimental models and clinical settings that model or represent malignant phenotypes of interest (Glinsky, G.V., Krones-Herzig, A., Glinskii, A.B., Gebauer, G. Microarray analysis of xenograft-derived cancer cell lines representing multiple experimental models of human prostate cancer. Molecular Carcinogenesis, 37: 209-221, 2003; Example 5, *supra*; Glinsky, G.V., Krones-Herzig, A., Glinskii, A.B. Malignancy-associated regions of transcriptional activation: gene expression profiling identifies common chromosomal regions of a recurrent transcriptional activation in human prostate, breast, ovarian, and colon cancers.

Neoplasia, 5: 21-228; Glinsky, G.V., Ivanova, Y.A., Glinskii, A.B. Common malignancy-

associated regions of transcriptional activation (MARTA) in human prostate, breast, ovarian, and colon cancers are targets for DNA amplification. Cancer Letters, in press, 2003). Thus, a primary criterion in selecting genes for inclusion within the cluster is the concordance of changes in expression rather than a magnitude of changes (e.g., fold change). Accordingly, transcripts of interest are expected to have a tightly controlled "rank order" of expression within a cluster of co-regulated genes reflecting a balance of up- and down-regulation as a desired regulatory end-point in a cell. A degree of resemblance of the transcript abundance rank order within a gene cluster between a test sample and reference standard is measured by a Pearson correlation coefficient and designated as a phenotype association index (PAI), as described fully in the introduction of the Detailed Description of Preferred Embodiments section. To identify genes with consistently concordant expression patterns across multiple data sets and various experimental conditions, we compared the expression profile of 218 genes (test samples) to the expression profiles of transcripts differentially regulated in multiple experimental models (reference standard) of human prostate cancer (Glinsky, G.V., Krones-Herzig, A., Glinskii, A.B., Gebauer, G. Microarray analysis of xenograft-derived cancer cell lines representing multiple experimental models of human prostate cancer. Molecular Carcinogenesis, 37: 209-221, 2003).

[00313] The transcripts comprising each signature were selected based on Pearson correlation coefficients (r > 0.95) reflecting a degree of similarity of expression profiles in clinical tumor samples (recurrent versus non-recurrent tumors) and experimental samples using the following protocol.

[00314] Step 1. Sets of differentially regulated transcripts were independently identified for each experimental conditions (see below) and clinical samples using the Affymetrix microarray processing and statistical analysis software package as described in this examples's Materials and Methods section.

[00315] Step 2. Sub-sets of transcripts exhibiting concordant expression changes in clinical and experimental samples were identified using the Affymetrix MicroDB and DMT software. Sub-sets of transcripts were identified with concordant changes of transcript abundance behavior in recurrent versus non-recurrent clinical tumor samples (218 transcripts) and experimental conditions independently defined for each signature (Signature 1: PC-3MLN4 orthotopic versus s.c. xenografts; Signature 2: PC-3MLN4 versus PC-3M & PC-3 orthotopic xenografts; Signature 3: PC-3/LNCap consensus class, Glinsky, G.V., Krones-Herzig, A., Glinskii, A.B., Gebauer, G. Microarray analysis of xenograft-derived cancer cell lines representing multiple experimental models of human prostate cancer. Molecular Carcinogenesis, 37: 209-221, 2003). Thus, from a set of 218 transcripts three concordant sub-sets of transcripts were identified corresponding to each binary comparison of clinical and experimental samples.

[00316] Step 3. Small gene clusters were selected as sub-sets of genes exhibiting concordant changes of transcript abundance behavior in recurrent versus non-recurrent clinical tumor samples (218 transcripts) and experimental conditions defined for each signature (Signature 1: PC-3MLN4 orthotopic versus s.c. xenografts; Signature 2: PC-3MLN4 versus PC-3M & PC-3 orthotopic xenografts; Signature 3: PC-3/LNCap consensus class, Glinsky, G.V., Krones-Herzig, A., Glinskii, A.B., Gebauer, G. Microarray analysis of xenograft-derived cancer cell lines representing multiple

experimental models of human prostate cancer. Molecular Carcinogenesis, 37: 209-221, 2003). Expression profiles were presented as log10 average fold changes for each transcript and processed for visualization and Pearson correlation analysis using Microsoft Excel software. The cut-off criterion for cluster formation was set to exceed a Pearson correlation coefficient 0.95 among the log10 transformed average expression values in the compared groups.

(training data set) by comparing the expression profiles of individual samples to the reference expression profiles of relevant experimental samples for each signature and an "average" expression profile of recurrent versus non-recurrent tumors. As explained above, we named the corresponding correlation coefficients calculated for individual samples the phenotype association indices (PAIs). We evaluated the prognostic power of identified clusters of co-regulated transcripts based on their ability to segregate the patients with recurrent and non-recurrent prostate tumors into distinct subgroups and selected a single best performing cluster for each binary condition (Figure 57; Tables 69 & 70).

[00318] Step 5. We used Kaplan-Meier survival analysis to assess the prognostic power of each best-performing cluster in predicting the probability that patients would remain disease-free after therapy (Figure 58-62). We selected the prognosis

discrimination cut-off value for each signature based on highest level of statistical significance in patient's stratification into poor and good prognosis groups as determined by the log-rank test (lowest P value and highest hazard ratio; Table 70 & Figures 58-62). Clinical samples having the Pearson correlation coefficient at or higher than the cut-off value were identified as having the poor prognosis signature. Clinical samples with the Pearson correlation coefficient lower the cut-off value were identified as having the good prognosis signature.

[00319] Step 6. We developed a prostate cancer recurrence predictor algorithm taking into account calls from all three individual signatures. We selected the common prognosis discrimination cut-off value for all three signatures based on highest level of statistical significance in patient's stratification into poor and good prognosis groups as determined by Kaplan-Meier survival analysis (lowest P value and highest hazard ratio defined by the log-rank test; Table 70 & Figure 58-62). Clinical samples having the Pearson correlation coefficient at or higher the cut-off value defined by at least two signatures were identified as having the poor prognosis signature. Clinical samples with the Pearson correlation coefficient lower than the cut-off value defined by at least two signatures were identified as having the good prognosis signature. We found that the cut-off value of PAIs > 0.2 scored in two of three individual clusters allowed to achieve the 90% recurrence prediction accuracy (Table 70).

[00320] Step 7. We validated the prognostic power of prostate cancer recurrence predictor algorithm alone and in combination with the established markers of outcome using an independent clinical set of 79 prostate cancer patients (Figures 58-6269 & 71).

## Results

[00321] Identification of molecular signatures distinguishing sub-groups of prostate cancer patients with distinct clinical outcomes after therapy. To identify the outcome predictor signatures, we utilized as a training data set the expression analysis of 12,625 transcripts in 21 prostate tumor samples obtained from prostate cancer patients with distinct clinical outcomes after therapy. Using biochemical evidence of relapse after therapy as a criterion of treatment failure, 21 patients were divided into two sub-groups, representing prostate cancer with recurrent (8 patients) and non-recurrent (13 patients) clinical behavior (14). We processed the original U95Av2 GeneChip CEL files using the Affymetrix Microarray Suite 5.0 software and performed statistical analysis of expression data set using the Affymetrix MicroDB and Affymetrix DMT software. This analysis identified a set of 218 genes (91 up-regulated and 127 down-regulated transcripts) differentially regulated in tumors from patients with recurrent versus non-recurrent prostate cancer at the statistically significant level (p<0.05) defined by both T-test and Mann-Whitney test (Table 70).

[00322] To reduce the number of hits in potential outcome predictor clusters and identify transcripts of potential biological relevance, we compared the expression profile of 218 genes to the expression profiles of transcripts differentially regulated in multiple experimental models of human prostate cancer (Glinsky, G.V., Krones-Herzig, A., Glinskii, A.B., Gebauer, G. Microarray analysis of xenograft-derived cancer cell lines representing multiple experimental models of human prostate cancer. Molecular Carcinogenesis, 37: 209-221, 2003, and Example 5, *supra*) in search for genes with consistently concordant expression patterns across multiple data sets and various experimental conditions. We identified several small gene clusters exhibiting highly

concordant pattern of expression (Pearson correlation coefficient, r > 0.95) in clinical and experimental samples. We evaluated the prognostic power of each identified cluster of co-regulated transcripts based on ability to segregate the patients with recurrent and nonrecurrent prostate tumors into distinct sub-groups. To assess a potential prognostic relevance of individual gene clusters, we calculated a Pearson correlation coefficient for each of 21 tumor samples by comparing the expression profiles of individual samples to the "average" expression profile of recurrent versus non-recurrent tumors and expression profiles of relevant experimental samples (Table 69 and Figure 57). Based on expected correlation of expression profiles of identified gene clusters with recurrent clinical behavior of prostate cancer, we named the corresponding correlation coefficients calculated for individual samples the phenotype association indices (PAIs). [00323] Using this strategy we identified several gene clusters (Tables 69 & 70) discriminating with 86-95% accuracy human prostate tumors exhibiting recurrent or nonrecurrent clinical behavior (Figure 57 and Tables 69 & 70). The transcripts comprising each signature in Table 69 were selected based on Pearson correlation coefficients (r > 0.95) reflecting a degree of similarity of expression profiles in clinical tumor samples (recurrent versus non-recurrent tumors) and experimental samples. Selection of transcripts was performed from sets of genes exhibiting concordant changes of transcript abundance behavior in recurrent versus non-recurrent clinical tumor samples (218 transcripts) and experimental conditions independently defined for each signature (Signature 1: PC-3MLN4 orthotopic versus s.c. xenografts; Signature 2: PC-3MLN4 versus PC-3M & PC-3 orthotopic xenografts; Signature 3: PC-3/LNCap consensus class, Glinsky, G.V., Krones-Herzig, A., Glinskii, A.B., Gebauer, G. Microarray analysis of

xenograft-derived cancer cell lines representing multiple experimental models of human prostate cancer. Molecular Carcinogenesis, 37: 209-221, 2003, and Example 5, *supra*). The expression profiles were presented as log10 average fold changes for each transcript.

Table 69. G	ene expression signatures associated with re	ecurrent pros	tate cancer.			
Signature 1						
LocusLink	Gene Name	GenBank	UniGene			
Name		ID	ID			
MGC5466	Hypothetical protein MGC5466	U90904	Hs.83724			
Wnt5A	proto-oncogene Wnt5A	L20861	Hs.152213			
KIAA0476	KIAA0476 protein	AB007945	Hs.6684			
ITPR1	inositol 1,4,5-trisphosphate receptor, type	D26070	Hs.198443			
TCF2	transcription factor 2, hepatic	X58840	Hs.169853			
Signature 2						
Gene	Gene Name	GenBank	UniGene			
		ID	ID			
MGC5466	Hypothetical protein MGC5466	U90904	Hs.83724			
CHAF1A	Chromatin assembly factor 1, subunit A	U20979	Hs.79018			
CDS2	CDP-diacylglycerol synthase 2	Y16521	Hs.24812			
IER3	Immediate early response 3	S81914	Hs.76090			
Signature 3						
LocusLink	Gene Name	GenBank	UniGene			
Name		ID	ID			
PPFIA3	Protein tyrosine phosphatase, receptor	AB014554	Hs.109299			
	type, f polypeptide					
COPEB	Core promoter element binding protein	AF001461	Hs.285313			
FOS	V-fos oncogene homolog	V01512	Hs.25647			
JUNB	Jun B proto-oncogene	X51345	Hs.400124			
ZFP36	zinc finger protein 36, C3H type	M92843	Hs.343586			

[00324] Table 70 illustrates data from 21 prostate cancer patients who provided tumor samples comprising a signature discovery (training) data set that were classified according to whether they had a good-prognosis signature or poor-prognosis signature based on PAI values defined by either individual recurrence predictor signatures or a recurrence predictor algorithm that takes into account calls from all three signatures. The number of correct predictions in the poor-prognosis and good-prognosis groups is shown as a fraction of patients with the observed clinical outcome after therapy (8 patients developed relapse and 13 patients remained disease-free). Correlation coefficients reflect a degree of similarity of expression profiles in clinical tumor samples (recurrent versus non-recurrent tumors) and experimental samples (Signature 1: PC-3MLN4 orthotopic versus s.c. xenografts; Signature 2: PC-3MLN4 versus PC-3M & PC-3 orthotopic xenografts; Signature 3: PC-3/LNCap consensus class, Glinsky, G.V., Krones-Herzig, A., Glinskii, A.B., Gebauer, G. Microarray analysis of xenograft-derived cancer cell lines representing multiple experimental models of human prostate cancer. Molecular Carcinogenesis, 37: 209-221, 2003; and Example 5, supra). P values were calculated with use of the log-rank test and reflect the statistically significant difference in the probability that patients would remain disease-free between poor-prognosis and good-prognosis subgroups.

Table 70. Prostate cancer recurrence prediction accuracy in a good-prognosis and a poorprognosis sub-group of patients defined according to whether they had a good-prognosis or a poor-prognosis signature. P value Recurrence Correlation Recurrent Non-recurrent Overall coefficient signature cancer cancer r = 0.983100% (8 of 8) 92% (12 of 13) 95% (20 of < 0.0001 Signature 1 21)

Signature 2	r = 0.963	88% (7 of 8)	92% (12 of 13)	90% (19 of	< 0.0001
				21)	
Signature 3	r = 0.996	75% (6 of 8)	92% (12 of 13)	86% (18 of	0.001
		, ,		21)	
Algorithm	NA	88 % (7 of 8)	92% (12 of 13)	90% (19 of	< 0.0001
				21)	

[00325] Figure 57 illustrates application of the five-gene cluster (Table 69, signature 1) to characterize clinical prostate cancer samples according to their propensity for recurrence after therapy. The expression pattern of the genes in the recurrence predictor cluster was analyzed in each of twenty-one separate clinical samples. The analysis produces a quantitative phenotype association index (plotted on the Y-axis) for each of the twenty-one clinical prostate cancer samples. Tumors that are likely to recur are expected to have positive phenotype association indices reflecting positive correlation of gene expression with metastasis-promoting orthotopic xenografts, while those that are unlikely to recur are expected to have negative association indices.

[00326] The figure shows the phenotype association indices for eight samples from patients who later had recurrence as bars 1 through 8, while the association indices for thirteen samples from patients whose tumors did not recur is shown as bars 11 through 23. Eight of the eight samples (or 100%) from patients who later experienced recurrence had positive phenotype association indices and so were properly classified. Twelve of the thirteen samples (or 92.3%) from patients whose tumors did not recur had negative phenotype association indices and so were properly classified as non-recurrent tumors. Thus, overall, twenty of the twenty-one samples (or 95.2%) were properly classified

using a five-gene recurrence predictor signature. Two alternative clusters identified using this strategy showed similar sample classification performance (Tables 69 & 70).

[00327] To further evaluate the prognostic power of the identified gene expression signatures, we performed Kaplan-Meier survival analysis using as a clinical end-point disease-free interval ("DFI") after therapy in prostate cancer patients with positive and negative PAIs. The Kaplan-Meier survival curves showed a highly significant difference in the probability that prostate cancer patients would remain disease-free after therapy between the groups with positive and negative PAIs defined by the signatures (Figures 58A-C), suggesting that patients with positive PAIs exhibit a poor outcome signature whereas patients with negative PAIs manifest a good outcome signature. The estimated hazard ration for disease recurrence after therapy in the group of patients with positive PAIs as compared with the group of patients with negative PAIs defined by the recurrence predictor signature 3 (Table 69) was 9.046 (Fig. 58 C)(95% confidence interval of ratio, 3.022 to 76.41; P = 0.001). 86% of patients with the positive PAIs had a disease recurrence within 5 years after therapy, whereas 85% of patients with the negative PAIs remained relapse-free at least 5 years (Figure 58C). Based on this analysis, we identified the group of prostate cancer patients with positive PAIs as a poor prognosis group and the group of prostate cancer patients with negative PAIs as a good prognosis group.

[00328] Theoretically, the recurrence predictor algorithm based on a combination of signatures should be more robust than a single predictor signature, particularly during the validation analysis using an independent test cohort of patients. Next we analyzed whether a combination of the three signatures would perform in the patient's

classification test with similar accuracy as the individual signatures. We found that the cut-off value of PAIs > 0.2 scored in two of three individual clusters allowed to achieve the 90% recurrence prediction accuracy (Table 70). This recurrence predictor algorithm correctly identified 88% of patients with recurrent and 92% of patients with non-recurrent disease (Table 70). The Kaplan-Meier survival analysis (Figure 58D) showed that the median relapse-free survival after therapy of patients in the poor prognosis group was 26 months. All patients in the poor prognosis group had a disease recurrence within 5 years after therapy, whereas 92% of patients in the good prognosis group remained relapse-free at least 5 years. The estimated hazard ration for disease recurrence after therapy in the poor prognosis group of patients as compared with the good prognosis group of patients defined by the recurrence predictor algorithm was 20.32 (95% confidence interval of ratio, 6.047 to 158.1; P < 0.0001).

[00329] Validation of the outcome predictor signatures using independent clinical data set. To validate the potential clinical utility of identified molecular signatures, we evaluated the prognostic power of signatures applied to an independent set of 79 clinical samples obtained from 37 prostate cancer patients who developed recurrence after the therapy and 42 patients who remained disease-free. The Kaplan-Meier survival analysis demonstrated that all three recurrence predictor signatures (Table 69) segregate prostate cancer patients into sub-groups with statistically significant differences in the probability of remaining relapse-free after therapy (Table 71). Interestingly, application of the recurrence predictor algorithm (requiring a cut-off value of PAIs > 0.2 scored in two of three individual clusters) appears to perform better than individual signatures in patient's stratification test using an independent data set (Table 71).

[00330] Table 71 summarizes classification of 79 prostate cancer patients who provided tumor samples. These samples comprise a signature validation (test) data set and were classified according to whether they had a good-prognosis signature or poor-prognosis signature based on PAI values defined by either individual recurrence predictor signatures or recurrence predictor algorithm that takes into account calls from all three signatures. Kaplan-Meier analysis was performed to evaluate the probability that patients would remain disease free according to whether they had a poor-prognosis or a good-prognosis signature and determine the proportion of patients who would remain disease-free at least 5 years after therapy in a poor-prognosis and a good-prognosis sub-groups. Hazard ratios, 95% confidence intervals, and P values were calculated with use of the log-rank test.

Table 71. Stratification of 79 prostate cancer patients into poor and good prognosis groups at					
time of diagnosis based on recurrence predictor signatures.					
Recurrence	Poor	Good	Hazard	95 % Confidence	P value
signature	prognosis,	prognosis,	ratio	interval of ratio	
	5-year	5-year			
	survival	survival			
Signature 1	41 %	78 %	2.858	1.405 to 5.143	0.0028
Signature 2	44 %	79 %	3.473	1.584 to 5.806	0.0008
Signature 3	41 %	76 %	3.351	1.810 to 6.907	0.0002
Algorithm	33 %	76 %	4.224	2.455 to 9.781	< 0.0001

[00331] Kaplan-Meier survival analysis (Figure 59A) showed that the median relapsefree survival after therapy of patients classified within the poor prognosis group (defined by the recurrence predictor algorithm) was 34.6 months. 67 % of patients in the poor prognosis group had a disease recurrence within 5 years after therapy, whereas 76 % of patients in the good prognosis group remained relapse-free at least 5 years. The estimated hazard ration for disease recurrence after therapy in the poor prognosis group as compared with the good prognosis group of patients defined by the recurrence predictor algorithm was 4.224 (95% confidence interval of ratio, 2.455 to 9.781; P < 0.0001). Overall, the application of the recurrence predictor algorithm allowed accurate stratification into poor prognosis group 82 % of patients who failed the therapy within one year after prostatectomy. The recurrence predictor algorithm seems to demonstrate more accurate performance in patient's classification compared to the conventional markers of outcome such as preoperative PSA level or RP Gleason sum (Figures 59-60 and Table 72).

[00332] Recurrence predictor signatures provide additional predictive value over conventional markers of outcome. Next we determined that application of the recurrence predictor signatures provides additional predictive value when combined with conventional markers of outcome such as preoperative PSA level and Gleason score.

Both preoperative PSA level and RP Gleason sum were significant predictors of prostate cancer recurrence after therapy in the validation cohort of 79 patients (Figures 59D and 60C).

[00333] Kaplan-Meier survival analysis (Figure 59D) showed that the median relapse-free survival after therapy of patients in the poor prognosis group defined by the high preoperative PSA level was 49.0 months. 60 % of patients in the poor prognosis group had a disease recurrence within 5 years after therapy, whereas 73 % of patients in the good prognosis group remained relapse-free at least 5 years. The estimated hazard ration for disease recurrence after therapy in the poor prognosis group as compared with the

good prognosis group of patients defined by the preoperative PSA level was 2.551 (95% confidence interval of ratio, 1.344 to 4.895; P = 0.0043). However, prediction of the outcome after therapy based on preoperative PSA level accurately stratified into the poor prognosis group only 65 % of patients who failed the therapy within one year after prostatectomy (Table 72).

[00334] Table 72 shows the number of correct predictions in poor-prognosis and good-prognosis groups as a fraction of patients with the observed clinical outcome after therapy (37 patients developed relapse and 42 patients remained disease-free). PSA and Gleason sum cut-off values for segregation of poor-prognosis and good-prognosis subgroups were defined to achieve the most accurate and statistically significant recurrence prediction in this cohort of patients. Multiparameter nomogram-based prognosis predictor was defined as described in this example's Materials & Methods using 50% relapse-free survival probability as a cut-off for patient's stratification into poor and good prognosis subgroups.

Table 72. Prostate cancer recurrence prediction accuracy in poor-prognosis and good-prognosis sub-groups of patients defined by a gene expression-based recurrence predictor algorithm alone or in combination with established biochemical and histopathological markers of outcome.

Recurrence	Recurrent	Non-recurrent	Year one	Overall
predictor	cancer	cancer	recurrence	
Recurrence	68% (25 of 37)	81% (34 of 42)	82% (14 of 17)	75% (59 of
Algorithm				79)
PSA	68% (25 of 37)	67% (28 of 42)	65% (11 of 17)	67% (53 of
	{			79)
PSA & Algorithm	84% (31 of 37)	71% (30 of 42)	88% (15 of 17)	77% (61 of
				79)

RP Gleason sum	38% (14 of 37)	90% (38 of 42)	47% (8 of 17)	66% (52 of
				79)
RP Gleason sum &	68% (25 of 37)	81% (34 of 42)	82% (14 of 17)	75% (59 of
Algorithm			}	79)
PSA & RP Gleason	81% (30 of 37)	67% (28 of 42)	82% (14 of 17)	73% (58 of
				79)
Nomogram	62% (23 of 37)	79% (33 of 42)	71% (12 of 17)	71% (56 of
				79)
Nomogram &	68% (25 of 37)	81% (34 of 42)	82% (14 of 17)	75% (59 of
Algorithm				79)

[00335] We next determined that application of the recurrence predictor algorithm identifies sub-groups of patients with distinct clinical outcome after therapy in both high and low PSA-expressing groups, thus adding additional predictive value to the therapy outcome classification based on preoperative PSA level alone.

[00336] In the group of patients with high preoperative PSA level (Figure 59B), the median relapse-free survival after therapy of patients in the poor prognosis sub-group defined by the recurrence predictor algorithm was 36.2 months. 73 % of patients in the poor prognosis sub-group had a disease recurrence within 5 years after therapy.

Conversely, 73 % of patients in the good prognosis sub-group remained relapse-free at least 5 years. The estimated hazard ration for disease recurrence after therapy in the poor prognosis sub-group as compared with the good prognosis sub-group of patients defined by the recurrence predictor algorithm was 4.315 (95% confidence interval of ratio, 1.338 to 7.025; P = 0.0081).

[00337] In the group of patients with low preoperative PSA level (Figure 59C), the median relapse-free survival after therapy of patients in the poor prognosis sub-group

defined by the recurrence predictor algorithm was 42.0 months. 53 % of patients in the poor prognosis sub-group had a disease recurrence within 5 years after therapy, whereas 92 % of patients in the good prognosis sub-group remained relapse-free at least 5 years. The estimated hazard ration for disease recurrence after therapy in the poor prognosis sub-group as compared with the good prognosis sub-group of patients defined by the recurrence predictor algorithm was 6.247 (95% confidence interval of ratio, 2.134 to 24.48; P = 0.0015). Overall, combining information from the recurrence predictor algorithm with preoperative PSA level measurement allowed 88 % of patients who failed the therapy within one year after prostatectomy to be accurately classified within the poor prognosis group (Table 72).

[00338] Radical prostatectomy ("RP") Gleason sum is a significant predictor of relapse-free survival in the validation cohort of 79 prostate cancer patients (Figure 60C). Kaplan-Meier survival analysis (Figure 60C) demonstrated that the median relapse-free survival after therapy of patients with the RP Gleason sum 8 & 9 was 21.0 months, thus defining the poor prognosis group based on histopathological criteria. 74 % of patients in the poor prognosis group had a disease recurrence within 5 years after therapy, whereas 69 % of patients in the good prognosis group (RP Gleason sum 6 & 7) remained relapse-free at least 5 years. The estimated hazard ration for disease recurrence after therapy in the poor prognosis group as compared with the good prognosis group of patients defined by the RP Gleason sum criteria was 3.335 (95% confidence interval of ratio, 2.389 to 13.70; P < 0.0001). RP Gleason sum-based outcome classification accurately stratified into poor prognosis group only 47 % of patients who failed the therapy within one year after prostatectomy (Table 72).

[00339] In the group of patients with RP Gleason sum 6 & 7 (Figure 60A), the median relapse-free survival after therapy of patients in the poor prognosis sub-group defined by the recurrence predictor algorithm was 61.0 months. 53 % of patients in the poor prognosis sub-group had a disease recurrence within 5 years after therapy, whereas 77 % of patients in the good prognosis sub-group remained relapse-free at least 5 years. The estimated hazard ration for disease recurrence after therapy in the poor prognosis sub-group as compared with the good prognosis sub-group of patients defined by the recurrence predictor algorithm was 3.024 (95% confidence interval of ratio, 1.457 to 8.671; P = 0.0055).

[00340] In the group of patients with RP Gleason sum 8 & 9 (Figure 60B), the median relapse-free survival after therapy in the poor prognosis sub-group defined by the recurrence predictor algorithm was 11.5 months. 100 % of patients in the poor prognosis sub-group had a disease recurrence within 5 years after therapy, whereas 67 % of patients in the good prognosis sub-group remained relapse-free at least 5 years. The estimated hazard ration for disease recurrence after therapy in the poor prognosis sub-group as compared with the good prognosis sub-group of patients defined by the recurrence predictor algorithm was 6.143 (95% confidence interval of ratio, 1.573 to 13.49; P = 0.0053). Overall, patient's classification using a combination of the recurrence predictor algorithm and RP Gleason sum allowed 82 % of patients who failed the therapy within one year after prostatectomy to be accurately classified as members of the poor prognosis group (Table 72). Based on this analysis we concluded that application of the recurrence predictor algorithm provides an additional predictive value to the therapy outcome classification based on established markers of outcome.

[00341] Recurrence predictor signatures provide additional predictive value over outcome prediction based on multiparameter nomogram. Classification nomograms are generally recognized most efficient clinically useful models currently available for prediction of the probability of relapse-free survival after therapy of individual prostate cancer patients (Kattan M. W., Eastham J. A., Stapleton A. M., Wheeler T. M., Scardino P. T. A preoperative nomogram for disease recurrence following radical prostatectomy for prostate cancer. J. Natl. Cancer Inst., 90: 766-771, 1998; D'Amico A. V., Whittington R., Malkowicz S. B., Fondurulia J., Chen M-H, Kaplan I., Beard C. J., Tomaszewski J. E., Renshaw A. A., Wein A., Coleman C. N. Pretreatment nomogram for prostatespecific antigen recurrence after radical prostatectomy or external-beam radiation therapy for clinically localised prostate cancer. J. Clin. Oncol., 17: 168-172, 1999; Graefen M., Noldus J., Pichlmeier A., Haese P., Hammerer S., Fernandez S., Conrad R., Henke E., Huland E., Huland H. Early prostate-specific antigen relapse after radical retropubic prostatectomy: prediction on the basis of preoperative and postoperative tumor characteristics. Eur. Urol., 36: 21-30, 1999; Kattan M. W., Wheeler T. M., Scardino P. T. Postoperative nomogram for disease recurrence after radical prostatectomy for prostate cancer. J. Clin. Oncol., 17: 1499-1507, 1999.). We applied the Kattan nomogram utilizing multiple postoperative parameters (Kattan, et al. (1999)) for prognosis prediction classification in the test group of 79 prostate cancer patients.

[00342] Kaplan-Meier survival analysis (Figure 61A) showed that the median relapsefree survival after therapy of patients in the poor prognosis group defined by the Kattan nomogram was 33.1 months. 72 % of patients in the poor prognosis group had a disease recurrence within 5 years after therapy, whereas 81 % of patients in the good prognosis group remained relapse-free at least 5 years. The estimated hazard ration for disease recurrence after therapy in the poor prognosis group as compared with the good prognosis group of patients defined by the Kattan nomogram was 3.757 (95% confidence interval of ratio, 2.318 to 9.647; P < 0.0001). Prediction of the outcome after therapy based on Kattan nomogram accurately stratified into poor prognosis group 71 % of patients who failed the therapy within one year after prostatectomy (Table 72).

[00343] Application of the recurrence predictor algorithm identified sub-groups of patients with distinct clinical outcome after therapy in both poor and good prognosis groups defined by the Kattan nomogram, thus adding additional predictive value to the therapy outcome classification based on nomogram alone.

[00344] In the poor prognosis group of patients defined by the Kattan nomogram the application of the recurrence predictor algorithm appears to identify two sub-groups of patients with statistically significant difference in the probability to remain relapse-free after therapy (Figure 61B). Median relapse-free survival after therapy of patients in the poor prognosis sub-group defined by the recurrence predictor algorithm was 11.5 months compared to median relapse-free survival of 71.1 months in the good prognosis sub-group (Figure 61B). 89 % of patients in the poor prognosis sub-group had a disease recurrence within 5 years after therapy. Conversely, 50 % of patients in the good prognosis sub-group remained relapse-free at least 5 years. The estimated hazard ration for disease recurrence after therapy in the poor prognosis sub-group as compared with the good prognosis sub-group of patients defined by the recurrence predictor algorithm was 3.129 (95% confidence interval of ratio, 1.378 to 7.434; P = 0.0068).

application of the Kattan nomogram, the recurrence predictor algorithm seems to define two sub-groups of patients with statistically significant difference in the probability to remain relapse-free after therapy (Figure 61C). Median relapse-free survival after therapy of patients in the poor prognosis sub-group defined by the recurrence predictor algorithm was 64.8 months. 41 % of patients in the poor prognosis sub-group had a disease recurrence within 5 years after therapy. Conversely, 87 % of patients in the good prognosis sub-group remained relapse-free at least 5 years. The estimated hazard ration for disease recurrence after therapy in the poor prognosis sub-group as compared with the good prognosis sub-group of patients defined by the recurrence predictor algorithm was 4.398 (95% confidence interval of ratio, 1.767 to 18.00; P = 0.0035). Overall, combination of the recurrence predictor algorithm and Kattan nomogram allowed accurate stratification into poor prognosis group 82 % of patients who failed the therapy within one year after prostatectomy (Table 72).

[00346] Recurrence predictor algorithm defines poor and good prognosis sub-groups of patients diagnosed with the early stage prostate cancer. Identification of sub-groups of patients with distinct clinical outcome after therapy would be particularly desirable in a cohort of patients diagnosed with the early stage prostate cancer. Next we determined that recurrence predictor signatures are useful in defining sub-groups of patients diagnosed with early stage prostate cancer and having a statistically significant difference in the likelihood of disease relapse after therapy.

[00347] In the group of patients diagnosed with the stage 1C prostate cancer (Figure 62A), the median relapse-free survival after therapy in the poor prognosis sub-group

defined by the recurrence predictor algorithm was 12 months. In contrast, the median relapse-free survival after therapy in the good prognosis group was 82.4 months. 77 % of patients in the poor prognosis sub-group had a disease recurrence within 5 years after therapy. Conversely, 81 % of patients in the good prognosis sub-group remained relapse-free at least 5 years. The estimated hazard ration for disease recurrence after therapy in the poor prognosis sub-group as compared with the good prognosis sub-group of patients defined by the recurrence predictor algorithm was 5.559 (95% confidence interval of ratio, 2.685 to 25.18; P = 0.0002).

[00348] In the group of patients diagnosed with the stage 2A prostate cancer (Figure 62B), the median relapse-free survival after therapy in the poor prognosis sub-group defined by the recurrence predictor algorithm was 35.4 months. 86 % of patients in the poor prognosis sub-group had a disease recurrence within 5 years after therapy, whereas 78 % of patients in the good prognosis sub-group remained relapse-free at least 5 years. The estimated hazard ratio for disease recurrence after therapy in the poor prognosis sub-group as compared with the good prognosis sub-group of patients defined by the recurrence predictor algorithm was 7.411 (95% confidence interval of ratio, 2.220 to 40.20; P = 0.0024). Based on this analysis we concluded that application of the recurrence predictor algorithm seems to provide potentially useful clinical information in stratification of patients diagnosed with the early stage prostate cancer into sub-groups with statistically significant difference in the likelihood of disease recurrence after therapy.

## Discussion

As a result of the broad application of measurements of PSA level in the blood [00349] for early detection of prostate cancer in the United States, an increasing proportion of prostate cancer patients are diagnosed with early-stage tumors that apparently confined to the prostate gland and many patients have seemingly indolent disease not affecting individual's survival (Potosky, A., Feuer, E., Levin, D. Impact of screening on incidence and mortality of prostate cancer in the United States. Epidemiol. Rev., 23: 181-186, 2001). The considerable clinical heterogeneity of the early stage prostate cancer represents a highly significant health care and socio-economic challenge because prostate cancer is expected to be diagnosed in ~ 200,000 individuals every year (Greenlee, R.T., Hill-Hamon, M.B., Murray, T., Thun, M. Cancer statistics, 2001. CA Cancer J. Clin., 51: 15-36, 2001). Consequently, it can be argued that, unlike other types of cancer, development of efficient prognostic tests rather than early detection is critical for improvement of clinical decision-making and management of prostate cancer. We hypothesized that clinically relevant genetic signatures can be found by [00350] searching for clusters of co-regulated genes that display highly concordant transcript abundance behavior across multiple experimental models and clinical settings that model or represent malignant phenotypes of interest (Glinsky, G.V., Krones-Herzig, A., Glinskii, A.B., Gebauer, G. Microarray analysis of xenograft-derived cancer cell lines representing multiple experimental models of human prostate cancer. Molecular Carcinogenesis, 37: 209-221, 2003; Glinsky, G.V., Krones-Herzig, A., Glinskii, A.B. Malignancy-associated regions of transcriptional activation: gene expression profiling identifies common chromosomal regions of a recurrent transcriptional activation in human prostate, breast, ovarian, and colon cancers. Neoplasia, 5: 21-228; Glinsky, G.V.,

Ivanova, Y.A., Glinskii, A.B. Common malignancy-associated regions of transcriptional activation (MARTA) in human prostate, breast, ovarian, and colon cancers are targets for DNA amplification. Cancer Letters, in press, 2003). Thus, according to this model the primary criterion in a transcript selection process should be the concordance of changes in expression rather the magnitude of changes (e.g., fold change). One of the predictions of this model is that transcripts of interest are expected to have a tightly controlled "rank order" of expression within a cluster of co-regulated genes reflecting a balance of up- and down-regulated mRNAs as a desired regulatory end-point in a cell. A degree of resemblance of the transcript abundance rank order within a gene cluster between a test sample and reference standard is measured by a Pearson correlation coefficient and designated a phenotype association index ("PAI").

[00351] Using this strategy we discovered and validated a prostate cancer recurrence predictor algorithm that is suitable for stratifying patients at the time of diagnosis into poor and good prognosis sub-groups with statistically significant differences in the disease-free survival after therapy. The algorithm is based on application of gene expression signatures associated with biochemical recurrence of prostate cancer. The signatures (Table 69) were defined using clusters of co-regulated genes exhibiting highly concordant expression profiles (r > 0.95) in metastatic nude mouse models of human prostate carcinoma and tumor samples from patients with recurrent prostate cancer (see Example 5).

[00352] A few previous studies have applied oligonucleotide or cDNA microarrays for identification of gene expression signatures associated with biochemical recurrence of human prostate cancer (Dhanasekaran, S.M., Barrette, T.R., Ghosh, D., Shah, R.,

Varambally, S., Kurachi, K., Pienta, K.J., Rubin, M.A., Chinnalyan, A.M. Delineation of prognostic biomarkers in prostate cancer. Nature, 412:822-826, 2001; Singh, D., Febbo, P.G., Ross, K., Jackson, D.G., Manola, C.L., Tamayo, P., Renshaw, A.A., D'Amico, A.V., Richie, J.P., Lander, E.S., Loda, M., Kantoff, P.W., Golub, T.R., Sellers, W.R. Gene expression correlates of clinical prostate cancer behavior. Cancer Cell, 1: 203-209, 2002; Varambally, S., Dhanasekaran, S.M., Zhou, M., Barrette, T.R., Kumar-Sinha, C., Sanda, M.G., Ghosh, D., Pineta, K.J., Sewalt, R.G., Otte, A.P., Rubin, M.A., Chinnalyan, A.M. The polycomb group protein EZH2 is involved in progression of prostate cancer. Nature, 419: 624-629, 2002; Henshall, S.M., Afar, D.E., Hiller, J., Horvath, L.G., Quinn, D.I., Rasiah, K.K., Gish, K., Willhite, D., Kench, J.G., Gardiner-Garden, M., Stricker, P.D., Scher, H.I., Grygiel, J.J., Agus, D.B., Mack, D.H., Sutherland, R.L. Survival analysis of genome-wide gene expression profiles of prostate cancers identifies new prognostic targets of disease relapse. Cancer Res., 63: 4196-4203, 2003). One of the major deficiencies of these studies that somewhat limited their significance was that a single clinical data set was utilized for both signature discovery and validation. To our knowledge, the work reported here is the first genome-wide expression profiling study of human prostate cancer that utilizes one clinical data set for signature discovery and algorithm development, and a second independent data set for validation of the prostate cancer recurrence predictor algorithm.

[00353] One of the interesting features of described here prostate cancer recurrence predictor algorithm is that it provides additional predictive value over conventional markers of outcome such as pre-operative PSA level and Gleason sum. Another important feature of identified recurrence predictor algorithm is its ability to stratify

patients diagnosed with the early stage prostate cancer into sub-groups with statistically-distinct likelihoods of biochemical relapse after therapy. Importantly, the recurrence predictor algorithm segregates into poor prognosis group 88% of patients who subsequently developed disease recurrence within one year after prostatectomy. Based on this analysis we concluded that identified in this study genetic signatures (as well as others that can be determined using the methods of the invention) have a significant potential for developing highly accurate clinical prognostic tests suitable for stratifying prostate cancer patients at the time of diagnosis with respect to likelihood of negative or positive clinical outcome after therapy.

[00354] The causal genetic, molecular, and biological distinctions between prostate tumors with recurrent and indolent clinical behavior remain largely unknown. The results reported in this example and in Example 5 provide the first experimental evidence of a clinically relevant transcriptional resemblance between metastatic human prostate carcinoma xenografts growing orthotopically in nude mice and primary prostate tumors from patients that subsequently developed a biochemical relapse after therapy. This work provides a model for investigation of the potential functional relevance of identified transcriptional aberrations and suggests that genetically defined metastasis-promoting features of primary tumors seem to be one of the major contributing factors of aggressive clinical behavior and unfavorable prognosis in prostate cancer patients. This conclusion is consistent with results of the several recent studies aimed at definition of metastasis predictor signatures in the primary human tumors representing multiple types of epithelial cancers (van 't Veer, L.J., Dai, H., van de Vijver, M.J., et al. Gene expression profiling predicts clinical outcome of breast cancer. Nature, 415: 530-536, 2002; van de

Vijver, M.J., He, Y.D., van 't Veer, L.J., et al. A gene expression signature as a predictor of survival in breast cancer. N. Engl. J. Med., 347: 1999-2009, 2002; Ramaswamy, S., Ross, K.N., Lander, E.S., Golub, T.R. A molecular signature of metastasis in primary solid tumors. Nature Genetics, 33: 49-54, 2003). Our results indicate that sub-groups of prostate cancer patients with poor and good prognosis gene expression signatures reflect the presence of two genetically defined sub-types of human prostate carcinoma manifesting dramatic statistically significant differences in response to therapy and clinically distinct courses of disease progression.

One of the dominant views on prostate cancer pathogenesis is the concept of [00355] progression from hormone-dependent early stage prostate cancer to hormone-refractory metastatic late stage disease with the apparent implication of increased proportion of patients with poor prognosis at the advanced stage of progression. However, in our validation data set of 79 samples the actual frequency of recurrence remains relatively constant among the patients with different stages of prostate cancer: 47% (16 of 34) in stage 1C; 56% (9 of 16) in stage 2A; and 41% (12 of 29) in stages 2B/2C/3A. These data suggest that progression of the disease occurs only in a sub-group of patients. Interestingly, in a sub-group of patients with good prognosis signatures the frequency of recurrence appears to increase in the patients with the late-stage prostate cancer: 24% (5 of 21) in stage 1C; 22% (2 of 9) in stage 2A; 33% (3 of 9) in stage 2B; 40% (2 of 5) in stage 2C/3A. These results seem to imply that patients with the good prognosis signatures may represent a sub-group undergoing a classical prostate cancer progression with a gradual increase in malignant potential. The patients with poor prognosis signatures may represent a genetically and biologically distinct sub-type of prostate cancer exhibiting

highly malignant behavior at the early stage of disease with the frequency of recurrence 85% (11 of 13) in stage 1C and 100% (7 of 7) in stage 2A patients.

[00356] In summary, using expression profiles of highly metastatic models of human prostate cancer in nude mice as a predictive reference of expected transcript abundance behavior in recurrent prostate tumors, we identified and validated recurrence predictor signatures of human prostate cancer. Prostate cancer recurrence predictor signatures provide additional predictive value to the conventional markers of outcome and will be clinically useful in stratifying prostate cancer patients into sub-groups with distinct clinical manifestation of disease and different response to therapy.

## REFERENCES

- 1. Holmberg, L., Bill-Axelson, A., Helgesen, F., Salo, J.O., Folmerz, P., Haggman, M., Andersson, S.O., Sapngberg, A., Busch, C., Nording, S., et al. 2002. N. Engl. J. Med. 347, 781-789.
- 2. Thomas, G.V., and Loda, M. 2002. Molecular staging of prostate cancer. In Prostate Cancer Principles & Practice. P.W. Kantoff, P.R. Carroll, and A.V. D'Amico, eds. (Philadelphia: Lippincott Williams & Wilkins), pp. 287-303.
- 3. DeMarzo, A.M., Nelson, W.G., Isaacs, W.B., Epstein, J.I. 2003. Pathological and molecular aspects of prostate cancer. Lancet, 361: 955-964.
- 4. Kattan M. W., Eastham J. A., Stapleton A. M., Wheeler T. M., Scardino P. T. A preoperative nomogram for disease recurrence following radical prostatectomy for prostate cancer. J. Natl. Cancer Inst., 90: 766-771, 1998.
- 5. D'Amico A. V., Whittington R., Malkowicz S. B., Fondurulia J., Chen M-H, Kaplan I., Beard C. J., Tomaszewski J. E., Renshaw A. A., Wein A., Coleman C. N.

Pretreatment nomogram for prostate-specific antigen recurrence after radical prostatectomy or external-beam radiation therapy for clinically localised prostate cancer. J. Clin. Oncol., 17: 168-172, 1999.

- 6. Graefen M., Noldus J., Pichlmeier A., Haese P., Hammerer S., Fernandez S., Conrad R., Henke E., Huland E., Huland H. Early prostate-specific antigen relapse after radical retropubic prostatectomy: prediction on the basis of preoperative and postoperative tumor characteristics. Eur. Urol., 36: 21-30, 1999.
- 7. Kattan M. W., Wheeler T. M., Scardino P. T. Postoperative nomogram for disease recurrence after radical prostatectomy for prostate cancer. J. Clin. Oncol., *17*: 1499-1507, 1999.
- 8. Magee, J.A., Araki, T., Patil, S., Ehrig, T., True, L., Humphrey, P.A., Catalona, W.J., Watson, M.A., Milbrandt, J. Expression profiling reveals hepsin overexpression in prostate cancer. Cancer Res., 61: 5692-5696, 2001.
- 9. Dhanasekaran, S.M., Barrette, T.R., Ghosh, D., Shah, R., Varambally, S., Kurachi, K., Pienta, K.J., Rubin, M.A., Chinnalyan, A.M. Delineation of prognostic biomarkers in prostate cancer. Nature, 412:822-826, 2001.
- 10. Welsh, J.B., Sapinoso, L.M., Su, A.I., Kern, S.G., Wang-Rodriguez, J., Moskaluk, C.A., Frierson, H.F., Jr., Hampton, G.M. Analysis of gene expression identifies candidate markers and pharmacological targets in prostate cancer. Cancer Res., 61: 5974-5978, 2001.
- 11. Luo, J., Duggan, D.J., Chen, Y., Sauvageot, J., Ewing, C.M., Bittner, M.L., Trent, J.M., Isaacs, W.B. Human prostate cancer and benign prostatic hyperplasia: molecular dissection by gene expression profiling. Cancer Res., 61: 4683-4688, 2001.

- 12. Stamey, TA, Warrington, JA, Caldwell, MC, Chen, Z, Fan, Z, Mahadevappa, M, McNeal, JE, Nolley, R, Zhang, Z. Molecular genetic profiling of Gleason grade 4/5 prostate cancers compared to benign prostatic hyperplasia. J. Urol., 166: 2171-2177, 2001.
- 13. Luo, J., Dunn, T, Ewing, C, Sauvageot, J., Chen, Y, Trent, J, Isaacs, W. Gene expression signature of benign prostatic hyperplasia revealed by cDNA microarray analysis. Prostate, 51: 189-200, 2002.
- 14. Singh, D., Febbo, P.G., Ross, K., Jackson, D.G., Manola, C.L., Tamayo, P., Renshaw, A.A., D'Amico, A.V., Richie, J.P., Lander, E.S., Loda, M., Kantoff, P.W., Golub, T.R., Sellers, W.R. Gene expression correlates of clinical prostate cancer behavior. Cancer Cell, 1: 203-209, 2002.
- 15. Rhodes, D.R., Barrette, T.R., Rubin, M.A., Ghosh, D., Chinnaiyan, A.M. Meta-analysis of microarrays: interstudy validation of gene expression profiles reveals pathways dysregulation in prostate cancer. Cancer Res., 62: 4427-4433, 2002.
- Varambally, S., Dhanasekaran, S.M., Zhou, M., Barrette, T.R., Kumar-Sinha, C., Sanda, M.G., Ghosh, D., Pineta, K.J., Sewalt, R.G., Otte, A.P., Rubin, M.A., Chinnalyan, A.M. The polycomb group protein EZH2 is involved in progression of prostate cancer. Nature, 419: 624-629, 2002.
- 17. Henshall, S.M., Afar, D.E., Hiller, J., Horvath, L.G., Quinn, D.I., Rasiah, K.K., Gish, K., Willhite, D., Kench, J.G., Gardiner-Garden, M., Stricker, P.D., Scher, H.I., Grygiel, J.J., Agus, D.B., Mack, D.H., Sutherland, R.L. Survival analysis of genome-wide gene expression profiles of prostate cancers identifies new prognostic targets of disease relapse. Cancer Res., 63: 4196-4203, 2003.

- 18. LaTulippe, E., Satagopan, J., Smith, A., Scher, H., Scardino, P., Reuter, V., Gerald, W.L. Comprehensive gene expression analysis of prostate cancer reveals distinct transcriptional programs associated with metastasis. Cancer Res., 62: 4499-4506, 2002.
- 19. Glinsky, G.V., Krones-Herzig, A., Glinskii, A.B., Gebauer, G. Microarray analysis of xenograft-derived cancer cell lines representing multiple experimental models of human prostate cancer. Molecular Carcinogenesis, 37: 209-221, 2003.
- 20. Potosky, A., Feuer, E., Levin, D. Impact of screening on incidence and mortality of prostate cancer in the United States. Epidemiol. Rev., 23: 181-186, 2001.
- 21. Greenlee, R.T., Hill-Hamon, M.B., Murray, T., Thun, M. Cancer statistics, 2001. CA Cancer J. Clin., 51: 15-36, 2001.
- 22. Glinsky, G.V., Krones-Herzig, A., Glinskii, A.B. Malignancy-associated regions of transcriptional activation: gene expression profiling identifies common chromosomal regions of a recurrent transcriptional activation in human prostate, breast, ovarian, and colon cancers. Neoplasia, 5: 21-228.
- 23. Glinsky, G.V., Ivanova, Y.A., Glinskii, A.B. Common malignancy-associated regions of transcriptional activation (MARTA) in human prostate, breast, ovarian, and colon cancers are targets for DNA amplification. Cancer Letters, in press, 2003.
- 24. van 't Veer, L.J., Dai, H., van de Vijver, M.J., et al. Gene expression profiling predicts clinical outcome of breast cancer. Nature, 415: 530-536, 2002
- 25. van de Vijver, M.J., He, Y.D., van 't Veer, L.J., et al. A gene expression signature as a predictor of survival in breast cancer. N. Engl. J. Med., 347: 1999-2009, 2002.
- 26. Ramaswamy, S., Ross, K.N., Lander, E.S., Golub, T.R. A molecular signature of metastasis in primary solid tumors. Nature Genetics, 33: 49-54, 2003.

## EXAMPLE 12 – USE OF EXPRESSION DATA WITH OTHER METRICS TO PREDICT BREAST CANCER PATIENT SURVIVAL

## Introduction

[00357] Highly accurate prognostic tests are essential for individualized decision-making process during clinical management of cancer patients leading to rational and more efficient selection of appropriate therapeutic interventions and improved outcome after therapy. In breast cancer, patients are classified into broad subgroups with poor and good prognosis reflecting a different probability of disease recurrence and survival after therapy. Distinct prognostic subgroups are identified using a combination of clinical and pathological criteria: age, primary tumor size, status of axillary lymph nodes, histologic type and pathologic grade of tumor, and hormone receptor status (Goldhirsch, A., Glick, J.H., Gelber, R.D., Coates, A.S., Seen, H.J. Meeting highlights: International Consensus Panel on the Treatment of Primary Breast Cancer: Seventh International Conference on Adjuvant Therapy of Primary Breast Cancer. J. Clin. Oncol., 19: 3817-3827, 2001; Eifel, P., Axelson, J.A., Costa, J., et al. National Institute of Health Consensus Development Conference Summary: adjuvant therapy for breast cancer, November 1-3, 2000. J. Natl. Cancer Inst., 93: 979-989, 2001.)

[00358] One of the most critical treatment decisions during the clinical management of breast cancer patients is the use of adjuvant systemic therapy. Adjuvant systemic therapy significantly improves disease-free and overall survival in breast cancer patients with both lymph-node negative and lymph-node positive disease (Early Breast Cancer Trialists' Collaborative Group. Polychemotherapy for early breast cancer: an overview of the randomized trials. Lancet, 352: 930-942, 1998; Early Breast Cancer Trialists' Collaborative Group. Tamoxifen for early breast cancer: an overview of the randomized

trials. Lancet, 351: 1451-1467, 1998). It is generally accepted that breast cancer patients with poor prognosis would gain the most benefits from the adjuvant systemic therapy (Goldhirsch, et al., 2001; Eifel et al., 2001).

[00359] Diagnosis of lymph-node status is important in therapeutic decision-making, prediction of disease outcome, and probability of breast cancer recurrence. Invasion into axillary lymph nodes is recognized as one of the most important prognostic factors (Krag, D., Weaver, D., Ashikaga, T., et al. The sentinel node in breast cancer – a multicenter validation study. N. Engl. J. Med., 339: 941-946, 1998; Singletary, S.E., Allred, C., Ashley, P., et al. Revision of the American Joint Committee on cancer staging system for breast cancer. J. Clin. Oncol., 20: 3628-3636, 2002; Jatoli, I., Hilsenbeck, S.G., Clark, G.M., Osborne, C.K. Significance of axillary lymph node metastasis in primary breast cancer. J. Clin. Oncol., 17: 2334-2340, 1999). Most patients diagnosed with lymph-node negative breast cancer can be effectively treated with surgery and local radiation therapy. However, results of several studies show that 22-33% of breast cancer patients with no detectable lymph-node involvement and classified into a good prognosis subgroup develop recurrence of disease after a 10-year follow-up (Early Breast Cancer Trialists' Collaborative Group. Tamoxifen for early breast cancer: an overview of the randomized trials. Lancet, 351: 1451-1467, 1998). Therefore, accurate identification of breast cancer patients with lymph-node negative tumors who are at high risk of recurrence is critically important for rational treatment decision and improved clinical outcome in the individual patient.

[00360] Microarray-based gene expression profiling of human cancers rapidly emerged as a new powerful screening technique generating hundreds of novel diagnostic,

prognostic, and therapeutic targets (Golub, T.R., Slonim, D.K., Tamayo, P., et al. Molecular classification of cancer: class discovery and class prediction by gene expression monitoring. Science, 286: 531-537, 1999; Alizadeh, A.A., Eisen, M.B., Davis, R.E., et al. Distinct types of diffuse large B-cell lymphoma identified by gene expression profiling. Nature, 403: 503-511, 2000; Alizadeh, A.A., Ross, D.T., Perou, C.M., van de Rijn, M. Towards a novel classification of human malignancies based on gene expression patterns. J. Pathol., 195: 41-52, 2001; Battacharjee, A., Richards, W.G., Staunton, J., et al. Classification of human lung carcinomas by mRNA expression profiling reveals distinct adenocarcinoma subclasses. Proc. Natl. Acad. Sci. USA, 98: 13790-13795, 2001; Yeoh, E.-J., Ross, M.E., Shurtleff, S.A., et al. Classification, subtype discovery, and prediction of outcome in pediatric acute lymphoblastic leukemia by gene expression profiling. Cancer Cell, 1: 133-143, 2002; Dyrskot, L., Thykjaer, T., Kruhoffer, M., Jensen, J.L., Marcussen, N., Hamilton-Dutoit, S., Wolf, H., Orntoft, T. Identifying distinct classes of bladder carcinoma using microarrays. Nature Genetics, 33: 90-96, 2003). Recently breast cancer gene expression signatures have been identified that are associated with the estrogen receptor and lymph node status of patients and can aid in classification of breast caner patients into subgroups with different clinical outcome after therapy (Perou, C.M., Sorlie, T., Eisen, M.B., et al. Molecular portrait of human breast tumors. Nature, 406: 747-752, 2000; Gruvberger, S., Ringner, M., Chen, Y., et al. Estrogen receptor status in breast cancer is associated with remarkably distinct gene expression patterns. Cancer Res., 61: 5979-5984, 2001; West, M., Blanchette, C., Dressman, H., et al. Predicting the clinical status of human breast cancer by using gene expression profiles. Proc. Natl. Acad. Sci. USA, 98: 11462-11467, 2001; Ahr, A., Karn,

T., Sollbach, C., et al. Identification of high risk breast cancer patients by gene expression profiling. Lancet, 359: 131-132, 2002; van 't Veer, L.J., dai, H., van de Vijver, M.J., et al. Gene expression profiling predicts clinical outcome of breast cancer. Nature, 415: 530-536, 2002; Sorlie, T., Perou, C.M., Tibshirani, R., et al. Gene expression patterns of breast carcinomas distinguish tumor subclasses with clinical implications. Proc. Natl. Acad. Sci. USA, 98: 10869-10874, 2001; Heedenfalk, I., Duggan, D., Chen, Y., et al. Gene-expression profiles in hereditary breast cancer. N. Engl. J. Med., 344: 539-548, 2001; van de Vijver, M.J., He, Y.D., van 't Veer, L.J., et al. A gene expression signature as a predictor of survival in breast cancer. N. Engl. J. Med., 347: 1999-2009, 2002; Huang, E., Cheng, S.H., Dressman, H., Pittman, J., Tsou, M.H., Horng, C.F., Bild, A., Iversen, E.S., Liao, M., Chen, C.M., West, M., Nevins, J.R., Huang, A.T. Gene expression predictors of breast cancer outcome. Lancet, 361: 1590-1596, 2003). [00361] One of the significant limitations of these array-based studies is that they generated vast data sets comprising many attractive targets with diagnostic and prognostic potential. Design and performance of meaningful follow-up experiments such as translation of the array-generated hits into quantitative RT-PCR-based analytical assays would require a significant data reduction. Furthermore, clinical implementation of novel prognostic tests would require integration of genomic data and best-established conventional markers of the outcome.

[00362] Here, we translate a large microarray-based breast cancer outcome predictor signature into quantitative RT-PCR-based assays of mRNA abundance levels of small gene clusters performing with similar classification accuracy. We demonstrate that identified molecular signatures provide additional predictive values over well-established

conventional prognostic markers for breast cancer such as hormone receptor status and lymph node involvement. These data indicate that quantitative laboratory tests measuring expression profiles of identified small gene clusters are useful for stratifying breast cancer patients into sub-groups with distinct likelihood of positive outcome after therapy and assisting in selection of optimal treatment strategies.

## Materials and Methods

[00363] The same general methods as described in Example 11 were used to carry out the work reported in this example.

## Results and Discussion

[00364] The 70-gene breast cancer metastasis and survival predictor signature represents a heterogeneous set of small gene clusters independently performing with high therapy outcome prediction accuracy. Recent study on gene expression profiling of breast cancer identifies 70 genes whose expression pattern is strongly predictive of a short post-diagnosis and treatment interval to distant metastases (van 't Veer, et al., 2002). The expression pattern of these 70 genes discriminates with 81% (optimized sensitivity threshold) or 83% (optimal accuracy threshold) accuracy the patient's prognosis in the group of 78 young women diagnosed with sporadic lymph-nodenegative breast cancer (this group comprises of 34 patients who developed distant metastases within 5 years and 44 patients who continued to be disease-free at least 5 years after therapy; they constitute clinically defined poor prognosis and good prognosis groups, correspondingly). We reduced the number of genes whose expression patterns represent genetic signatures of breast cancer with "poor prognosis" or "good prognosis."

Measurements of mRNA expression levels of 70 genes in established human breast carcinoma cell lines (MCF7; MDA-MB-435; MDA-MB-468; MDA-MB-231; MDA-MB-435Br1; MDA-MB-435BL3) and primary cultures of normal human breast epithelial cells were performed utilizing Q-RT-PCR method, which is generally accepted as the most reliable method of gene expression analysis and unambiguous confirmation of a gene identity. For each breast cancer cell line concordant sets of genes were identified exhibiting both positive and negative correlation between fold expression changes in cancer cell lines versus control cell line and poor prognosis group versus good prognosis group patient samples. Minimum segregation sets were selected from corresponding concordance sets and individual phenotype association indices were calculated. The four top-performing breast cancer metastasis predictor gene clusters are listed in Table 73. A breast cancer poor prognosis predictor cluster comprising 6 genes was identified (r = 0.981) using MDA-MB-468 cell line gene expression profile as a reference standard. 32 of 34 samples from the poor prognosis group had positive phenotype association indices, whereas 29 of 44 samples from the good prognosis group had negative phenotype association indices yielding 78% overall accuracy in sample classification. Another breast cancer poor prognosis predictor cluster comprising 4 genes was identified (r = 0.944) using MDA-MB-435BL3 cell line gene expression profile as a reference standard. Using this 4-gene cluster, 28 of 34 samples from the poor prognosis group had positive phenotype association indices, whereas 28 of 44 samples from the good prognosis group had negative phenotype association indices overall yielding 72 % accuracy in sample classification.

[00366] A breast cancer good prognosis predictor cluster comprising 14 genes was identified (r = -0.952) using MDA-MB-435Br1 cell line gene expression profile as a reference standard. 30 of 34 samples from the poor prognosis group had negative phenotype association indices, whereas 34 of 44 samples from the good prognosis group had positive phenotype association indices yielding 82% overall accuracy in sample classification. Another breast cancer good prognosis predictor cluster comprising 13 genes (r = -0.992) was identified using MCF7 cell line gene expression profile as a reference standard. 30 of 34 samples from the poor prognosis group had negative phenotype association indices, whereas 32 of 44 samples from the good prognosis group had positive phenotype association indices yielding 79% overall accuracy in sample classification.

[00367] The transcripts comprising each signature listed in Table 73 were selected based on Pearson correlation coefficients (r > 0.95) reflecting a degree of similarity of expression profiles in clinical tumor samples (34 recurrent versus 44 non-recurrent tumors) and experimental cell line samples. Selection of transcripts was performed from sets of genes exhibiting concordant changes of transcript abundance behavior in recurrent versus non-recurrent clinical tumor samples (70 transcripts) and experimental conditions independently defined for each signature (6-gene signature: MDA-MB468 cells versus control; 4-gene signature: MDA-MB-435BL3 cells versus control; 13-gene signature: MCF7 cells versus control; 14-gene signature: MDA-MB-435Br1 cells versus control)(see also Example 2). mRNA expression levels of 70 genes comprising parent microarray-defined signature (van't Veer, L.J., et al., 2002; van de Vijver, M.J., et al., 2002) were measured by standard quantitative RT-PCR method in multiple established

human breast cancer cell lines using GAPDH expression for normalization and compared to the expression in a control cell line. Control cells were primary cultures of normal human breast epithelial cells. Expression profiles were presented as log10 average fold changes for each transcript.

Table 73. Gene expression signatures predicting survival of breast cancer patients.							
6-gene signature (same as Table 27)							
LocusLink	Description	Gene ID (Chip identified in	UniGene				
Name		van't Veer, L.J., et al.,2002)	ID				
	Fms-related tyrosine		Hs.381093				
FLT1	kinase 1	NM_002019					
	BCL2 binding component		Hs.87246				
BBC3	3	U82987					
	Transforming growth		Hs.2025				
TGFB3	factor, beta 3	NM_003239					
	Membrane-spanning 4-		Hs.11090				
MS4A7	domains	AF201951					
	Glutathione S-transferase		Hs.2006				
GSTM3	M3	NM_000849					
	Fibroblast growth factor		Hs.49585				
FGF18	18	NM_003862					
	4-gene	signature					
LocusLink	Description	Gene ID (Chip identified in	UniGene				
Name		van't Veer, L.J., et al.,2002)	ID				
	Highly expressed in		Hs.58169				
HEC	cancer	NM_006101					
	Minichromosome		Hs.155462				
мсм6	maintenance deficient 6	NM_005915					
<del></del>	Glutathione S-transferase		Hs.2006				
GSTM3	M3	NM_000849					

	Fibroblast growth factor		Hs.49585
FGF18	18	NM_003862	
		(same as Table 29)	
LocusLink	Description	Gene ID (Chip identified in	UniGene
Name	1	van't Veer, L.J., et al.,2002)	
	SCUBE2 signal peptide,		
CEGP1	CUB domain	NM_020974	Hs.222399
	Fibroblast growth factor		40505
FGF18	18	NM_003862	Hs.49585
	Glutathione S-transferase		
GSTM3	M3	NM_000849	Hs.2006
	Transforming growth		
TGFB3	factor, beta 3	NM_003239	Hs.2025
	Membrane-spanning 4-		
MS4A7	domains	AF201951	Hs.11090
EST	Hypothetical protein	Contig55377_RC	Hs.218182
	Adaptor-related protein		
AP2B1	complex 2	NM_001282	Hs.74626
CCNE2	Cyclin E2	· NM_004702	Hs.30464
	Maternal embryonic		101000
KIAA0175	leucine zipper kinase	NM_014791	Hs.184339
EXT1	Exostoses (multiple) 1	NM_000127	Hs.184161
LOC341692	Similar to Diap3 protein	Contig46218_RC	Hs.283127
	CDC42 binding protein		TT 10506
PK428	kinase alpha	NM_003607	Hs.18586
	14-gene signatu	re (same as Table 28)	TI-:Como
Gene	Description	Gene ID (Chip identified in	ì
		van't Veer, L.J., et al.,2002	
	Membrane-spanning 4-		Hs.11090
MS4A7	domains	AF201951	

	Transforming growth		Hs.2025
TGFB3	factor, beta 3	NM_003239	
	BCL2 binding component		Hs.87246
BBC3	3	U82987	
	Adaptor-related protein		Hs.74626
AP2B1	complex 2	NM_001282	
	Aldehyde dehydrogenase		Hs.77448
ALDH4A1	4 family, member A1	NM_003748	
	Chromosome 20, open		Hs.155071
FLJ11190	reading frame 46	NM_018354	
DC13	DC13 protein	NM_020188	Hs.6879
	Guanine monophosphate		Hs.5398
GMPS	synthetase	NM_003875	
	A kinase (PRKA) anchor		Hs.42322
AKAP2	protein	Contig57258_RC	
DCK	Deoxycytidine kinase	NM_000788	Hs.709
	Epithelial cell		Hs.122579
ECT2	transforming sequence 2	Contig25991	
	ESTs, weakly similar to		
EST	quiescin	Contig38288_RC	
OXCT	3-oxoacid CoA transferase	NM_000436	Hs.177584
EXT1	Exostoses (multiple) 1	NM_000127	Hs.184161

[00368] To demonstrate the ability to reduce the number of genes in the cluster, while maintaining predictive power, we selected subsets of genes within a minimum segregation set so as to raise the correlation coefficient, and tested the performance of the cluster as the set was reduced from 9 to 2 genes. Specifically, classification was performed in a cohort of 78 breast cancer patients. The outcome predictor clusters were

identified using MDA-MB-435BL3 human breast carcinoma cell line as a reference standard. These results are shown in Tables 73.1 and 73.2.

Table 73.1. Classification accuracy of breast cancer outcome predictor algorithm based on 9-gene parent cluster and smaller gene clusters derived from the parent 9-gene cluster.

Number of genes	Correlation	Poor	Good	
in cluster	coefficient	prognosis	prognosis	Overall
<del></del>	0.945	31 of 34	27 of 44	58 of 78
9 genes		(91%)	(61%)	(74%)
	0.900	20 of 34	36 of 44	56 of 44
5 genes		(59%)	(82%)	(72%)
	0.956	28 of 34	28 of 44	56 of 44
4 genes		(82%)	(64%)	(72%)
	1.000	27 of 34	30 of 44	57 of 44
2 genes		(79%)	((68%)	(73%)

Table 73.2 Genes contained within reduced clusters							
9-gene cluster	5-gene cluster	4-gene cluster	2-gene cluster				
HEC	HEC	HEC	HEC				
AI377418	MCM6	MCM6	FGF18				
MCM6	BBC3	GSTM3					
BBC3	ALDH4	FGF18					
ALDH4	AP2B1						
AP2B1							
PECI							
GSTM3							
FGF18							

[00369] As described in Example 2, we validated the classification accuracy using an independent data set, and tested performance of the 13 genes good prognosis predictor

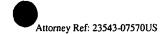
cluster on a set of 19 samples obtained from 11 breast cancer patients who developed distant metastases within five years after diagnosis and treatment and 8 patients who remained disease free for at least five years (van 't Veer, L.J., et al., 2002). 9 of 11 samples from the poor prognosis group had negative phenotype association indices, whereas 6 of 8 samples from the good prognosis group had positive phenotype association indices yielding 79% overall accuracy in sample classification.

[00370] Kaplan-Meier analysis showed that metastasis-free survival after therapy was significantly different in breast cancer patients segregated into good and poor prognosis groups based on relative values of expression signatures defined by all four small gene clusters (Figure 65A). These data indicate that quantitative laboratory tests measuring expression profiles of identified small gene clusters are useful in stratifying breast cancer patients into sub-groups with statistically distinct probabilities of remaining disease-free after therapy.

therapy outcome prediction accuracy in an independent cohort of 295 breast cancer patients. Recently the breast cancer prognosis prediction accuracy of the 70-gene signature was validated in a large cohort of 295 patients with either lymph node-negative or lymph node-positive breast cancer (van de Vijver, M.J., et al., 2002). The expression profile of the 70-gene breast cancer outcome predictor signature was highly informative in forecasting the probability of remaining free of distant metastasis and predicting the overall survival after therapy (*id.*). We compared the classification accuracy of small gene clusters and a large 70-gene parent signature applied to a cohort of 295 patients.

[00372] As shown in the Table 74, identified small gene clusters and a large parent signature perform similarly in identifying sub-groups of breast cancer patients with poor and good prognosis defined by differences in the probability of the overall survival after therapy. At the several classification threshold levels small gene clusters fully recapitulate or even outperform the 70-gene parent signature in classification accuracy of the 295 breast cancer patients (Table 74). Taken together these data are consistent with the idea that the 70-gene breast cancer prognosis signature represents a heterogeneous set of small gene clusters with high therapy outcome prediction potential. Consistent with this idea, the application of the 14-gene survival predictor signature was highly informative in classification of breast cancer patients into sub-groups with statistically significant difference in the probability of survival after therapy (Figure 68). Interestingly, the highly significant difference (p < 0.0001) in the survival probability between poor and good prognosis groups defined by the 14-gene signature was achieved using multiple classification threshold levels providing additional flexibility in selection of a desirable 5-or 10-year survival level defining good prognosis group (Figure 68B). To generate the data in Table 74, 295 breast cancer patients were classified [00373] according to whether they had a good-prognosis signature or poor-prognosis signature defined by individual therapy outcome predictor signatures. Kaplan-Meier analysis was performed to evaluate the probability that patients would survive according to whether they had a poor-prognosis or a good-prognosis signature and determine the proportion of patients who would survive at least 5 or 10 years after therapy in poor-prognosis and good-prognosis sub-groups. Hazard ratios, 95% confidence intervals, and P values were calculated with use of the log-rank test. The number of correct predictions in poorprognosis and good-prognosis groups is shown as a fraction of patients with the observed clinical outcome after therapy (79 patients died and 216 patients remained alive). The classification performance of different signatures were evaluated using one common threshold level (0.00) and optimized threshold levels adjusted for each gene cluster to achieve the most statistically significant (highest hazard ratio and lowest P value) discrimination in survival probability between patients assigned to poor and good prognosis groups.

Table 74. Stratification of 295 breast cancer patients at the time of diagnosis into poor and									
good prognosis groups using different therapy outcome predictor signatures									
Outcome	Poor	Good	Correct	Correct	Hazard	95%	P value		
signature	prognosis,	prognosis,	predictions,	predictions,	ratio	Confidence			
(cut off	5-(10)-	5-(10)-	poor	good	} }	interval			
value)	year	year	outcome	outcome					
ļ	survival	survival							
70-gene	75%	97%	70 of 79	106 of 216	6.327	2.498 to	< 0.0001		
(0.45)	(56%)	(92%)	(89%)	(49%)		6.077			
70-gene	64%	91%	42 of 79	174 of 216	3.867	3.405 to	< 0.0001		
(0.00)	(46%)	(80%)	(53%)	(81%)		9.809			
13-gene	73%	98%	71 of 79	106 of 216	7.005	2.560 to	< 0.0001		
(0.12)	(56%)	(93%)	(90%)	(49%)		6.237			
13-gene	73%	97%	69 of 79	115 of 216	6.519	2.728 to	< 0.0001		
(0.04)	(54%)	(92%)	(87%)	(53%)		6.610			
13-gene	73%	96%	67 of 79	118 of 216	5.698	2.663 to	< 0.0001		
(0.00)	(54%)	(90%)	(85%)	(55%)		6.450			
14-gene	77%	96%	72 of 79	79 of 216	5.220	1.912 to	<0.0001		
(0.37)	(62%)	(91%)	(91%)	(37%)		4.874			
14-gene	76%	95%	69 of 79	95 of 216	4.701	2.038 to	<0.0001		
(0.28)	(59%)	(89%)	(87%)	(44%)		5.016	!		



14-gene	75%	92%	58 of 79	130 of 216	3.637	2.217 to	<0.0001
(0.00)	(55%)	(85%)	(73%)	(60%)	) }	5.419	
14-gene	65%	91%	45 of 79	176 of 216	4.171	3.632 to	< 0.0001
(-0.55)	(45%)	(81%)	(57%)	(81%)		10.21	
6-gene (-	78%	96%	70 of 79	85 of 216	4.543	1.901 to	< 0.0001
0.12)	(62%)	(88%)	(89%)	(39%)		4.756	
6-gene	78%	92%	64 of 79	101 of 216	3.314	1.757 to	< 0.0001
(0.00)	(60%)	(86%)	(81%)	(47%)		4.282	
4-gene	73%	93%	60 of 79	136 of 216	4.389	2.723 to	< 0.0001
(0.20)	(53%)	(85%)	(76%)	(63%)	}	6.735	
4-gene	75%	93%	60 of 79	119 of 216	3.519	2.050 to	<0.0001
(0.00)	(58%)	(84%)	(76%)	(55%)		4.983	

[00374] The 70-gene signature, in contrast to small gene clusters, is not suitable for breast cancer outcome prediction in patients with estrogen receptor negative tumors. Consistent with well-established prognostic value of the estrogen receptor status of breast tumors (see Introduction), 97 percent of patients in the good prognosis group defined by the 70-gene signature had estrogen receptor positive (ER+) tumors (van de Vijver, M.J., et al., 2002). Conversely, ninety six percent of breast cancer patients with the estrogen receptor negative (ER-) tumors (66 of 69 patients at the cut off level <0.45) had expression profile of the 70 genes predictive of a poor outcome after therapy. Two important conclusions can be drawn from this association. First, breast cancer patients with ER+ tumors and poor prognosis expression profile of the 70 genes may have yet unidentified functional defect within an ER-response pathway. Second, a 70-gene signature appears to assign rather uniformly a vast majority of the patients with ER-tumors into poor prognosis category and, therefore, is not suitable for prognosis prediction in this group of breast cancer patients.

[00375] In agreement with many previous observations, patients with ER- tumors had significantly worst survival after therapy compared to the patients with ER+ tumors in the cohort of 295 breast cancer patients (Figure 64A). The Kaplan-Meier survival analysis (Figure 64A) showed that the median relapse-free survival after therapy of patients with the ER- tumors was 9.7 years. Only 47.1 % of patients with ER-negative tumors survived 10 years after therapy compared to 77.4 % patients with ER+ tumors. The estimated hazard ration for survival after therapy in the poor prognosis group as compared with the good prognosis group of patients defined by the ER status was 3.258 (95% confidence interval of ratio, 2.792 to 8.651; P < 0.0001).

[00376] Next we determined that application of a survival predictor algorithm would identify sub-groups of patients with distinct clinical outcome after therapy in breast cancer patients with ER-negative tumors, thus providing additional predictive value to the therapy outcome classification based on ER status alone. We were unable to generate statistically meaningful prognostic stratification of ER-negative breast cancer patients using a parent 70-gene signature (data not shown). However, we were able to identify two small gene clusters comprising 5 and 3 genes (Table 75) that appear highly informative in classifying breast cancer patients with ER-negative tumors into good and poor prognosis sub-groups with statistically distinct probability of survival after therapy (Figure 64B).

Table 75. Gene expression signatures predicting survival of breast cancer patients with estrogen receptor-negative tumors.

5-gene signature

Gene	Description	Gene ID (Chip identified in	UniGene	
		van't Veer, L.J., et	ID	
		al.,2002)		
EST	Unknown	Contig63649_RC		
	RA-regulated nuclear		Hs.126774	
	matrix-associated			
L2DTL	protein	NM_016448		
DCK	Deoxycytidine kinase	NM_000788	Hs.709	
	G protein-coupled		Hs.44197	
DKFZP564D0462	receptor 126	AL080079		
	Hypothetical protein		Hs.100691	
LOC286052	LOC286052	AA555029_RC		
	3-gene si	gnature	<del></del>	
Gene	Description	Gene ID (Chip identified in	UniGene	
		van't Veer, L.J., et	ID .	
		al.,2002)		
	Guanine nucleotide		Hs.92002	
GNAZ	binding protein	NM_002073		
<del></del>	CDC42 binding protein		Hs.18586	
PK428	kinase alpha	NM_003607		
LYRIC	LYRIC/3D3	AK000745	Hs.243901	

[00377] In the group of 69 breast cancer patients with ER-negative tumors (Figure 64B), the median survival after therapy of patients in the poor prognosis sub-group defined by the survival predictor algorithm was 5.2 years. Only 30 % of patients in the poor prognosis sub-group survived 10 years after therapy compared to 77 % patients in the good prognosis sub-group. The estimated hazard ration for survival after therapy in the poor prognosis sub-group as compared with the good prognosis sub-group of patients

defined by the survival predictor algorithm was 3.609 (95% confidence interval of ratio, 1.477 to 5.792; P = 0.0021).

Outcome classification of breast cancer patients with ER-positive tumors [00378] using a 14-gene survival predictor signature. To further validate the clinical utility of identified signatures, we determined that application of a 14-gene survival predictor cluster is informative in classifying breast cancer patients with ER-positive tumors. Kaplan-Meier analysis showed that application of the 14-gene survival predictor signature identified three sub-groups of patients with statistically distinct probabilities of survival after therapy in the cohort of 226 breast cancer patients with ER-positive tumors (Figures 67 A&B). The median survival after therapy of patients in the poor prognosis sub-group defined by the 14-gene survival predictor signature was 7.2 years (Figure 67A). Only 41 % of patients in the poor prognosis sub-group survived 10 years after therapy compared to 100 % patients in the good prognosis sub-group (P < 0.0001). A large, statistically distinct sub-group of patients with an intermediate expression pattern of the 14-gene signature and an intermediate prognosis was identified by Kaplan-Meier survival analysis (Figure 67B). The patients in the sub-group with an intermediate prognosis had 90% 5-year survival and 76% 10-year survival after therapy (Figure 67B). Thus, the 14-gene survival predictor signature is highly informative in classifying breast cancer patients with ER-positive tumors into good, intermediate, and poor prognosis subgroups with statistically significant differences in the probability of survival after therapy (Figures 67 A&B).

[00379] Therapy outcome prediction in breast cancer patients with lymph nodenegative disease using survival predictor signatures. Invasion into axillary lymph nodes is considered as one of the most important negative prognostic factors in breast cancer and patients with no detectable lymph node involvement are classified as having good prognosis (Krag, et al., 1998; Singletary, et al., 2002; Jatoli, et al., 1999). Breast cancer patients with lymph node negative disease typically would not be selected for adjuvant systemic therapy and usually treated with surgery and radiation. Recent data demonstrated that up to 33% of these patients would fail therapy and develop recurrence of the disease after a 10-year follow-up (Early Breast Cancer Trialists' Collaborative Group. Tamoxifen for early breast cancer: an overview of the randomized trials. Lancet, 351: 1451-1467, 1998). Therefore, we tested whether application of the 14-gene survival predictor signature would aid in identifying breast cancer patients with lymph-node negative tumors that are at high risk of treatment failure.

[00380] Kaplan-Meier analysis showed that the 14-gene survival predictor signature (Tables 29 and 73) identified two sub-groups of patients with statistically distinct probability of survival after therapy in the cohort of 151 breast cancer patients with lymph node negative disease (Figure 63A). The median survival after therapy of patients in the poor prognosis sub-group defined by the 14-gene survival predictor signature was 7.7 years (Figure 63A). Only 46 % of patients in the poor prognosis sub-group survived 10 years after therapy compared to 82 % patients in the good prognosis sub-group (P < 0.0001). The estimated hazard ration for survival after therapy in the poor prognosis sub-group as compared with the good prognosis sub-group of patients defined by the 14-gene survival predictor signature was 5.067 (95% confidence interval of ratio, 3.174 to 11.57; P < 0.0001).

[00381] Kaplan-Meier analysis also demonstrated that the 14-gene survival predictor signature identified two sub-groups of patients with statistically distinct probability of survival after therapy in the cohort of 109 breast cancer patients with ER-positive tumors and lymph node negative disease (Figure 63B). The median survival after therapy of patients in the poor prognosis sub-group defined by the 14-gene survival predictor signature was 11.0 years (Figure 63B). 10-year survival after therapy in the poor prognosis sub-group was 57% compared to 86% patient's survival in the good prognosis sub-group (P < 0.0001). The estimated hazard ration for survival after therapy in the poor prognosis sub-group as compared with the good prognosis sub-group of patients defined by the 14-gene survival predictor signature was 5.314 (95% confidence interval of ratio, 2.775 to 17.79; P < 0.0001).

[00382] Next we determined that application of small gene clusters comprising 5 and 3 genes (Table 75) that appear highly informative in classification of breast cancer patients with ER-negative tumors into good and poor prognosis sub-groups with statistically distinct probability of survival after therapy (Figure 64B), also are informative in classification of sub-group of ER-negative patients with lymph node-negative disease. In the group of 42 breast cancer patients with ER-negative tumors and lymph node-negative disease (Figure 63C), the median survival after therapy of patients in the poor prognosis sub-group defined by the survival predictor algorithm was 5.2 years. Only 34 % of patients in the poor prognosis sub-group survived 10 years after therapy compared to 74 % patients in the good prognosis sub-group. The estimated hazard ration for survival after therapy in the poor prognosis sub-group as compared with the good prognosis sub-group of patients defined by the survival predictor algorithm was 3.237 (95% confidence

interval of ratio, 1.139 to 6.476; P = 0.0243). Thus, the survival predictor signatures identified in accordance with the methods of the invention are highly informative in classifying breast cancer patients with lymph node-negative disease and either ER-positive or ER-negative tumors into good and poor prognosis sub-groups with statistically significant difference in the probability of survival after therapy (Figures 63 B&C).

[00383] Therapy outcome prediction in breast cancer patients with lymph nodepositive disease using survival predictor signatures. Breast cancer patients with
invasion into axillary lymph node are considered as having a poor prognosis and usually
treated with adjuvant systemic therapy. The patients with poor prognosis are thought to
benefit most from adjuvant systemic therapy (see Introduction). In the cohort of 295
breast cancer patients, ten of 151 (6.6%) patients who had lymph node-negative disease
and 120 of the 144 (83.3%) patients who had lymph node-positive disease had received
adjuvant systemic therapy (van de Vijver, et al. 2002). This treatment strategy was clearly
beneficial for patients with lymph node-positive disease, because sub-groups of patients
with distinct lymph node status in the cohort of 295 patients had statistically
indistinguishable survival after therapy (data not shown). Next we determined therapy
outcome prediction using survival predictor signatures identified in accordance with the
present invention to be informative in breast cancer patients with lymph node-positive
disease.

[00384] Kaplan-Meier analysis show that application of the 14-gene survival predictor signature identify three sub-groups of patients with statistically distinct probability of survival after therapy in the cohort of 144 breast cancer patients with lymph node positive

disease (Figure 66A). The median survival after therapy of patients in the poor prognosis sub-group defined by the 14-gene survival predictor signature was 9.5 years (Figure 66A). Only 43 % of patients in the poor prognosis sub-group survived 10 years after therapy compared to 98 % patients in the good prognosis sub-group (P < 0.0001). Large statistically distinct sub-group of patients with an intermediate expression pattern of the 14-gene signature and an intermediate prognosis was identified by Kaplan-Meier survival analysis (Figure 66A). The patients in the sub-group with an intermediate prognosis had 86% 5-year survival and 73% 10-year survival after therapy (Figure 66A). Thus, 14-gene survival predictor signature appears highly informative in classification of breast cancer patients with lymph node-positive disease into good, intermediate, and poor prognosis sub-groups with statistically significant difference in the probability of survival after therapy (Figures 66A).

[00385] Using the 14-gene survival predictor signature we identified two sub-groups of patients with statistically distinct probabilities of survival after therapy in the cohort of 117 breast cancer patients with ER-positive tumors and lymph node positive disease (Figure 66B). The median survival after therapy of patients in the poor prognosis subgroup defined by the 14-gene survival predictor signature was 11.0 years (Figure 66B). 10-year survival after therapy in the poor prognosis sub-group was 68% compared to 98% patient's survival in the good prognosis sub-group (P = 0.0026). The estimated hazard ration for survival after therapy in the poor prognosis sub-group as compared with the good prognosis sub-group of patients defined by the 14-gene survival predictor signature was 6.810 (95% confidence interval of ratio, 1.566 to 8.358; P = 0.0026).

[00386] Next we determined that the small gene clusters comprising 5 and 3 genes (Table 75) also are informative in classifying sub-groups of ER-negative patients with lymph node-positive disease. In the group of 27 breast cancer patients with ER-negative tumors and lymph node-positive disease (Figure 66C), the median survival after therapy of patients in the poor prognosis sub-group defined by the survival predictor algorithm was 4.4 years. Only 24 % of patients in the poor prognosis sub-group survived 10 years after therapy compared to 82 % patients in the good prognosis sub-group. The estimated hazard ration for survival after therapy in the poor prognosis sub-group as compared with the good prognosis sub-group of patients defined by the survival predictor algorithm was 3.815 (95% confidence interval of ratio, 0.9857 to 9.660; P = 0.0530). Thus, survival predictor signatures identified in accordance with the present invention also is informative in classifying breast cancer patients with lymph node-positive disease into good and poor prognosis sub-groups with statistically significant differences in the probability of survival after therapy (Figures 66A & 66B).

as a component of multiparameter therapy outcome classification of breast cancer patients. Next we estimated the potential clinical benefits of applying gene expression survival predictor signatures identified in accordance with the methods of the present invention for classifying breast cancer patients at the time of diagnosis into sub-groups with distinct probabilities of survival after therapy. In our estimate we used the assignment of the patient into a poor outcome classification sub-group as a criterion of treatment failure and reason for prescription of additional cycle(s) of adjuvant systemic therapy. We have made the estimate of potential therapeutic benefits in the cohort of 295

breast cancer patients (van de Vijver, et al. 2002) and based our estimate on the assumption that the use of additional cycle(s) of adjuvant systemic therapy would be prescribed to patients classified within a poor prognosis sub-group. In the cohort of 295 breast cancer patients, ten of 151 (6.6%) patients who had lymph node-negative disease and 120 of the 144 (83.3%) patients who had lymph node-positive disease had received adjuvant systemic therapy (id.), indicating that a major difference in treatment protocols between LN+ and LN- sub-groups was the application of adjuvant systemic therapy in patients with lymph node positive disease. We accepted the actual 5- and 10-year survival in the corresponding classification categories as the expected therapy outcome for a given sub-group. We assumed that each additional cycle of adjuvant systemic therapy would result in the same therapy outcome as was actually documented in the most relevant subgroups of the 295 patients. Therapy outcome for patients classified into poor prognosis sub-groups and treated with additional cycle(s) of adjuvant systemic therapy is expected to be in 37% of patients in good therapy outcome category for ER+LN+ and ER+LNpoor signature sub-groups and in 41% of patients in good therapy outcome category for ER-LN+ and ER-LN- poor signature sub-groups (Table 76). Finally, we assumed that patients classified into good prognosis sub-groups would receive the same treatment and would have the same outcome as in the original cohort of 295 patients (van de Vijver, et al., 2002). Based on these assumptions we calculated the number of patients that would be expected to have good and poor survival outcome after therapy and estimated the expected 10-year survival in each classification sub-groups (Table 76).

[00388] The estimate of potential therapeutic benefits provided in Table 76 is based on the cohort of 295 breast cancer patients (van de Vijver, et al. 2002) and premised on the

assumption that additional cycle(s) of adjuvant systemic therapy would be prescribed to patients classified into poor prognosis sub-groups. In the cohort of 295 breast cancer patients, ten of 151 (6.6%) patients who had lymph node-negative disease and 120 of the 144 (83.3%) patients who had lymph node-positive disease had received adjuvant systemic therapy (id.). We accepted the actual 5- and 10-year survival in the corresponding classification categories as the expected therapy outcome for a given sub-group. We assumed that each additional cycle of adjuvant systemic therapy would result in the same therapy outcome as was actually documented in the most relevant sub-groups of the 295 patients. Therapy outcome for patients classified into poor prognosis sub-groups and treated with additional cycle(s) of adjuvant systemic therapy is expected to be in 37% of patients in good therapy outcome category for ER+LN+ and ER+LN- poor signature sub-groups and in 41% of patients in good therapy outcome category for ER-LN+ and ER-LN- poor signature sub-groups.

Table 76. Estimated therapeutic benefits of using gene expression survival predictor								
signatures for classification of breast cancer patients								
Classification	5-year	10-year	Number	Good	Good	Estimated increase in 10-year survival,		
	]	}	}		(municated)	%		
category	survival	survival	patients	(current)	(projected)	70		
			151/295					
LN-negative	82%	69%	(51%)					
			144/295					
LN-positive	85%	72%	(49%)					
LN- Good			95/151			0.00		
signature	92%	82%	(63%)	95	95			

LN- Poor		<del></del>	56/151		17 (56 x	23%
signature	64%	46%	(37%)	0	0.3)	
LN+ Good			43/144			0.00
signature	98%	98%	(30%)	43	43	
LN+			67/144		20 (67 x	10%
Intermediate	86%	73%	(47%)	0	0.3)	
LN+ Poor			34/144		10 (34 x	13%
signature	68%	43%	(24%)	0	0.3)	
				138/295	185/295	5%
Overall				(47%)	(63%)	
	<del> </del>		226/295			
ER+ tumors	90%	77%	(77%)			
			69/295			
ER- tumors	62%	47%	(23%)			
ER+ LN-						
Good	1		69/109			0.00
signature	97%	86%	(63%)	69	69	
Poor			40/109		15 (40 x	17%
signature	76%	57%	(37%)	0	0.37)	
ER- LN-		<del></del>				
Good			16/42			0.00
signature	74%	74%	(38%)	16	16	
Poor			26/42		11 (25 x	44%
signature	50%	34%	(62%	0	0.41)	
ER+ LN+						
Good			43/117			0.00
signature	98%	98%	(37%)	43	43	
Poor	-		74/117		27 (74 x	16%
signature	86%	68%	(63%)	0	0.37)	
ER- LN+						

Good			11/27			0.00
signature	82%	82%	(41%)	11	11	
Poor	<u> </u>		16/27		7 (16 x	100%
signature	47%	24%	(59%)	0	0.41)	
} <del>-</del>				139/295	199/295	6%
Overall				(47%)	(67%)	

[00389] One of the most interesting end-points of this analysis is the prediction that patients with ER-LN- and ER-LN+ breast cancer classified into poor prognosis subgroups would be expected to show a most dramatic increase in 10-year survival after therapy (Table 76). This prediction is consistent with the generally accepted notion that breast cancer patients with poor prognosis would benefit most from adjuvant systemic therapy (see Introduction). The estimated modest increase in the overall 10-year survival (Table 76) may translate every year into ~7,000-9,000 more breast cancer survivors after 10-year follow-up. Our ability to accurately segregate at the time of diagnosis breast cancer patients with low probability of survival after therapy should lead to more rapid development of novel efficient therapeutic modalities specifically targeting most aggressive therapy-resistant breast cancers.

[00390] While the invention has been described with reference to specific methods and embodiments, it will be appreciated that various modifications may be made without departing from the invention, the scope of which is limited only by the appended claims. All references cited, including scientific publications, patent applications, and issued patents, are herein incorporated by reference in their entirety for all purposes.